

*Stress assemblies:  
Defining pathways leading to their formation  
and identifying their components*

*Chujun Zhang*

张楚珺





*Stress assemblies:  
Defining pathways leading to their formation  
and identifying their components*

*Chujun Zhang*

张楚珺

*Utrecht, 2022*

The research described in the thesis was performed at the Hubrecht Institute of The Royal Netherlands School of Arts and Sciences (KNAW), Utrecht, The Netherlands

Copyright © 2022 Chujun Zhang

**ISBN:** 9789464238037

No part of this publication may be reproduced, stored in a retrieval system, or transmitted in any form or by any means, electronic, photocopying, recording or otherwise, without the prior permission in writing from the author.

**Printed by:** ProefschriftMaken || [www.proefschriftmaken.nl](http://www.proefschriftmaken.nl)

**Layout by:** Chujun Zhang

**Cover design by:** Chujun Zhang designed the cover based on the illustration from Shutterstock under Article ID 1697114038.



# **Stress assemblies: Defining pathways leading to their formation and identifying their components**

**Stress-assemblages: paden definiëren die leiden tot hun vorming en  
hun componenten identificeren**  
(met een samenvatting in het Nederlands)

## **Proefschrift**

ter verkrijging van de graad van doctor aan de Universiteit Utrecht op gezag  
van de rector magnificus, prof.dr. H.R.B.M. Kummeling, ingevolge het besluit  
van het college voor promoties in het openbaar te verdedigen op  
woensdag 25 mei 2022 des middags te 4.15 uur

door

**Chujun Zhang**

geboren op 18 september 1991  
te Huibei, China

**Promotoren:**

Prof. dr. A. van Oudenaarden

Prof. dr. C. Rabouille

## *Table of contents*

<i>Chapter1</i>	<i>General introduction</i>	<i>8</i>
	<i>Cellular stress and Stress assemblies</i>	
<i>Chapter2</i>	<i>Membrane-Bound Meet Membraneless in Health and Disease</i>	<i>24</i>
<i>Chapter3</i>	<i>Activation of IRE1, PERK and saltinducible kinases leads to Sec body formation in Drosophila S2 cells</i>	<i>56</i>
<i>Chapter4</i>	<i>Osmotic stress via calmodulin lead to the formation of stress granule in Drosophila S2 cells</i>	<i>100</i>
<i>Chapter5</i>	<i>Novel components of the stress assembly Sec body identified by proximity labeling</i>	<i>126</i>
<i>Chapter6</i>	<i>Summary and general discussion</i>	<i>148</i>
<i>Chapter7</i>	<i>Addendum</i>	<i>162</i>
	<i>Nederlandse samenvatting</i>	
	<i>List of publications</i>	
	<i>Acknowledgements</i>	
	<i>Curriculum vitae</i>	



# *Chapter1*

*General Introduction*  
*Cellular stress and Stress assemblies*

Chujun Zhang and Catherine Rabouille (2022)

---

## *General Introduction*

### *Cellular stress and Stress assemblies*

#### **1**

#### *1 Cellular stress*

A cell in an organism or an organ can be subjected to many stresses. Cellular stress can be induced by internal and external signals. Cells respond to different kinds of stresses that activates multiple processes in order to promote cellular homeostasis or when the stress is too strong, commit to cell death.

##### *1.1 ER stress and UPR*

One internal stress that cells can experience is ER stress. Endoplasmic reticulum (ER) is one of the largest compartments that serves in the synthesis of secretory protein, in their folding and proper oligomerization, and where a multitude of posttranslational modifications including glycosylation, the formation of disulfide bonds takes place (Horstmann, 2002; Jamieson and Palade, 1968). After a process termed quality-control, only correctly folded proteins exit the ER (at ER, see below) and will be delivered to the Golgi apparatus. Misfolded proteins remain in the ER to complete the folding process until it is correct or are degraded (Ellgaard. et al., 1999; Palade, 1975). In addition, ER also functions  $\text{Ca}^{2+}$  storage and lipid and carbohydrate metabolism (Krause, 1991).

Disruption of any of these processes causes ER stress and results in the activation of Unfolded Protein Response (UPR) (Boyce and Yuan, 2006; Hetz, 2012; Ron and Walter, 2007). This activation has first been identified as a response to an increased load of unfolded proteins in the ER. The outcome is multiple and comprises the increased transcription and translation of target genes. Those encode ER chaperones (such as BIP) (Gardner et al., 2013; Munro and Pelham, 1987), those leading to an increased capacity of ER exit (see below), an increased ER degradation along a general stalling of translation, especially of ER inserted proteins, in order to resolve and decrease the ER load and restore its homeostasis (Palade, 1975).

The UPR is regulated by three membrane sensors: The inositol-requiring enzyme 1 (IRE1), the protein kinase R (PKR)-like ER kinase (PERK), and the activating transcription factor 6 (ATF6) (Harding et al., 2000b; Hetz, 2012; Lin et al., 2007). ATF6 is a transcription factor which contains a large ER luminal domain. Upon ER stress conditions, ATF6 is delivered from the ER to Golgi apparatus via transport vesicles and is cleaved twice at

Golgi by two Golgi-resident proteases (Gardner et al., 2013). S1P (site 1 protease) removes the luminal domain of ATF6 and S2P (site 2 protease) cut the transmembrane region. After that, only the N-terminal cytosolic domain of ATF6 moves into the nucleus and results in the activation expression of target genes (Brown et al., 2000; Ye. et al., 2000).

The other two branches of UPR are mediated by PERK and IRE1 which are very similar in structure and function. Both of them are ER localized type I transmembrane proteins and contain a luminal domain while the kinase domain localizes in the cytosolic part of the protein (Gardner et al., 2013; Harding et al., 2000b; Harding et al., 1999). Upon ER stress, PERK oligomerizes and phosphorylates both itself and the  $\alpha$ -subunit of eukaryotic translation initiation factor-2 (eIF2 $\alpha$ ) at Ser51 (DuRose et al., 2009; McInerney et al., 2005). Phosphorylation of eIF2 $\alpha$  inactivates eIF2 and results in the induction of transcription factor ATF4 translation (Baird and Wek, 2012; Donnelly et al., 2013; Harding et al., 2000a). ATF4 target genes are involved in apoptosis which contribute signals to cell death pathways (Harding et al., 2000a; Mateju et al., 2020).

On the other hand, IRE1 cytosolic region contains a kinase domain but also an RNase domain. In response to the increase in unfolded protein load, IRE1 oligomerizes leading to the activation of the kinase domain by autophosphorylation. This leads to the activation of the RNase activity that cleaves the unspliced mRNA of XBP1 (X-box binding protein 1 in metazoans and Hac1 (homologous to ATF/CREB1) in yeast) (Korennykh et al., 2009; Mori. et al., 1996; Shamu et al., 1994). Unspliced XBP1 (XBP1u) is an UPR inhibitor, whereas spliced XBP1 (XBP1s) is a UPR-specific transcription factor, which induces ER-associated degradation (ERAD) (Arai et al., 2006; Travers et al., 2000). Importantly, XBP1s also communicates with cleaved ATF6 and upregulated ATF4, all leading to the increasing of the transcription of UPR target genes together.

## 1.2 Oxidative stress and ROS production

Molecular oxygen and antioxidants are required for cell survival (Ali et al., 2004; Haynes et al., 2003). Oxygen products include reactive oxygen species (ROS) such as the superoxide anion (O<sub>2</sub><sup>-</sup>), hydrogen peroxide (H<sub>2</sub>O<sub>2</sub>) and hydroxyl radicals (OH<sup>-</sup>) and are toxic to the cell (John et al., 2005; Kato et al., 2019). Antioxidants include catalase, glutathione peroxidase, and superoxide dismutase (SOD) (Dupuis et al., 2004). In growing conditions, the production of ROS is counterbalanced by antioxidants that remove them in cells are keep in equilibrium. The oxidative stress appears when the conditions results in a disbalance in the equilibrium between ROS production and antioxidant activity (Trachootham et al., 2008).

---

ROS are involved in positively many important cellular processes one of the most well-known one is ROS and  $\text{Ca}^{2+}$  homeostasis in aging. People found that the plasma ROS level increased in aged rats (Luceri et al., 2018). And increase ROS production can change  $\text{Ca}^{2+}$  hemostasis during aging (Castelli et al., 2019). Interestingly, many proteins that are involved in  $\text{Ca}^{2+}$  signaling are modified by ROS, and  $\text{Ca}^{2+}$  also regulates ROS generation (Gorlach et al., 2015a; Gorlach et al., 2015b). ROS have effect on several  $\text{Ca}^{2+}$  transport proteins on the plasma membrane, such as the transient receptor potential (TRP) channels, and the second messenger adenosine diphosphate (ADP)-ribose (Perraud et al., 2005).

### *1.3 Salt stress and NaK-ATPase/SIK1 complex*

Another common stress is salt stress that can be induced by high NaCl concentration (Dmitrieva and Burg, 2007). The intake of increasing of  $\text{Na}^+$  concentration in the circulating medium leads to the NaK-ATPase and salt inducible kinase (SIK) activation (Jaitovich and Bertorello, 2010; Wehr et al., 2013). NaK-ATPase is a plasma membrane transporter that allows the transport of three  $\text{Na}^+$  ions out of the cell against the import of two  $\text{K}^+$  ions inside the cell. Ouabain is a NaK-ATPase inhibitor which can bind to NaK-ATPase and keeps NaK-ATPase in a closed stage, therefore inhibiting the transport of the ions via NaK-ATPase (Kaplan, 2002; Zatti et al., 2005).

SIK (Salt Inducible Kinase) was first found in five-week-old rats after a high  $\text{Na}^+$  diet treatment for a week (Wang. et al., 1999). Interestingly, Sjöström and his colleagues found that SIK1 activation regulates NaK-ATPase activity, not directly, but via Protein Phosphatase 2A (PP2A) (Sjöström. et al., 2007). SIK1, NaK-ATPase and PP2A are form the NaK-ATPase/SIK1 complex. The activation of SIK1 causes the complex dissociation and in the activation of NaK-ATPase(Sjöström. et al., 2007).

## *2 Stress assemblies are membraneless organelles*

Cellular stress not only activates many signaling pathways, but also lead to the remodeling of the cytoplasm through the formation of biocondensates/stress assemblies.

### *2.1 Membraneless organelles*

There are numerous compartments or organelles in eukaryotic cells and eukaryotic cells are compartmentalized by membrane-bound compartments to ensure the biochemical reactions and cellular functions(Blobel and Dobberstein, 1975; John et al., 2005; Zhang and Rabouille, 2019). The endoplasmic reticulum, Golgi apparatus and the vesicles are



membrane bound compartments specialized in protein sorting and trafficking through the cell (Fullekrug and Nilsson, 1998; Lippincott-Schwartz et al., 1989).

However, the advent of light microscopy has led to the discovery that cells also contain organelles that lack membrane. These membranesless organelles are present both in the nucleus (such as the nucleolus, nuclear speckles), but also form in the cytoplasm of cells that experience stress, as stress assemblies, in particular stress granules and Sec bodies (Gomes and Shorter, 2018; Nott et al., 2015; Zhang and Rabouille, 2019).

It is important to note that membrane bound and membraneless organelles interact with one another, many of the later forming around membranes (**Chapter 2**, (Zhang and Rabouille, 2019)).

## *2.2 Membraneless organelles form by phase separation*

Those membraneless organelles were discovered decades ago and nowadays people are focused on understanding the biophysical principles underlying their formation.

Phase separation can be a transition which can concentrate specific molecules seemingly diffuse, leading to a liquid-liquid phase separation (LLPS, (liquid into a liquid) or a liquid-solid transition (Chong and Forman-Kay, 2016; Hyman et al., 2014). Membraneless organelles can form via macromolecular condensation which happens when a critical molecular concentration, temperature, pH or salt concentration threshold is crossed (Banani et al., 2017; Weber and Brangwynne, 2012). They are often liquid-like. In 2009, Brangwynne, Jülicher and Hyman proved that P granules (also named germ granules) have liquid-like properties and formed via phase separation (Brangwynne et al., 2009). In particular, the time-laps imaging showed that the smaller droplets tended to fused into larger droplets over time (Li et al., 2012).

## *2.3 Phase separation of proteins with low complexity domains and intrinsically disordered regions*

Proteins associated with membraneless organelles often exhibit multivalent interactions and triggers in different ways. Folded proteins are proteins with well-defined interaction surfaces which can form stable secondary structures (Bah and Forman-Kay, 2016). Intrinsically disordered protein regions are proteins that cannot form stable secondary structures and many IDRs (Intrinsically disordered regions) contain a small biased amino acid composition which referred to as low complexity domains (Coletta et al., 2010; Das et al., 2014).

---

In this regard, specific domains have been shown to drive phase separation. NCK (Non-Catalytic region of tyrosine Kinase) and N-WASP (Wiskott–Aldrich syndrome protein) are two signaling proteins that regulate actin polymerization which can interact with each other via the SH3 domain from NCK and PRM (proline-rich motif) domain of N-WASP (Jones et al., 2006). Li and colleagues found that when amplifying and mixing SH3 and PRM in vitro, the mixed solution keeps clear at low concentrations and turns to form liquid droplets at high concentrations (Li et al., 2012).

Similar research was found from the phase separation of a unimolecular RNA helicase, Ddx4 (Nott et al., 2015). Ddx4 contains a disordered N terminus which can spontaneously self-associate both in cells and in vitro with a highly similar structure. The N terminus of Ddx4 is very sensitive to temperature change as it can transform from droplets to diffusion when the temperature increases (Nott et al., 2015). In addition, the droplet formed upon low temperature can become destabilized at higher NaCl concentration, the chains in the interior of the droplet become more mobile (Nott et al., 2015).

### *3 Sec bodies*

One of the stress assemblies that form in stress *Drosophila* S2 cells are Sec bodies that are linked to the early secretory pathway.

#### *3.1 The early secretory pathway*

The early secretory pathway mediates and delivers secretory proteins from the ER (see above) to the correct cellular space (Dancourt and Barlowe, 2010; Nickel et al., 1998). The delivery proceeds start from ER where the newly synthesized proteins are folded and assembled (see above) (Palade, 1975; Rothman and Wieland, 1996). The properly folded proteins are transported from the ER to Golgi complex via coat protein complex II (COPII) transport vesicles which bud at the ER exit site (ERES) (Schekman and Orci, 1996). Conversely, COPI coated mediated the retrograde traffic from the Golgi complex back to the ER and this balances the COPII mediate transport (Barlowe et al., 1994; Schekman and Orci, 1996). Proteins are further sorted at Golgi complex and delivered to their final destinations (Barlowe, 2015).

#### *3.2 COPII coat*

The COPII coat was first identified in yeast (Peter Novick. et al., 1980) and mediate proteins export out of ER (Bannykh. et al., 1996). Formation of the COPII vesicle requires the activation of Sar1 (a small 21-kDa Ras-like GTPase protein) (Nakano and Muramatsu, 1989; Oka et al., 1991). Sec12 is an ER-bound transmembrane guanine nucleotide exchange

factor (GEF) and mediates this Sar1-GDP to –GTP activation (Barlowe and Schekman, 1993; d'Enfert et al., 1991). Sar1-GDP to –GTP transition leads to the N-terminal of itself insert into the ER membrane (Lee et al., 2005). After activation, Sar1-GTP recruits the Sec23/24 subcomplex and form the “prebudding complex” together with transmembrane cargo (Barlowe et al., 1994), forming the inner layer of the COPII coat. The transmembrane cargos interact with Sec24 through independent cargo binding sites (Miller et al., 2002). These prebudding complex is then recruited by the Sec13/31 complex onto the prebudding complex, forming the outer layer of the COPII coat (Stagg et al., 2008). The recruitment of outer layer Sec13/31 leads to the increase of Sec23 activity towards Sar1 and that completes the entire assembly of COPII coat (Antonny et al., 2001; Espenshade et al., 1995; Gimeno et al., 1996).

### 3.3 *Sec16*

COPII coat formed at ERES and the question remains how is this formation organized at ERES? Sec16 is an important factor in contribution to the optimal formation of COPII coat (Supek et al., 2002; Watson et al., 2006). The function of Sec16 in Secretory pathway was first identified in yeast (Peter Novick. et al., 1980) where mutated Sec16 was found to inhibit the COPII mediated protein transport to the Golgi (Novick. et al., 1981; Sprangers and Rabouille, 2015). Sec16 is a large (~240kDa) hydrophilic protein which contains three functional domains: ELD (ERES localization domain) /UCR (Upstream conserved region), the CCD (Central conserved domain) and CTCD (C-terminal conserved domain) from N-terminal to C-terminal (Espenshade et al., 1995; Sprangers and Rabouille, 2015).

Sec16 directly interacts with COPII coat subunits Sec23, Sec24, Sec13 and Sec31 (Bharucha et al., 2013; Bhattacharyya and Glick, 2007; Connerly et al., 2005; Ivan et al., 2008; Whittle and Schwartz, 2010; Yorimitsu and Sato, 2012), suggesting that Sec16 serves as a scaffold protein for COPII coat formation. Multiple researches have been done in different species. In 2008, Rabouille group found that Sec16 localizes at ERES doesn't change upon Sec23 depletion in *Drosophila* S2 cells (Ivan et al., 2008). But Sec16 depletion disrupts ERES and inhibits ER transport via COPII coat. Moreover, the localization of Sec16 at ERES is also upstream of Sar1. This Indicates that in *Drosophila* cells the localization of Sec16 at ERES is independent of COPII subunits. This is consistent with *drosophila* Sec16 that Sec16 provides a platform for COPII coat assembly.

In addition to that, the importance of Sec16 is also confirmed in mammalian cells. There are two Sec16 orthologues in mammalian cells: Sec16A(250kDa) and Sec16B(117kDa) (Bhattacharyya and Glick, 2007). Sec16A is more similar to Sec16 in other

---

species and shows a typical ERES localization (Bhattacharyya and Glick, 2007; Watson et al., 2006). Interestingly, both overexpression and depletion of Sec16A results in the disorganization of the ERES, and the absence of Sec16A inhibits ER export (Aguilera-Gomez et al., 2016).

### *3.4 Sec bodies*

Amino acid starvation in the Krebs Ringer bicarbonate buffer (KRB) leads to the phase separation of Sec16 and COPII subunits into the stress assemblies, the Sec bodies (Zacharogianni et al., 2014). Sec body formation takes place at ERES and contains multiple Sec proteins of ERES components, Sec16, Sec23, Sec24(AB and CD) and Sec31. Sec bodies formation is optimal after 4 hours amino acid starvation in KRB ( $7 \pm 3$  Sec bodies per cell). Electron microscopy showed that they are membraneless and they display a diameter between 0.6 and 0.8  $\mu$ M (Zacharogianni et al., 2014).

Sec16 and Sec24AB seem to be the drivers of Sec body formation. Sec16 and Sec24AB depletion decreases the Sec body formation in S2 cells (Aguilera-Gomez et al., 2016; Zacharogianni et al., 2014). Interestingly, Both of Sec24AB and Sec16 contain a high level of low complexity sequences (LCS). LCS domains of Sec24AB located at the N-terminal and Sec16 LCS are throughout the sequence. The overexpressed Sec24AB N-terminal region tagged to GFP leads to its recruitment to Sec bodies under amino acid starvation in KRB. Conversely, Sec24AB without N-terminal (non LCS region) is hardly recruited.

The first question that I address in my thesis is the identification of the pathways triggering Sec body formation in *Drosophila* cells upon incubation in KRB (**Chapter 3**). The second is the identification of the Sec body components by proximity labeling (**Chapter 5**).

## *4 Stress granules*

Critically, KRB incubation of S2 cells also leads to the formation of a different stress assembly, the stress granules (Aguilera-Gomez et al., 2016). Stress granules are also submicron stress assemblies that form in eukaryotic cells upon many cellular stresses, including those that induce inhibition of translation initiation and polysome disassembly (Anderson and Kedersha, 2008, 2009; Kedersha and Anderson, 2002). This leads to an accumulation of untranslated, 80S ribosome-free mRNAs in the cytoplasm that can bind RNA-binding proteins that phase separate into stress granules (Buchan and Parker, 2009; Kedersha et al., 2005; Protter and Parker, 2016). There is also non-canonical pathways lead to stress granule formation like osmotic stress (Aulas et al., 2017; van Leeuwen and Rabouille, 2019).

Given that the same stress (KRB incubation and high salt stress) of S2 cells leads to the formation of both Sec bodies and stress granules, The question whether both are formed downstream of the same pathways (**Chapter 4**).

### *Scope of this thesis*

7

After the presentation of some stress signaling pathways and stress assemblies (**Chapters 1 and 2**), the main scope of this thesis is to unravel the signaling pathways leading to the formation of stress assemblies, Sec bodies and Stress granules. It is articulated around 2 chapters.

**Chapter 3**, describes the signaling pathways leading to Sec body formation. Here, we have found that amino acid starvation in KRB comprises two branches. First, KRB induces a NaCl stress due to its 2.6-fold increased (moderate) NaCl concentration when compared to the growing Schneider's medium. Interestingly, a larger (4-fold) increase in NaCl concentration in Schneider's (SCH150) is sufficient to lead to Sec body formation. NaCl stress activates the Salt inducible Kinases (SIK) and their pharmacological inhibition (using the pan SIK inhibitor HG-9-91-01) reduces Sec body formation. The second pathway activated in KRB is due to amino acid starvation that elicits oxidative stress and ER stress. However, either ROS or ER stress or combined is not enough to trigger Sec body formation. To form Sec bodies, ER stress (through the activation of IRE1 and PERK) needs to be combined to moderate NaCl stress.

Conversely, **Chapter 4** describes the Signaling pathways leading to stress granule formation and we have compared these to Sec bodies. Here, we show that both KRB and high NaCl stress (SCH150) also lead to the formation of stress granules. However, neither SIKs, nor IRE1 nor PERK are involved in their formation. Instead, we found osmotic stress through the addition of any salt or sucrose leads to the formation of stress granules that is also partly modulated by calmodulin activation, in stark contrast to Sec body formation.

In **Chapter 5**, we report how I have addressed the protein content of Sec body using APEX2 followed by mass spectroscopy. 52 proteins have been identified specifically enriched in Sec body, including a large proportion of ER and Golgi protein.

We summary and discuss our findings in **Chapter 6**.

---

## References

- Aguilera-Gomez, A., van Oorschot, M.M., Veenendaal, T., and Rabouille, C. (2016). In vivo visualization of mono-ADP-ribosylation by dPARP16 upon amino-acid starvation. *eLife* 5.
- Ali, M.H., Pearlstein, D.P., Mathieu, C.E., and Schumacker, P.T. (2004). Mitochondrial requirement for endothelial responses to cyclic strain: implications for mechanotransduction. *American journal of physiology Lung cellular and molecular physiology* 287, L486-496.
- Anderson, P., and Kedersha, N. (2008). Stress granules: the Tao of RNA triage. *Trends in biochemical sciences* 33, 141-150.
- Anderson, P., and Kedersha, N. (2009). Stress granules. *Current Biology* 19, R397-398.
- Antonny, B., Madden, D., Hamamoto, S., Orci, L., and Schekman, R. (2001). Dynamics of the COPII coat with GTP and stable analogues. *Nature cell biology* 3, 531-537.
- Arai, T., Hasegawa, M., Akiyama, H., Ikeda, K., Nonaka, T., Mori, H., Mann, D., Tsuchiya, K., Yoshida, M., Hashizume, Y., et al. (2006). TDP-43 is a component of ubiquitin-positive tau-negative inclusions in frontotemporal lobar degeneration and amyotrophic lateral sclerosis. *Biochemical and biophysical research communications* 351, 602-611.
- Aulas, A., Fay, M.M., Lyons, S.M., Achorn, C.A., Kedersha, N., Anderson, P., and Ivanov, P. (2017). Stress-specific differences in assembly and composition of stress granules and related foci. *Journal of cell science* 130, 927-937.
- Bah, A., and Forman-Kay, J.D. (2016). Modulation of Intrinsically Disordered Protein Function by Post-translational Modifications. *Journal of biology chemistry* 291, 6696-6705.
- Baird, T.D., and Wek, R.C. (2012). Eukaryotic initiation factor 2 phosphorylation and translational control in metabolism. *Advances in nutrition* 3, 307-321.
- Banani, S.F., Lee, H.O., Hyman, A.A., and Rosen, M.K. (2017). Biomolecular condensates: organizers of cellular biochemistry. *Nature reviews Molecular cell biology* 18, 285-298.
- Bannykh, S.I., Rowe, T., and Balch, W.E. (1996). The organization of endoplasmic reticulum export complexes. *Journal of cell biology* 135, 19-35.
- Barlowe, C. (2015). Membrane trafficking: ER export encounters dualism. *Current biology* 25, R151-153.
- Barlowe, C., Orci, L., Yeung, T., Hosobuchi, M., Hamamoto, S., Salama, N., Rexach, M.F., Ravazzola, M., Amherdt, M., and Schekman, R. (1994). COPII: a membrane coat formed by Sec proteins that drive vesicle budding from the endoplasmic reticulum. *Cell* 77, 895-907.
- Barlowe, C., and Schekman, R. (1993). SEC12 encodes a guanine-nucleotide-exchange factor essential for transport vesicle budding from the ER. *Nature* 365, 347-349.
- Bharucha, N., Liu, Y., Papanikou, E., McMahon, C., Esaki, M., Jeffrey, P.D., Hughson, F.M., and Glick, B.S. (2013). Sec16 influences transitional ER sites by regulating rather than organizing COPII. *Molecular biology of the cell* 24, 3406-3419.
- Bhattacharyya, D., and Glick, B.S. (2007). Two mammalian Sec16 homologues have nonredundant functions in endoplasmic reticulum (ER) export and transitional ER organization. *Molecular biology of the cell* 18, 839-849.
- Blobel, G., and Dobberstein, B. (1975). Transfer of proteins across membranes. I. Presence of proteolytically processed and unprocessed nascent immunoglobulin light chains on membrane-bound ribosomes of murine myeloma. *Journal of cell biology* 67, 835-851.
- Boyce, M., and Yuan, J. (2006). Cellular response to endoplasmic reticulum stress: a matter of life or

- death. *Cell Death & Differentiation* 13, 363-373.
- Brangwynne, C.P., Eckmann, C.R., Courson, D.S., Rybarska, A., Hoege, C., Gharakhani, J., Julicher, F., and Hyman, A.A. (2009). Germline P granules are liquid droplets that localize by controlled dissolution/condensation. *Science* 324, 1729-1732.
- Brown, M.S., Ye, J., Rawson, R.B., and Goldstein, J.L. (2000). Regulated Intramembrane Proteolysis. *Cell* 100, 391-398.
- Buchan, J.R., and Parker, R. (2009). Eukaryotic stress granules: the ins and outs of translation. *Molecular cell* 36, 932-941.
- Castelli, V., Benedetti, E., Antonosante, A., Catanesi, M., Pitari, G., Ippoliti, R., Cimini, A., and d'Angelo, M. (2019). Neuronal Cells Rearrangement During Aging and Neurodegenerative Disease: Metabolism, Oxidative Stress and Organelles Dynamic. *Frontiers in molecular neuroscience* 12, 132.
- Chong, P.A., and Forman-Kay, J.D. (2016). Liquid-liquid phase separation in cellular signaling systems. *Current Opinion in Structural Biology* 41, 180-186.
- Coletta, A., Pinney, J.W., Solis, D.Y., Marsh, J., Pettifer, S.R., and Attwood, T.K. (2010). Low-complexity regions within protein sequences have position-dependent roles. *BMC systems biology* 4, 43.
- Connerly, P.L., Esaki, M., Montegna, E.A., Strongin, D.E., Levi, S., Soderholm, J., and Glick, B.S. (2005). Sec16 is a determinant of transitional ER organization. *Current biology : CB* 15, 1439-1447.
- d'Enfert, C., Wuestehube, L.J., Lila, T., and Schekman, R. (1991). Sec12p-dependent membrane binding of the small GTP-binding protein Sar1p promotes formation of transport vesicles from the ER. *Journal of cell biology* 114, 663-670.
- Dancourt, J., and Barlowe, C. (2010). Protein sorting receptors in the early secretory pathway. *Annual review of biochemistry* 79, 777-802.
- Das, S., Pal, U., Das, S., Bagga, K., Roy, A., Mrigwani, A., and Maiti, N.C. (2014). Sequence complexity of amyloidogenic regions in intrinsically disordered human proteins. *PloS one* 9, e89781.
- Dmitrieva, N.I., and Burg, M.B. (2007). High NaCl promotes cellular senescence. *Cell Cycle* 6, 3108-3113.
- Donnelly, N., Gorman, A.M., Gupta, S., and Samali, A. (2013). The eIF2alpha kinases: their structures and functions. *Cellular and molecular life sciences* 70, 3493-3511.
- Dupuis, L., Gonzalez de Aguilar, J.L., Oudart, H., de Tapia, M., Barbeito, L., and Loeffler, J.P. (2004). Mitochondria in amyotrophic lateral sclerosis: a trigger and a target. *Neurodegenerative diseases* 1, 245-254.
- DuRose, J.B., Scheuner, D., Kaufman, R.J., Rothblum, L.I., and Niwa, M. (2009). Phosphorylation of eukaryotic translation initiation factor 2alpha coordinates rRNA transcription and translation inhibition during endoplasmic reticulum stress. *Molecular and cellular biology* 29, 4295-4307.
- Ellgaard, L., Molinari, M., and Helenius, A. (1999). Setting the standards: quality control in the secretory pathway. *Science* 286, 7.
- Espenshade, P., Gimeno, R.E., Holzmacher, E., Teung, P., and Kaiser, C.A. (1995). Yeast SEC16 gene encodes a multidomain vesicle coat protein that interacts with Sec23p. *Journal of cell biology* 131, 311-324.
- Fullekrug, J., and Nilsson, T. (1998). Protein sorting in the Golgi complex. *Biochimica et biophysica acta-molecular cell research* 1404, 77-84.
- Gardner, B.M., Pincus, D., Gotthardt, K., Gallagher, C.M., and Walter, P. (2013). Endoplasmic reticulum stress sensing in the unfolded protein response. *Cold Spring Harbor perspectives in biology* 5,

---

a013169.

Gimeno, R.E., Espenshade, P., and Kaiser, C.A. (1996). COPII coat subunit interactions: Sec24p and Sec23p bind to adjacent regions of Sec16p. *Molecular biology of the cell* 7, 1815-1823.

Gomes, E., and Shorter, J. (2018). The molecular language of membraneless organelles. *Journal of Biological Chemistry* 294, 7115-7127.

Gorlach, A., Bertram, K., Hudecova, S., and Krizanova, O. (2015a). Calcium and ROS: A mutual interplay. *Redox biology* 6, 260-271.

Gorlach, A., Dimova, E.Y., Petry, A., Martinez-Ruiz, A., Hernansanz-Agustin, P., Rolo, A.P., Palmeira, C.M., and Kietzmann, T. (2015b). Reactive oxygen species, nutrition, hypoxia and diseases: Problems solved? *Redox biology* 6, 372-385.

Harding, H.P., Novoa, I., Zhang, Y., Zeng, H., Wek, R., Schapira, M., and Ron, D. (2000a). Regulated translation initiation controls stress-induced gene expression in mammalian cells. *Molecular cell* 6, 1099-1108.

Harding, H.P., Zhang, Y., Bertolotti, A., Zeng, H., and Ron, D. (2000b). Perk is essential for translational regulation and cell survival during the unfolded protein response. *Molecular cell* 5, 897-904.

Harding, H.P., Zhang, Y., and Ron, D. (1999). Protein translation and folding are coupled by an endoplasmic-reticulum-resident kinase. *Nature* 397, 271-274.

Haynes, V., Elfering, S., Squires, R., Traaseth, N., Solien, J., Ettl, A., and Giulivi, C. (2003). Mitochondrial Nitric-oxide Synthase: Role in Pathophysiology. *IUBMB life* 55, 599-603.

Hetz, C. (2012). The unfolded protein response: controlling cell fate decisions under ER stress and beyond. *Nature reviews molecular cell biology* 13, 89-102.

Horstmann, H. (2002). Ultrastructural characterization of endoplasmic reticulum -- Golgi transport containers (EGTC). *Journal of cell science* 115, 4263-4273.

Hyman, A.A., Weber, C.A., and Julicher, F. (2014). Liquid-liquid phase separation in biology. *Annual review of cell and developmental biology* 30, 39-58.

Ivan, V., de Voer, G., Xanthakis, D., Spoorendonk, K.M., Kondylis, V., and Rabouille, C. (2008). Drosophila Sec16 mediates the biogenesis of tER sites upstream of Sar1 through an arginine-rich motif. *Molecular biology of the cell* 19, 4352-4365.

Jaitovich, A., and Bertorello, A.M. (2010). Intracellular sodium sensing: SIK1 network, hormone action and high blood pressure. *Biochimica et Biophysica Acta (BBA) - Molecular Basis of Disease* 1802, 1140-1149.

Jamieson, J.D., and Palade, G.E. (1968). Intracellular transport of secretory proteins in the pancreatic exocrine cell. IV. Metabolic requirements. *Journal of cell biology* 39, 589-603.

John, G.B., Shang, Y., Li, L., Renken, C., Mannella, C.A., Selker, J.M., Rangell, L., Bennett, M.J., and Zha, J. (2005). The mitochondrial inner membrane protein mitofilin controls cristae morphology. *Molecular biology of the cell* 16, 1543-1554.

Jones, N.L., Blasutig, I.M., Eremina, V., Ruston, J.M., Bladt, F., Li, H., Huang, H.L., Larose, L., Li, S.S.C., Takano, T., et al. (2006). Nck adaptor proteins link nephrin to the actin cytoskeleton of kidney podocytes. *Nature* 440, 818-823.

Kaplan, J.H. (2002). Biochemistry of Na,K-ATPase. *Annual review of biochemistry* 71, 511-535.

Kato, M., Yang, Y.-S., Sutter, B.M., Wang, Y., McKnight, S.L., and Tu, B.P. (2019). Redox State Controls Phase Separation of the Yeast Ataxin-2 Protein via Reversible Oxidation of Its Methionine-Rich Low-Complexity Domain. *Cell* 177, 711-721.e718.



- Kedersha, N., and Anderson, P. (2002). Stress granules: sites of mRNA triage that regulate mRNA stability and translatability. *Biochemical Society Transactions* 30, 963.
- Kedersha, N., Stoecklin, G., Ayodele, M., Yacono, P., Lykke-Andersen, J., Fritzler, M.J., Scheuner, D., Kaufman, R.J., Golan, D.E., and Anderson, P. (2005). Stress granules and processing bodies are dynamically linked sites of mRNP remodeling. *Journal of cell biology* 169, 871-884.
- Korennykh, A.V., Egea, P.F., Korostelev, A.A., Finer-Moore, J., Zhang, C., Shokat, K.M., Stroud, R.M., and Walter, P. (2009). The unfolded protein response signals through high-order assembly of Ire1. *Nature* 457, 687-693.
- Krause, K.-H. (1991). Ca<sup>2+</sup>-storage organelles. *FEBS Letters* 285, 5.
- Lee, M.C., Orci, L., Hamamoto, S., Futai, E., Ravazzola, M., and Schekman, R. (2005). Sar1p N-terminal helix initiates membrane curvature and completes the fission of a COPII vesicle. *Cell* 122, 605-617.
- Li, P., Banjade, S., Cheng, H.C., Kim, S., Chen, B., Guo, L., Llaguno, M., Hollingsworth, J.V., King, D.S., Banani, S.F., et al. (2012). Phase transitions in the assembly of multivalent signalling proteins. *Nature* 483, 336-340.
- Lin, J.H., Li, H., Yasumura, D., Cohen, H.R., Zhang, C., Panning, B., Shokat, K.M., Lavail, M.M., and Walter, P. (2007). IRE1 signaling affects cell fate during the unfolded protein response. *Science* 318, 944-949.
- Lippincott-Schwartz, J., Yuan, L.C., Bonifacino, J.S., and Klausner, R.D. (1989). Rapid redistribution of Golgi proteins into the ER in cells treated with brefeldin A: evidence for membrane cycling from Golgi to ER. *Cell* 56, 801-813.
- Luceri, C., Bigagli, E., Femia, A.P., Caderni, G., Giovannelli, L., and Lodovici, M. (2018). Aging related changes in circulating reactive oxygen species (ROS) and protein carbonyls are indicative of liver oxidative injury. *Toxicology reports* 5, 141-145.
- Mateju, D., Eichenberger, B., Voigt, F., Eglinger, J., Roth, G., and Chao, J.A. (2020). Single-Molecule Imaging Reveals Translation of mRNAs Localized to Stress Granules. *Cell* 183, 1801-1812.
- McInerney, G.M., Kedersha, N.L., Kaufman, R.J., Anderson, P., and Liljestrom, P. (2005). Importance of eIF2 $\alpha$  phosphorylation and stress granule assembly in alphavirus translation regulation. *Molecular biology of the cell* 16, 3753-3763.
- Miller, E., Antonny, B., Hamamoto, S., and Schekman, R. (2002). Cargo selection into COPII vesicles is driven by the Sec24p subunit. *The EMBO journal* 21, 6105-6113.
- Mori, K., Kawahara, T., Yoshida, H., Yanagi, H., and Yura, T. (1996). Signalling from endoplasmic reticulum to nucleus transcription factor with a basic-leucine zipper motif is required for the unfolded protein-response pathway. *Genes to Cells*, 15.
- Munro, S., and Pelham, H.R. (1987). A C-terminal signal prevents secretion of luminal ER proteins. *Cell* 48, 899-907.
- Nakano, A., and Muramatsu, M. (1989). A novel GTP-binding protein, Sar1p, is involved in transport from the endoplasmic reticulum to the Golgi apparatus. *Journal of cell biology* 109, 2677-2691.
- Nickel, W., Brugger, B., and Wieland, F.T. (1998). Protein and lipid sorting between the endoplasmic reticulum and the Golgi complex. *Seminars in cell & developmental biology* 9, 493-501.
- Nott, T.J., Petsalaki, E., Farber, P., Jervis, D., Fussner, E., Plochowitz, A., Craggs, T.D., Bazett-Jones, D.P., Pawson, T., Forman-Kay, J.D., et al. (2015). Phase transition of a disordered nuage protein generates environmentally responsive membraneless organelles. *Molecular cell* 57, 936-947.
- Novick, P., Ferro, S., and Schekman, R. (1981). Order of events in the yeast secretory pathway. *Cell*

---

25, 461-469.

Oka, T., Nishikawa, S., and Nakano, A. (1991). Reconstitution of GTP-binding Sar1 protein function in ER to Golgi transport. *Journal of cell biology* 114, 671-679.

Palade, G. (1975). Intracellular aspects of the process of protein synthesis. *Science* 189, 347-358.

Perraud, A.L., Takanishi, C.L., Shen, B., Kang, S., Smith, M.K., Schmitz, C., Knowles, H.M., Ferraris, D., Li, W., Zhang, J., et al. (2005). Accumulation of free ADP-ribose from mitochondria mediates oxidative stress-induced gating of TRPM2 cation channels. *Journal of biological chemistry* 280, 6138-6148.

PeterNovick., CharlesField., and RandySchekman. (1980). Identification of 23 complementation groups required for post-translational events in the yeast secretory pathway. *Cell* 21, 205-215.

Protter, D.S., and Parker, R. (2016). Principles and Properties of Stress Granules. *Trends in cell biology* 26, 668-679.

Ron, D., and Walter, P. (2007). Signal integration in the endoplasmic reticulum unfolded protein response. *Nature reviews molecular cell biology* 8, 519-529.

Rothman, J.E., and Wieland, F.T. (1996). Protein sorting by transport vesicles. *Science* 272, 227-234.

Schekman, R., and Orci, L. (1996). Coat proteins and vesicle budding. *Science* 271, 1526-1533.

Shamu, C.E., Cox, J.S., and Walter, P. (1994). The unfolded-protein-response pathway in yeast. *Trends in cell biology* 4, 56-60.

Sjöström., M., Stenström., K., Eneling., K., Zwiller., J., Katz., A.I., Takemori., H., and Bertorello., A.M. (2007). SIK1 is part of a cell sodium-sensing network that regulates active sodium transport through a calcium-dependent process. *PNAS* 104, 16922-16927.

Sprangers, J., and Rabouille, C. (2015). SEC16 in COPII coat dynamics at ER exit sites. *Biochemical Society transactions* 43, 97-103.

Stagg, S.M., LaPointe, P., Razvi, A., Gurkan, C., Potter, C.S., Carragher, B., and Balch, W.E. (2008). Structural basis for cargo regulation of COPII coat assembly. *Cell* 134, 474-484.

Supek, F., Madden, D.T., Hamamoto, S., Orci, L., and Schekman, R. (2002). Sec16p potentiates the action of COPII proteins to bud transport vesicles. *Journal of cell biology* 158, 1029-1038.

Trachootham, D., Lu, W., Ogasawara, M.A., Nilsa, R.D., and Huang, P. (2008). Redox regulation of cell survival. *Antioxidants & redox signaling* 10, 1343-1374.

Travers, K.J., Patil, C.K., Wodicka, L., Lockhart, D.J., Weissman, J.S., and Walter, P. (2000). Functional and genomic analyses reveal an essential coordination between the unfolded protein response and ER-associated degradation. *Cell* 101, 249-258.

van Leeuwen, W., and Rabouille, C. (2019). Cellular stress leads to the formation of membraneless stress assemblies in eukaryotic cells. *Traffic* 0.

Wang., Z., Takemori., H., Halder., S.K., Nonaka., Y., and Okamoto., M. (1999). Cloning of a novel kinase (SIK) of the SNF1/AMPK family from high salt diet-treated rat adrenal. *FEBS Letters* 453, 135-139.

Watson, P., Townley, A.K., Koka, P., Palmer, K.J., and Stephens, D.J. (2006). Sec16 defines endoplasmic reticulum exit sites and is required for secretory cargo export in mammalian cells. *Traffic* 7, 1678-1687.

Weber, S.C., and Brangwynne, C.P. (2012). Getting RNA and protein in phase. *Cell* 149, 1188-1191.

Wehr, M.C., Holder, M.V., Gailite, I., Saunders, R.E., Maile, T.M., Ciirdaeva, E., Instrell, R., Jiang, M., Howell, M., Rossner, M.J., et al. (2013). Salt-inducible kinases regulate growth through the Hippo signalling pathway in *Drosophila*. *Nature cell biology* 15, 61-71.

Whittle, J.R., and Schwartz, T.U. (2010). Structure of the Sec13-Sec16 edge element, a template for

assembly of the COPII vesicle coat. *Journal of cell biology* 190, 347-361.

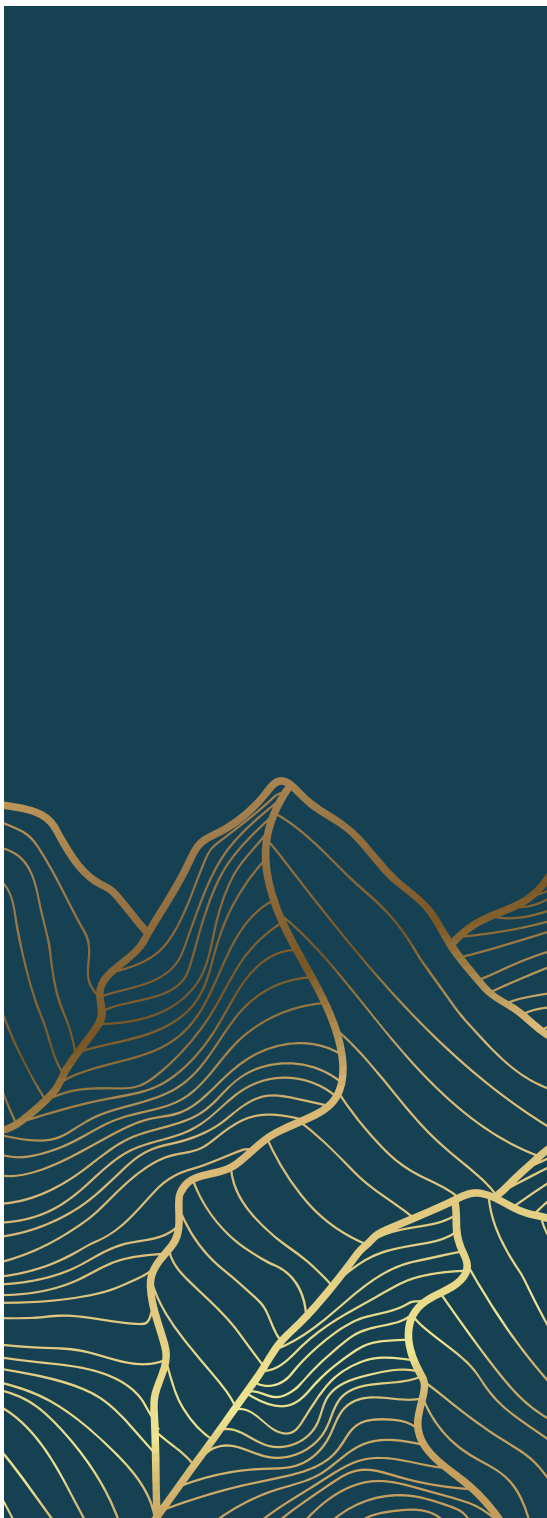
Ye., J., Rawson., R.B., Komuro., R., Chen., X., Davé., U.P., Prywes., R., Brown., M.S., and Goldstein., J.L. (2000). ER Stress Induces Cleavage of Membrane-Bound ATF6 by the Same Proteases that Process SREBPs. *Molecular cell* 6, 10.

Yorimitsu, T., and Sato, K. (2012). Insights into structural and regulatory roles of Sec16 in COPII vesicle formation at ER exit sites. *Molecular biology of the cell* 23, 2930-2942.

Zacharogianni, M., Aguilera-Gomez, A., Veenendaal, T., Smout, J., and Rabouille, C. (2014). A stress assembly that confers cell viability by preserving ERES components during amino-acid starvation. *eLife* 3.

Zatti, A., Chauvet, V., Rajendran, V., Kimura, T., Pagel, P., and Caplan, M.J. (2005). The C-terminal tail of the polycystin-1 protein interacts with the Na,K-ATPase alpha-subunit. *Molecular biology of the cell* 16, 5087-5093.

Zhang, C., and Rabouille, C. (2019). Membrane-Bound Meet Membraneless in Health and Disease. *Cells* 8.



## *Chapter2*

# *Membrane-Bound Meet Membraneless in Health and Disease*

Chujun Zhang and Catherine Rabouille (2019)  
Cells 2019

---

## *Membrane-bound meet membraneless in health and disease*

### *Abstract*

Membraneless organelles (MLOs) are defined as cellular structures that are not sealed by a lipidic membrane and are shown to form by phase separation. They exist in both the nucleus and the cytoplasm that is also heavily populated by numerous membrane-bound organelles. Even though the name membraneless suggests that MLOs are free of membrane, both membrane and factors regulating membrane trafficking steps are emerging as important components of MLO formation and function. As a result, we name them biocondensates. In this review, we examine the relationships between biocondensates and membrane. First, inhibition of membrane trafficking in the early secretory pathway leads to the formation of biocondensates (P-bodies and Sec bodies). In the same vein, stress granules have a complex relationship with the cyto-nuclear transport machinery. Second, membrane contributes to the regulated formation of phase separation in the cells and we will present examples including clustering at the plasma membrane and at the synapse. Finally, the whole cell appears to transit from an interphase phase-separated state to a mitotic diffuse state in a DYRK3 dependent manner. This firmly establishes a crosstalk between the two types of cell organization that will need to be further explored.

### *Introduction*

Cell compartmentalization has been largely defined by the formation and maintenance of membrane-bound organelles, such as those displayed in the compartments of the secretory pathway, the endosomal-lysosomal pathway, the mitochondria, the peroxisomes, and the lipid droplets. Each sustains specific functions and biochemical reactions. However, this has recently been complexified by the discovery of membrane-contact sites between all these membrane-bound compartments through which lipids and ions traffic (Scorrano et al., 2019), as well as by the (re-)discovery of the so-called membraneless organelles (MLOs) (Forman-Kay et al., 2018).

MLOs define a class of compartments that are not membrane-bound, i.e., not surrounded by a sealed phospholipid membrane. They are formed by phase separation either liquid-liquid or liquid-solid (Gomes and Shorter, 2018). Phase separation defines the behavior of a homogeneous solution of dispersed macromolecules that segregate into two distinct phases either liquid or solid/gel/fibrillar. The differences in the material properties of the separated phases can be distinguished by FRAP (Fluorescence Recovery After Photobleaching). In the case of liquid droplets, bleaching half of the structure would result

in a quick recovery through the efficient movement of the non-bleached molecules to the bleached area within the droplet. This is the case for P granules (reviewed in (Marnik and Updike, 2019)), P-bodies, stress granules (Patel et al., 2015) and Sec bodies (Zacharogianni et al., 2014). When the structure is solid and crystalline, the recovery does not occur as the molecules within the structure are immobile. For instance, metabolic enzyme foci that form in starved yeast are solid (Petrovska et al., 2014). Note that in this case, these material properties do not affect their reversibility. However, stress granules tend to transit from liquid droplets to solid entities, and this transition is accompanied by their irreversibility (Molliex et al., 2015; Patel et al., 2015), a feature that is proposed to coincide with the onset of neurodegenerative diseases.

Phase separation is driven by “driver/scaffold” proteins (Banani et al., 2016) that are essential and sufficient to drive phase separation and formation of MLOs. When they are absent, these compartments are not formed or are not stable. Drivers coalesce and attract other proteins or macromolecules with which they normally interact. Drivers engage in multivalency, i.e., in low affinity multivalent interactions (Banani et al., 2016). They often contain domains of intrinsically disordered regions that contain repeating sequences or high frequency of the same amino-acid, such as proline, arginine, glutamine that can interact with Other amino acids such as tyrosines (Ruff et al., 2019). The interactions involved in liquid phase separation are electrostatic but also cation/pi as well as pi/pi (Vernon et al., 2018). Overall, phase separation results in the formation of low affinity coalescence containing proteins and often (but not always) Ribonucleic acids (RNAs). These condensates are also referred to “quinary structures” in which the abundance of components is not entirely defined and may vary (Kroschwald and Alberti, 2017). As such, they are different from the ribosome or the proteasome, which are complexes with a fixed subunit stoichiometry (Alberti, 2017). Last, as membrane-bound organelles, MLOs also sustain specific biochemistries. For instance, the RNA-binding protein Otu was shown to form MLOs that exhibit deubiquitination activity. Notably, this enzymatic activity only emerges when Otu coalesces, not as monomers (Ji et al., 2019). Other examples of signaling regulated by MLOs is available in (Chong and Forman-Kay, 2016).

MLOs exist both in the cell nucleoplasm and in the cytoplasm, in basal steady state conditions (such as the nucleolus, nuclear speckles, centrosome, P granules in *C.elegans* (Marnik and Updike, 2019), germ granules in *Drosophila* (Trcek and Lehmann, 2019), the plant pyrenoid (Wunder et al., 2019), and neuronal RNA granules (Formicola et al., 2019)). MLOs also formed upon cellular stress, among which the best studied are the P-bodies and stress granules (recently reviewed in (van Leeuwen and Rabouille, 2019)).

---

However, the name “membraneless organelles” is misleading because, although they are not sealed by a membrane, they are not devoid of interaction with membrane. First, the formation of some MLOs is related to inhibition/modulation of specific membrane transport steps in the early secretory pathway (**Appendix A**). They are also related to the cyto-nuclear transport (**Appendix B**). In this regard, some MLOs may incorporate proteins that normally function in these trafficking steps (part 1 and 2). Second, some MLOs form and are located near a membrane, and membrane can enhance their coalescence (part 3). Last, the entire cell is now proposed to transit from a phase-separated state in interphase to a dispersed state in mitosis (part 4).

Here, we will review what is known of the link/interface between MLOs, membrane, membrane traffic, and its components. However, because this review will illustrate that the term MLOs is not appropriate, we will not use it further (although we keep it in the title). Instead we will use the term “phase-separated biocondensates” when they occur in basal conditions and “stress assemblies” when they are triggered by cellular stress.

## *1 Stress Assemblies and the Inhibition of Trafficking in the Early Secretory Pathway*

### *1.1 P-Bodies Form in Yeast Mutant for Secretory Pathway Components*

P-bodies are submicron dynamic cytoplasmic stress assemblies comprising translationally inactive mRNAs and proteins that are normally associated with translation repression, mRNA turnover such as 30-deadenylation, 50-decapping, 50-30 exonuclease activity, nonsense mediated decay, and miRNA-targeted gene silencing in all eukaryotic cells so far examined (Parker and Sheth, 2007). Mammalian P-bodies are characterized by the presence of AGO1/3, DCP2, EDC3 among many other protein (Guzikowski et al., 2019; Hubstenberger et al., 2017) whereas Dcp1p, Dcp2p, Edc3p mark the yeast P-bodies (Teixeira and Parker, 2007). In yeast, P-bodies are only visible where they are stressed for instance by oxidative stress, endoplasmic reticulum (ER) stress, osmotic shock, glucose starvation (Buchan et al., 2008; Wang et al., 2018a). In mammalian cells, P-bodies are visible as small microscopic entities even in the absence of stress (reflecting RNA degradation needed for cell homeostasis), but stress triggers their enlargement (Souquere et al., 2009). Given their concentration in RNA decay factors, P-bodies have been proposed to be the site of mRNA degradation and turnover, but it appears that they are more involved in RNA storage without degradation (Horvathova et al., 2017; Hubstenberger et al., 2017). The contradictory presence of intact mRNAs and RNA decay factors in P-bodies is puzzling but



may reflect protection of the mRNAs by specific RNA-binding proteins and translational repressors that inhibit degradation.

With their proposed role in RNA biology, P-bodies are not intuitively linked to membrane and membrane trac. Yet, a first link has been made with the discovery that in the yeast thermosensitive mutant *arf1-11* (Yahara et al., 2001), the P-body number increases even at normal growth temperature, a phenotype that is referred to, as the “multiple P-body phenotype” (Kilchert et al., 2010). This phenotype is even more pronounced upon stress by heat shock (Kilchert et al., 2010). Arf1 (ADP-ribosylation factor 1) is a small GTPase that plays an important role in vesicular trafficking especially in the Golgi where it appears characteristically concentrated. Indeed, Arf1 activation is the first step in the assembly Coatamer complex I coat (COPI) that mediates the retrograde transport from the Golgi to the ER (Aguilera-Gomez and Rabouille, 2016). At the Golgi, Arf1 also modulates the activity of phospholipase D (Jackson and Bouvet, 2014). In addition, Arf1 is proposed to have novel and conserved roles in the morphological and functional maintenance of mitochondria (Ackema et al., 2014; Walch et al., 2018).

As mentioned above, P-bodies are hardly visible in wildtype yeast in growing conditions, but their number increased in growing *arf1* mutants. This increase is strikingly strong because neither starvation nor oxidative/redox stress leads to such an increase in wildtype yeast. Interestingly, the multiple P-body phenotype is not specific for *arf1* mutant. It is also observed in other secretory mutants (Kilchert et al., 2010), suggesting that this phenotype is most likely related to a general defect in secretion. Of note, it is unrelated to the activation of the unfolded protein response (Kilchert et al., 2010).

In yeast, the secretory pathway is massively used for the transport and secretion of the components of the cell wall that is important to protect cells from osmotic shock. Accordingly, *arf1* and other secretory yeast mutants are more sensitive to osmotic stress. When treated with high salt, P-body formation increased further. However, this is specific to salt and not to glycerol, suggesting that this phenotype is not downstream of osmotic stress per se, but is related to salt stress.

Salt stress can lead to a transient increase in intracellular calcium (Batiza et al., 1996; Matsumoto et al., 2002). Accordingly, adding  $\text{CaCl}_2$  (but not  $\text{MgCl}_2$ ) to the medium induces the multiple P-body phenotype in wildtype cells. Furthermore, treatment of *arf1* mutants with the calcium chelating agent BAPTA (1,2-bis(o-aminophenoxy)ethane-N, N, N', N'-tetraacetic acid) results in the reduction of the number of P-bodies that form in this

---

mutant. Taken together, the multiple P-body phenotype observed in secretory mutants is largely dependent on a change in intracellular calcium. In line with it, Calmodulin, a major player in calcium signaling is required for this phenotype. However, it is required only for the multiple P-body phenotype observed in secretory mutants, not when this phenotype is induced by other stresses (Kilchert et al., 2010) (**Figure 1A**).

This suggests that P-body formation can be induced by differential signaling pathways. Specific P-body components could therefore be required for P-body formation upon one stress but not another. In this regard, Pat1 (that contains an EF-hand, which might coordinate a calcium) and Scd6 (an Sm-like protein most likely involved in the regulation of mRNA translation and/or degradation in PBs (Decker and Parker, 2012)) are both required for P-body formation in secretory mutants, but do not play a role in their formation upon glucose starvation (Kilchert et al., 2010).

How the inhibition of the early secretory pathway triggers calcium imbalance in the cytoplasm that leads to the formation of P-bodies (related to RNA mutant homeostasis) remain to be further investigated, especially if it does not trigger ER stress. This opens interesting avenues to integrate membrane traffic and the formation of phase-separated biocondensates.

### *1.2 Sec body Formation and the ER Exit Sites (ERES)*

In the previous section, yeast mutants inhibiting the function of the early secretory pathway displayed an increase in their cytoplasmic calcium resulting in P-body formation. Here, we address how nutrient stress modulates the early secretory pathway (**Appendix A**) leading to the phase separation of ERES components into a different organelle, the stress assembly named Sec bodies.

Amino-acid starvation of *Drosophila* S2 cells leads to inhibition of protein transport out of the ER (Zacharogianni et al., 2014). This is also the case in mammalian cells, at least when measured with the Sec-luciferase reporter (Aguilera-Gomez et al., 2017). In S2 cells, this stress also leads to the coalescence/condensation of Sec bodies (Zacharogianni et al., 2014). Although Sec body composition is still not firmly established despite the analysis by mass spectrometry (Aguilera-Gomez et al., 2017), they definitely contain ERES components, Sec16, and COPII subunits Sec23, Sec24, and Sec31. In other words, they contain components related to the trafficking step that is inhibited. Of note, Sec bodies, unlike P-bodies are not RNA-based.

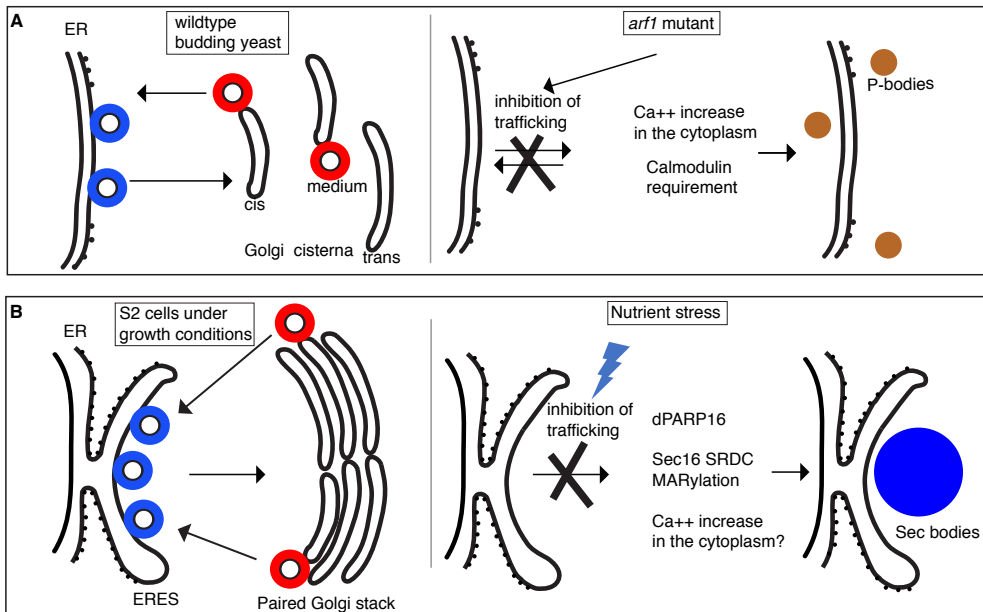


**Figure 1. Stress assemblies and the inhibition of tracking in the early secretory pathway.** In growing conditions, COPII (Coatamer complex II) coated vesicles (blue) bud from ER (budding yeast) and ER Exit Sites (ERES) (Drosophila S2 cells) whereas COPI (Coatamer complex I) coated vesicles (red) bud from the Golgi. **(A)**: In yeast, a subset of secretory transport mutants causes inhibition of tracking in the early secretory pathway and leads to the formation of multiple P-bodies. These mutants are more sensitive to salt leading to an increase of calcium in the cytoplasm and triggering the formation of specific P-bodies containing Pat1 and Scd6 in a calmodulin dependent manner. **(B)**: In Drosophila S2 cells, the nutrient stress of amino acid starvation also inhibits protein transport in the early secretory pathway and leads to the formation of Sec bodies. Amino-acid starvation appears to lead to dPARP16 activation that MARYlates the Sec16 SRDC (Serum Responsive Domain Conserved) leading to Sec body formation. Whether  $\text{Ca}^{++}$  imbalance is also important remains to be established.

Sec bodies have a diameter between 0.6–0.8  $\mu\text{m}$  and they were shown by electron microscopy to not be sealed by a membrane although they are often close to ER. This agrees with the fact that they form at the ER cup marking the ERES in non-stressed cells. Two lines of evidence suggest this. First, live cell imaging reveals that out of the 15–20 ERES in growing cells, only a couple are “selected” and will form Sec bodies, while the other disappear. The model is that the selected ERES will be remodeled into nascent Sec bodies while the ERES components of the other ERES are released and recaptured by the growing Sec bodies. Second, marking the ER cup with a form of Sec16 that only contains the domain that targets it to ERES (Ivan et al., 2008) but that is not incorporated in Sec

---

bodies (Zacharogianni et al., 2014), clearly showed that Sec bodies form very close to the ER cup, even though they can later be displaced. This suggests that Sec bodies initially form where ERES were present.

Sec bodies have the material properties compatible with being a liquid droplet. FRAP experiment of a small part of the structure showed a relatively fast recovery, emphasizing that this condensate is not an aggregate. Sec bodies also reversible very quickly upon amino-acid addition. Sec16 and COPII subunits form functional ERES upon addition of amino-acids after the starvation and they also appear protected against degradation during the starvation period (Zacharogianni et al., 2014). Last, Sec bodies are pro-survival during the period of stress and upon stress relief as many nutrient stress assemblies are (reviewed in (van Leeuwen and Rabouille, 2019)).

Given that they incorporate COPII coat subunits (although not Sar1, and not COPI coat components), the role of trafficking in the early secretory pathway in their formation has been investigated. However, neither Sar1 depletion that leads to a reduction in the COPII coated vesicle formation nor treatment with Brefeldin A (BFA) that blocks COPI coated vesicle formation affects Sec body formation. This supports the notion that that protein transport in COPI and COPII coated vesicles is not necessary for Sec body formation (Zacharogianni et al., 2014).

What is? As mentioned in the introduction, drivers in the phase separation into liquid droplets are known to be components displaying low complexity sequences with intrinsically disordered domains, such as those found in RNA-binding proteins (see part 2). Interestingly, the ERES components mentioned above, Sec16 and the two Sec24 isoforms in *Drosophila* (Sec24AB and CD) display a higher content of low complexity sequences when compared to the overall *Drosophila* proteome (Zacharogianni et al., 2014). Accordingly, depletion of Sec24AB (but not of Sec24 CD) (Zacharogianni et al., 2014) and Sec16 (Aguilera-Gomez et al., 2016) reduces Sec body formation. The low complexity sequences of Sec24AB are clustered at its N-terminus. When those are tagged with the Green Fluorescent Protein (GFP), they can recruit GFP to Sec bodies, suggesting that they are sufficient to mediate this recruitment. For Sec16, the situation is more complex as only the central conserved domain of the protein is folded, the rest being largely intrinsically disordered. A domain of 140 amino acids at the C-terminus of the protein has been shown to be required for Sec body formation (Zacharogianni et al., 2014). Within this region, a smaller conserved domain of 44 amino acids (that we named SRDC for Serum Responsive Domain Conserved) appears to play a major role in Sec body formation. First, a full-length

version of Sec16 deleted of this domain does not support Sec body formation. Second, overexpression of SRDC in the absence of stress leads to Sec body formation even if it is not itself recruited to Sec bodies (Di Paola et al., 2012). The mechanism behind this finding is still lacking. One tentative explanation is that this peptide displaces Sec16 from the ERES by competing its interaction with COPII subunits. This is however unlikely as Sec16 without this domain still localizes to ERES (Aguilera-Gomez et al., 2016) and that overexpression of full-length Sec16 does not lead to ectopic Sec body formation (unpublished). We propose instead that upon stress Sec16 changes slightly its conformation and exposes its SRDC that becomes a clear cis acting factor in Sec body formation. Overexpression of this domain could somehow mimic or induce this change in conformation.

2

The change in conformation could be triggered by post-translation modifications. In this regard, *Drosophila* PARP16 appears to play a key role in Sec body formation. Human PARP16 is a mono ADP-ribosylation (MARylation) enzyme (Di Paola et al., 2012; Jwa and Chang, 2012) suggesting that dPARP16 has the same activity even though the catalytic site of the *Drosophila* enzyme is not entirely conserved. Depletion of dPARP16 prevents their formation and its overexpression in growing cells leads to their ectopic formation. Critically, the depletion of dPARP16 in S2 cells increased the sensitivity to amino-acid starvation and the cells do not recover after stress relief. Interestingly, dPARP16 appears to MARylate SRDC, adding a large pi contribution to its interaction. Overexpression of SRDC in dPARP16 depleted cells does not result in Sec body formation (Aguilera-Gomez et al., 2016). This suggested that the MARylation of SRDC in a dPARP16 dependent manner is necessary and sufficient for Sec body formation. How does amino-acid starvation activate dPARP16 remains to be established.

Taken together, these two examples show that inhibition of the early secretory pathway leads to the formation of stress assemblies. Whether the pathways are the same in both cases needs to be further defined. For instance, it will be interesting to also establish if calcium plays a key role in Sec body formation as it does for P-bodies.

What is remarkable in the case of Sec bodies is that the driver for their formation is a protein (Sec16) that organizes the step that is inhibited (optimal formation of COPII coated vesicles at ERES) (Sprangers and Rabouille, 2015). The formation of Sec bodies in turn acts as a protection again Sec16 (and COPII subunits) degradation. This opens the possibility that inhibition or activation of membrane traffic steps (for instance in the endocytic pathway) triggers the formation of other condensates to be discovered. Why not imagine that inhibition of endocytosis leads to clathrin-based condensate that would also serve as a protective reservoir?

---

## *2 The Complex Relationship between Stress Granules, Cyto-Nuclear Transport, and Amyotrophic Lateral Sclerosis (ALS)*

### *2.1 Stress Granules*

Stress granules are also submicron stress assemblies that form in eukaryotic cells upon many cellular stresses as long as they induce inhibition of translation initiation and polysome disassembly. This leads to an accumulation of untranslated, 80S ribosome-free mRNAs in the cytoplasm that can bind RNA-binding proteins that phase separate into membraneless compartments, the stress granules (Anderson and Kedersha, 2002). They often form adjacent to, or overlapping with, P-bodies, yet their two functions appear distinct. Stress granules have been proposed to act as triage centers for mRNAs (Anderson and Kedersha, 2008) protecting capped and polyadenylated mRNAs from degradation in P-bodies (Protter and Parker, 2016). Stress granules would then store these protected mRNAs in such a way that they can be immediately translated upon stress relief (Anderson and Kedersha, 2009; Buchan and Parker, 2009; Protter and Parker, 2016).

As Sec bodies, Stress granules are rapidly reversible upon stress relief and they are pro-survival. Indeed, cells that do not form stress granules survive less well during stress and thrive less upon stress relief (recently reviewed in (van Leeuwen and Rabouille, 2019)).

### *2.2 Stress Granules and ALS: A Role for FUS, TDP43, and C9orf72*

There is a solid relationship between stress granules and ALS (and frontotemporal dementia). ALS is a disease characterized by the degeneration of motor neurons and ultimately neuronal death leading to muscle weakness. Genetically, ALS can be linked to mutations in RNA-binding proteins, such as Ataxin2, Fused in Sarcoma (FUS), TAR DNA-binding protein 43 (TDP43), and C9orf72 (the latter accounting for 40% of familial forms of ALS).

The pathological hallmark of ALS is the presence of inclusion bodies (i.e., abnormal aggregations of proteins) in the cytoplasm of motor neurons. In about 97% of people with ALS, the main component of the inclusion bodies is TDP-43 protein (Scotter et al., 2015) except in the case of FUS mutations where the main component of these inclusions is FUS itself (Birsá et al., 2019; Scotter et al., 2015).

FUS and TPD43 are both RNA-binding proteins containing prion-like domains that

are intrinsically disordered and prone to “coalescence”. For wildtype purified FUS (Murray et al., 2017; Patel et al., 2015; Scotter et al., 2015) and TDP43 in vitro, this coalescence corresponds to a phase separation into liquid droplets (Guo et al., 2018; Maharana et al., 2018; Patel et al., 2015). This is driven either by cation- $\pi$  interactions including those between tyrosine residues present in the prion-like domain and arginine present in the RNA-binding domain (Wang et al., 2018b) or through LARK (low-complexity, aromatic-rich, kinked segments) interactions (Hughes et al., 2018) (reviewed in (Gomes and Shorter, 2018)). In cells, wildtype FUS localizes to stress granules that are formed upon oxidative stress (such as arsenite treatment) at least in mammalian cultured cells (Patel et al., 2015). Conversely, mutated FUS and TDP43 in vitro also phase separate, but in assemblies that become increasingly solid, fibrillar, and irreversible with time. In vivo, when mutated FUS and TDP43 proteins are expressed at the same time as stress granules form (for instance upon oxidative stress that is shown to probably be, at least partly, at the origin of the disease onset), they affect their dynamics. Stress granules are no longer liquid and no longer reversible.

There are two slightly different models explaining how mutated FUS and TDP43 mutations exert their deleterious effect on stress granules dynamics and material properties. Mutated FUS is still recruited to stress granules (as wildtype FUS), but it starts forming irreversible aggregates within the granules leading to modifications of their properties (Bowden and Dormann, 2016) (**Figure 2B**). TDP43 acts differently (**Figure 2B**). The recruitment of wildtype TDP43 to stress granules (that is mediated by a Tankyrase dependent mechanism (McGurk et al., 2018)) is proposed to prevent TDP43 phosphorylation. It appears that TDP43 phosphorylation is a key event leading to its pathological aggregation. In this regard, mutated TDP43 that is not recruited to stress granules is therefore prone to phosphorylation and consequently aggregate outside stress granules (McGurk et al., 2018). Despite the lack of overlap, stress granule dynamic is nevertheless affected, perhaps because TDP43 aggregates interfere with their ability to regulate the RNA targeting to them, or through signaling (Li et al., 2013) (**Figure 2B**).

The mutation of C9orf72 causing ALS consists on a hexanucleotide GGGGCC repeat expansion (Bigio, 2011). In healthy individuals, this hexanucleotide is typically present less than 20–30 times (Fong et al., 2012) but in ALS patients, it can be repeated more than a few hundred times (Khan et al., 2012). There are several theories about how C9orf72 GGGGCC repeat expansion causes ALS. It appears that the RNA transcribed from the C9orf72 gene containing the expansion is translated through a non-ATG initiated mechanism leading to the synthesis and accumulation of dipeptide repeat proteins that

can affect cellular homeostasis in multiple ways. One of them is that this accumulation compromises cyto-nuclear transport (Freibaum et al., 2015; Jovičić et al., 2015; Zhang et al., 2015). The second is that this dipeptide repeat proteins themselves phase separate/aggregates and impair stress-granule dynamics in such a way that they also become irreversible (Boeynaems et al., 2017).

The relationship between stress granules and cyto-nuclear transport is complex. Cyto-nuclear transport is mediated by nuclear transport receptors, including nuclear import receptors, NIRs that import cognate proteins to the nucleus (**Appendix B**). Certain NIRs do localize to stress granules and consequently, stress granule formation inhibits cyto-nuclear transport (**Figure 2A**). Conversely, NIRs can act as chaperones for RNA-binding proteins containing prion-like domains (such as FUS and TDP43) and prevents their deleterious aggregation that affect stress granule dynamics (**Figure 2B**). Below we review both bodies of evidences.

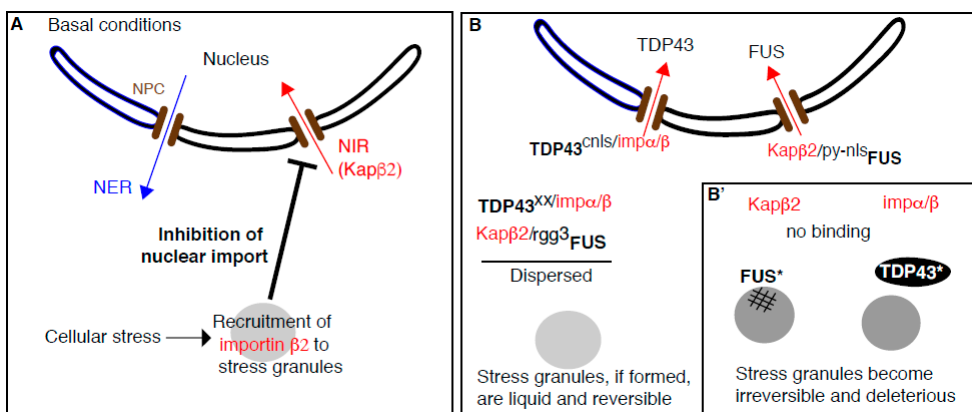


**Figure 2. The complex relationship between stress granules, cyto-nuclear transport and ALS. (A):** In basal growth conditions, the nuclear import receptor (NIR) Karyopherin β2 (Kapβ2) associates to its cognate cargoes and imports them to the nucleus through the nuclear pore complex (brown bars on the nuclear envelope). Upon cellular stress, Kapβ2 is recruited to stress granules and is no longer available to function as a receptor. As a result, stress granule formation triggered by cellular stress causes inhibition of cyto-nuclear transport. **(B):** The RNA-binding protein FUS and TDP43 are normally imported in the nucleus by binding to their cognate NIRs (Kapβ2 and Impα/β, respectively). The pool of FUS and TDP43 that is present in the cytoplasm remains dispersed through their binding to Kapβ2 and Impα/β, respectively but via other domains (such as FUS-rgg3). **(B'):** Upon cellular stress and/or expression of mutated FUS and TDP43 that prevent their binding to their NIRs, mutated FUS (FUS\*) and TDP43 (TDP43\*) aggregates in a deleterious manner but in two different ways. FUS\* is recruited to stress granules and aggregates within, leading stress granules to become solid and irreversible. On the other hand, TDP43\* aggregates on its own next to stress granules and negatively impact their dynamics via a mechanism that is still to be elucidated.



### *2.3 Stress Granules Assembly Negatively Regulates Cytoplasm to Nucleus Import*

The first observation that components of nuclear transport machinery localize to membraneless organelles was made in *C. elegans*. There, the nucleoporin NUP98 that localizes on the nucleoplasmic face of nuclear pore complexes also associates to the large cytoplasmic membraneless RNA-based P granules (Patterson et al., 2011). This observation was extended to stress granules where several nuclear transport receptors were shown to assemble to stress granules in mammalian HeLa cells treated by arsenite, diethyl maleate as well as in cells subjected to heat stress (Mahboubi et al., 2013). Interestingly, P-bodies are not targeted.

If indeed, nuclear transport receptors are present in, and recruited to, stress granules under conditions of cellular stress, it might ultimately inhibit the nuclear trafficking through the nuclear pore. This is exactly what was found for the NIR Karyopherin  $\beta 2$  (also called importin 2 and transportin 1) that also localizes to stress granules in arsenite treated cells (Zhang et al., 2018). This recruitment is concomitant with the strong inhibition of nuclear import as shown by using a Shuttle-tdTomato (with both a nuclear localization signal (NLS) and nuclear export signal (NES) flanking the tomato dDNA) that was found accumulating in the cytoplasm (Zhang et al., 2018) (**Figure 2A**).

Furthermore, as stress-granule dynamics have been linked to ALS pathology triggered by mutated C9orf72 and TDP43, the role of these mutations on nuclear transport was assessed. Accordingly, expression of the C9orf72 Dipeptide repeat proteins (Freibaum et al., 2015; Jovičić et al., 2015; Zhang et al., 2015) and mutated TDP43 (Gasset-Rosa et al., 2019) disrupt nucleocytoplasmic transport. Critically, the inhibition in nuclear transport is due to the formation of impaired stress granules that contain NIRs, such as Karyopherin  $\beta 2$ . Consequently, inhibiting stress granule assembly, for instance by depleting Ataxin 2, suppresses nucleocytoplasmic transport defects as well as neurodegeneration in C9ORF72-mediated ALS and Frontotemporal dementia (Zhang et al., 2018).

### *2.4 Beyond Nuclear Transport: NIRs Act as Chaperones to Prevent Stress-Granule-Related Pathological Aggregation in ALS (Figure 2B)*

As summarized above, certain nuclear transport receptors can be recruited to stress granules, the formation of which affects cyto-nuclear trafficking. What is also clearly shown is that NIRs has other functions that are independent of their role in nuclear import. Indeed, they act as cytoplasmic chaperones and promote the physiological dynamics of stress granules. Briefly, when FUS and TDP43 are bound to their cognate NIRs, they can enter the nucleus, and the pool that is present in the cytoplasm is dispersed. When FUS

---

and TDP43 can no longer bind their cognate NIRs (either because there are mutated or the level of NIRs is lower or mutated), they form irreversible aggregates that interfere with stress granule function, dynamics, and reversibility leading to the proteinopathy observed in ALS. Experimental evidences underlying this exciting new biology has been gathered both in vitro and in vivo by three independent groups in back-to-back articles (Guo et al., 2018; Hofweber et al., 2018; Yoshizawa et al., 2018) and we outline them below.

#### *2.4.1 Purifies FUS Phase Separation into Liquid Droplets is Specifically Inhibited by Karyopherin $\beta$ 2*

As reported above, purified FUS and hnRNPA1 phase separate in vitro into liquid droplets. Strikingly, addition of their cognate purified NIRs (i.e. Karyopherin  $\beta$ 2) (Zhang and Chook, 2012) efficiently prevent their phase separation (Guo et al., 2018; Hofweber et al., 2018; Yoshizawa et al., 2018). Furthermore, when added to preformed FUS and hnRNPA1 liquid droplets, Karyopherin  $\beta$ 2 also rapidly disperses them (Guo et al., 2018).

FUS phase separation is however not affected by adding NIRs that do not bind FUS, such as importin 5 (Hofweber et al., 2018) and Imp $\alpha/\beta$  (Yoshizawa et al., 2018). Kap121, a NIR that binds weakly to FUS only partially prevents FUS phase separation (Yoshizawa et al., 2018). This suggests that when NIRs have a low affinity for a cargo, they are not able to prevent their phase separation in vitro. Accordingly, FUS chimera harboring an NLS that is recognized by Imp  $\alpha/\beta$  phase separates and addition of purified Imp $\alpha/\beta$  then prevents it.

In vitro, many different RNA binding proteins such as FUS (as well as hnRNPA1, hnRNPA2, TAF15 and EWSR1) can be made to fibrillate, and addition of purified Karyopherin  $\beta$ 2 strongly inhibits this fibrillization. As above, addition of either a mutant Karyopherin  $\beta$ 2 that cannot bind its cargoes or the complex Imp $\alpha/\beta$  do not alter FUS fibrillation (Guo et al., 2018). Importantly, the effect of NIRs to chaperone RNA binding proteins and prevent their aggregation is not limited to Karyopherin  $\beta$ 2. Indeed, the fibrillization of TDP43 (TDP43<sup>Q331K</sup>) that is a cognate substrate for Imp $\alpha/\beta$  is prevented by addition of this specific NIR. As predicted, Karyopherin  $\beta$ 2 does not prevent seeded TDP43 fibrillization.

Taken together, the presence of Karyopherin  $\beta$ 2 and Imp $\alpha/\beta$  strongly reduces the in vitro phase separation/fibrillation of FUS and TDP43, respectively (**Figure 2B**).

#### *2.4.2 Does Karyopherin $\beta$ 2 Antagonize the Coalescence/Aggregation of FUS in Cellulo?*

Human FUS overexpressed in yeast mis-localizes to the cytoplasm and aggregates, as in neurodegenerative diseases (Couthouis et al., 2011). However, co-expression of human Karyopherin  $\beta 2$  prevents the formation of these aggregated foci and allows FUS to localize to the nucleus. In addition, FUS<sup>P525L</sup> and FUS<sup>R495X</sup> that cannot bind Karyopherin 2 remain aggregated and are not affected by the expression of Karyopherin  $\beta 2$ , validating the in vitro results (Guo et al., 2018).

In human stressed cells, endogenous FUS is recruited to stress granules upon cellular stress and elevating Karyopherin  $\beta 2$  expression inhibits this accumulation. This is independent from the role of Karyopherin  $\beta 2$  in nuclear import because Karyopherin  $\beta 2$  expression has the same effect on wildtype FUS and a FUS version deleted of its PY-NLS, the binding motif to Karyopherin  $\beta 2$  that is critical for nuclear import (Guo et al., 2018).

Additional evidence is provided by mammalian cells expressing a version of FUS that is not imported in the nucleus. It is maintained in a diffused state in cytoplasm because of the presence of Karyopherin  $\beta 2$ . When EGF-M9M (a peptide that inhibits Karyopherin  $\beta 2$  binding to its cargoes) is co-expressed, FUS localizes into stress granules. This further indicates that FUS binding to Karyopherin  $\beta 2$  prevents its recruitment to stress granules and therefore prevents its deleterious effect on their dynamics. Accordingly, when Karyopherin  $\beta 2$  is not present or prevented to bind FUS, FUS is efficiently recruited to stress granules (**Figure 2B**). Conversely, in cells expressing EGFP-biMax (a peptide that inhibits the binding of importin to its cargoes), cytoplasmic FUS remains diffuse because it does not affect its binding to Karyopherin  $\beta 2$  (Hofweber et al., 2018). This was further tested in a semi-intact cell system in which stress granules are first formed, followed by the cell permeabilization that washes out endogenous Karyopherin  $\beta 2$  and blocking the nuclear pores. When FUS is then added with purified Karyopherin  $\beta 2$ , its recruitment to stress granules is significantly reduced (Hofweber et al., 2018) (**Figure 2B**).

Taken together, Karyopherin  $\beta 2$  reduces FUS accumulation and aggregation in stress granules, thus preventing them to become dysfunctional and irreversible.

#### *2.4.3 Where Does Karyopherin $\beta 2$ Bind FUS to Prevent Their Condensation/Fibrilization?*

Karyopherin  $\beta 2$  binds stably the PY-NLS of FUS and this allows FUS import to the nucleus. Interestingly, PY-NLS is also critical for Karyopherin  $\beta 2$  to prevent FUS phase separation in vitro. As in cells (see above), the ability of Karyopherin  $\beta 2$  to prevent FUS phase separation is abolished by adding the inhibitory peptide M9M (Yoshizawa et al., 2018). However,

---

the binding domain of Karyopherin  $\beta 2$  to FUS is not restricted to the NLS and extends to other domains. In depth Nuclear Magnetic Resonance spectroscopy analysis reveals that Karyopherin  $\beta 2$  directly binds the RGG2 and RGG3 of FUS (Yoshizawa et al., 2018). Karyopherin  $\beta 2$  binding to the FUS RGG3-PY was confirmed independently (Hofweber et al., 2018). Importantly, this purified arginine rich domain (RGG3-PY) phase separates on its own, in agreement with (Chong et al., 2018), and addition of Karyopherin  $\beta 2$  suppresses it. Strikingly, both phase separation and binding to Karyopherin  $\beta 2$  is inhibited when these arginines are mutated to lysines (Hofweber et al., 2018).

The role of RGG3 in FUS phase separation properties was also examined in the context of full-length FUS. Indeed, deletion of the PY-NLS does not affect FUS liquid phase separation but mutating all arginine residues in RGG2 and RGG3 of full-length FUS to lysines strongly decreases phase separation, demonstrating a clear role of the RGG3 domain (Yoshizawa et al., 2018). In conclusion, Karyopherin  $\beta 2$  chaperones FUS through its binding the RGG3-PY domain to prevent its condensation.

#### *2.4.4 How Does This Relate to ALS and FTD? Could NIR be Used as A Treatment of ALS?*

FUS<sup>R495X</sup> and FUS<sup>P525L</sup> are two ALS-linked FUS variants which can cause aggressive juvenile ALS, and these two mutations reduce FUS binding to Karyopherin  $\beta 2$  (Hofweber et al., 2018; Zhang and Chook, 2012). In vivo Karyopherin  $\beta 2$  reduced FUS<sup>P525L</sup> aggregation by ~50% while having limited activity against FUS<sup>R495X</sup> (Guo et al., 2018). In vitro, both wildtype and mutated proteins phase separate but Karyopherin  $\beta 2$  only reduces the condensation of wildtype FUS, not this of mutant proteins (Hofweber et al., 2018). Thus, the presence of these mutations has similar effect as reducing the level of Karyopherin  $\beta 2$ , and results in irreversible aggregation.

As mentioned above, Karyopherin  $\beta 2$  can rapidly dissolve preformed FUS fibrils and hydrogel in vitro. In parallel, Imp $\alpha/\beta$  also leads to the disaggregation of TDP-43 and TDP-43<sup>Q331K</sup> fibrils. The effect of Karyopherin  $\beta 2$  in reverting pathological aggregates was tested in a Drosophila model for neurodegeneration. Elevating Karyopherin  $\beta 2$  rescues FUS-Linked Neurodegeneration and partially rescues the lifespan of the flies (Guo et al., 2018). This parallels the finding that elevated Karyopherin  $\beta 2$  also mitigates FUS<sup>R521H</sup>-mediated motor neuron degeneration in Drosophila (Daigle et al., 2012). This indicates that NIRs could be used to prevent prion-like spread of self-seeding aggregates during ALS as well as other neurodegenerative diseases (Guo et al., 2019).

Taken together, Karyopherin  $\beta 2$  appears to behave in two different manners regarding stress granules: On one hand, it is incorporated to stress granules resulting in the inhibition of cyto-nuclear import that is a hallmark of ALS. On the other hand, it acts as cytoplasmic chaperone for ALS related FUS, thus preventing its recruitment to stress granules. Note that Imp $\alpha/\beta$  similarly chaperones TDP43. In this case, TDP43 is prevented to aggregate next to stress granules and exert its deleterious effect at a distance. In both cases, the interaction between stress granules and NIRs is at the center of this disease, but in two opposite manners. In the first case, stress granule formation appears to promote the disease as they recruit NIRs and contribute to the inhibition of cyto-nuclear transport observed in C9orf72. In the second case, stress granules are protected by NIRs (that do not appear to localize with them) as they chaperone FUS and TDP43 and prevent these proteins to affect the dynamics and reversibility of stress granules. More work is of course needed to sort out the role of other NIRs.

### *3 Membrane Enhances the Formation of Phase-Separated Condensates*

#### *3.1 P-Body Formation is regulated by ER Proteins*

As mentioned above in the introduction, the term “membraneless” is not completely appropriate to define biological condensates that arise from phase separation in vivo. For instance, P-bodies that form in yeast are often localized in close proximity to ER membranes (Kilchert et al., 2010) in line with what has been observed in the oocyte *Drosophila* bodies that form around the ER membrane (Weil et al., 2012).

To identify ER proteins mediating the ER localization of P-bodies in yeast, and more generally to shed light on the relationship between ER and P-bodies, a deletion screen targeted to ER proteins was conducted in wildtype yeast in which P-bodies (marked by Dcp2 and Scd6) were induced upon heat shock. Bfr1 and Scp160 were identified as modulating P-body formation, but not their localization near the ER (Weidner et al., 2014). Scp160 is an mRNA-binding protein that, together with Bfr1 (whose function is still unclear), associates with actively translating polysomes at the ER (Lang et al., 2001). They both localize to the ER membrane whether the yeast are stressed or not, and both Scp160 and Bfr1 are shown by immunoprecipitations to interact with P-body components (such as Dcp2) (Weidner et al., 2014) (**Figure 3A**).

However, the phenotype observed in Bfr1 or Scp160 deletion is complex. There are more P-bodies in these mutants when compared to wildtype, but only in basal conditions. When the growth temperature shifts up, the mutant cells have less P-bodies

---

than wildtype. Therefore, Scp160/ Bfr1 negatively regulate P-body formation under normal stress-free growth conditions (Weidner et al., 2014).

### *3.2 Plasma Membrane Receptors Promotes Phase Separation*

Not only stress assemblies form in contact with membrane but phase separation can also occur and be enhanced directly at biological membranes through transmembrane proteins. At the plasma membrane, this would lead to efficient receptors clustering together with their cytoplasmic interactors and potentially their ligands. Furthermore, the proximity of a membrane (a 2D flat lipid bilayer) could enhance phase separation perhaps by concentrating components and facilitating their pi-pi and cation/pi interaction.

As briefly reported in the introduction, specific interactions between protein domains can drive phase separation. In vitro reconstitution with purified components have shown that purified SH3 domains and proline-rich motifs support phase separation into liquid droplets, even though their affinity for each other is not very high (Li et al., 2012). In vivo, the ability of these domains to phase separate is used to create domains on the plasma membrane that enhance enzymatic reactions, for instance polymerization of actin cytoskeleton around the transmembrane adhesion receptor Nephhrin. Nck and N-WASP are two cytoplasmic SH2 and SH3 domains containing proteins that are involved in the formation of actin filaments. Through its SH2 domain, Nck first associates with three phosphorylated tyrosines present in the long disordered cytoplasmic tail of Nephhrin (Jones et al., 2006). Once bound, the three SH3 domains of Nck binds the proline-rich domain of N-WASP, an event that drives phase separation in the plane of the plasma membrane and leads to the clustering of Nephhrin. As Nephhrin binds the Arp2/3 complex, it becomes activated and efficiently drive the polymerization of actin (**Figure 3B**).

Similar clustering and condensation of SH3- and SH2- domains containing plasma membrane adapters has also been reported in the context of T cell receptor activation mediated by the T cell receptor complex protein LAT (linker for activation of T cells). In this case, LAT coalescence attracts specific proteins (such as ZAP70) and repulse others such as CD45. This would then create a micro-environment where specific, spatially restricted and efficient T cell receptor signaling reactions takes place. Altogether, this leads to an amplification of T cell signaling (Douglass and Vale, 2005; Su et al., 2016). Membrane clustering therefore appears to be a common mechanism in cellular signaling, which may serve to stabilize active conformations, amplify signals and may introduce switch-like behavior (Chong and Forman-Kay, 2016).

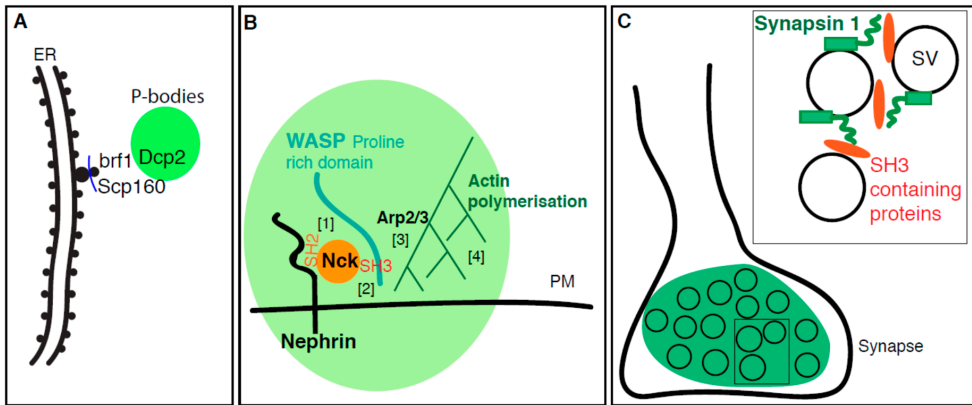


**Figure 3. Membrane enhances the formation of phase-separated condensates. (A):** P-bodies form near the ER as DCP2 interacts with the ER proteins Scp160 and Brf1 themselves interacting with translating ribosomes present at the translocon. **(B):** Nephtrin is a transmembrane adhesion receptor resident of the plasma membrane (PM). It binds to Nck-SH2 domain via its long disorder cytoplasmic tail [1]. Nck contains also three SH3 domain can binds the proline-rich domain of N-WASP [2]. This forms a biocondensation (green) that recruits Arp2/3 [3], resulting in actin polymerization around Nephtrin[4] **(C):** Synapsin 1 at synapse interacts with several SH3 domain containing proteins (in orange such as Intersectin and Gbr2) via its intrinsically disordered region. These interactions are proposed to lead to the phase separation of these components and coalescence of synaptic vesicles (SV) as observed at the synapse.

### 3.3 The Synapse, A Phase Separation Mediated by Small Lipid Carriers?

As reported above, a flat plasma membrane can help promoting phase separation in acting as a platform or a crucible. However, small lipid carriers can also enhance phase separation as observed in an in vitro system mimicking the synapse (Milovanovic et al., 2018).

Synapsin1 is a protein that is present at the synapse. It harbors an ATP (Adenosine triphosphate) binding module that is flanked by an intrinsically disordered C-terminal regions that are, in principle, prone to separate into liquid phase. To test this, in vitro purified GFP-tagged synapsin 1 forms micrometer-size droplets that tend to fuse together. Furthermore, FRAP of a small area within the droplet reveals that the phase is liquid and that Synapsin1 moves in and out of the droplet rapidly. Analysis of two purified fragments of Synapsin1 confirmed that the intrinsically disorder region is responsible for droplet formation, not its folded central ATP binding module (Milovanovic et al., 2018).

As mentioned above, SH2 and SH3 domains containing proteins interact with

---

intrinsically proline-rich domains containing proteins, such as synapsin 1. Interestingly, two SH3 domains containing proteins normally present at the synapse are intersectin (an endocytic multidomain scaffold protein and an regulator of synaptic vesicle replenishment) (Gerth et al., 2017) and Grb2 (McPherson et al., 1994) (growth factor receptor-bound 2) and they both interact with Synapsin1 via its proline-rich intrinsically disorder tail. When tested in vitro, incubation of purified Synapsin1 with intersectin and Grb2 leads to their co-phase separation into larger droplets. The use of the sole SH3 domain of intersectin yields a similar effect, supporting as above, the role of SH3 domain and its interaction with proline-rich domain in phase separation.

Synapsin1 is normally present at the synapse that is, a crowded environment. Accordingly, the phase separation propensity of purified Synapsin1 (alone and in the presence of its SH3 binding partners) is enhanced by presence the crowding agent Polyethylene glycol (PEG). Given that SH3 containing proteins and PEG play a positive role in Synapsin1 phase separation, and given that at the synapse, Synapsin1, intersectin and Grb2 are all present at the cytoplasmic leaflet of synaptic vesicles (Cesca et al., 2010), this infers that Synapsin1 phase separates at the synapse in a manner that depends on its interaction with SH3 domain proteins and on crowding.

However, the presence of small lipidic synaptic vesicles could also play a role in this phase separation. This was tested in vitro. Small artificial 50–150 nm diameter lipid vesicles devoid of proteins (but labeled by the lipid dye Cy5-DOPE) were added to purified synapsin1. Strikingly, the formation of synapsin liquid droplets correlated with the accumulation of lipid dye in the droplets. No droplets were observed in the absence of synapsin 1 and the vesicles do not condensate on their own. Analysis by electron microscopy showed that these droplets are clusters of small vesicles connected by synapsin 1, while in the absence of synapsin 1, vesicles remained dispersed. Importantly, synapsin 1 condensates did not recruit vesicles lacking negatively charged phospholipid suggesting that those are necessary for synapsin1 binding to vesicles even in the absence of Grb2 and intersectin (Milovanovic et al., 2018).

These results show that the clustering of small lipid carriers and synapsin 1 might mimic the synapse in a minimalistic manner. Indeed, observed a few decades ago by EM, synapses are characterized by a collection of clustered synaptic vesicles seemingly glued together by a protein gel. This gel is likely to contain synapsin 1 (Milovanovic and De Camilli, 2017). Of course, at the synapse, the vesicles would also harbor SH3 containing proteins at their surface and in addition to lipids, this will likely help the phase separation of synapsin 1. The next step of the in vitro assay will be to mix purified synapsin 1 together



with small lipidic carriers carrying SH3 domains (**Figure 3C**).

Taken together, these findings opens the possibility to study the two forms of cell compartmentalization (membrane-bound and non-membrane-bound) in an integrated manner, refining further how membrane drives phase separation and what molecular contact are established between these two classes of organelles, in the same way as membrane contacts sites are now studied. For instance, are the ER anchored P-bodies moving together with the ER? Is there an exchange of components, including protein and RNAs between condensates/stress assemblies and membrane-bound organelles? Furthermore, as membrane enhances the formation of condensates, it also facilitates biochemical reactions taken place in these condensates. What are those reactions and how are they different from those that occur in more dispersed state remains to be investigated? Finally, it will be important to understand how biological condensates influence membrane dynamics, membrane traffic, and the function of membrane-bound organelles in general.

#### *4 The Cell Cycle Appears to be A Global Transition from An Interphasic Phase-Separated State to A Mitotic Dispersed State*

Last, the concept of phase transition has recently been extended to the whole cell during the cell cycle. What is proposed is that the cell in interphase is characterized by the presence of many MLOs, which become diffuse at the onset of mitosis in a DYRK3 dependent manner (Rai et al., 2018). This is proposed to ensure optimal partitioning in the two daughter cells, a phenomenon that is reminiscent of membrane-bound organelles that fragment at the onset of mitosis. DYRK3 is a kinase that has been identified previously as being required for the dissolution of stress granules upon stress relief. This DYRK3 dependent dissolution links to TORC1 signaling as it releases the TOR kinase that was trapped in the granule during stress (Wippich et al., 2013).

To understand the role of DYRK3 in non-stressed cells, DYRK3 was overexpressed which resulted in its spontaneous phase separation that occurs at a specific concentration threshold. At low expression level in interphase cells, DYRK3 shows a diffuse distribution within the nucleus and the cytoplasm with some enrichment at centrosomes and in nuclear splicing speckles. Interestingly, at high expression, it leads to the dissolution of these splicing speckles, an effect that was reverted by treating cells with the DYRK3 inhibitor. Furthermore, when DYRK3 is prevented to enter the nucleus, the splicing speckles are no longer dissolved. Overexpression of DYRK3 also dissolves pericentriolar satellites and prevents the induction of stress granules with arsenite in the cytoplasm in a kinase-

---

activity-dependent manner. However, nucleoli of overexpressed DYRK3 cells were still intact. In mitotic cells, overexpressed DYRK3 localizes to spindle poles and biochemically, DYRK3 interacts with proteins that are heavily phosphorylated during mitosis (Rai et al., 2018).

Therefore, what is the role of DYRK3 when the content of both cellular compartments mixes at the onset of mitosis? The first clue is that inhibition of DYRK3 in mitotic cells leads to the aberrant condensation of the splicing-speckle marker SC35, the stress-granule marker PABP (PolyA-binding protein) and the pericentriolar material protein PCM1. They were found to co-condense into a so-called liquid phase-separated hybrid mitotic granules that also contain for polyadenylated RNA and accumulated inhibited DYRK3. However, these structures are not positive for P-body, Cajal body markers, and ubiquitin. It therefore appears that DYRK3 kinase activity is essential during mitosis to prevent the formation of liquid-liquid phase-separated mitotic granules (Rai et al., 2018).

Overall, overexpression of DYRK3 in interphase cells leads to the dissolution of many MLOs (but not the nucleolus) while inhibition of DYRK3 in mitosis leads to the formation of a non-physiological hybrid granule. DYRK3 is therefore proposed to act as a dissolvase of multiple liquid-unmixed/phase separated/condensate compartments to prevent their aberrant condensation during mitosis.

How would the same enzyme have a low activity in interphase and be activated at the onset of mitosis? DYRK3 expression increases gradually as cells progress from late S to the end of G2 (mitosis) with sudden increase in DYRK3 levels as cells enter mitosis. Accordingly, the DYRK3-to-substrate ratio has been proposed to modulate the phase transition. The notion is that when the ratio is high, the phase separates should disperse (like during mitosis). Conversely, when this ratio is low, condensation should take place (like in interphase). To investigate this, non-mitotic cells were transfected with inducible DYRK3 and SRRM1 (a protein a splicing-speckle with a high content in low complexity regions), and the changes in their concentration was recorded by time-lapse imaging, from G1 to mitosis exit. As expected, the DYRK3/SRRM1 ratio increases over time and SRRM1 remains dissolved in cells that display a high DTRK3/SRRM1 ratio. This indicated that this ratio is required to maintain the dissolved phase during mitosis. Conversely, when the ratio is low, SRRM1 is present in granules, as observed in interphase.

In conclusion, interphase cells appear to exhibit a low level of DYRK3 which allows the phase separation of many physiological MLOs. Conversely, mitotic cells have a higher

level of DYRK3 as well as many mitotic phosphor-proteins that allow the dissolution of these MLOs.

## *5 Conclusions*

In this review, we have reported that the two forms of cell compartmentalization, membrane-bound organelles and MLOs, interact with one another more than was anticipated. Inhibition of membrane traffic steps by mutations or cellular stress leads to the formation of specific stress assemblies, some of them based upon proteins that are key for optimizing on of this step (such as Sec16, part 1). We also report how stress granules interact in a complex manner with nuclear transport receptors and as such are involved in ALS (part 2). In the third part, we report that although the two forms of cell compartmentalization (membrane-bound and membraneless) are often studied independently of one another by different groups of researchers, they in fact interact. Even better, membrane enhances phase separation of condensates (part 3). Last, it appears that the whole cell transits from a phase-separated state at interphase to a more dispersed state at the onset of mitosis, an observation that is reminiscent to what happens to membrane-bound compartments that fragment and disperse at mitosis. The notion behind this is that it would enhance the chances of equal partitioning between the two daughter cells even if we now know that it is in fact not stochastic.

Altogether, the link between membrane-bound organelles and phase-separated condensates has several consequences. First, although the term “membraneless organelle” is language-wise correct when defined as non-sealed by a membrane, it also alludes to the notion that phase separation in cellulo “has nothing to do” with membrane. Consequently, the term membraneless organelles should be replaced by “phase-separated condensates” or “stress assemblies” as we have done in this review. Second, the contact between these condensates/assemblies and membrane needs to be defined in a more systematic manner as they influence each other’s biology. P-bodies appear to form near the ER and what about other condensates given that the ER pervades the entire cell? Third, a large amount of data leading to the deep understanding of the biophysical and material properties of these condensates are performed in vitro using purifying proteins. However, given that the cell is an environment crowded with membrane-bound organelles that interact with condensates, now is a good time to add membrane to in vitro phase separation experiments. In this regard, the pioneering experiments performed with synapsin 1 and small lipid carriers in vitro are paving this avenue to recreate in a small (and still reductionist) manner the cell interior.

### *Appendix A: The Early Secretory Pathway*

The secretory pathway is conserved in the eukaryotic kingdom and mediates the export of proteins and lipids from the endoplasmic Reticulum (ER) to the extracellular medium, the plasma membrane, and nearly all cellular membrane-bound compartments. The early secretory pathway refers to a series of membrane-bound compartments, the ER, the ER exit sites (ERES), the ERGIC (ER-to-Golgi intermediate compartments, for mammalian cells) and the Golgi. In the ER, newly synthesized proteins are folded, assembled, glycosylated and they exported to the Golgi via the ERGIC in COPII coated transport vesicles that bud at specialized cup-shaped regions of the ER, the ERES (Gomez-Navarro and Miller, 2016; Peotter et al., 2019). COPII coated vesicle formation requires the small GTPase Sar1 (GTP-bound state) that is activated by its GEF Sec12. Once inserted at the ER membrane, Sar1 bound to Guanosine triphosphate (GTP) recruits the inner coat Sec23/Sec24 heterodimer that is coupled to cargo selection and recruitment by Sec24 (Barlowe, 2015). The outer coat Sec13/Sec31 is then recruited resulting in the formation of a cargo loaded COPII coated vesicle (Miller and Schekman, 2013). One large hydrophilic ERES protein Sec16 acts as a ER exit site scaffold and plays an important role in optimizing COPII dynamics Sec16 directly binds nearly all COPII subunits and it contributes to ERES stability (reviewed in (Sprangers and Rabouille, 2015)).

After exiting the ER via these COPII vesicles, proteins reach the Golgi complex where they are further processed, sorted, and dispatched to their correct destination (Bonifacino and Glick, 2004). Some proteins need to be retrieved back to the ER in COPI coated vesicles (Arakel and Schwappach, 2018; Béthune and Wieland, 2018).

### *Appendix B: The Cyto-Nuclear Trafficking*

The cyto-nuclear trafficking refers to the regulated movement through the nuclear pore complex (NPC) of molecules with a molecular mass above 50 kDa. Protein entry to the nucleus is mediated by the so-called nuclear import receptors (NIRs). They tightly bind the NLS (nuclear localization signal) of proteins cargo and break hydrophobic contacts between FG-repeat-rich nucleoporins of the NPC as they traverse the nuclear pore during nuclear transport. Once the complex is in the nucleoplasm, it dissociates in an energy dependent manner that requires the small Ran GTPase. The NIRs are then re-exported from the nucleus to the cytoplasm where GTP hydrolysis releases Ran.

Among NIRs, the family of importin  $\beta$ /Karyopherins  $\beta$  plays an important role. For instance, Karyopherins  $\beta$  2 (also called transportin 1 or importin  $\beta$  2) imports M9-containing proteins, such as FUS, hnRNPA1, and hnRNPA2, TAF15, and EWSR1 through

their PY-NLS (Kimura and Imamoto, 2014). On the other hand, TDP-43 contains a C-ter NLS instead of N-ter PY-NLS which can recognize by Imp $\alpha$ . Imp $\alpha$  is then bound by Kap  $\beta$  1 allowing transport through the nuclear pores (Guo et al., 2019).

Conversely, proteins exit from the nucleus is mediated by nuclear export receptors also called exportins that bind NES (Nuclear export signals) that are not very well defined (Kimura and Imamoto, 2014).

### *Acknowledgments*

We thank Wessel van Leeuwen for critically reading the manuscript.

### *Funding*

C.Z. is supported by a scholarship of the China Scholarship Council (201706670014).

### *References*

- Ackema, K.B., Hench, J., Bockler, S., Wang, S.C., Sauder, U., Mergentaler, H., Westermann, B., Bard, F., Frank, S., and Spang, A. (2014). The small GTPase Arf1 modulates mitochondrial morphology and function. *The EMBO journal* 33, 2659-2675.
- Aguilera-Gomez, A., and Rabouille, C. (2016). Intra-Golgi Transport. In: Ralph A Bradshaw and Philip D Stahl (Editors-in-Chief), *Encyclopedia of Cell Biology*, Waltham, MA: Academic Press Vol 2, 354-362.
- Aguilera-Gomez, A., van Oorschot, M.M., Veenendaal, T., and Rabouille, C. (2016). In vivo visualization of mono-ADP-ribosylation by dPARP16 upon amino-acid starvation. *Elife* 5.
- Aguilera-Gomez, A., Zacharogianni, M., van Oorschot, M.M., Genau, H., Grond, R., Veenendaal, T., Sinsimer, K.S., Gavis, E.R., Behrends, C., and Rabouille, C. (2017). Phospho-Rasputin Stabilization by Sec16 Is Required for Stress Granule Formation upon Amino Acid Starvation. *Cell Rep* 20, 935-948.
- Alberti, S. (2017). The wisdom of crowds: regulating cell function through condensed states of living matter. *J Cell Sci* 130, 2789-2796.
- Anderson, P., and Kedersha, N. (2002). Stressful initiations. *Journal of Cell Science* 115, 3227-3234.
- Anderson, P., and Kedersha, N. (2008). Stress granules: the Tao of RNA triage. *Trends in biochemical sciences* 33, 141-150.
- Anderson, P., and Kedersha, N. (2009). Stress granules. *Current Biology* 19, R397-398.
- Arakel, E.C., and Schwappach, B. (2018). Formation of COPI-coated vesicles at a glance. *Journal of Cell Science* 131, jcs209890.
- Banani, S.F., Rice, A.M., Peeples, W.B., Lin, Y., Jain, S., Parker, R., and Rosen, M.K. (2016). Compositional Control of Phase-Separated Cellular Bodies. *Cell* 166, 651-663.
- Barlowe, C. (2015). Membrane trafficking: ER export encounters dualism. *Current biology : CB* 25, R151-153.
- Batiza, A.F., Schulz, T., and Masson, P.H. (1996). Yeast respond to hypotonic shock with a calcium pulse. *Journal of Biological Chemistry* 271, 23357-23362.

- Béthune, J., and Wieland, F.T. (2018). Assembly of COPI and COPII Vesicular Coat Proteins on Membranes. *Annual Review of Biophysics* 47, 63-83.
- Bigio, E.H. (2011). C9ORF72, the new gene on the block, causes C9FTD/ALS: new insights provided by neuropathology. *Acta Neuropathologica* 122, 653-655.
- Birsa, N., Benthham, M.P., and Fratta, P. (2019). Cytoplasmic functions of TDP-43 and FUS and their role in ALS. *Seminars in Cell & Developmental Biology*.
- Boeynaems, S., Bogaert, E., Kovacs, D., Konijnenberg, A., Timmerman, E., Volkov, A., Guharoy, M., De Decker, M., Jaspers, T., Ryan, V.H., et al. (2017). Phase Separation of C9orf72 Dipeptide Repeats Perturbs Stress Granule Dynamics. *Mol Cell* 65, 1044-1055 e1045.
- Bonifacino, J.S., and Glick, B.S. (2004). The mechanisms of vesicle budding and fusion. *Cell* 116, 153-166.
- Bowden, H.A., and Dormann, D. (2016). Altered mRNP granule dynamics in FTLD pathogenesis. *Journal of Neurochemistry* 138, 112-133.
- Buchan, J.R., Muhlrads, D., and Parker, R. (2008). P bodies promote stress granule assembly in *Saccharomyces cerevisiae*. *J Cell Biol* 183, 441-455.
- Buchan, J.R., and Parker, R. (2009). Eukaryotic stress granules: the ins and outs of translation. *Mol Cell* 36, 932-941.
- Cesca, F., Baldelli, P., Valtorta, F., and Benfenati, F. (2010). The synapsins: Key actors of synapse function and plasticity. *Progress in Neurobiology* 91, 313-348.
- Chong, P.A., and Forman-Kay, J.D. (2016). Liquid-liquid phase separation in cellular signaling systems. *Current Opinion in Structural Biology* 41, 180-186.
- Chong, P.A., Vernon, R.M., and Forman-Kay, J.D. (2018). RGG/RG Motif Regions in RNA Binding and Phase Separation. *Journal of Molecular Biology* 430, 4650-4665.
- Couthouis, J., Hart, M.P., Shorter, J., DeJesus-Hernandez, M., Erion, R., Oristano, R., Liu, A.X., Ramos, D., Jethava, N., Hosangadi, D., et al. (2011). A yeast functional screen predicts new candidate ALS disease genes. *Proceedings of the National Academy of Sciences* 108, 20881.
- Daigle, J.G., Lanson, N.A., Jr., Smith, R.B., Casci, I., Maltare, A., Monaghan, J., Nichols, C.D., Kryndushkin, D., Shewmaker, F., and Pandey, U.B. (2012). RNA-binding ability of FUS regulates neurodegeneration, cytoplasmic mislocalization and incorporation into stress granules associated with FUS carrying ALS-linked mutations. *Human Molecular Genetics* 22, 1193-1205.
- Decker, C.J., and Parker, R. (2012). P-Bodies and Stress Granules: Possible Roles in the Control of Translation and mRNA Degradation. *Cold Spring Harbor Perspectives in Biology* 4.
- Di Paola, S., Micaroni, M., Di Tullio, G., Buccione, R., and Di Girolamo, M. (2012). PARP16/ARTD15 is a novel endoplasmic-reticulum-associated mono-ADP-ribosyltransferase that interacts with, and modifies karyopherin-ss1. *PLoS one* 7, e37352.
- Douglass, A.D., and Vale, R.D. (2005). Single-Molecule Microscopy Reveals Plasma Membrane Microdomains Created by Protein-Protein Networks that Exclude or Trap Signaling Molecules in T Cells. *Cell* 121, 937-950.
- Fong, J.C., Karydas, A.M., and Goldman, J.S. (2012). Genetic counseling for FTD/ALS caused by the C9ORF72 hexanucleotide expansion. *Alzheimer's Research & Therapy* 4, 27.
- Forman-Kay, J.D., Kriwacki, R.W., and Seydoux, G. (2018). Phase Separation in Biology and Disease. *Journal of Molecular Biology* 430, 4603-4606.
- Formicola, N., Vijayakumar, J., and Besse, F. (2019). Neuronal ribonucleoprotein granules: Dynamic

sensors of localized signals. *Traffic* 20, 639-649.

Freibaum, B.D., Lu, Y., Lopez-Gonzalez, R., Kim, N.C., Almeida, S., Lee, K.H., Badders, N., Valentine, M., Miller, B.L., Wong, P.C., et al. (2015). GGGGCC repeat expansion in C9orf72 compromises nucleocytoplasmic transport. *Nature* 525, 129-133.

Gasset-Rosa, F., Lu, S., Yu, H., Chen, C.C., Melamed, Z., Guo, L., Shorter, J., Da Cruz, S., and Cleveland, D.W. (2019). Cytoplasmic TDP-43 De-mixing Independent of Stress Granules Drives Inhibition of Nuclear Import, Loss of Nuclear TDP-43, and Cell Death. *Neuron* 102, 339-357.e337.

Gerth, F., Jäpel, M., Pechstein, A., Kochlamazashvili, G., Lehmann, M., Puchkov, D., Onofri, F., Benfenati, F., Nikonenko, A.G., Fredrich, K., et al. (2017). Intersectin associates with synapsin and regulates its nanoscale localization and function. *Proceedings of the National Academy of Sciences* 114, 12057.

Gomes, E., and Shorter, J. (2018). The molecular language of membraneless organelles. *Journal of Biological Chemistry*, pii: jbc.TM118.001192. doi:.

Gomez-Navarro, N., and Miller, E. (2016). Protein sorting at the ER-Golgi interface. *J Cell Biol* 215, 769-778.

Guo, L., Fare, C.M., and Shorter, J. (2019). Therapeutic Dissolution of Aberrant Phases by Nuclear-Import Receptors. *Trends in Cell Biology* 29, 308-322.

Guo, L., Kim, H.J., Wang, H., Monaghan, J., Freyermuth, F., Sung, J.C., O'Donovan, K., Fare, C.M., Diaz, Z., Singh, N., et al. (2018). Nuclear-Import Receptors Reverse Aberrant Phase Transitions of RNA-Binding Proteins with Prion-like Domains. *Cell* 173, 677-692.e620.

Guzikowski, A.R., Chen, Y.S., and Zid, B.M. (2019). Stress-induced mRNP granules: Form and function of processing bodies and stress granules. *Wiley Interdisciplinary Reviews: RNA* 10, e1524.

Hofweber, M., Hutten, S., Bourgeois, B., Spreitzer, E., Niedner-Boblentz, A., Schifferer, M., Ruepp, M.-D., Simons, M., Niessing, D., Madl, T., et al. (2018). Phase Separation of FUS Is Suppressed by Its Nuclear Import Receptor and Arginine Methylation. *Cell* 173, 706-719.e713.

Horvathova, I., Voigt, F., Kotrys, A.V., Zhan, Y., Artus-Revel, C.G., Eglinger, J., Stadler, M.B., Giorgetti, L., and Chao, J.A. (2017). The Dynamics of mRNA Turnover Revealed by Single-Molecule Imaging in Single Cells. *Molecular cell* 68, 615-625.e619.

Hubstenberger, A., Courel, M., Bénard, M., Souquere, S., Ernoult-Lange, M., Chouaib, R., Yi, Z., Morlot, J.-B., Munier, A., Fradet, M., et al. (2017). P-Body Purification Reveals the Condensation of Repressed mRNA Regulons. *Molecular cell* 68, 144-157.e145.

Hughes, M.P., Sawaya, M.R., Boyer, D.R., Goldschmidt, L., Rodriguez, J.A., Cascio, D., Chong, L., Gonen, T., and Eisenberg, D.S. (2018). Atomic structures of low-complexity protein segments reveal kinked  $\beta$  sheets that assemble networks. *Science* 359, 698.

Ivan, V., de Voer, G., Xanthakis, D., Spoorendonk, K.M., Kondylis, V., and Rabouille, C. (2008). *Drosophila* Sec16 mediates the biogenesis of tER sites upstream of Sar1 through an arginine-rich motif. *Mol Biol Cell* 19, 4352-4365.

Jackson, C.L., and Bouvet, S. (2014). Arfs at a Glance. *Journal of Cell Science* 127, 4103.

Ji, S., Luo, Y., Cai, Q., Cao, Z., Zhao, Y., Mei, J., Li, C., Xia, P., Xie, Z., Xia, Z., et al. (2019). LC Domain-Mediated Coalescence Is Essential for Otu Enzymatic Activity to Extend *Drosophila* Lifespan. *Molecular cell* 74, 363-377.e365.

Jones, N.L., Blasutig, I.M., Eremina, V., Ruston, J.M., Bladt, F., Li, H., Huang, H.L., Larose, L., Li, S.S.C., Takano, T., et al. (2006). Nck adaptor proteins link nephrin to the actin cytoskeleton of kidney

podocytes. *Nature* 440, 818-823.

Jovičić, A., Mertens, J., Boeynaems, S., Bogaert, E., Chai, N., Yamada, S.B., Paul Iii, J.W., Sun, S., Herdy, J.R., Bieri, G., et al. (2015). Modifiers of C9orf72 dipeptide repeat toxicity connect nucleocytoplasmic transport defects to FTD/ALS. *Nature Neuroscience* 18, 1226.

Jwa, M., and Chang, P. (2012). PARP16 is a tail-anchored endoplasmic reticulum protein required for the PERK- and IRE1 $\alpha$ -mediated unfolded protein response. *Nat Cell Biol* 14, 1223-1230.

Khan, B.K., Yokoyama, J.S., Takada, L.T., Sha, S.J., Rutherford, N.J., Fong, J.C., Karydas, A.M., Wu, T., Ketelle, R.S., Baker, M.C., et al. (2012). Atypical, slowly progressive behavioural variant frontotemporal dementia associated with <em>C9ORF72</em> hexanucleotide expansion. *Journal of Neurology, Neurosurgery & Psychiatry* 83, 358.

Kilchert, C., Weidner, J., Prescianotto-Baschong, C., and Spang, A. (2010). Defects in the secretory pathway and high Ca<sup>2+</sup> induce multiple P-bodies. *Mol Biol Cell* 21, 2624-2638.

Kimura, M., and Imamoto, N. (2014). Biological Significance of the Importin- $\beta$  Family-Dependent Nucleocytoplasmic Transport Pathways. *Traffic* 15, 727-748.

Kroschwald, S., and Alberti, S. (2017). Gel or Die: Phase Separation as a Survival Strategy. *Cell* 168, 947-948.

Lang, B.D., Li, A.-m., Black-Brewster, H.D., and Fridovich-Keil, J.L. (2001). The brefeldin A resistance protein Bfr1p is a component of polyribosome-associated mRNP complexes in yeast. *Nucleic Acids Research* 29, 2567-2574.

Li, P., Banjade, S., Cheng, H.C., Kim, S., Chen, B., Guo, L., Llaguno, M., Hollingsworth, J.V., King, D.S., Banani, S.F., et al. (2012). Phase transitions in the assembly of multivalent signalling proteins. *Nature* 483, 336-340.

Li, Y.R., King, O.D., Shorter, J., and Gitler, A.D. (2013). Stress granules as crucibles of ALS pathogenesis. *J Cell Biol* 201, 361-372.

Maharana, S., Wang, J., Papadopoulos, D.K., Richter, D., Pozniakovsky, A., Poser, I., Bickle, M., Rizk, S., Guillén-Boixet, J., Franzmann, T.M., et al. (2018). RNA buffers the phase separation behavior of prion-like RNA binding proteins. *Science* 360, 918.

Mahboubi, H., Seganathy, E., Kong, D., and Stochaj, U. (2013). Identification of Novel Stress Granule Components That Are Involved in Nuclear Transport. *PLoS one* 8, e68356.

Marnik, E.A., and Updike, D.L. (2019). Membraneless organelles: P granules in *Caenorhabditis elegans*. *Traffic* 0.

Matsumoto, T.K., Ellsmore, A.J., Cessna, S.G., Low, P.S., Pardo, J.M., Bressan, R.A., and Hasegawa, P.M. (2002). An Osmotically Induced Cytosolic Ca<sup>2+</sup> Transient Activates Calcineurin Signaling to Mediate Ion Homeostasis and Salt Tolerance of *Saccharomyces cerevisiae*. *Journal of Biological Chemistry* 277, 33075-33080.

McGurk, L., Gomes, E., Guo, L., Mojsilovic-Petrovic, J., Tran, V., Kalb, R.G., Shorter, J., and Bonini, N.M. (2018). Poly(ADP-Ribose) Prevents Pathological Phase Separation of TDP-43 by Promoting Liquid Demixing and Stress Granule Localization. *Molecular cell* 71, 703-717.e709.

McPherson, P.S., Czernik, A.J., Chilcote, T.J., Onofri, F., Benfenati, F., Greengard, P., Schlessinger, J., and De Camilli, P. (1994). Interaction of Grb2 via its Src homology 3 domains with synaptic proteins including synapsin I. *Proceedings of the National Academy of Sciences* 91, 6486.

Miller, E.A., and Schekman, R. (2013). COPII - a flexible vesicle formation system. *Curr Opin Cell Biol* 25, 420-427.

Milovanovic, D., and De Camilli, P. (2017). Synaptic Vesicle Clusters at Synapses: A Distinct Liquid



Phase? *Neuron* 93, 995-1002.

Milovanovic, D., Wu, Y., Bian, X., and De Camilli, P. (2018). A liquid phase of synapsin and lipid vesicles. *Science* 361, 604.

Molliex, A., Temirov, J., Lee, J., Coughlin, M., Kanagaraj, A.P., Kim, H.J., Mittag, T., and Taylor, J.P. (2015). Phase Separation by Low Complexity Domains Promotes Stress Granule Assembly and Drives Pathological Fibrillization. *Cell* 163, 123-133.

Murray, D.T., Kato, M., Lin, Y., Thurber, K.R., Hung, I., McKnight, S.L., and Tycko, R. (2017). Structure of FUS Protein Fibrils and Its Relevance to Self-Assembly and Phase Separation of Low-Complexity Domains. *Cell* 171, 615-627.

Parker, R., and Sheth, U. (2007). P bodies and the control of mRNA translation and degradation. *Mol Cell* 25, 635-646.

Patel, A., Lee, H.O., Jawerth, L., Maharana, S., Jahnel, M., Hein, M.Y., Stoykov, S., Mahamid, J., Saha, S., Franzmann, T.M., et al. (2015). A Liquid-to-Solid Phase Transition of the ALS Protein FUS Accelerated by Disease Mutation. *Cell* 162, 1066-1077.

Patterson, J.R., Wood, M.P., and Schisa, J.A. (2011). Assembly of RNP granules in stressed and aging oocytes requires nucleoporins and is coordinated with nuclear membrane blebbing. *Dev Biol* 353, 173-185.

Peotter, J., Kasberg, W., Pustova, I., and Audhya, A. (2019). COPII-mediated trafficking at the ER/ERGIC interface. *Traffic* 20, 491-503.

Petrovska, I., Nuske, E., Munder, M.C., Kulasegaran, G., Malinovska, L., Kroschwald, S., Richter, D., Fahmy, K., Gibson, K., Verbavatz, J.M., et al. (2014). Filament formation by metabolic enzymes is a specific adaptation to an advanced state of cellular starvation. *Elife*.

Protter, D.S., and Parker, R. (2016). Principles and Properties of Stress Granules. *Trends in cell biology* 26, 668-679.

Rai, A.K., Chen, J.-X., Selbach, M., and Pelkmans, L. (2018). Kinase-controlled phase transition of membraneless organelles in mitosis. *Nature* 559, 211-216.

Ruff, K.M., Pappu, R.V., and Holehouse, A.S. (2019). Conformational preferences and phase behavior of intrinsically disordered low complexity sequences: insights from multiscale simulations. *Current Opinion in Structural Biology* 56, 1-10.

Scorrano, L., De Matteis, M.A., Emr, S., Giordano, F., Hajnóczky, G., Kornmann, B., Lackner, L.L., Levine, T.P., Pellegrini, L., Reinisch, K., et al. (2019). Coming together to define membrane contact sites. *Nature Communications* 10, 1287.

Scotter, E.L., Chen, H.J., and Shaw, C.E. (2015). TDP-43 Proteinopathy and ALS: Insights into Disease Mechanisms and Therapeutic Targets. *Neurotherapeutics* 12, 352-363.

Souquere, S., Mollet, S., Kress, M., Dautry, F., Pierron, G., and Weil, D. (2009). Unravelling the ultrastructure of stress granules and associated P-bodies in human cells. *J Cell Sci* 122, 3619-3626.

Sprangers, J., and Rabouille, C. (2015). SEC16 in COPII coat dynamics at ER exit sites. *Biochemical Society transactions* 43, 97-103.

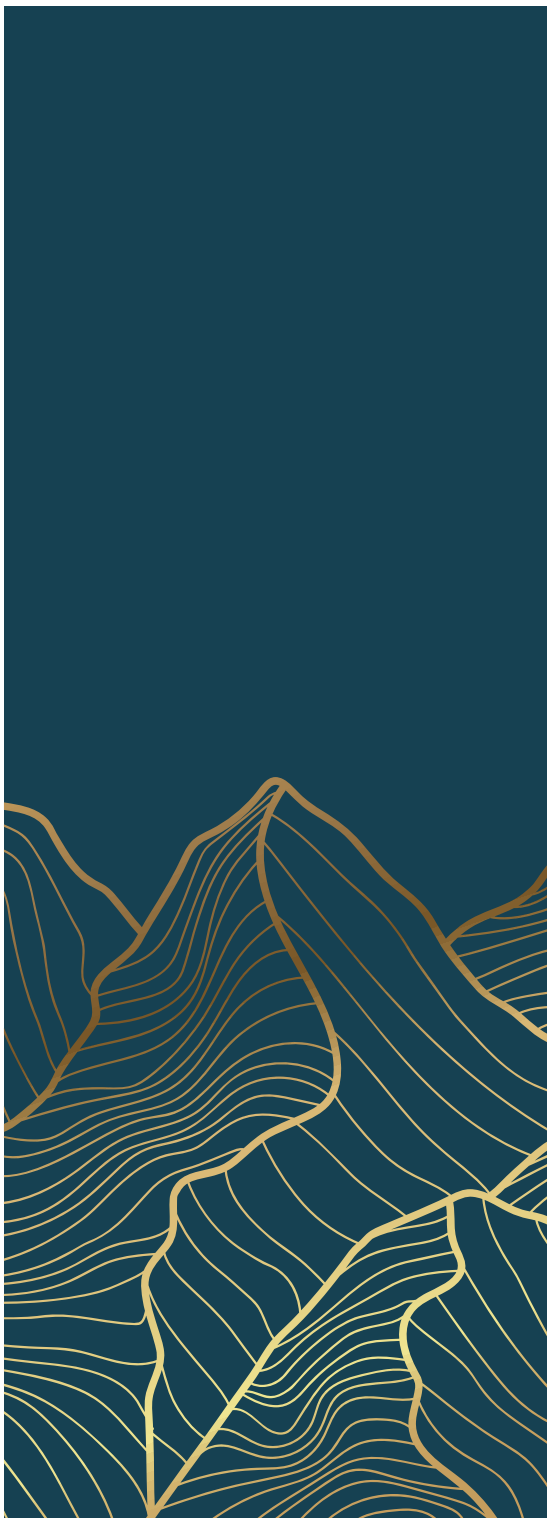
Su, X., Ditlev, J.A., Hui, E., Xing, W., Banjade, S., Okrut, J., King, D.S., Taunton, J., Rosen, M.K., and Vale, R.D. (2016). Phase separation of signaling molecules promotes T cell receptor signal transduction. *Science* 352, 595-599.

Teixeira, D., and Parker, R. (2007). Analysis of P-Body Assembly in *Saccharomyces cerevisiae*. *Molecular biology of the cell* 18, 2274-2287.

Trcek, T., and Lehmann, R. (2019). Germ granules in *Drosophila*. *Traffic* 20, 650-660.

- van Leeuwen, W., and Rabouille, C. (2019). Cellular stress leads to the formation of membraneless stress assemblies in eukaryotic cells. *Traffic* 0.
- Vernon, R.M., Chong, P.A., Tsang, B., Kim, T.H., Bah, A., Farber, P., Lin, H., and Forman-Kay, J.D. (2018). Pi-Pi contacts are an overlooked protein feature relevant to phase separation. *eLife* 7, e31486.
- Walch, L., Pellier, E., Leng, W., Lakisic, G., Gautreau, A., Contremoulins, V., Verbavatz, J.-M., and Jackson, C.L. (2018). GBF1 and Arf1 interact with Miro and regulate mitochondrial positioning within cells. *Scientific Reports* 8, 17121.
- Wang, C., Schmich, F., Srivatsa, S., Weidner, J., Beerenwinkel, N., and Spang, A. (2018a). Context-dependent deposition and regulation of mRNAs in P-bodies. *eLife* 7, e29815.
- Wang, J., Choi, J.-M., Holehouse, A.S., Lee, H.O., Zhang, X., Jahnel, M., Maharana, S., Lemaître, R., Pozniakovsky, A., Drechsel, D., et al. (2018b). A Molecular Grammar Governing the Driving Forces for Phase Separation of Prion-like RNA Binding Proteins. *Cell* 174, 688-699.e616.
- Weidner, J., Wang, C., Prescianotto-Baschong, C., Estrada, A.F., and Spang, A. (2014). The polysome-associated proteins Scp160 and Bfr1 prevent P body formation under normal growth conditions. *J Cell Sci* 127, 1992-2004.
- Weil, T.T., Parton, R.M., Herpers, B., Soetaert, J., Veenendaal, T., Xanthakis, D., Dobbie, I.M., Halstead, J.M., Hayashi, R., Rabouille, C., et al. (2012). Drosophila patterning is established by differential association of mRNAs with P bodies. *Nat Cell Biol* 14, 1305-1313.
- Wippich, F., Bodenmiller, B., Trajkovska, M.G., Wanka, S., Aebersold, R., and Pelkmans, L. (2013). Dual specificity kinase DYRK3 couples stress granule condensation/dissolution to mTORC1 signaling. *Cell* 152, 791-805.
- Wunder, T., Oh, Z.G., and Mueller-Cajar, O. (2019). CO<sub>2</sub>-fixing liquid droplets: Towards a dissection of the microalgal pyrenoid. *Traffic* 0.
- Yahara, N., Ueda, T., Sato, K., and Nakano, A. (2001). Multiple Roles of Arf1 GTPase in the Yeast Exocytic and Endocytic Pathways. *Molecular biology of the cell* 12, 221-238.
- Yoshizawa, T., Ali, R., Jiou, J., Fung, H.Y.J., Burke, K.A., Kim, S.J., Lin, Y., Peeples, W.B., Saltzberg, D., Soniat, M., et al. (2018). Nuclear Import Receptor Inhibits Phase Separation of FUS through Binding to Multiple Sites. *Cell* 173, 693-705.e622.
- Zacharogianni, M., Aguilera-Gomez, A., Veenendaal, T., Smout, J., and Rabouille, C. (2014). A stress assembly that confers cell viability by preserving ERES components during amino-acid starvation. *Elife* 3.
- Zhang, K., Daigle, J.G., Cunningham, K.M., Coyne, A.N., Ruan, K., Grima, J.C., Bowen, K.E., Wadhwa, H., Yang, P., Rigo, F., et al. (2018). Stress Granule Assembly Disrupts Nucleocytoplasmic Transport. *Cell* 173, 958-971.e917.
- Zhang, K., Donnelly, C.J., Haeusler, A.R., Grima, J.C., Machamer, J.B., Steinwald, P., Daley, E.L., Miller, S.J., Cunningham, K.M., Vidensky, S., et al. (2015). The C9orf72 repeat expansion disrupts nucleocytoplasmic transport. *Nature* 525, 56-61.
- Zhang, Z.C., and Chook, Y.M. (2012). Structural and energetic basis of ALS-causing mutations in the atypical proline-tyrosine nuclear localization signal of the Fused in Sarcoma protein (FUS). *Proceedings of the National Academy of Sciences* 109, 12017.





## *Chapter3*

*Activation of IRE1, PERK and saltinducible  
kinases leads to Sec body formation in  
Drosophila S2 cells*

Chujun Zhang , Wessel van Leeuwen, Marloes Blotenburg,  
Angelica Aguilera-Gomez, Sem Brussee, Rianne Ground,  
Harm H. Kampinga and Catherine Rabouille (2021)  
Journal of Cell Science 2021

---

## *Activation of IRE1, PERK and salt-inducible kinases leads to Sec body formation in Drosophila S2 cells*

### *Abstract*

The phase separation of the non-membrane bound Sec bodies occurs in Drosophila S2 cells by coalescence of components of the endoplasmic reticulum (ER) exit sites under the stress of amino acid starvation. Here, we address which signaling pathways cause Sec body formation and find that two pathways are critical. The first is the activation of the salt-inducible kinases (SIKs; SIK2 and SIK3) by Na<sup>+</sup> stress, which, when it is strong, is sufficient. The second is activation of IRE1 and PERK (also known as PEK in flies) downstream of ER stress induced by the absence of amino acids, which needs to be combined with moderate salt stress to induce Sec body formation. SIK, and IRE1 and PERK activation appear to potentiate each other through the stimulation of the unfolded protein response, a key parameter in Sec body formation. This work shows the role of SIKs in phase transition and re-enforces the role of IRE1 and PERK as a metabolic sensor for the level of circulating amino acids and salt.

3

### *Introduction*

Cell compartmentalization is not only mediated by membrane-bound organelles. It also relies on non-membrane bound biomolecular condensates (so-called membraneless organelles) that populate the nucleus and the cytoplasm.

The formation of membraneless organelles has been shown to occur through phase separation, which can be driven by stress (such as ER, oxidative, proteostatic or nutrient stress), resulting in the formation of stress assemblies (van Leeuwen and Rabouille, 2019). Those are mesoscale coalescence of specific and defined components that phase separate. For instance, nutrient stress leads to the formation of many biocondensates. Most of them are RNA based, such as stress granules and P-bodies (van Leeuwen and Rabouille, 2019), but some are not. This is the case for glucosestarved yeast where metabolic enzymes foci (Munder et al., 2016; Petrovska et al., 2014) and proteasome storage granules (Peters et al., 2013; van Leeuwen and Rabouille, 2019) form, as well as Drosophila S2 cells that form Sec bodies under conditions of amino acid starvation (Zacharogianni et al., 2014).

Sec bodies are related to the inhibition of protein secretion in the early secretory pathway. The early secretory pathway comprises the endoplasmic reticulum (ER), where newly synthesized proteins destined to the plasma membrane and the extracellular medium are synthesized. Proteins exit the ER at the ER exit sites (ERES) to reach the Golgi. The ERES are characterized by the concentration of COPI-coated vesicles whose formation requires six proteins, including Sec12 and Sar1, the inner coat proteins Sec23 and Sec24, and the outer coat proteins Sec13 and Sec31 (Gomez-Navarro and Miller, 2016). In addition, a larger hydrophilic protein called Sec16, has been identified as a key regulator of the ERES organization and COPII vesicle budding (Sprangers and Rabouille, 2015). Many additional lines of evidence support the role of Sec16 in optimizing COPII-coated vesicle formation and export from the ER (Farhan et al., 2010; Joo et al., 2016; Wilhelmi et al., 2016).

Upon the stress of amino acid starvation in Krebs Ringer bicarbonate buffer (KRB), the ERES of *Drosophila* S2 cells are remodeled into large round non-membrane bound phase-separated Sec bodies. They are typically observed by immunofluorescence after staining of endogenous Sec16, Sec23 and expressed Sec24–GFP (Zacharogianni et al., 2014) (see **Fig. 1A,A'**). Importantly, Sec bodies are very quickly resolved upon stress relief (addition of growth medium). Finally, they appear to protect the components of the ERES from degradation (Zacharogianni et al., 2014) and they help cells to survive under conditions of amino acid shortage (Aguilera-Gomez et al., 2016; Zacharogianni et al., 2014).

Phase separation has been shown to be driven by specific components, the so-called drivers, either RNAs or proteins harboring structural features that become exposed or modified under certain conditions. In the case of Sec bodies, Sec24AB (Aguilera-Gomez et al., 2016; Zacharogianni et al., 2014) and Sec16 have been shown to drive Sec body coalescence (Aguilera-Gomez et al., 2016) in a manner that depends on a small stretch of 44 residues in Sec16 and on the mono-ADP-ribosylation enzyme by PARP16 (Aguilera-Gomez et al., 2016). This illustrates the critical role of post-translational modifications in phase separation (Bah and Forman-Kay, 2016; Owen and Shewmaker, 2019).

In parallel, changes in cytoplasmic biophysical properties have also been shown to be important in phase separation (Rabouille and Alberti, 2017), such as a drop of cytoplasmic pH within minutes, without post-translational modifications (Munder et al., 2016; Peters et al., 2013; van Leeuwen and Rabouille, 2019).

Here, we seek out to (1) identify the pathways elicited in S2 cells upon incubation

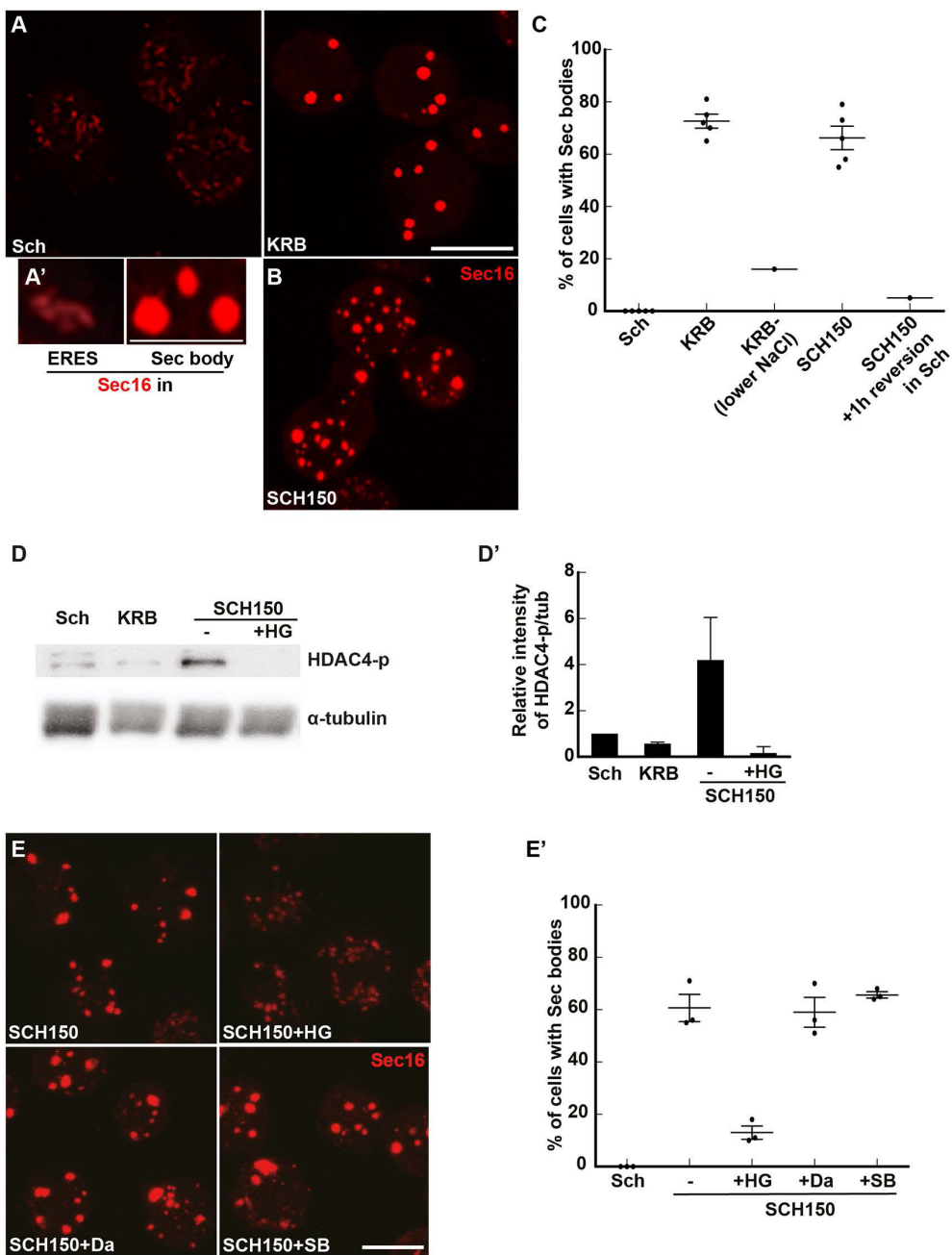




**Fig. 1. Salt stress activates the SIKs, which are involved in Sec body formation.** (A,A') Immunofluorescence (IF) visualization of endogenous Sec16 in S2 cells growing in Schneider's medium (Sch) and in cells incubated in KRB (A). Note the difference in the Sec16 pattern; Sec16 is at ER exit sites in growing cells and in Sec bodies in cells incubated in KRB. Upon KRB incubation, ERES remodel into larger structures, the Sec bodies, that are brighter than ERES. (B) IF visualization of Sec body formation (marked by Sec16) in cells incubated in Schneider's medium supplemented with 10 mM sodium bicarbonate and 150 mM of NaCl (SCH150) for 4 h at 26°C. (C) Quantification of Sec body formation (marked by Sec16) in cells incubated in Sch, KRB, KRB with lower NaCl (containing only 60 mM NaCl) and SCH150 for 4 h at 26°C as well as SCH150 and then in Sch for 1 h (reversion), showing that SCH150-induced Sec bodies are formed reversibly. (D,D') Western blot of S2 cells protein extract after incubation in Schneider's medium (Sch), KRB and SCH150 with and without HG-9-91-01 (5 µM) for 4 h at 26°C blotted for HDAC4-p and α-tubulin. Quantification of the ratio HDAC4-p to α-tubulin (D'). (E,E') IF Visualization (E) and quantification (E') of Sec body formation (marked by Sec16) in cells incubated in SCH150 supplemented or not with the SIK inhibitor HG-9-91-01 (HG, 5 µM), the Src inhibitor dasatinib (Da, 20 µM) and the p38 MAPK inhibitor SB203580 (SB, 30 µM) for 4 h at 26°C. Scale bars: 10 µm. Errors bars: s.e.m.

in the starvation medium KRB that lead to Sec body formation, and (2) to assess whether changes in the cytoplasmic biophysical properties play a role in the phase transition leading to Sec body formation. We show that amino acid starvation in KRB stimulates ER stress and activation of two downstream kinases, IRE1 and PERK (also known as PEK in flies) leading to the stimulation of the unfolded protein response (UPR) (Boyce and Yuan, 2006; Walter and Ron, 2011). However, the sole activation of the IRE1 and PERK does not lead to Sec body formation. To form Sec bodies in KRB, IRE1 and PERK activation needs to be combined with a moderate salt stress. Accordingly, KRB incubation is faithfully mimicked by cell incubation with dithiothreitol (DTT) and addition of 100 mM NaCl. Interestingly, a high-salt stress addition of 150 mM NaCl, which activates the salt-inducible kinases (SIKs; SIK2 and SIK3), is sufficient to efficiently drive Sec body formation. Importantly, we found that a decrease in the cytoplasmic ATP concentration, a general RNA degradation and the stimulation of the UPR are factors strongly correlated to Sec body formation.

## *Results*

### *Salt stress is necessary and sufficient for Sec body formation*

In an attempt to understand Sec body formation upon incubation in the starvation buffer KRB (Fig. 1A,A'), we noticed that the salt concentration of the Schneider's medium, in which S2 cells are grown, is much lower than that in mammalian tissue culture media [such as Dulbecco's modified Eagle's medium (DMEM)] and KRB, which is used as a starvation medium [for instance, 3-fold lower for Na<sup>+</sup> (i.e. 51 mM in Schneider's medium and 138 mM in KRB); Table 1]. Accordingly, we found that lowering the concentration of NaCl in KRB

---

(to 60 mM instead of the 120 mM in normal KRB (78 mM instead of 138 mM  $\text{Na}^+$ , Table 1) resulted in a decrease in Sec body formation (**Fig. 1C**), showing that NaCl is necessary for their formation. Conversely, the addition of 150 mM NaCl together with 10 mM sodium bicarbonate (SCH150, resulting in 211 mM  $\text{Na}^+$ ; **Table 1**) to Schneider's medium led to a substantial formation of reversible Sec bodies, as efficiently as incubating the cells in KRB (**Fig. 1A–C**).

Osmotic shock has been reported to trigger the formation of different stress assemblies, such as stress granules (Aulas et al., 2017; Bounedjah et al., 2012) and P-bodies (Jalihal et al., 2020; Kilchert et al., 2010). However, addition of 0.4–0.6 M sucrose does not elicit Sec body formation (**Fig. S1C**), even though the cell diameter significantly decreased by 22% (**Fig. S1A,B**). This shows that the shrinkage of the cell volume is not a factor leading to Sec body formation. Furthermore, neither the addition of 150 mM of KCl nor of sodium acetate instead of NaCl led to a substantial formation of Sec bodies (**Fig. S1C**). Taken together, these results suggest that increasing the  $\text{Na}^+$  concentration in Schneider's medium by 4-fold (referred to as salt stress), but not osmotic shock or  $\text{K}^+$  increase (**Table 1**), triggers a pathway that leads to Sec body formation.

To test this further, we aimed to increase cytoplasmic  $\text{Na}^+$  concentration and assess whether that was sufficient for Sec body formation by manipulating the abundant NaK ATPase present at the plasma membrane. NaK ATPase extrudes three  $\text{Na}^+$  ions against two  $\text{K}^+$  ions, and is the main pump that maintains the intracellular  $\text{Na}^+$  concentration low and compatible with cellular function. We found that the localization of NaK ATPase changes dramatically from intracellular puncta for cells in Schneider's medium to a strong plasma membrane localization in cells in SCH150 (**Fig. S1D**) together with a strong increase in its protein level (**Fig. S1E**), suggesting its involvement. Accordingly, incubation of cells with the NaK ATPase inhibitor ouabain in the growing medium SCH100 (161 mM  $\text{Na}^+$ , **Table 1**) led to a robust Sec body formation (**Fig. S1F,F'**), presumably because the cytoplasmic  $\text{Na}^+$  concentration increases, as  $\text{Na}^+$  can no longer be extruded. This shows that increasing  $\text{Na}^+$  in the cytoplasm is sufficient to drive Sec body formation, perhaps by mobilizing the NaK ATPase.

We then asked which pathway is activated downstream of increased  $\text{Na}^+$ . An increase in intracellular  $\text{Na}^+$  concentration is known to activate the SIKs, and in this regard, two SIKs (SIK2 and SIK3) are expressed in *Drosophila* (Teesalu et al., 2017; Wehr et al., 2013). To test this, we monitored the phosphorylation of a known SIK target, Histone Deacetylase 4 (HDAC4), which is phosphorylated upon SIK2 and SIK3 activation, and found

that it was also strongly (4-fold) activated in SCH150. Importantly, this SCH150-induced phosphorylation is 97% inhibited by addition of a pan-SIK inhibitor HG-9-91-01 (HG) (**Fig. 1D,D'**).

We then used HG to test the role of SIK activation in Sec body formation. Addition of HG reduces Sec body formation in 85% of the cells incubated in SCH150 (**Fig. 1E,E'**). As HG can also inhibit p38 MAPKs and Src (Clark et al., 2012), we used specific inhibitors for these two groups of kinases and assessed their potential to inhibit Sec body formation with SCH150. Neither the p38 MAPK inhibitor SB203580 nor the Src inhibitor Dasatinib, inhibited Sec body formation (**Fig. 1E,E'**), showing that the effect of HG can be attributed to SIK inhibition.

The above results not only show that S2 cells are fully responsive to HG, but also that SIK activation by increased NaCl concentration in the medium (inducing Na<sup>+</sup> stress) is a key pathway for Sec body formation.

*In addition to salt stress, amino acid starvation activates other pathways necessary for Sec body formation*

The data above opens the possibility that the formation of Sec bodies in the starvation medium KRB is simply be due to an elevated salt concentration (**Table 1**), unrelated to the absence of amino acids. However, this is not the case. When the Na<sup>+</sup> concentration in Schneider's medium and KRB are set to the same values (around 140 mM, KRB versus SCH84, **Table 1**), Sec bodies form very efficiently in KRB but not at all in SCH84 (**Fig. 2A'**). The major difference between these two media is that SCH84 contains 78 mM amino acids and serum, whereas KRB contains none. Since we have demonstrated previously that serum (that was dialyzed to remove free amino acids) does not play a role in Sec body formation (Aguilera-Gomez et al., 2016; Zacharogianni et al., 2014), this indicates that the presence of amino acids prevents Sec body formation even upon a moderate Na<sup>+</sup> stress.

**Table 1. Ion concentration in the different cell incubation media and buffers**

Total	Schneider's (Sch)	KRB	KRB lower NaCl	SCH84	SCH100	SCH150	Sch buffer	DMEM
Na <sup>+</sup> (mM)	51	138 (×2.7)*	78 (×1.52)	144 (×2.8)	161 (×3.15)	211 (×4.13)	56 (×1)	151 (×2.9)
Cl <sup>-</sup> (mM)	67	126 (×1.9)	66 (×1)	151 (×2.3)	168 (×2.5)	218 (×3.3)	87 (×1.3)	126 (×2.2)
K <sup>+</sup> (mM)	21	4.5 (×0.2)	4.5 (×0.2)	21 (×1)	21 (×1)	21 (×1)	21 (×1)	4.5 (×0.2)
HCO <sub>3</sub> <sup>-</sup> (mM)	5	15 (×3)	15 (×3)	15 (×3)	15 (×3)	15 (×3)	15 (×3)	29 (×6)
Glucose (mM)	11	10	10	11	11	11	10	25
Amino acids (mM)	78	-	-	78	78	78	-	10.4
Serum	10%	-	-	10%	10%	10%	-	10%
Sec bodies	No	Yes	No	No	No	Yes	No	

\*The (×) in bracket indicates the fold difference over the concentration in Schneider's medium.

To demonstrate this further, cells were incubated with KRB supplemented or not with amino acids. Addition of 5–40 mM amino acids to KRB strongly prevented Sec body formation (**Fig. 2A,A'**), and led to the reversion of KRB-triggered Sec bodies back to ERES (**Fig. 2A,A'**), almost as efficiently as the reversion in Schneider's medium (Zacharogianni et al., 2014). This suggests that, for an equivalent salt concentration, the presence of amino acids indeed prevents Sec body formation. This shows that amino acid starvation is instrumental to Sec body formation by potentiating  $\text{Na}^+$  stress. Alternatively, the presence of salt might potentiate pathways induced by amino acid starvation leading to Sec body formation, perhaps through SIK activation. To test this, we incubated cells in KRB in the presence of the SIK inhibitor HG, and found that Sec body formation was inhibited by 38% (**Fig. 2B**), suggesting their involvement.

However, HDAC4 (the SIK target mentioned above) does not appear to be phosphorylated upon incubation in KRB (**Fig. 1D,D'**). As above, to rule out an unspecific inhibition of other kinases by HG, we tested p38 MAPK and Src inhibitors, but found that these inhibitors do not affect KRB-induced Sec body formation (**Fig. 2C**). Furthermore, as SIKs are member of the AMPK family, we tested whether known inhibitors of AMPK affect KRB-induced Sec body formation. However, neither Dorsomorphin (compound C) (Weiss et al., 2010), nor ON123300 (Zhang et al., 2014) affected this (**Fig. 2C**), as was also the case for SCH150, showing that salt stress is largely mediated by SIKs. Furthermore, addition of the AMPK agonist AICAR (Ducommun et al., 2014) to Schneider's medium, even in the absence of amino acids (Sch buffer), did not lead to Sec body formation. This suggests that no AMPK family members other than SIKs are required for Sec body formation in cells incubated in KRB. Either HDAC4 is not a SIK target in KRB, or the HDAC4 protein is degraded in KRB, making the increased phosphorylation difficult to show experimentally.

As HG only inhibits KRB-triggered Sec body formation by 38%, not 80% as seen with SCH150 (**Fig. 2B**), these results show that the Sec body formation in KRB is the result of an interplay between  $\text{Na}^+$  stress (through increased NaCl concentration in the medium) and the absence of amino acids that triggers another stress. We therefore investigated which other pathways are triggered upon amino acid starvation in KRB.

*The sole inhibition of mTORC1 is neither sufficient nor necessary to trigger Sec body formation*

Mechanistic Target of Rapamycin Complex 1 (mTORC1) is the major sensor of amino acid level in the circulating medium (Kim and Guan, 2019). When amino acids are absent or low, the complex is inhibited, resulting in the inhibition of many anabolic pathways, and

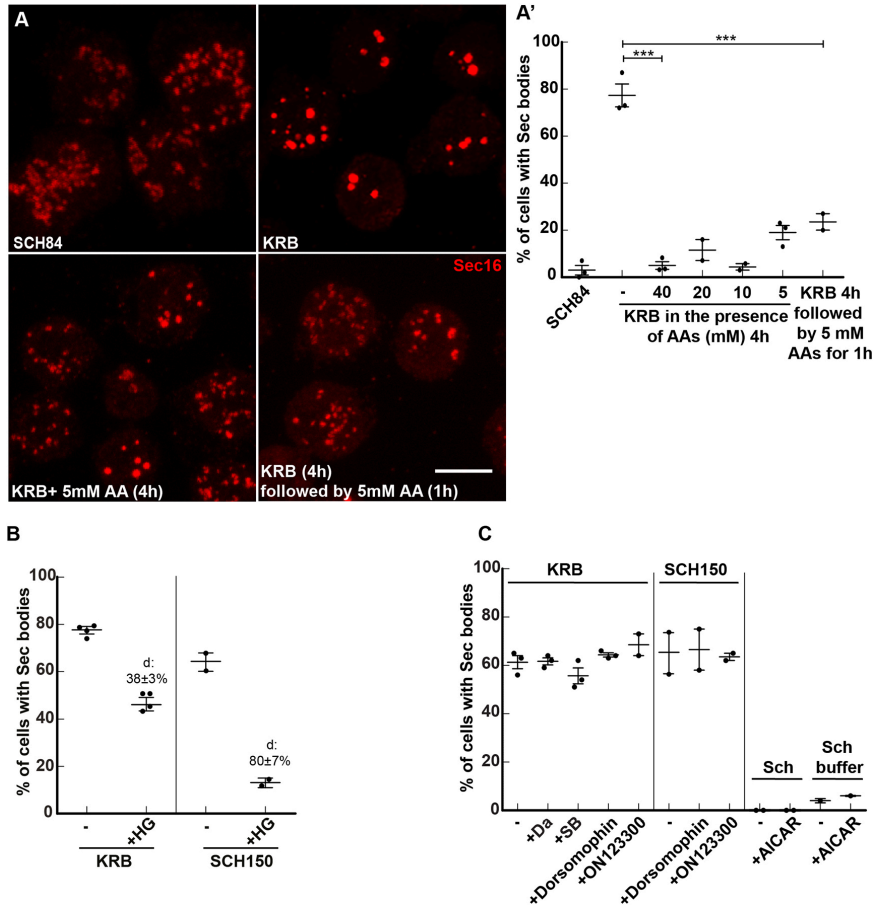


**Fig. 2. Amino acid starvation enhances cell salt stress-induced Sec body formation. (A,A') Immunofluorescence (IF) visualization (A) and quantification (A') of Sec body formation (marked by Sec16) in cells incubated in SCH84, KRB, KRB supplemented with 5–40 mM amino acids (AA) for 4 h at 26°C, as well as KRB for 4 h followed by addition of 5 mM amino acids for 1 h at 26°C. (B) Quantification of Sec body formation (marked by Sec16) in cells incubated in KRB and SCH150 with or without the SIK inhibitor HG-9-91-01(5 μM). (C) Quantification of Sec body formation (marked by Sec16) in cells incubated in KRB and SCH150 with or without the Src inhibitor dasatinib (Da, 20 μM), the p38 MAPK inhibitor SB203580 (SB, 30 μM), Dorsomorphin (1 μM) and ON123300 (10 μM) for 4 h at 26°C, as well in cells incubated in Schneider's medium (Sch) and Schneider's medium buffer supplemented with or without the AMPK activator AICAR (1 mM). 'd' indicates the mean±s.e.m. decrease in Sec body formation when compared to the absence of inhibitors. Scale bars: 10 μm. Errors bars: s.e.m.**

the activation of the degradative pathway of autophagy. We have previously shown that in S2 cells incubated with KRB, protein synthesis is inhibited very quickly, and the mTORC1 target S6 Kinase is no longer phosphorylated (**Fig. S2A**), and the autophagic pathway is activated (Zacharogianni et al., 2014). We also showed that the sole inhibition of mTORC1 by Rapamycin (Zacharogianni et al., 2014) and Torin (**Fig. S2B,B'**) is not enough to trigger the formation of Sec bodies. Similarly, depleting Raptor, the main subunit of mTORC1, does not trigger Sec body formation in growing cells (Zacharogianni et al., 2014). Finally, overexpression of TCS1, an endogenous inhibitor of mTORC1 (Condon and Sabatini, 2019) also failed to trigger the formation of Sec bodies (**Fig. S2C**). Taken together, although amino acid starvation does inhibit mTORC1 in S2 cells, Sec body formation is not a consequence of its sole inhibition.

*KRB incubation leads to oxidative stress but oxidative stress alone is not enough to trigger Sec body formation*

In order to determine which other pathways are stimulated by amino acid starvation in KRB, we performed bulk RNA sequencing and compared the results to those of cells grown in Schneider's medium. We detected 15,679 genes, including 1070 downregulated and 1635 upregulated (**Fig. S3A, Table S1**; see GEO: GSE143810). Interestingly, the strongest GO term associated with upregulated genes is oxidoreductase activity, including 20 genes expressing glutathione-S-transferase that are unregulated as well as a strong reduction in peroxiredoxin expression, suggesting that KRB could elicit oxidative stress (**Fig. S3B**), perhaps through reactive oxygen species (ROS) production.

To visualize the ROS production upon KRB incubation, we used DCF fluorescence measurements. KRB incubation elicits a specific, robust and steady increase of ROS production that is significantly inhibited by the ROS inhibitor N-acetyl-L-cysteine (NAC) (**Fig. S3C**). However, this does not prevent Sec body formation (**Fig. S3D'**). Furthermore, generating oxidative stress with arsenite (**Fig. S3D,D'**), ammonium persulfate (APS), or H<sub>2</sub>O<sub>2</sub> (data not shown) in growing cells in Schneider's medium does not lead to Sec body formation. Taken together, ROS are produced during KRB incubation but this is not sufficient to trigger Sec body formation.

*KRB incubation stimulates IRE1 activation*

Since Sec bodies are linked to the inhibition of the exit of newly synthesized proteins out of the ER, we investigated whether incubation in KRB stimulates ER stress, which is known to activate one or more of the three known downstream signaling pathways mediated by IRE1, PERK and ATF6 (Hetzel, 2012; Korennykh et al., 2009; Moore and Hollien, 2012).

IRE1 is an ER transmembrane protein that, when activated, dimerizes in the plane of the ER membrane, resulting in the autophosphorylation of its kinase domain (Walter and Ron, 2011). Cells incubated in the starvation medium KRB display a clear phosphorylated IRE1 (IRE1-p) signal when compared to cells in Schneider's medium, which is as strong as that seen upon addition of DTT, a known IRE1-activating agent (**Fig. 3A**). In the absence of antibodies to *Drosophila* IRE1, we tested whether the expression level of the kinase was modified by KRB treatment by monitoring the level of its mRNA by PCR, but this is not increased by this treatment (**Fig. 3B**). Importantly, we tested whether IRE1 activation was modulated by the presence of amino acids in the medium. We found that IRE1 is 34% less phosphorylated when KRB was replenished with amino acids than in KRB alone (**Fig. 3A**), partly sustaining the notion that amino acid starvation activates IRE1. Importantly, addition of the IRE1 kinase attenuator AMG18 (see below) completely prevented its phosphorylation (**Fig. 3A**).

The autophosphorylation of IRE1 in turn stimulates its nuclease activity, leading to the specific splicing of *xbp1* mRNA that is then translated into a potent transcription factor transcriptionally upregulating molecular machineries that resolve the overload of misfolded proteins in the ER (Walter and Ron, 2011), such as the UPR. IRE1 nuclease activity also triggers IRE1-dependent decay of mRNA (RIDD), a less-specific degradation of mRNAs that are largely associated to the ER (Hollien et al., 2009), which is also likely to relieve the ER burden of translocation and protein folding.

Both incubation in KRB and addition of DTT to Schneider's medium led to a clear spliced *xbp1* [*xbp1s*, representing 40% of the total in KRB, and 69% in DTT when compared to in Schneider's medium (**Fig. 3C**)]. In agreement with the decrease in IRE1-p, *xbp1* splicing in KRB was also 25% less pronounced in the presence of amino acids (**Fig. 3C**). This confirms that amino acid starvation leads, at least partly, to the activation of IRE1. Accordingly, inhibition of IRE1 nuclease activity by 4u8C totally inhibited *xbp1* splicing in KRB (**Fig. 3C**), suggesting that IRE1 is involved and that the drug works efficiently in S2 cells.

To test whether activation of IRE1 triggers the UPR, we first monitored the Bip (also known as Hsc70-3 in flies) protein level, and found that this was increased 4-fold upon DTT addition (as expected) and 2.3-fold upon KRB, suggesting that the UPR is stimulated via IRE1 activation (**Fig. 3D,D'**). However, we found that 4u8C was only moderately powerful in suppressing Bip upregulation, suggesting that other pathways are likely to promote the UPR (such as that mediated by PERK, **Fig. 4E**, see below). Indeed only the combined inhibition of IRE1 and PERK suppressed Bip upregulation (**Fig. 3D'**). Surprisingly, we also



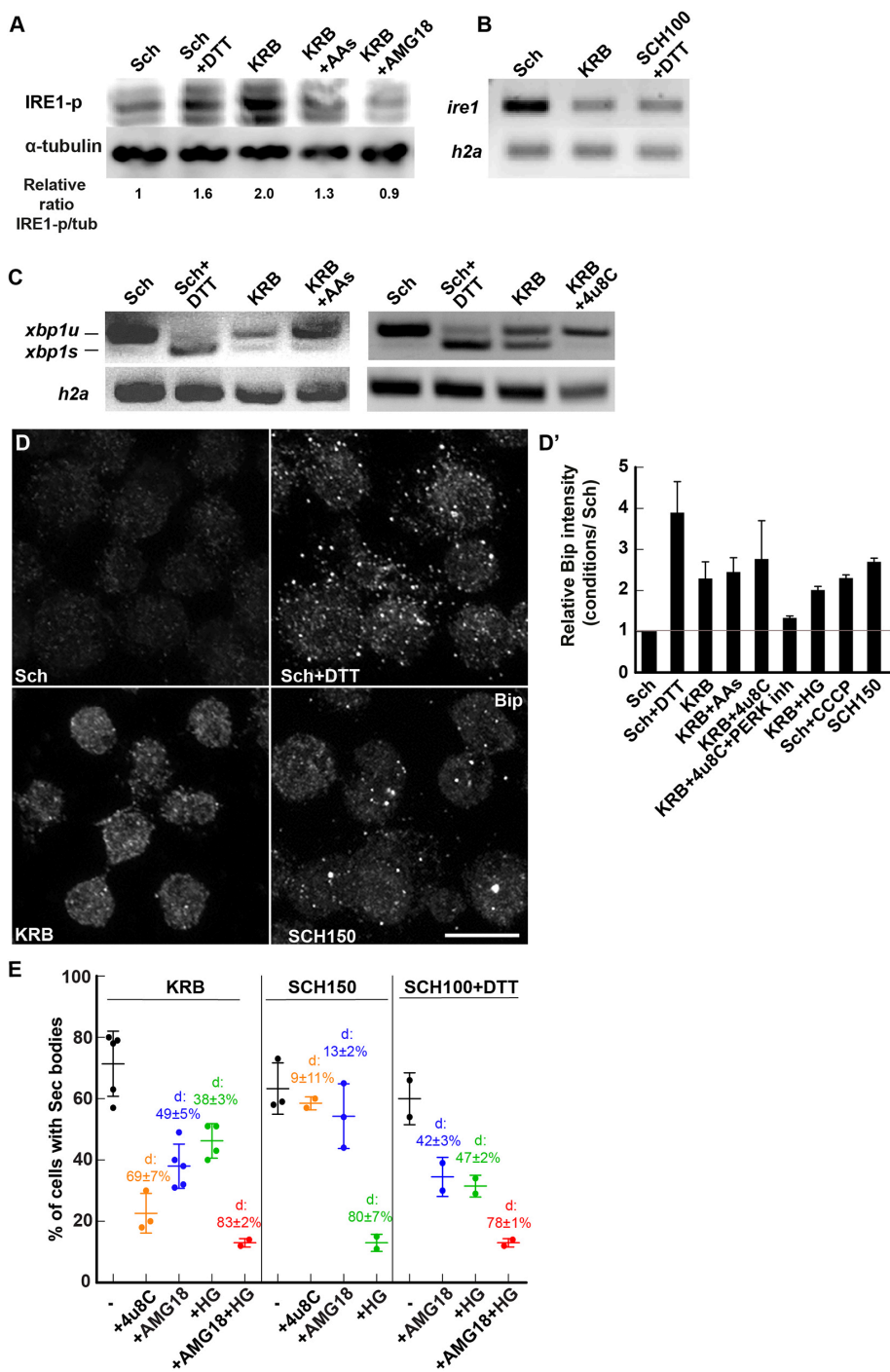




**Fig. 3. KRB incubation activates IRE1.** (A) Western blot visualization of IRE1-p (using the anti IRE1-p antibody, Genentech) in cells in Schneider's medium (Sch), Sch+DTT (5 mM), KRB, KRB+amino acids (AAs) (5 mM) and KRB+AMG18 (10  $\mu$ M) for 4 h after blotting. Note that KRB incubation elicits IRE1-p more strongly than Sch+DTT, and that addition of AAs to KRB partially reverses this phosphorylation. Addition of the IRE1 kinase attenuator AMG18 (10  $\mu$ M) strongly inhibits IRE1-p formation. Quantification underneath is the ratio of IRE1-p (middle band) to  $\alpha$ -tubulin for the blot shown. (B) Visualization of the PCR products of *ire1* and *h2a* mRNAs from cells incubated in Sch, KRB and SCH100+DTT for 4 h at 26°C. (C) Visualization of spliced (*xbp1s*) and unspliced (*xbp1u*) PCR products of *xbp1* upon conditions indicated on the panel. (D,D') Immunofluorescence visualization (D) of the protein Bip in cells incubated in the conditions indicated on the panel. Quantification is in D'. Note that the UPR is stimulated in KRB and many other conditions. (E) Quantification of Sec body formation (marked by Sec16) in cells incubated in KRB, SCH150 or SCH100+DTT with or without 4u8C (30  $\mu$ M), AMG18 (10  $\mu$ M), HG (5  $\mu$ M) or AMG18+HG. 'd' indicates the mean $\pm$ s.e.m. decrease in Sec body formation when compared to the absence of inhibitors. P-value (SCH150 and SCH150+AMG18) is 0.104 and the P-value (KRB and KRB+HG) is 0.0019. The other differences are highly significant (<10<sup>-4</sup>). Errors bars: s.e.m. Scale bar: 10  $\mu$ m.

3

found that incubating S2 cells in high salt (SCH150) also triggered an increase in Bip protein level, suggesting a yet-to-be-elucidated interplay between salt stress and the UPR stimulation (Fig. 3D'). This appears to be independent of SIK activation, as HG addition did not modify the observed Bip upregulation (Fig. 3D').

To further test the stimulation of the UPR in KRB, we also monitored the level of UPR RNA targets, such as *bip* RNA, *xbp1* itself and *gadd45* (Fig. 3C, Fig. S4A,D). All were elevated upon addition of DTT, as expected (Fig. S4A,D), but not in KRB. In fact, except for *gadd45*, which did not change, the level of both *bip* and *xbp1* mRNAs were only 70% of the level in Schneider's medium, suggesting that these RNAs are partially degraded (Fig. S4A,D), making it difficult to precisely evaluate the stimulation of the UPR.

To test RIDD, we monitored the mRNA level of three RIDD targets, *indy*, *PIG-Wa* and *sparc* (Gaddam et al., 2012; Hollien and Weissman, 2006). We found that both *indy* and *PIG-Wa* (but not *sparc*) expression was lower in cells incubated in KRB when compared to cells in Schneider's medium (Fig. S4B,D). These results suggest that KRB incubation leads to IRE1 activation in turn activating the UPR, but also to RNA degradation, perhaps via RIDD.

If RIDD is the mechanism underlying the observed decreased level of these RNAs, it should be inhibited in the presence of 4u8C. We therefore monitored *bip* and *indy* RNA levels under this condition, but this treatment did not strongly rescue the *bip* and *indy*

level (**Fig. S4C,D**) suggesting that the overall RNA degradation observed in KRB is likely not to occur via RIDD. In parallel, we tested the effect of the amino acid starvation on the degradation of these mRNAs (UPR and RIDD targets), and found that they all are rescued by addition of 5 or 40 mM amino acids (**Fig. S4A,B,D**). These results indicate that RNA degradation is downstream of the amino acid starvation but does not occur via RIDD. Altogether, we conclude that KRB activates IRE1, the UPR and a non RIDD general pathway of RNA degradation that is strongly modulated by the absence of amino acids.

### *IRE1 activation is necessary for Sec body formation but not sufficient*

We then asked whether IRE1 activation is necessary for Sec body formation. To test this, we used the IRE1 kinase activity attenuator AMG18 and 4u8C to monitor KRB-induced Sec body formation. Both inhibitor treatments substantially inhibited Sec body formation (49% for AMG18 and 69% for 4u8C) (**Fig. 3E**), indicating that IRE1 activity is necessary for Sec body formation. Of note, AMG18 is fully functional on *Drosophila* IRE1. Indeed, the kinase site of *Drosophila* IRE1 is very similar to the human enzyme (**Fig. S4E**). Furthermore, using AMG18 at either 10, 20 or 50  $\mu$ M during the KRB incubation inhibits Sec body formation to the same extent (**Fig. S4F**). Finally, the drug is 84% effective at blocking IRE1-p formation induced by thapsigargin (**Fig. S4G**). These results show that AMG18 is fully active in S2 cells.

The above results show that IRE1 activation is necessary for Sec body formation. However, it is not sufficient. First, activating IRE1 (through incubation with DTT) does not lead to Sec body formation (**Fig. 4A,B**). This is further supported by the finding that expression of a constitutive active form of IRE1 in which the three serine residues of the catalytic site have been mutated to aspartic acid (S703D, S705D and S708D) (Chang et al., 2018b; Yan et al., 2019) also does not lead to Sec body formation (**Fig. 4B,C**). This indicates that in addition to IRE1 activation, other pathways are stimulated.

As mentioned above, ER stress can also activate PERK (Hetz, 2012). In this regard, we found that eIF2 $\alpha$ , an important PERK target that regulates translation, is strongly phosphorylated in cells in KRB, as much with addition of DTT to Schneider's medium (**Fig. 4D**). We then tested whether PERK activity was required for Sec body formation. Both PERK depletion by RNAi and PERK pharmacological inhibition by GSK2606414 led to a 50% reduction of Sec body formation upon KRB incubation (**Fig. 4E**). On the other hand, ATF6, the third pathway downstream of ER stress is not involved, as of ATF6 depletion by RNAi did not modify the degree of KRB-induced Sec body formation (**Fig. 4E**). This suggests that, parallel to IRE1 activation, PERK activity (but not ATF6) is also necessary for Sec body

formation. This is also supported by the fact that combined inhibition of IRE1 and PERK in KRB leads to an 84% inhibition of Sec body formation (**Fig. 4E**). This is in line with the combined inhibition of PERK and IRE1 inhibiting the stimulation of the UPR (**Fig. 3D'**).

*A combination of moderate salt stress with IRE1 and PERK activation leads to Sec body formation*

Although addition of DTT to Schneider's medium activates both IRE1 and PERK, it still does not lead to Sec body formation (**Fig. 4A, D**). Given the effect of the SIK inhibitor HG on KRB-stimulated Sec body formation (suggesting of SIKs activation) (**Fig. 2B**), we tested whether Sec body formation in KRB is recapitulated by activating IRE1 and PERK activation through DTT (5 mM) together with applying a moderate salt stress [SCH100 (161 mM Na<sup>+</sup>), equivalent to KRB (138Mm Na<sup>+</sup>); Table 1]. Strikingly, we found that SCH100 plus DTT (**Fig. 4F,F'**) is as efficient as KRB in inducing the formation of largely reversible Sec bodies. To assess further the equivalence between SCH100 plus DTT and KRB, we again used AMG18 and 4u8C (**Fig. 3E**), combined with the SIK inhibitor HG. AMG18 and 4u8C incubation resulted in a similar decrease in the Sec body response in both KRB and SCH100 plus DTT (~45%). When IRE1 and SIK were inhibited together, the Sec body formation was also similarly strongly inhibited (**Fig. 3E**).

Taken together, Sec body formation in KRB is largely recapitulated by a moderate salt stress activating SIKs combined with ER stress triggered by amino acid starvation, which activates IRE1 and PERK (SCH100 plus DTT).

*The cytoplasm acidifies upon KRB incubation*

As mentioned in the introduction, signaling pathways and/or change in the biophysical properties of the cytoplasm (Rabouille and Alberti, 2017; van Leeuwen and Rabouille, 2019) are critical for phase separation leading to the formation of stress assemblies. We therefore questioned how the biophysical cytoplasmic features are affected by the activation of these two pathways.

In glucose-starved yeast, the phase separation of proteasome subunits into proteasome storage granules and the formation of metabolic enzymes foci have been shown to occur through a drop in the cytoplasmic pH in a necessary and sufficient manner (Munder et al., 2016; Peters et al., 2013; van Leeuwen and Rabouille, 2019). We hence asked whether the cytoplasmic pH of the S2 cell cytoplasm also changed upon incubation in KRB and whether this is relevant to Sec body formation.

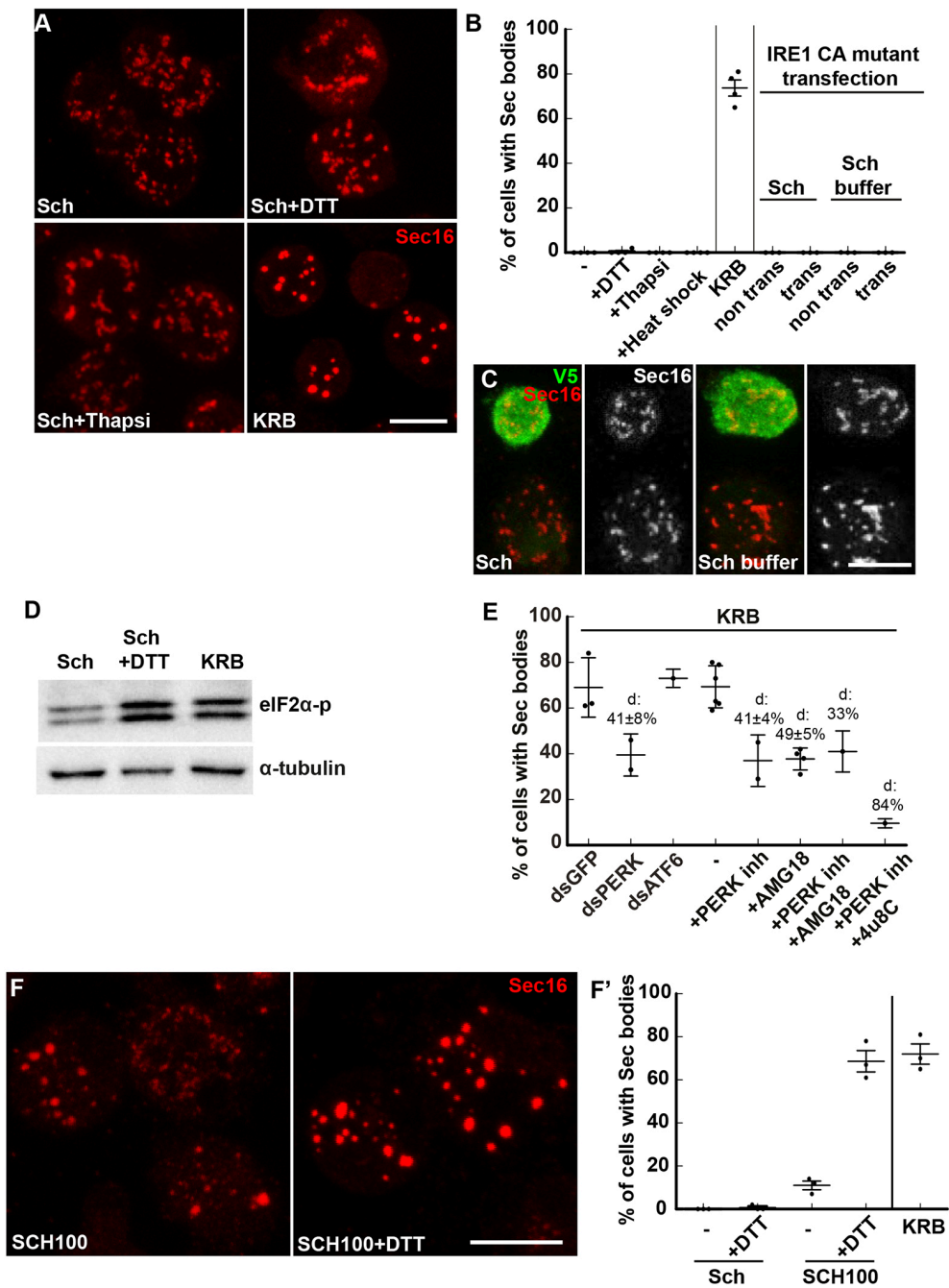


**Fig. 4. KRB incubation is mimicked by a moderate salt stress combined with activation of IRE1 and PERK. (A–C)** Immunofluorescence (IF) micrographs of Sec16 in cells in Schneider’s medium (Sch), KRB, Sch supplemented with DTT (5 mM) and thapsigargin (Thapsi, 2  $\mu$ M) for 4 h at 26°C **(A)**. Overexpression of the constitutively active (CA) IRE1 mutant tagged by V5 (in green) in cells incubated in Sch and Schneider’s buffer **(C)**. A quantification of the percentage of cells with Sec bodies is shown in B. Trans, transfected. **(D)** Western blot visualization of eIF2 $\alpha$ -p in cells in Sch, Sch+DTT (5 mM) and KRB. **(E)** Quantification of Sec body formation (marked by Sec16) upon PERK depletion, PERK inhibition (5  $\mu$ M), combined inhibition of PERK and IRE1 kinase (AMG18), and PERK and IRE1 nuclease (4u8C), as well as ATF6 depletion upon KRB incubation for 4 h at 26°C. ‘d’ indicates the mean $\pm$ s.e.m. decrease in Sec body formation. **(F,F’)** Visualization **(F)** of Sec body formation (marked by Sec16) in cells incubated in SCH100 and SCH100+DTT (5 mM) for 4 h at 26°C. Quantification in **F’**. Errors bars: s.e.m. Scale bars: 10  $\mu$ m.

---

To do this, we used a cell-based assay to estimate the ratio of intensity of pHluorin versus mCherry in cells transfected with a pHluorin–mCherry cytoplasmic probe (Brett et al., 2005; Miesenböck et al., 1998). pHluorin is a pH-sensitive GFP mutant that changes its fluorescent spectrum at certain pHs. Upon KRB incubation, we observed that the cytoplasmic pH decreased, illustrated by a decrease in the ratio of pHluorin to mCherry when compared to cells grown in Schneider’s medium where it remains largely constant (**Fig. S5A,A’**). We estimate that the cytoplasm of growing cells is at pH 6.8, whereas the pH of the cytoplasm of KRB-incubated cells is 6 (**Fig. S5A,A’**), suggesting a drop of nearly 1 pH unit. Interestingly, this result suggests that, similar to what occurs in yeast, nutrient starvation leads to a reduction of the cytoplasmic pH pointing to a conserved mechanism (Rabouille and Alberti, 2017; van Leeuwen and Rabouille, 2019). However, we found that arsenite treatment of S2 cells also leads to a similar pH drop. Given that this treatment does not lead to Sec body formation and this indicates that the decrease in pH is likely not to be a prime driver for Sec body formation.

*Sec body formation is largely associated to a drop in the cytoplasmic ATP concentration*

In glucose-starved yeast, the pH drop has been shown to be the consequence of a decrease in the intracellular ATP concentration (due to a reduction of glycolysis) (Munder et al., 2016). Using a luciferase-based assay, we therefore measured the intracellular ATP concentration in S2 cells in KRB. The intracellular concentration steadily and specifically decreases after 1 h incubation in KRB incubated cells (**Fig. 5A**). We estimate the intracellular ATP concentration to be 1.7 mM (**Fig. 5B**) in growing cells, a concentration that decreases by 50% after 3 h incubation in KRB (**Fig. 5A,B**). These results show that the sharp decrease in intracellular ATP concentration correlates with Sec body formation.

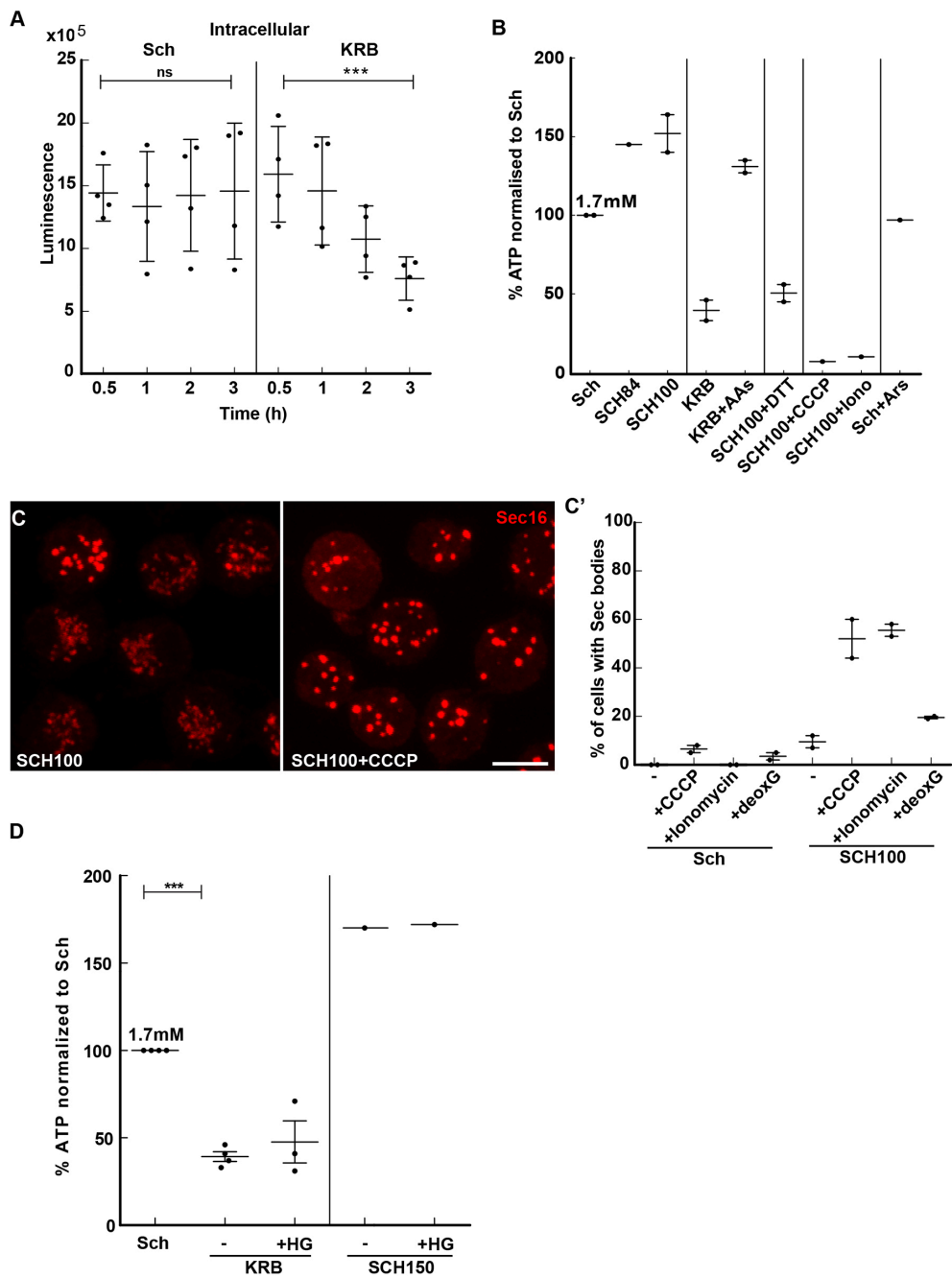


**Fig. 5. The decrease of the intracellular ATP level is one driving factor for Sec body formation. (A)** Luminescence intensity measuring the intracellular ATP concentration of S2 cells during incubation in Schneider's medium (Sch) and KRB. Note that the ATP concentration decreases by 48% after 4 h incubation in KRB. ns, not significant; \*\*\* $P < 0.001$ . **(B)** Quantification of the change in the intracellular ATP concentration (percentage when compared to Sch, which is set to 100%) after 4 h incubation in the different conditions presented on the panel (see Table 1 and Table S2). AA, amino acids; Iono, ionomycin; Ars, arsenite. **(C,C')** Visualization of Sec16 **(C)** and quantification **(C')** of Sec body formation (marked by Sec16) in cells supplemented by CCCP (25  $\mu$ M), ionomycin (2.8  $\mu$ M) and 2-deoxyglucose (deoxG; 20 mM) for 4 h at 26°C. **(D)** Quantification of the change in the intracellular ATP concentration (percentage when compared to Sch, which is set to 100%) upon SIK inhibition with HG-9-91-01 (HG, 5  $\mu$ M) in KRB and SCH150. Scale bar: 10  $\mu$ m. Errors bars: s.e.m.

To investigate further whether the decrease in cytoplasmic ATP could be a driving factor in Sec body formation, we assessed the ATP level in experimental conditions that induce Sec body formation (**Fig. 5B**). In particular, incubation in SCH100 plus DTT induces a severe drop in the intracellular ATP. Furthermore, incubation with ouabain leads to an ATP decrease (and Sec body formation; **Fig. S1F**). Conversely, in cells incubated in KRB supplemented with 5 mM amino acids, where Sec body formation is largely inhibited, the intracellular ATP concentration is not decreased (**Fig. 5B**). Similarly, arsenite (which also does not lead to Sec body formation) also does not cause a drop in ATP. Overall, the conditions where Sec bodies form appear to be those where the ATP is the lowest.

To test whether a drop in intracellular ATP drives Sec body formation, we used two approaches. We first inhibited the ATP production of growing cells by blocking the mitochondrial OXPHOS with CCCP and ionomycin (**Fig. 5C,C'**), as well as by blocking glycolysis with 2-deoxyglucose. Strikingly, cells incubated in SCH100 supplemented by either CCCP or ionomycin had a robust Sec body formation, supporting the idea that a drop in intracellular ATP induces the formation of Sec bodies (**Fig. 5C,C'**). Incubation with 2-deoxyglucose also induced a consistent but small degree of Sec body formation (**Fig. 5C'**), suggesting that S2 cells rely more on mitochondrial respiration than on glycolysis.

Second, we developed a semi-intact cell (SIC) system using digitonin to gently permeabilize the S2 cell plasma membrane (**Fig. 6A**). The specific incubation of the permeabilized cells with KRB at pH 7.4 for 2 h led to Sec body formation in 38% of the cells (**Fig. 6B**). We confirmed that the pH of the buffer and the presence of NaCl is critical, as KRB at pH 6 and replacing Cl<sup>-</sup> in the KRB with acetate did not lead to Sec body formation (**Fig. 6B**). To test the role of a low concentration of ATP in Sec body formation, KRB was supplemented with 0.5 mM ATP and this led to a strong inhibition of Sec body formation



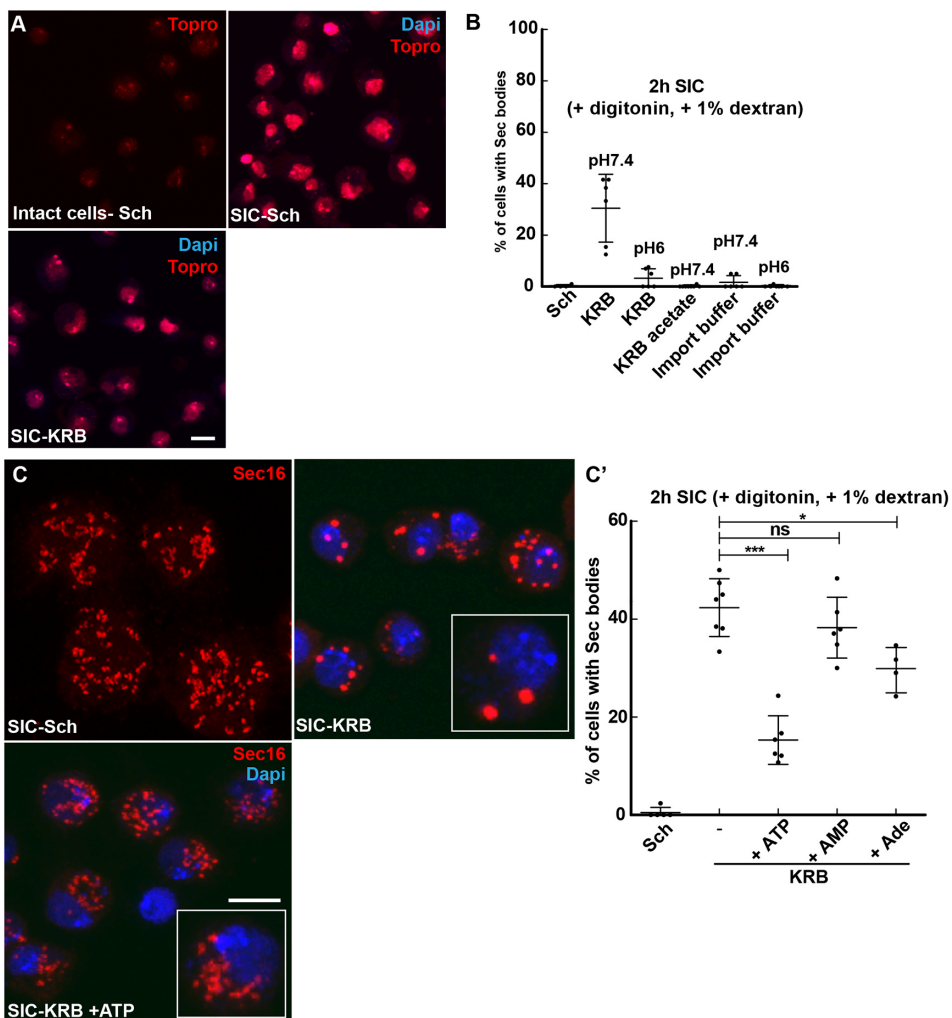


**Fig. 6. Addition of ATP to semi-intact cells prevents Sec body formation. (A)** Visualization of S2 cells permeabilization using the non-membrane permeant TO-PRO-3 in intact cells in Schneider's medium (Sch) and in semi-intact cells (SICs;+10  $\mu$ g/ml digitonin,+1% dextran) incubated in Sch and KRB for 2 h at 26°C. Note that TO-PRO-3 stains the nucleus only in the SIC system. **(B)** Effect of buffer composition in the formation of Sec bodies in SICs for 2 h at 26°C. Decreasing the pH of KRB from 7.4 to 6 decreases the efficiency of Sec body formation. Replacing Cl<sup>-</sup> by acetate in the KRB and replacing KRB by the import buffer (20 mM HEPES, 110 mM KAc, 2 mM MgAc and 0.5 mM EGTA) abolishes Sec body formation. **(C,C')** Immunofluorescence visualization of Sec16 (red, **C**) and quantification of Sec body formation (**C'**) (marked by Sec16) in the SIC system for cells incubated in Sch, in KRB and in KRB supplemented with 0.5 mM ATP, 0.5 mM AMP and 0.5 mM Adenosine. Cells in the white box are magnified 2.5 times. Scale bars: 10  $\mu$ m. Errors bars: s.d. ns, not significant; \*P<0.05, \*\*\*P<0.001.



(**Fig. 6C,C'**). This is specific for ATP, as addition of AMP or adenosine did not lead to this strong inhibition (**Fig. 6C,C'**). These two results indicate that the intracellular ATP concentration modulates the phase separation of Sec bodies.

We then assessed whether the ATP drop is upstream or downstream of ER stress (activation of both IRE1 and PERK leading to UPR). To test this, we monitored the Bip protein level in CCCP-treated cells (**Fig. 3D'**) and found that it was increased, as in KRB. This suggests that lowering ATP cytoplasmic concentration appears to be upstream of ER stress and UPR activation. Taken together, the lowering in the cytoplasmic ATP concentration appears to be a key factor driving Sec body formation.

However, in conditions of high-salt stress through SCH150, the cytoplasmic concentration of cytoplasmic ATP does not change. Furthermore, addition of the SIK inhibitor has also no effect on the ATP change (**Fig. 5D**). This suggests that SIK activity is not instrumental to this ATP drop, and that Sec bodies can form even when the concentration of the ATP is not lowered.

### *RNA degradation*

The above results show the decrease in the ATP cytoplasmic concentration does not appear to be a common factor underlying Sec body formation in both KRB and SCH150. In search for a communality, we further investigated the overall decrease in RNA levels that we observed in both cells incubated in KRB and SCH150 (**Fig. S5C**). This decrease was also more specifically measured for bip, xbp1, indy and PIG-Wa (**Fig. S4C**). We therefore explored the possibility that Sec body formation is linked to RNA degradation. We first examined whether Sec bodies form to protect a set of RNAs from degradation, similar to what is thought to be the case for stress granules (Leung et al., 2006). We first monitored whether Sec bodies contain full-length RNAs by performing single-molecule fluorescence in situ hybridization (smFISH) using an oligo(dT) probe. As expected, stress granules (which also form upon incubation in KRB, marked here by the RNA-binding protein FMR1; Aguilera-Gomez et al., 2016), strongly colocalize with polyA-tailed RNAs, but Sec bodies are negative (**Fig. S5D**). This indicates that Sec bodies do not contain polyA-tailed RNAs, at least not in sufficient amounts to be detected by this method.

We then explored whether Sec bodies template around degraded RNAs. To test this, we used the SIC system of cells incubated in Schneider's medium where Sec bodies do not form (**Fig. 6C**), to which was added RNase 1 to degrade RNAs to nucleotides. However, this did not lead to Sec body formation (not shown). Finally, we added the total pool of

---

RNAs from cells incubated in KRB to the SIC system in Schneider's medium. However, this also did not lead to Sec body formation (not shown). Consequently, in our hand, RNA degradation is not functionally linked to Sec body formation.

In conclusion, we propose that the UPR activation both by amino acid starvation in KRB and salt stress in SCH150 is more likely to be a key factor in Sec body formation.

### *Discussion*

Here, we show that the Sec bodies that form in *Drosophila* S2 cells incubated in KRB are fully recapitulated by activation of SIKs, IRE1 and PERK (through SCH100 plus DTT), leading to the activation of a downstream UPR. Strikingly, the strong activation of SIKs in (SCH150) also induces the UPR and leads to Sec body formation. The resulting structures in each condition appear to be similar in size and number, and their formation is reversible. Whether their content is strictly similar has not been addressed here.

3

Taken together, our results show that Sec body formation requires the stimulation of two main signaling pathways (**Fig. 7**). The first is the salt stress pathway (addition of 150 mM NaCl), which activates the SIKs in a necessary and sufficient manner. It also does not lead to a change in the cytoplasmic ATP concentration. It does induce RNA degradation and it stimulates the UPR in an unexpected manner, given that PERK and IRE1 inhibitors do not alter SCH150 driven Sec body formation (**Fig. 7**).

The second pathway is the activation of IRE1 and PERK (but not ATF6), downstream of ER stress, which is partly induced by the absence of amino acids in KRB. Activation of either IRE1 or PERK is necessary but not sufficient. To form Sec bodies, this activation needs to be combined with a moderate salt stress. We propose that IRE1 and PERK activation combined with SIK activation occur in KRB, which is recapitulated by SCH100 plus DTT. This is associated with a decrease in the cytoplasmic concentration of ATP, with RNA degradation and with a stimulation of the UPR. Interestingly, both strong salt stress (SCH150) and KRB lead to the activation of the UPR (measured by the increase in Bip protein level), leading to the possibility that SIKs, IRE1 and PERK interact with and/or activate, each other. Either IRE1 and/or PERK activate the SIKs, or SIK activation activates IRE1 and/or PERK. This still needs to be refined.

#### *The prominent role of salt stress and SIKs in remodeling the cytoplasm*

Strong salt stress is induced by a 4-fold increase of Na<sup>+</sup> in the medium combined with bicarbonate. This triggers an increase of Na<sup>+</sup> in the cytoplasm that activates one or more SIK (as shown by the phosphorylation of the SIK target HDAC4). Accordingly, SIK inhibition

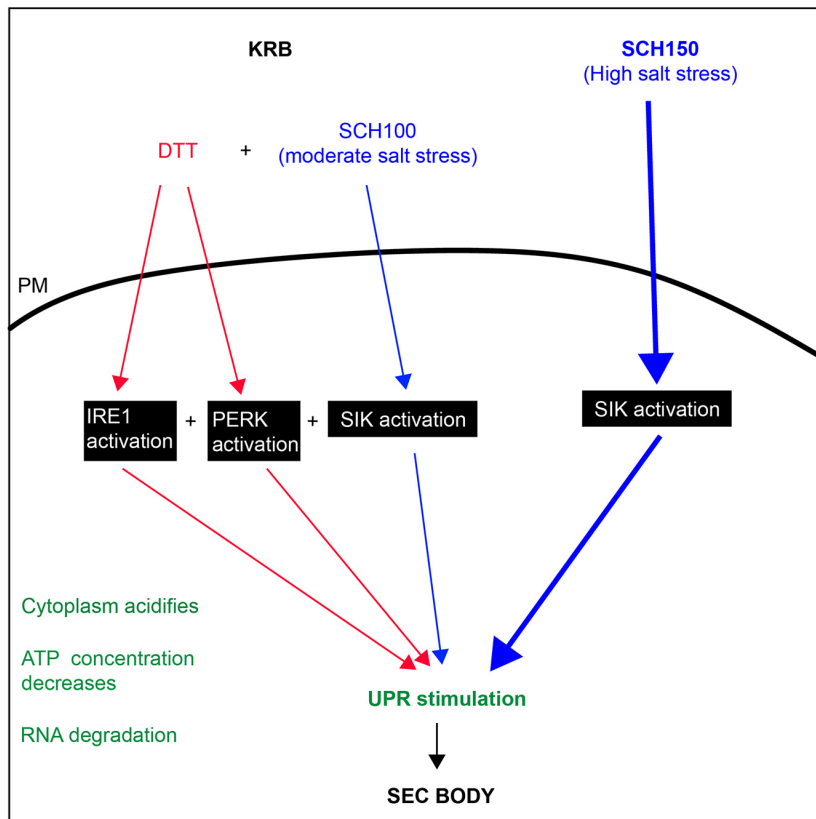


**Fig. 7. Activation of SIK, IRE1 and PERK and SIK to form Sec bodies.** Blue pathway, Sec bodies can form upon high-salt stress (SCH150) through SIK activation, which, when strong is sufficient. A moderate salt stress also activates SIKs, but it is not enough to stimulate Sec body formation. Red pathway: amino acid starvation in KRB leads to IRE1, PERK and SIK activation leading to Sec body formation (mimicked by SCH100+DTT). IRE1 and PERK activation are necessary but not sufficient. In green are features appearing upon KRB incubation, such as cytoplasm acidification, a decrease in the cytoplasmic ATP concentration and the stimulation of the UPR that we propose to be a key factor in Sec body formation.

decreases Sec body formation.

Keeping intracellular  $\text{Na}^+$  as near as possible to physiological concentrations (5 mM) is critical for cellular life, and the cell spends 40% of its available ATP to extrude  $\text{Na}^+$  against  $\text{K}^+$  with the NaK ATPase (Jaitovich and Bertorello, 2010). It is therefore not surprising that  $\text{Na}^+$  stress would elicit a cytoprotective response, such as prominent as

Sec body formation (and stress granule formation in mammalian cells; Yan et al., 2014). This will need to be further elucidated, as many organisms and tissues are subjected to increased circulating  $\text{Na}^+$ . We show, however, that it is not equivalent to an osmotic shock and that this addition of salt does not lead to a decrease in a cell volume. In contrast to P-bodies in yeast (Jalihal et al., 2020; Kilchert et al., 2010), osmotic stress does not induce Sec bodies. Interestingly,  $\text{Na}^+$ /salt stress has recently been shown to induce the biogenesis of the lysosomal pathway (i.e. more endo/lysosomes as well as an increase in its activity) via TFEB and TOR (Lopez-Hernandez et al., 2020).

Increased  $\text{Na}^+$  activates the intracellular  $\text{Na}^+$ -sensor network revolving around the SIKs (Jaitovich and Bertorello, 2010). The SIKs belong to the family of AMPKs, and have been shown to be part of a nutrient-sensing mechanism so far revolving around glucose (Wein et al., 2018) and unbalance of the ATP-to-ADP ratio. In mammals, there are three genes encoding SIK (SIK1–SIK3) but only 2 in *Drosophila*. *Drosophila* SIK2 is the ortholog of human SIK1 and SIK2, and has been shown to have a link to the fly Hippo pathway (Wehr et al., 2013), possibly linking nutrient to growth. *Drosophila* SIK3 is required for glucose sensing in the fly (Teesalu et al., 2017). Which SIK is involved in Sec body formation has not been clarified, as overexpression of each SIK individually has not proven enough to trigger Sec body formation, even when combined to some excess salt (SCH84 or SCH100). However, at least two SIKs appear to change their intracellular localization in KRB, that is, SIK2 and the long SIK3 isoform, which appear to cluster near the plasma membrane and localize to the nuclear envelope (data not shown). The role of SIKs in the formation of stress assemblies (here the Sec bodies) appears important and novel, and needs to be investigated further. Other members of the AMPK family do not appear to be involved and changing the ratio ADP-to-ATP did not alter Sec body formation in our SIC system (not shown).

#### *IRE1 and PERK activation combined to SIK activation*

Although a high salt stress is sufficient to trigger Sec body formation, the Sec body formation observed during incubation in the amino acid starvation buffer KRB elicits another pathway, the ER stress pathway, leading to the activation of both IRE1 and PERK. Indeed, KRB-induced Sec body formation is entirely mimicked by a moderate salt stress (SCH100, **Table 1**) combined with activation of IRE1 and PERK induced by DTT (SCH100 plus DTT).

#### *UPR stimulation*

Surprisingly, we find that salt stress as well as KRB induces the UPR, which we find is a common downstream event in all conditions inducing Sec body formation. How salt stress

activates the UPR and the exact role of IRE1 and PERK is still not fully understood. It does not appear to be via SIKs, as HG does not modulate the UPR, yet strongly reduces Sec body formation. Conversely, IRE1 and PERK inhibitors do not influence SCH150-induced Sec body formation, so the exact link between IRE1, PERK, SIKs and the UPR remains to be further investigated.

How UPR stimulation induces Sec body formation is not completely understood. It could occur through the clustering of IRE1 and PERK, two membrane kinases, and them forming a template in the plane of the ER membrane. In this regard, UPR stimulation has been linked to the MARYlation enzyme *Drosophila* PARP16 (Jwa and Chang, 2012), which is also a transmembrane protein of the ER that undergoes a remodeling in KRB (Aguilera-Gomez et al., 2016). What other roles are played by events downstream of the UPR, for example, Bip upregulation itself, and cytoplasmic changes, remains to be elucidated in detail. One interesting aspect is whether the activation of UPR might affect biophysical properties, membrane association dynamics, and conformation and post-translational modifications of Sec16 and COPII subunits, which would lead to their enhanced phase separation properties under stress.

*Lowering the cytoplasmic ATP concentration is one parameter that induces Sec body formation*

The lowering of the cytoplasmic ATP concentration occurs in KRB and SCH100 plus DTT. Forcing this lowering or preventing it has a strong incidence on Sec body formation. This finding is consistent with the hydrotropic property of ATP, that is, it being able to prevent phase separation in the cytoplasm. At least in vitro, addition of 8 mM ATP dissolves or prevents the phase separation of purified FUS and TAF15 (Patel et al., 2017). This is a concentration matching physiological range of ATP level in mammalian cells (1–10 mM) (Traut, 1994) and that is also compatible with the S2 cell ATP concentration (1.7 mM).

One possibility to explain the decrease of ATP concentration is the activation of kinases (among them, IRE1, PERK and SIK) that would consume the ATP pool. However, we propose that the decrease in the intracellular ATP concentration is upstream of the kinase activation. Indeed, incubating cells in KRB induces a ROS shock (as we showed experimentally), which could damage mitochondrial respiration, resulting, in turn, in ER stress, and UPR activation. Taken together, although we unravel a strong causality between low ATP and Sec body formation, the noticeable exception of such formation in SCH150 suggests other possibilities.

In conclusion, this work illustrates the complexity of amino acid starvation,

the number of pathways it activates and how they interact with each other, as well as the different cellular cytoplasmic biophysical parameters it affects. We propose that the formation of Sec bodies depends on the activation of signaling pathways leading to activation of SIKs, IRE1 and PERK, altogether leading to the activation of the UPR, one of the common features of all pathways leading to Sec body formation.

## *Materials and Methods*

### *Cell culture, KRB incubation, drug treatments and depletions by RNAi*

*Drosophila* S2 cells (R69007, Thermo Fisher Scientific) were cultured in Schneider's medium (Sch, S0146; Sigma) supplemented with 10% insecttested fetal bovine serum (F4135; Sigma) at 26°C. S2 cells (between passages 5 and 18) were pelleted at 200 g in a microfuge for 3 min, washed once in fresh Schneider's medium, and diluted to 106/ml. 1 ml of cell suspension were plated per well in a 12-well plate containing coverslips. Cells were allowed to attach for 1.5 h before starting the treatment.

Amino acid starvation was performed in Krebs Ringers bicarbonate buffer (KRB) comprising 0.7 mM Na<sub>2</sub>HPO<sub>4</sub>, 1.5 mM NaH<sub>2</sub>PO<sub>4</sub>, 15mM NaHCO<sub>3</sub> (sodium bicarbonate, BIC), 120.7 mM NaCl, 4.53 mM KCl, 0.5 mM MgCl and 10 mM flucose at pH 7.4 as reported in Zacharogianni et al. (2014) (Table 1). SCH84, SCH100 and SCH150 correspond to Sch supplemented with 84, 100 and 150 mMNaCl. KRB21 corresponds to KRB supplemented to 21 mM KCl.

Wild-type *Drosophila* S2 cells were depleted by dsRNA, as previously described (Kondylis and Rabouille, 2003). Cells were analyzed after incubation with dsRNAs for 5 days, typically leading to depletion in more than 90% of the cells. Primers for depletion used were: dsPERK forward, 5'-TAATACGACTCACTATAGGGAGCTGGAGCTGGCTGTTTT-3'; dsPERK reverse, 5'- TAATACGACTCACTATAGGGTACTGGCGGATATCGGCTTC-3', dsATF6 forward, 5'- TAATACGACTCACTATAGGGAGCGGCATGTCATAGCTGTA-3', dsATF6 reverse, 5'- TAATACGACTCACTATAGGGTTGACGAGAAATGCAATCCA-3'.

### *Cell treatments*

Drugs were used at the concentrations mentioned in Table S2, including the IRE1 kinase inhibitor amgen small molecule 18 (AMG18) (Harrington et al., 2015). Drug treatment was performed on the plated cells at 26°C for 4 h incubated either in Schneider's medium or in KRB or any of the modified versions of these two media (Table 1). Heat shock was performed on 2×10<sup>6</sup> S2 cells plated on coverslip in 3 cm dish at 38°C in an incubator for 1 h.

### *Antibodies*

For immunofluorescence, we used the rabbit polyclonal anti-Sec16 (1:800; Ivan et al., 2008) to detect Sec16, mouse monoclonal antibody a5 (1:20, deposited by Fambrough, D.M., DSHB) to detect NaK ATPase, mouse monoclonal anti-FMR1 (1:20, deposited by Siomi, H. DSHB) and rabbit polyclonal anti-GRP78 (Bip) (1:100, SPC-180, StressMarq) (Coelho et al., 2013; Sunderhaus et al., 2019). Donkey anti-rabbit-IgG conjugated to Alexa Fluor 568 (1:200, A10042, Invitrogen) and a goat anti-mouse-IgG conjugated to Alexa Fluor 488 (1:200, A11001, Invitrogen) were used as secondary antibodies.

For western blotting, we used a mouse monoclonal anti-phospho-p70 S6 Kinase (1:1000, 9206S, Cell Signaling), a rabbit monoclonal anti-human IRE1-p (1:1000, gift from Genentech (Chang et al., 2018a), a mouse monoclonal antibody anti NaK ATPase a5 (1:1000, deposited by Fambrough, D.M., DSHB), a rabbit monoclonal anti-phospho-HDAC4/ HDAC5/ HDAC7 (1:1000, 3424S, Cell Signaling), a rabbit monoclonal antibody anti-Phospho-eIF2 $\alpha$  (Ser51) (1:1000, 9721S, Cell Signaling) and a mouse monoclonal anti- $\alpha$ -tubulin (1:2500, T5168, Sigma-Aldrich) followed by anti-rabbit-IgG and mouse-IgG antibodies coupled to HRP (1:2000, NA934, NA931, GE Healthcare).

### *Immunofluorescence*

For immunofluorescence, cells were fixed with 4% paraformaldehyde in PBS (pH 7.4) for 20 min. Cells were then washed three times with PBS and subsequently quenched by incubation in 50 mM NH<sub>4</sub>Cl in PBS for 5 min. Followed by permeabilization with 0.11% Triton X-100 for 5 min. Thereafter, cells were washed three times in PBS and blocked in PBS supplemented with 0.5% fish skin gelatin (G7765, Sigma-Aldrich) for 20 min. Cells were then incubated with the primary antibody (in blocking buffer) for 25 min, washed three times with blocking buffer and incubated with the secondary antibody (in blocking buffer) coupled to a fluorescent dye for 20 min. Cells on the coverslip were washed twice in milliQ water and dried for 3 min on a tissue with cells facing up. Finally, each coverslip with cells was mounted with Prolong antifade medium (+DAPI, P36935, Invitrogen) on a microscope slide. Samples were viewed with a Leica SPE confocal microscope using a 63 $\times$  oil lens and 2 $\times$  zoom.

### *Quantification of Sec body formation*

Cells positive for Sec bodies contain at least two large (>0.5  $\mu$ m) (typically 3–10) round Sec16-positive structures, whereas the typical ERES pattern observed in Schneider's medium has largely disappeared (see Fig. 1A,A') (Zacharogianni et al., 2014). For all

---

conditions, immunofluorescence analysis was performed three times or more unless otherwise stated and at least four to five fields (~25–30 cells per field) were recorded and analyzed per experiment. The response per field was determined by dividing the total amount of cells with Sec bodies by the total amount of cells. Finally, the average between all the fields was calculated and statistical analyses was performed using a one-tailed paired t-test.

#### *Cell diameter measurement*

After incubation with different buffers, S2 cells were stained with phalloidin–TRITC 1: 4000 (P1951, Sigma-Aldrich) for 20 min to detect F-actin. To measure the cell cross-sectional diameter, confocal images of equatorial cell sections were taken. The diameter was drawn by hand and measured using the ‘Measure’ function of ImageJ.

#### *Cell fluorescence intensity measurement*

To measure the Bip immunofluorescence intensity in the cells under different conditions, confocal images of full projections were analyzed. The measuring tool of ImageJ was used to measure the Bip immunofluorescence intensity cell by cell. The intensity in Schneider’s medium was set as 1 and the intensity of the other conditions was expressed relative to that in Schneider’s medium.

#### *XBP1/RIDD assay and IRE1 PCR*

10×10<sup>6</sup> cells grown in Schneider’s medium and 20×10<sup>6</sup> cells incubated in KRB for 4 h were spun down (5 min at 200 g) and washed in PBS-MilliQ prior to RNA extraction. For each condition, RNA was extracted using the RNeasy Mini Kit (Qiagen). The RNA concentrations were measured on the NanoDrop ND-1000 UV-Vis Spectrophotometer (Thermo Scientific). 1 µg RNA were used to synthesize cDNA using the GoScript Reverse Transcription System kit (Promega). For each condition, a PCR was performed using Taq polymerase (Promega) and visualized on agarose gel to assess xbp1, bip, gadd45, sparc, indy, PIG-Wa, ire1 and h2a (control) PCR product. Primers used were:

xbp1 forward, 5'- CAGATGCATCAGCCAATCCAAC-3';

xbp1 reverse, 5'-CACAACCTTCCAGAGTGAG- 3';

bip forward, 5'-CTGCAGGTGATGCGCATCATCAA-3';

bip reverse, 5'-CTTGCCCTTCTTCTTGTACAGCTTGA-3';

gadd45 forward, 5'-ATGGTCGTCGAGGAGAACTGCAG-3';

gadd45 reverse, 5'- CTCCAGCAGTACCTCGTGCATGT-3';

indy forward, 5'-CCATGAGCCTCAATACCAAATCGTTGGA- 3';

indy reverse, 5'-TGTAGACCAACATGGATGGCACCG- 3';



PIG-Wa forward, 5'-TTCTGGCTGTGGATTTCCCTTCGTATC- 3';  
PIG-Wa reverse, 5'-TTTCGTGAATCCCAGTATGAAGAAGGCATT- 3';  
sparc forward, 5'-GTCGGACTGCTCTGTGTATC-3';  
sparc reverse, 5'-ATGGTCCTTGTGGAGTCGC-3';  
h2a forward, 5'- GTGGAAAAGGTGGCAAAGTGAA-3';  
h2a reverse, 5'-TTCTTGTGTGCACGAGCAGCAT- 3';  
ire1 forward, 5'ATGAGAAGACGGACTGCACG- 3';  
and ire1 reverse, 5'-GATCTGCTCGCCCTCCTTAC-3'.

### *ROS detection assay*

The stock solution of H2DCFDA (10 mM in DMSO) was diluted to 5  $\mu$ M in Schneider's medium directly before usage. 106 cells/ml were incubated with 5  $\mu$ M H2DCFDA in Schneider's medium in the dark for 1 h (and up to 4 h) at 26°C in a 48-well plate. After incubation, the cells were washed three times with Schneider's medium to remove excess H2DCFDA that might be noncovalently associated with the extracellular leaflet of the plasma membrane. The cells were then incubated in the treatment medium (as described above) and the fluorescence intensity of the dye was immediately recorded over a period of 1 h at 26°C using a Spark multimode microplate reader (Tecan) with an excitation of 480 nm and an emission of 530 nm. The fluorescence intensity of five fields of cells per condition was measured every 5 min for a period of 1 h. Each experiment was performed at least three times or more.

The difference in DCF intensity for each condition was calculated by using the last value (1 h) minus the first value (0 h). The difference in intensity of Schneider's medium (usually very small, less than 10%) was used and set as the baseline at the value of 1. The difference in any other conditions was calculated as 'Difference in DCF intensity (condition x)/ Difference in DCF intensity (Schneider's medium)'. The fold difference was then expressed as a fold change over this baseline.

### *Western blotting*

A total of 4×10<sup>6</sup> cells per condition were treated as described above. After treatment, the cells were harvested on ice and lysed in the following buffer [50 mM Tris-HCl pH 7.5, 150 mM NaCl, 1% Triton X-100, 50 mM NaF, 1 mM Na<sub>3</sub>VO<sub>4</sub>, 25mM Na<sub>2</sub>- $\beta$ -glycerophosphate supplemented with a protease inhibitor tablet (11836153001, Roche)]. The lysates were cleared by centrifugation at 20,000 g for 20 min at 4°C. Supernatants were collected and the protein concentration was determined with a BCA protein assay kit (Thermo Fisher Scientific). 50  $\mu$ g of protein was mixed with 5× SDS loading dye, boiled for 5 min and

---

separated on an 8% SDS-PAGE gel. Then, separated proteins were transferred to a PVDF membrane. Hereafter, the PVDF membrane was blocked in TBS plus 0.05% Tween-20 and 5% BSA (Sigma-Aldrich) (blocking buffer). Primary antibodies were added to blocking buffer. After an overnight incubation at 4°C, the membrane was washed three times in TBS plus 0.05% Tween-20 over 45 min and incubated with secondary antibodies for 1 h at room temperature. The membrane was washed three times washing in TBS+0.05%Tween-20 and developed by enhanced chemiluminescence (Bio-Rad) with Image Quant™ LAS 4000.

### *Cytoplasmic pH measurement*

The cytoplasmic pH was estimated by using the ratiometric fluorescent GFPmutant pHluorin2 (Mahon, 2011) attached to mCherry in a cell-based assay. Cloning of pHluorin2-mCherry was performed by amplifying the fragment out of pAG304GPD-ypHluorin2 [a gift from Simon Alberti, Biotechnology Center (BIOTEC), Center for Molecular and Cellular Bioengineering (CMCB), Technische Universität Dresden, Dresden, Germany] using forward primer, 5'-GAGGGTACCATGGTGAGCAAGGGCG-3' and reverse primer, 5'-CGACTCGAGTTATT TGTATAGTTCATCCATGCCA -3'.

The fragment was cloned into the pMT-V5 vector using KpnI and XhoI restriction sites. pMT-pHluorin2-mCherry was transfected in S2 cells using Effectene transfection reagent (Qiagen) with a 1:10 ratio of DNA to Effectene Reagent. Upon acidification, pHluorin2 excitation wavelength decreases, while the mCherry excitation signal remains largely unchanged. The ratio was calculated from the fluorescence intensity of pHluorin2 and mCherry determined using a Leica SP8 confocal microscope. The average ratio was calculated from 120 cells over five viewing fields. A pH calibration curve was made by incubating transfected cells for 30 min in buffers with a different pH supplemented with 75  $\mu$ M monensin (M5273, Sigma-Aldrich), 10  $\mu$ M nigericin (N7143, Sigma-Aldrich), 10 mM 2-deoxyglucose (D6134, Sigma-Aldrich) and 10 mM NaN<sub>3</sub> (10325720, Thermo Fisher Scientific) to allow equilibration of the intracellular and extracellular pH. The ratio was calculated as described above.

### *ATP measurement*

To measure the ATP concentration, we used the CellTiter-Glo 2.0 kit (Promega) and followed the manufacturer's instruction. In brief, S2 cells (8×10<sup>4</sup>) were plated in a transparent 96-well plate and treated as indicated above. Every treatment was performed at least in triplicate and each experiment was performed two or three times. To determine the intracellular ATP concentration, 100  $\mu$ l of fresh incubation medium was added to the treated cells and a 0.5× volume CellTiter-Glo 2.0 (Promega) was added to each well. The background signal was determined by adding CellTiter-Glo 2.0 (Promega) to medium

without cells. The total volume was transferred to a 96-well Greiner flat white plate. Luminescence was measured with a Tecan Spark multimode microplate reader (emission wavelength 560 nm). To determine the extracellular ATP level, the incubation medium was transferred to a 96-well Greiner flat white plate and 0.5× volume CellTiter- Glo 2.0 (Promega) was added to each well. The luminescence was measured as above. An ATP calibration curve was made by measuring different known concentrations of ATP (Sigma-Aldrich) in Schneider's medium.

#### *Semi-intact cell assay*

Wild-type S2 cells ( $1.5 \times 10^6$ ) were plated on coverslips and permeabilized with 10 µg/ml digitonin (D141, Sigma-Aldrich) in KRB for 2 h at 26°C. Subsequently, cells were fixed and Sec bodies were visualized by immunostaining of Sec16. To test the effect of ATP, AMP or adenosine on Sec body formation, the semi-intact cells were incubated in the presence of 0.5 mM ATP (A1852, Sigma-Aldrich), 0.5 mM AMP (01930, Sigma-Aldrich) or 0.5 mM adenosine (A9251, Sigma-Aldrich). Note that the digitonin was not removed. The permeabilization efficiency was determined by using the non-membrane-permeable dye TO-PRO-3 iodide (T3605, Thermo Fisher Scientific) (Fig. 6A). The import buffer used in the SIC system was 20 mM HEPES, 110 mM KAc, 2 mM MgAc, 5 mM NaAc and 0.5 mM EGTA (pH was set at either 6.0 or 7.4 with KOH). For the RNA degradation experiment in the SIC system, we incubated S2 cells on coverslips for 2 h at 26°C in Schneider's medium containing 10 µg/ml digitonin (Sigma-Aldrich) with or without 0.25 U/µl RNase 1 (EN0602, Thermo Fisher Scientific).

#### *RNA sequencing*

A total of  $10 \times 10^6$  S2 cells were incubated in KRB and in Schneider's medium for 4 h as described above. Two biological replicates were performed. Total RNA was isolated using the RNeasy mini kit (Qiagen). The Utrecht Sequencing Facility (USEQ) generated RNA libraries using a RiboZero (Illumina) and TruSeq Stranded Total RNA Library Prep kit (Illumina). Hereafter, libraries were sequenced on Illumina NextSeq500 1×75 bp high output. Read quality was checked using fastqc. Reads were mapped to the *Drosophila melanogaster* Dm6 reference genome (UCSC) using STAR (2.4.0.1) with default parameters (Dobin et al., 2013). We generated the read count per transcript table with an in-house Python2.7 script using pysam (<https://github.com/pysam-developers/pysam>) and the Dm6 annotation file (Ensembl). Differential expression between the conditions was determined using EdgeR (3.24.3) analysis in the R bioconductor package (Robinson et al., 2010). The DAVID web tool was used for GO analysis with default parameters (<https://david.ncifcrf.gov/summary.jsp>). The GEO accession number for the RNA-seq data reported in this paper is GSE143810.

---

### *smFISH*

Plated wild-type S2 cells were first treated with KRB (see above), and fixed and labeled for endogenous FMR1 or Sec16 as described above in the immunofluorescence section. After incubation with the secondary antibody, cells were washed three times with PBS and cells were post-fixed in 4% paraformaldehyde in PBS (pH 7.4) for 10 min. Following a washing three times in PBS, cells were further incubated for 5 min in 10% formamide (17899, Thermo Fisher Scientific) in DEPC-treated water. They were then incubated overnight on a droplet containing one fluorescent smFISH probe [125 nM in 1% dextran sulfate (D8906, Sigma-Aldrich), 10% formamide in DEPC-treated water at 37°C] in a moistened chamber to avoid drying. Cells were washed twice for 30 min with 10% formamide in DEPC-treated water and mounted with Prolong antifade medium (plus DAPI) on a microscopeslide. The TMR-oligo(dT)30× was purchased from IDT. A widefield Leica MM-AF microscope was used with a 100× lens for imaging.

### *Statistics*

Significance of the data was calculated and made by using GraphPad Prism 5.02. Statistical analyses were performed by using a one-tailed paired t-test and denoted \* $P < 0.05$ , \*\* $P < 0.01$ , \*\*\* $P < 0.001$ . Error bars represent s.e.m. except for Fig. 6B,C', Figs S2B' and S5A,A',B where they represent s.d.

### *Acknowledgements*

We thank our colleagues in the field for critics and comments. We thank Apfrida Kendek (UMCU) for Fig. S2C. We acknowledge Genentech for providing us with the AMG18 and the anti IRE1-p monoclonal antibody.

### *Funding*

C.Z. is supported by a scholarship of the China Scholarship Council (201706670014). Deposited in PMC for immediate release.

### *Data availability*

The GEO accession number for the RNA-seq data reported in this paper is GSE143810.

Supplemental Figures

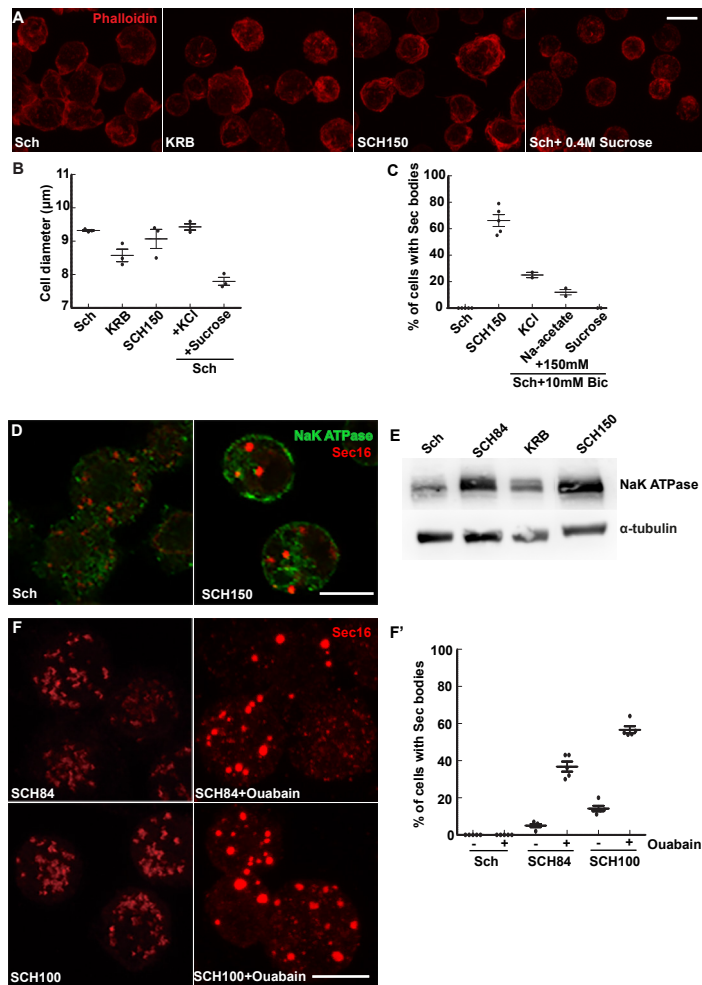


**Fig. S1. High salt stress is not equivalent to osmotic shock**

**A:** Visualization of the cell perimeter by Phalloidin staining (A) in cells incubated in Schneider's (Sch), KRB and SCH150 for 4h at 26°C as well as Sch+0.4M sucrose for 1.5h at 26°C.

**B:** Measurement (in μm) of the cell diameter after incubations in conditions mentioned on the panel. Note that incubation in 0.4M sucrose leads to a 22% decrease of the cell diameter.

**C:** Quantification of Sec body formation (marked by Sec16) in cells incubated in Sch and Schneider's supplemented with 10mM sodium bicarbonate and 150mM of NaCl (SCH150), KCl, Na-acetate, and sucrose for 4h at 26°C. Note that the strong Sec body formation response is specific for addition of 150mM NaCl.

**D:** IF visualization of the NaK ATPase (green) and Sec16 (red) in cells incubated in Sch and SCH150 for 4h at 26°C. Note the strong increase of NaK ATPase on the cell plasma membrane after incubation in

SCH150.

**E:** Western blot of S2 cells extract after incubation in Sch, SCH84, KRB and SCH150 for 4h at 26°C stained for NaK ATPase and  $\alpha$ -tubulin. Note that the NaK ATPase level increased after incubation in SCH150.

**F, F':** IF visualization (F) and quantification (F') of Sec body formation (marked by Sec16) in cells incubated in Sch, SCH84 and SCH100 supplemented by ouabain (1 $\mu$ M) for 4h at 26°C.

Scale bar: 10 $\mu$ m. Errors bars: SEM

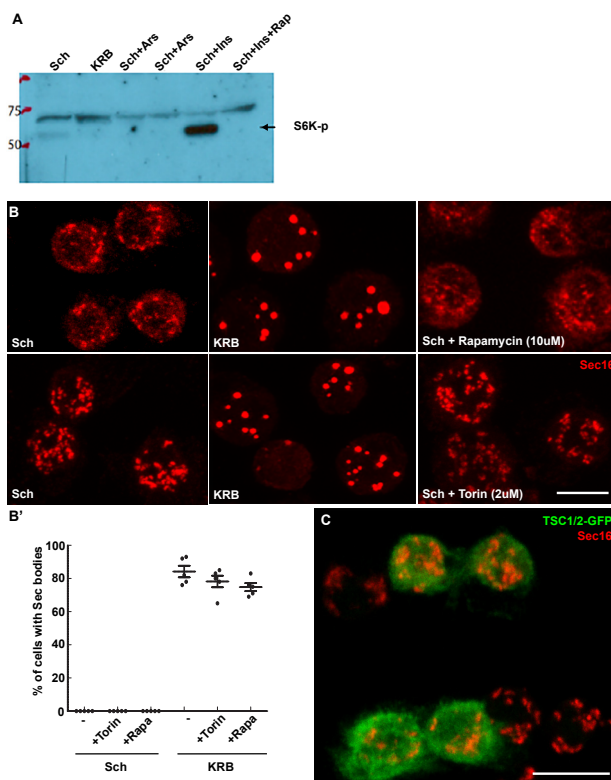


**Fig. S2. TORC1 inhibition does not lead to Sec body formation.**

**A:** Western blot of extract of S2 cells incubated as mentioned and stained for S6K-p. This shows that S6K is no longer phosphorylated after KRB incubation for 4h and that rapamycin inhibits S6K-p stimulated by insulin.

**B, B':** IF visualization (B) and quantification (B') of Sec body formation (marked by Sec16) in cells grown in Schneider's (Sch) also supplemented by mTORC1 inhibitors Rapamycin (10 $\mu$ M) and Torin (2 $\mu$ M) for 4h at 26°C. Note that the sole inhibition of mTORC1 does not lead to Sec body formation contrary to incubation in KRB.

**C:** IF Visualization of Sec16 in cells overexpressing the mTORC1 inhibitor TSC1/2-GFP. Note that Sec bodies do not form in these transfected cells.

Scale bar: 10 $\mu$ m Error bars: SD

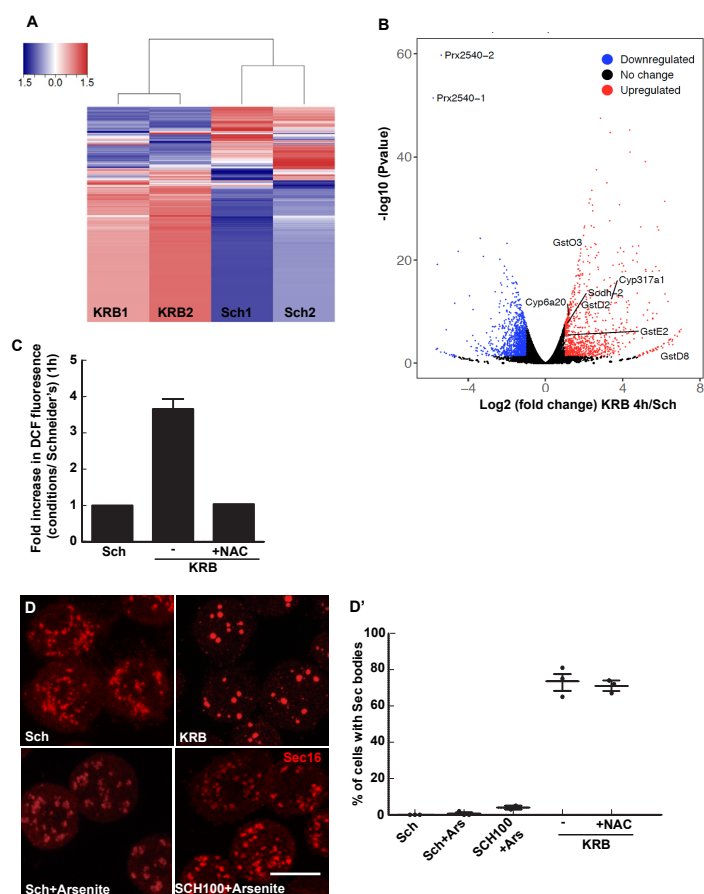


**Fig. S3. KRB incubation leads to oxidative stress but oxidative stress does not lead to Sec body formation.**

**A:** Heatmap generated from all detected transcripts highlighting the similarities of the number of reads between the conditions based on the Euclidean distance. The replicates of each condition clusters together.

**B:** Volcano plot mRNAs identified by RNA sequencing that are differentially modulated between Schneider's and KRB.

**C:** Graph showing the increase in DCF fluorescence measuring the production of ROS upon KRB for 4h at 26°C when compared to Schneider's (Sch). Sec body formation is quantified in D'. Note that addition of N-acetyl-L-cysteine (NAC) suppresses ROS production but has no effect on Sec body formation.

**D, D':** IF visualization (**D**) and quantification (**D'**) of Sec body formation in cells in Schneider's supplemented with sodium arsenite (Ars, 2.5mM) and SCH100+Ars (2.5mM) for 4h at 26°C. Note that none of these conditions elicit Sec body formation.

Scale bar: 10µm Errors bars: SEM

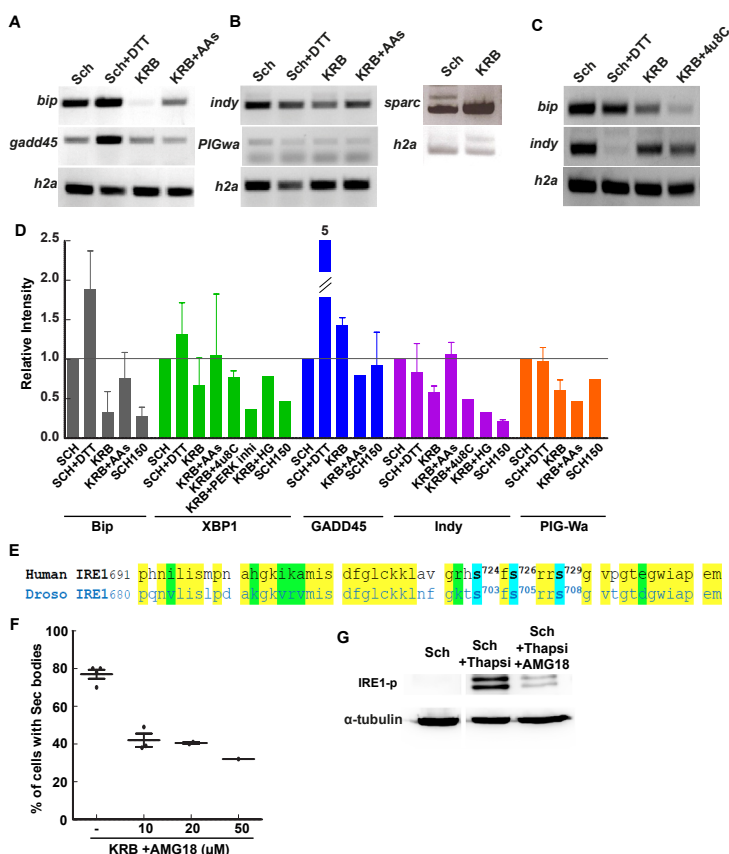


**Fig. S4. Drosophila IRE1 and specificity and efficacy of AMG18**

**A:** Visualization of the PCR products of UPR *bip*, *gadd45*, and mRNAs from cells grown in the conditions mentioned in the panel for 4h at 26°C with *h2a* as a control.

**B:** Visualization of the PCR RIDD products of *indy*, *PIGwa* and *sparc* from cells grown in the conditions mentioned in the panel for 4h at 26°C with *h2a* as a control.

**C:** Visualization of the PCR products of *bip* and *indy* from cells in KRB supplemented or not with 4u8C for 4h at 26°C.

**D:** Quantification of the PCR results upon different conditions mentioned. Normalized to Schneider's (set at 1).

**E:** Comparison of the IRE1 catalytic sites sequences in human (H) and Drosophila (D). The green highlights the identity in and around the kinase site (underlined). The serine (S) in blue is the autophosphorylated site. Note that the two other serines (in blue) are also conserved.

**F:** Quantification of Sec body formation (marked by Sec16) in cells incubated in KRB supplemented by 10, 20 and 50μM AMG18.

**G:** Western blot of S2 cells extract after their incubation in Schneider's supplemented with Thapsigargin (2μM) and AMG18 (10μM) using the IRE1-p specific antibody and an α-tubulin antibody. Errors bars: SEM



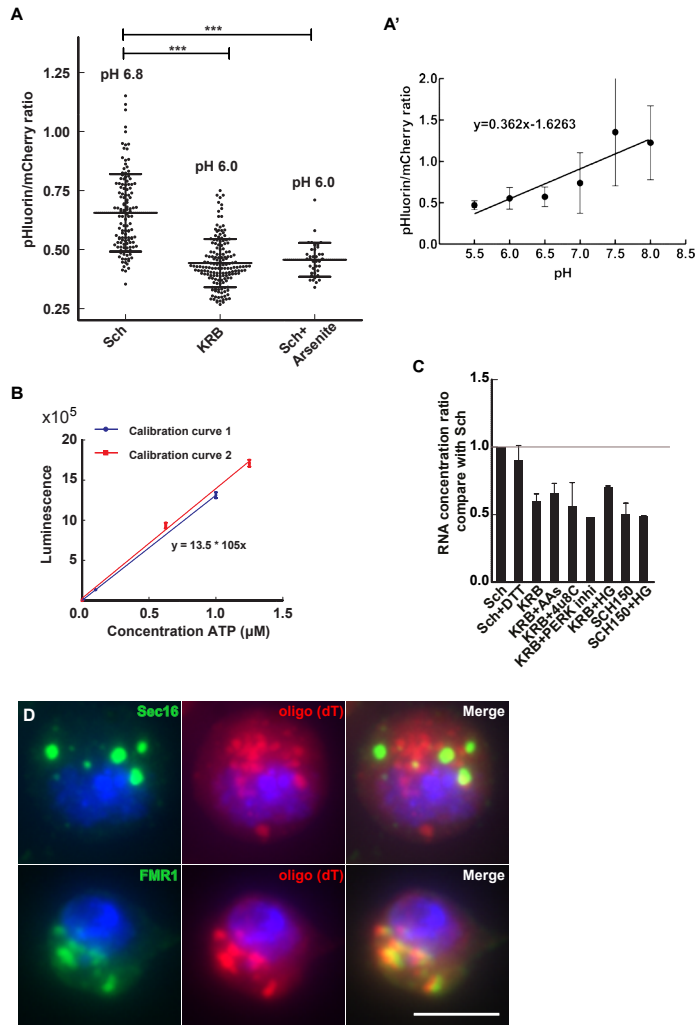


Fig. S5. pH measurements, calibration curves and oligo(dT) smFISH

A, A': Measurement of the intracellular pH (using the pHluorin-mCherry- fusion protein) in cells incubated in Schneider's (Sch), KRB and Sch+0.5mM arsenite (A). pH calibration curve, plotting the ratio between pHluorin and mCherry in buffers with a different pH (A')

B: ATP concentration calibration curve, plotting the ATP concentration versus the luminescence intensity.

C: RNA concentration after extraction from the conditions mentioned in the panel when compared with Schneider's (Sch) (set as 1).

D: Single molecule FISH using oligo(dT) probes (red) on cells incubated in KRB for 4h and labeled for Sec16 (green, to mark Sec bodies, and with FMR1 (green) to mark stress granules). Note that as expected polyA tailed RNAs co-localize with stress granules but not with Sec bodies.

Scale bar: 10 $\mu\text{m}$  Error bars: SD (A, A', B), SEM(C).

**Table S1 (related to Suppl Figure S3).** List of genes up and down regulated upon KRB incubation. Differential gene expression between 4h starved (KRB) and 4h fed (Schneider's) using EdgeR. The gene name, log fold change, P-value and FDR are shown. Significant (Empirical Bayes  $p < 0.05$ ) up regulated genes are highlighted in red and down regulated genes in blue. This table is available in the online version of this manuscript.

**Table S2. List of drug with providers and concentrations.**

Chemicals	Suppliers	Article number	Stock concentrations	Solvent	Final concentrations
Adenosine	Sigma-Aldrich	A9251	10mM	MilliQ	0.5mM
AICAR	Sigma-Aldrich	A9978	100mM	MilliQ	1mM
Amino-acids solution	Sigma-Aldrich	R7131	228.7mM	KRB	5.72mM
AMP (Adenosine 5'-monophosphate disodium salt)	Sigma-Aldrich	O1930	100mM	MilliQ	0.5mM
AMG18 (IRE1 kinase activity)	Gift from Genentech		10mM	DMSO	10μM 20μM 50μM
APS (Ammonium persulfate)	Sigma-Aldrich	A7460	1M	MilliQ	500μM
Arsenite (Na (meta) arsenite)	Sigma-Aldrich	S7400	0.5M	MilliQ	2.5mM
ATP (Adenosine 5'-triphosphate disodium salt hydrate)	Sigma-Aldrich	A1852	100mM	MilliQ	0.5mM
CCCP (Carbonyl cyanide 3-chlorophenylhydrazone)	Sigma-Aldrich	C2759	100mM	DMSO	25μM
Dasatinib	Sigma-Aldrich	SML2589	80mM	DMSO	20μM
2-Deoxy-D-glucose	Sigma-Aldrich	D6134	1M	MilliQ	20mM
DTT (Dithiothreitol)	Biorad	161-0611	2M	DMSO	5mM
Dorsomorphin	Sigma-Aldrich	P5499	1mM	DMSO	1μM
H <sub>2</sub> O <sub>2</sub> (Hydrogen peroxide)	Sigma-Aldrich	H1009	2M	MilliQ	1mM
HG-9-91-01 (pan SIK inhibitor)	MedChemExpress/Bio-Connect	HY-15776	5mM	DMSO	5μM
KCl (Potassium Chloride)	Sigma-Aldrich	P9541	2M	MilliQ	150mM
Ionomycin from Streptomyces conglobatus	Sigma-Aldrich	I9657	2.8mM	DMSO	2.8μM
Na-acetate (Sodium acetate)	Fisher Scientific	S/2040/53	2M	MilliQ	150mM
N-Acetyl-L-cysteine	Sigma-Aldrich	A7250	30mM	MilliQ	300μM
NaCl (Sodium Chloride)	J.T.Baker	O278	2M	MilliQ	84mM, 100mM, 150mM
ON123300	Selleckchem	S8161	10mM	DMSO	10μM
Ouabain octahydrate	Sigma-Aldrich	O3125	50mM	MilliQ	1μM
PERK inhibitor I	Sigma-Aldrich	S16535	10mM	DMSO	5μM
Rapamycin	Sigma-Aldrich	R0395	10mM	DMSO	10μM
RNase I	ThermoFisher	EN0602	10U/μl		0.25U/μl
SB203580	Sigma-Aldrich	S8307	30mM	DMSO	30μM
Sucrose	Sigma-Aldrich	S0389	2M	MilliQ	0.4M
Thapsigargin	Sigma-Aldrich	SML1845	1mM	DMSO	2μM
Torin	Invivogen	inh-tor1	3mM	DMSO	2μM
4u8C (IRE1 nuclease activity Inhibitor)	Merck Millipore	412512	122mM	DMSO	30μM

*References*

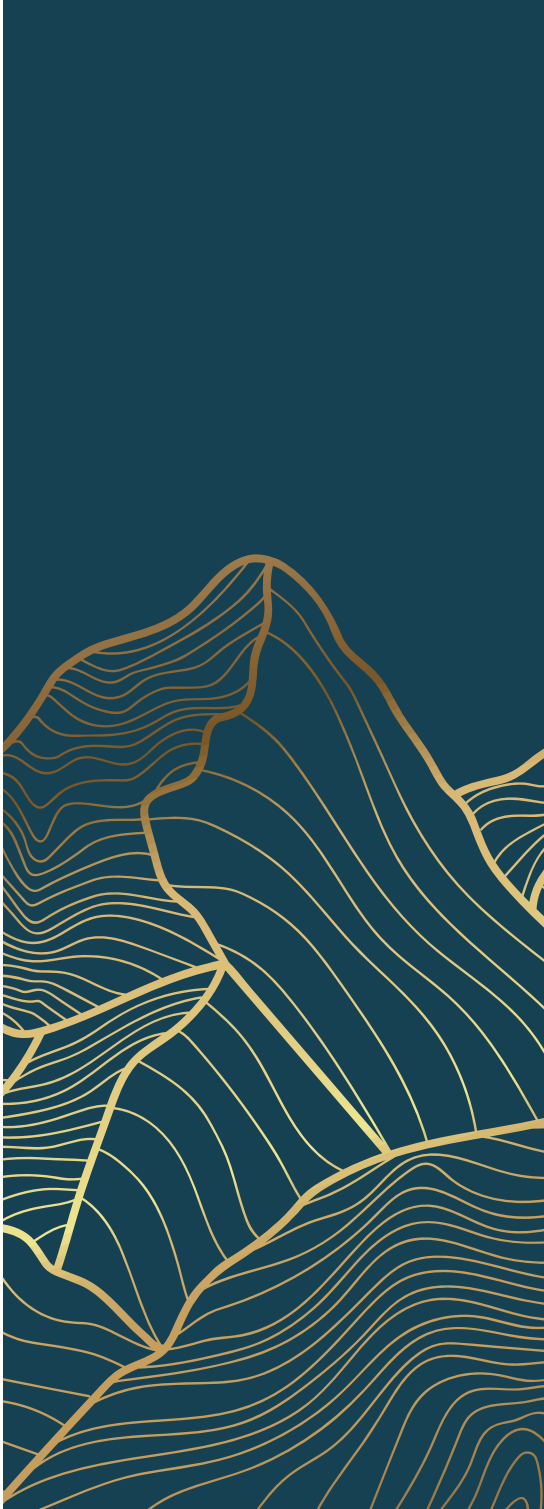
- Aguilera-Gomez, A., van Oorschot, M. M., Veenendaal, T. and Rabouille, C. (2016). In vivo visualization of mono-ADP-ribosylation by dPARP16 upon aminoacid starvation. *eLife* 5, e21475. doi:10.7554/eLife.21475
- Aulas, A., Fay, M. M., Lyons, S. M., Achorn, C. A., Kedersha, N., Anderson, P. and Ivanov, P. (2017). Stress-specific differences in assembly and composition of stress granules and related foci. *J. Cell Sci.* 130, 927-937.
- Bah, A. and Forman-Kay, J. D. (2016). Modulation of intrinsically disordered protein function by post-translational modifications. *J. Biol. Chem.* 291, 6696-6705. doi:10.1074/jbc.R115.695056
- Bounedjah, O., Hamon, L., Savarin, P., Desforages, B., Curmi, P. A. and Pastré, D. (2012). Macromolecular crowding regulates assembly of mRNA stress granules after osmotic stress: new role for compatible osmolytes. *J. Biol. Chem.* 287, 2446-2458. doi:10.1074/jbc.M111.292748
- Boyce, M. and Yuan, J. (2006). Cellular response to endoplasmic reticulum stress: a matter of life or death. *Cell Death Differ.* 13, 363-373. doi:10.1038/sj.cdd.4401817
- Brett, C. L., Tukaye, D. N., Mukherjee, S. and Rao, R. (2005). The yeast endosomal Na<sup>+</sup>(K<sup>+</sup>)/H<sup>+</sup> exchanger Nhx1 regulates cellular pH to control vesicle trafficking. *Mol. Biol. Cell* 16, 1396-1405. doi:10.1091/mbc.e04-11-0999
- Chang, T.-K., Lawrence, D. A., Lu, M. M., Tan, J., Harnoss, J. M., Marsters, S. A., Liu, P., Sandoval, W., Martin, S. E. and Ashkenazi, A. (2018a). Coordination between two branches of the unfolded protein response determines apoptotic cell fate. *Mol. Cell* 71, 629-636.e625. doi:10.1016/j.molcel.2018.06.038
- Chang, T. K., Lawrence, D. A., Lu, M., Tan, J., Harnoss, J. M., Marsters, S. A., Liu, P., Sandoval, W., Martin, S. E. and Ashkenazi, A. (2018b). Coordination between two branches of the unfolded protein response determines apoptotic cell fate. *Mol. Cell* 71, 629-636.e625.
- Clark, K., MacKenzie, K. F., Petkevicius, K., Kristariyanto, Y., Zhang, J., Choi, H. G., Pegg, M., Plater, L., Pedrioli, P. G., McIver, E. et al. (2012). Phosphorylation of CRT3 by the salt-inducible kinases controls the interconversion of classically activated and regulatory macrophages. *Proc. Natl. Acad. Sci. U.S.A.* 42, 6986-6991.
- Coelho, D. S., Cairrao, F., Zeng, X., Pires, E., Coelho, A. V., Ron, D., Ryoo, H. D. and Domingos, P. M. (2013). Xbp1-independent Ire1 signaling is required for photoreceptor differentiation and rhabdome morphogenesis in *Drosophila*. *Cell reports* 5, 791-801. doi:10.1016/j.celrep.2013.09.046
- Condon, K. J. and Sabatini, D. M. (2019). Nutrient regulation of mTORC1 at a glance. *J. Cell Sci.* 132, jcs222570. doi:10.1242/jcs.222570
- Dobin, A., Davis, C. A., Schlesinger, F., Drenkow, J., Zaleski, C., Jha, S., Batut, P., Chaisson, M. and Gingeras, T. R. (2013). STAR: ultrafast universal RNA-seq aligner. *Bioinformatics* 29, 15-21. doi:10.1093/bioinformatics/bts635
- Ducommun, S., Ford, R. J., Bultot, L., Deak, M., Bertrand, L., Kemp, B. E., Steinberg, G. R. and Sakamoto, K. (2014). Enhanced activation of cellular AMPK by dual-small molecule treatment: AICAR and A769662. *Am. J. Physiol. Endocrinol. Metab.* 306, E688-E696. doi:10.1152/ajpendo.00672.2013
- Farhan, H., Wendeler, M. W., Mitrovic, S., Fava, E., Silberberg, Y., Sharan, R., Zerial, M. and Hauri, H. P. (2010). MAPK signaling to the early secretory pathway revealed by kinase/phosphatase functional screening. *J. Cell Biol.* 189, 997-1011. doi:10.1083/jcb.200912082
- Gaddam, D., Stevens, N. and Hollien, J. (2012). Comparison of mRNA localization and regulation

- during endoplasmic reticulum stress in *Drosophila* cells. *Mol. Biol. Cell* 24, 14-20. doi:10.1091/mbc.e12-06-0491
- Gomez-Navarro, N. and Miller, E. (2016). Protein sorting at the ER-Golgi interface. *J. Cell Biol.* 215, 769-778. doi:10.1083/jcb.201610031
- Harrington, P. E., Biswas, K., Malwitz, D., Tasker, A. S., Mohr, C., Andrews, K. L., Dellamaggiore, K., Kendall, R., Beckmann, H., Jaekel, P. et al. (2015). Unfolded protein response in cancer: IRE1 $\alpha$  inhibition by selective kinase ligands does not impair tumor cell viability. *ACS Med. Chem. Lett.* 6, 68-72. doi:10.1021/ml500315b
- Hetz, C. (2012). The unfolded protein response: controlling cell fate decisions under ER stress and beyond. *Nat. Rev. Mol. Cell Biol.* 13, 89-102. doi:10.1038/nrm3270
- Hollien, J. and Weissman, J. S. (2006). Decay of endoplasmic reticulum-localized mRNAs during the unfolded protein response. *Science* 313, 104-107. doi:10.1126/science.1129631
- Hollien, J., Lin, J. H., Li, H., Stevens, N., Walter, P. and Weissman, J. S. (2009). Regulated Ire1-dependent decay of messenger RNAs in mammalian cells. *J. Cell Biol.* 186, 323-331. doi:10.1083/jcb.200903014
- Ivan, V., de Voer, G., Xanthakis, D., Spoorendonk, K. M., Kondylis, V. and Rabouille, C. (2008). *Drosophila* Sec16 mediates the biogenesis of tER sites upstream of Sar1 through an arginine-rich motif. *Mol. Biol. Cell* 19, 4352-4365. doi:10.1091/mbc.e08-03-0246
- Jaitovich, A. and Bertorello, A. M. (2010). Intracellular sodium sensing: SIK1 network, hormone action and high blood pressure. *Biochim. Biophys. Acta* 1802, 1140-1149.
- Jalihal, A. P., Pitchaiya, S., Xiao, L., Bawa, P., Jiang, X., Bedi, K., Parolia, A., Cieslik, M., Ljungman, M., Chinnaiyan, A. M. et al. (2020). Multivalent proteins rapidly and reversibly phase-separate upon osmotic cell volume change. *Mol. Cell* 79, 978-990.e975. doi:10.1016/j.molcel.2020.08.004
- Joo, J. H., Wang, B., Frankel, E., Ge, L., Xu, L., Iyengar, R., Li-Harms, X., Wright, C., Shaw, T. I., Lindsten, T. et al. (2016). The noncanonical role of ULK/ ATG1 in ER-to-golgi trafficking is essential for cellular homeostasis. *Mol. Cell* 62, 491-506.
- Jwa, M. and Chang, P. (2012). PARP16 is a tail-anchored endoplasmic reticulum protein required for the PERK- and IRE1 $\alpha$ -mediated unfolded protein response. *Nat. Cell Biol.* 14, 1223-1230. doi:10.1038/ncb2593
- Kilchert, C., Weidner, J., Prescianotto-Baschong, C. and Spang, A. (2010). Defects in the secretory pathway and high Ca<sup>2+</sup> induce multiple P-bodies. *Mol. Biol. Cell* 21, 2624-2638. doi:10.1091/mbc.e10-02-0099
- Kim, J. and Guan, K.-L. (2019). mTOR as a central hub of nutrient signalling and cell growth. *Nat. Cell Biol.* 21, 63-71. doi:10.1038/s41556-018-0205-1
- Kondylis, V. and Rabouille, C. (2003). A novel role for dp115 in the organization of tER sites in *Drosophila*. *J. Cell Biol.* 162, 185-198. doi:10.1083/jcb.200301136
- Korennnykh, A. V., Egea, P. F., Korostelev, A. A., Finer-Moore, J., Zhang, C., Shokat, K. M., Stroud, R. M. and Walter, P. (2009). The unfolded protein response signals through high-order assembly of Ire1. *Nature* 457, 687-693. doi:10.1038/nature07661
- Leung, A. K., Calabrese, J. M. and Sharp, P. A. (2006). Quantitative analysis of Argonaute protein reveals microRNA-dependent localization to stress granules. *Proc. Natl. Acad. Sci. USA* 103, 18125-18130. doi:10.1073/pnas.0608845103
- Lopez-Hernandez, T., Puchkov, D., Krause, E., Maritzen, T. and Haucke, V. (2020). Endocytic regulation

- of cellular ion homeostasis controls lysosome biogenesis. *Nat. Cell Biol.* 22, 815-827. doi:10.1038/s41556-020-0535-7
- Mahon, M. J. (2011). pHluorin2: an enhanced, ratiometric, pH-sensitive green fluorescent protein. *Adv. Biosci. Biotechnol.* 2, 132-137. doi:10.4236/abb.2011.23021
- Miesenböck, G., De Angelis, D. A. and Rothman, J. E. (1998). Visualizing secretion and synaptic transmission with pH-sensitive green fluorescent proteins. *Nature* 394, 192-195.
- Moore, K. A. and Hollien, J. (2012). The unfolded protein response in secretory cell function. *Annu. Rev. Genet.* 46, 165-183. doi:10.1146/annurev-genet-110711-155644
- Munder, M. C., Midtvedt, D., Franzmann, T., Nuske, E., Otto, O., Herbig, M., Ulbricht, E., Müller, P., Taubenberger, A., Maharana, S. et al. (2016). A pH-driven transition of the cytoplasm from a fluid- to a solid-like state promotes entry into dormancy. *eLife* 5, e09347. doi:10.7554/eLife.09347
- Owen, I. and Shewmaker, F. (2019). The role of post-translational modifications in the phase transitions of intrinsically Disordered proteins. *Int. J. Mol. Sci.* 20, 5501. doi:10.3390/ijms20215501
- Patel, A., Malinovska, L., Saha, S., Wang, J., Alberti, S., Krishnan, Y. and Hyman, A. A. (2017). ATP as a biological hydrotrope. *Science* 356, 753. doi:10.1126/science.aaf6846
- Peters, L. Z., Hazan, R., Breker, M., Schuldiner, M. and Ben-Aroya, S. (2013). Formation and dissociation of proteasome storage granules are regulated by cytosolic pH. *J. Cell Biol.* 201, 663-671. doi:10.1083/jcb.201211146
- Petrovska, I., Nuske, E., Munder, M. C., Kulasegaran, G., Malinovska, L., Kroschwald, S., Richter, D., Fahmy, K., Gibson, K., Verbavatz, J. M. et al. (2014). Filament formation by metabolic enzymes is a specific adaptation to an advanced state of cellular starvation. *eLife* 3, e02409. doi:10.7554/eLife.02409.036
- Rabouille, C. and Alberti, S. (2017). Cell adaptation upon stress: the emerging role of membrane-less compartments. *Curr. Opin. Cell Biol.* 47, 34-42. doi:10.1016/j.cob.2017.02.006
- Robinson, M. D., McCarthy, D. J. and Smyth, G. K. (2010). edgeR: a Bioconductor package for differential expression analysis of digital gene expression data. *Bioinformatics* 26, 139-140. doi:10.1093/bioinformatics/btp616
- Sprangers, J. and Rabouille, C. (2015). SEC16 in COPII coat dynamics at ER exit sites. *Biochem. Soc. Trans.* 43, 97-103. doi:10.1042/BST20140283
- Sunderhaus, E. R., Law, A. D. and Kretschmar, D. (2019). ER responses play a key role in Swiss-Cheese/Neuropathy Target Esterase-associated neurodegeneration. *Neurobiol. Dis.* 130, 104520. doi:10.1016/j.nbd.2019.104520
- Teesalu, M., Rovenko, B. M. and Hietakangas, V. (2017). Salt-inducible kinase 3 provides sugar tolerance by regulating NADPH/NADP<sup>+</sup> redox balance. *Curr. Biol.* 27, 458-464. doi:10.1016/j.cub.2016.12.032
- Traut, T. W. (1994). Physiological concentrations of purines and pyrimidines. *Mol. Cell. Biochem.* 140, 1-22. doi:10.1007/BF00928361
- van Leeuwen, W. and Rabouille, C. (2019). Cellular stress leads to the formation of membraneless stress assemblies in eukaryotic cells. *Traffic* 20, 623-638. doi:10.1111/tra.12669
- Walter, P. and Ron, D. (2011). The unfolded protein response: from stress pathway to homeostatic regulation. *Science* 334, 1081. doi:10.1126/science.1209038
- Wehr, M. C., Holder, M. V., Gailite, I., Saunders, R. E., Maile, T. M., Ciirdaeva, E., Instrell, R., Jiang, M., Howell, M., Rossner, M. J. et al. (2013). Salt-inducible kinases regulate growth through the Hippo

- 
- signalling pathway in *Drosophila*. *Nat. Cell Biol.* 15, 61-71. doi:10.1038/ncb2658
- Wein, M. N., Foretz, M., Fisher, D. E., Xavier, R. J. and Kronenberg, H. M. (2018). Salt-inducible kinases: physiology, regulation by cAMP, and therapeutic potential. *Trends Endocrinol. Metab.* 29, 723-735. doi:10.1016/j.tem.2018.08.004
- Weiss, A., Charbonnier, E., Ellertsdottir, E., Tsirigos, A., Wolf, C., Schuh, R., Pyrowolakis, G. and Affolter, M. (2010). A conserved activation element in BMP signaling during *Drosophila* development. *Nat. Struct. Mol. Biol.* 17, 69-76. doi:10.1038/nsmb.1715
- Wilhelmi, I., Kanski, R., Neumann, A., Herdt, O., Hoff, F., Jacob, R., Preussner, M. and Heyd, F. (2016). Sec16 alternative splicing dynamically controls COPII transport efficiency. *Nat. Commun.* 7, 12347. doi:10.1038/ncomms12347
- Yan, C., Yan, Z., Wang, Y., Yan, X. and Han, Y. (2014). Tudor-SN, a component of stress granules, regulates growth under salt stress by modulating GA2ox3 mRNA levels in *Arabidopsis*. *J. Exp. Bot.* 65, 5933-5944. doi:10.1093/jxb/eru334
- Yan, C., Liu, J., Gao, J., Sun, Y., Zhang, L., Song, H., Xue, L., Zhan, L., Gao, G., Ke, Z. et al. (2019). IRE1 promotes neurodegeneration through autophagydependent neuron death in the *Drosophila* model of Parkinson's disease. *Cell Death Dis.* 10, 800. doi:10.1038/s41419-019-2039-6
- Zacharogianni, M., Aguilera-Gomez, A., Veenendaal, T., Smout, J. and Rabouille, C. (2014). A stress assembly that confers cell viability by preserving ERES components during amino-acid starvation. *eLife* 3, e04132. doi:10.7554/eLife.04132
- Zhang, X., Lv, H., Zhou, Q., Elkholi, R., Chipuk, J. E., Reddy, M. V., Reddy, E. P. and Gallo, J. M. (2014). Preclinical pharmacological evaluation of a novel multiple kinase inhibitor, ON123300, in brain tumor models. *Mol. Cancer Ther.* 13, 1105-1116. doi:10.1158/1535-7163.MCT-13-0847





## *Chapter4*



*Osmotic stress via calmodulin lead to the  
formation of stress granule  
in Drosophila S2 cells*

Chujun Zhang, Rianne Ground, J. Mirjam A. Damen,  
Wei Wu and Catherine Rabouille (2022)  
Submitted to bioRxiv

---

## *Osmotic stress via calmodulin lead to the formation of stress granule in Drosophila S2 cells*

### *Abstract*

Cellular stress of S2 cells leads to the formation of stress assemblies by phase separation of cytoplasmic components. We have shown that the cellular stresses of either high increase of the NaCl concentration in the extracellular medium, or a moderate one combined to amino acid starvation, leads to the formation of Sec bodies where components of the endoplasmic Reticulum exit sites (ERES) coalesce. These extracellular stresses lead to both the activation of salt inducible kinase (SIK), and to ER stress triggering the activation of the two downstream kinases IRE1 and PERK. Interestingly, the same stresses also result in the formation of a second stress assembly, the stress granules, which stores specific RNAs and RNA binding proteins. Here we asked whether stress granule formation is governed by the same pathways as Sec bodies. However, we found that the inhibition of SIK, IRE1 and PERK does not affect stress granule formation. Instead, we found that osmotic stress through the addition of either salts (including calcium chloride) or sucrose leads to the formation of stress granules. Interestingly, stress granule formation is partly modulated by calmodulin activation, suggesting the involvement of calcium signaling. Furthermore, as Sec body formation is driven by entirely different pathways, these results show that the same cells under the same stress, form two different stress assemblies by non-overlapping downstream pathway activation, perhaps explaining that they do not coalesce into a single structure.

### *Introduction*

There are two forms of cell compartmentalization: membrane-bound organelles and membrane-less organelles (MLOs). Unlike membrane-bound organelles, MLOs are not surrounded by a sealed phospholipid membrane and are formed by phase separation (Banani et al., 2016; Gomes and Shorter, 2018; Patel et al., 2015). Phase separation drives a homogeneous solution of dispersed macromolecules into two distinct phase which can be either liquid or solid. MLOs (such as nucleolus) exist in cells in basal conditions, but it is now well established that cellular stress leads to phase separation and the formation of many different MLOs (van Leeuwen and Rabouille, 2019), including stress granules (Anderson and Kedersha, 2002; Aulas et al., 2017) and Sec bodies (Zacharogianni et al., 2014).

Sec bodies are stress assemblies that first have been identified in Drosophila S2 cells under the condition of amino acid starvation in the Krebs Ringer Bicarbonate buffer,

KRB. KRB incubation results in the remodeling and coalescence of ER exit site (ERES) components into round, membrane-less, reversible, liquid-like, Sec bodies of 0.6-0.8  $\mu\text{m}$  in diameter (Zacharogianni et al., 2014). KRB contains a 2.6-fold higher NaCl concentration than the growing medium Schneider's and does not contain amino acids. Interestingly, a 4-fold increase in NaCl concentration in Schneider's (through the specific addition of 150mM NaCl, SCH150) also leads to Sec body formation in S2 cells (Zhang et al., 2021).

This led us to identify signaling pathways necessary for Sec body formation. The first one is the activation of Salt Inducible Kinases (SIKs) by NaCl, which is sufficient when the NaCl stress is high, for instance in SCH150. The second is the activation of IRE1 and PERK downstream of ER stress (Walter and Ron, 2011) that is induced by amino acid starvation (Zhang et al., 2021). IRE1 and PERK activation in solo does not lead to Sec body formation. It needs to be combined with moderate salt stress, as in KRB. Accordingly, addition to dithiothreitol (DTT that activates both IRE1 PERK) together with 100mM NaCl to Schneider's leads to the same efficient Sec body formation as KRB incubation (Zhang et al., 2021).

We have reported that upon KRB incubation, not only Sec body formed, but also stress granules in close proximity and with a similar kinetics (Aguilera-Gomez and Rabouille, 2017; Zacharogianni et al., 2014). Stress granule is another class membrane-less and reversible MLOs that has been widely reported to contain mRNAs bound to RNA-binding proteins (Anderson and Kedersha, 2002). The RNAs that phase separated into stress granules are stored there during the stress and can be immediately translated upon stress relief. In *Drosophila* S2 cells, they can be visualized by labeling several RNA binding proteins, such as FMR1 (Zacharogianni et al., 2014), Caprin and Rasputin (Aguilera-Gomez et al., 2017). Most of the stress granules formation is dependent on eIF2alpha phosphorylation resulting in translational stalling (canonical pathways). However, they can also form in an independent manner (non-canonical pathways) like those activated upon osmotic stress (Aulas et al., 2017; Kedersha et al., 2016). In this regard, in our study, we show that stress granule formation is also induced by incubating cells in SCH150, i.e., addition of NaCl to the growing medium (**Figure 1A**).

Here, we asked whether, stress granule formation in response to KRB and SCH150 is governed by the activation of the same kinases as Sec bodies. However, we found that the inhibition of SIK, IRE1 and PERK in solo does not inhibit stress granule formation upon KRB and SCH150. Instead, we found that the addition of several different salts (including  $\text{CaCl}_2$ ) to the growing medium Schneider's as well as osmotic stress (by addition of sucrose) is enough to lead to stress granule formation. This is strikingly different than for Sec bodies,

which formation strictly depends in the specific presence and the addition of NaCl and do not form upon addition of sucrose (Zhang et al., 2021). Mass spectrometry reveals that calmodulin is one of the most upregulated proteins during KRB incubation, and we found that its depletion partially prevents stress granule formation both in KRB and SCH150. This suggests that calcium signaling plays a role in stress granule formation, in line with the presence of calcium binding proteins in these structures (Markmiller et al., 2019; Marmor-Kollet et al., 2020). Furthermore, these results show that the same cells, under the same stresses form two different stress assemblies by non-overlapping downstream kinase activation.

## Results

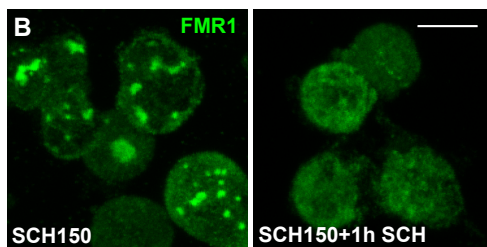
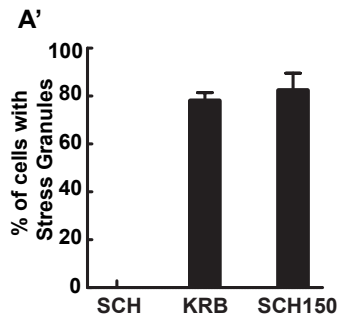
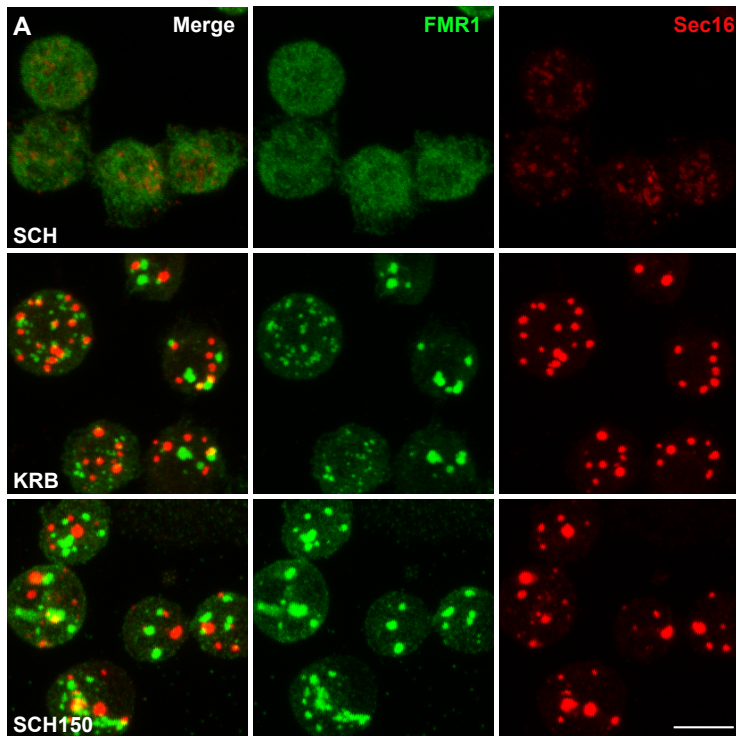
### *KRB and high NaCl stress leads to stress granule formation*

As mentioned in the introduction, the same cellular stresses (KRB and SCH150 for 4h) of S2 cells not only lead to the formation of Sec body (Zacharogianni et al., 2014; Zhang et al., 2021), but also of stress granule that are marked here by FMR1 (**Figure 1A, A'**). We have shown that the stress granules formed upon KRB appears to be bona fide stress granules, as in addition to FMR1, they contain several RNA binding proteins and are membraneless and are reversible (Aguilera-Gomez et al., 2017). Here, we confirmed that SCH150 induced stress granules are reversible. Indeed, they dissolved upon furthermore incubation in growing medium for 1h following the stress period (**Figure 1B**). Furthermore, they contain Rox8, the homolog of TIA1 in mammalian cells (Ma et al., 2017), a key stress granule marker in mammalian cells (**Figure 4D**). Furthermore, stress granules form around poly-adenylated (polyA) mRNAs that are stored in these structures during the period of stress (Kedersha et al., 1999). Here, we showed the stress granule formed in KRB and SCH150 contain polyA mRNAs using fluorescence in situ hybridization (FISH) with an oligo (dT) probe (**Figure 5**). Taken together, these results indicate that the stress granules formed in high salt stress (SCH150) are bona fide stress granules.

Given that the same stress leads to the simultaneous formation of two distinct stress assemblies (**Figure 1A**), it leads us to question whether stress granule formation follow the same pathways and are governed by the same activation of the same kinases as Sec bodies.

### *SIK and three ER stress sensors are not involved in stress granule formation upon KRB and SCH150*

As mentioned above, we have shown that SIK activation is an important contributor in



---

**Figure 1: KRB and SCH150 incubation leads to reversible stress granule formation.**

**(A, A')** Immunofluorescence (IF) visualization of endogenous FMR1 and Sec16 in S2 cells in growing medium Schneider's (SCH) and in cells incubated in KRB and SCH150 (addition of 150mM of NaCl to Schneider's) for 4 h at 26°C **(A)**. Note that, upon KRB and SCH150 incubation FMR1 and Sec16 remodel into two distinct large structures, the stress granules and Sec bodies, respectively **(A)**. Quantification of stress granule formation in KRB and SCH150 **(A')**.

**(B)** IF visualization of stress granule formation (marked by FMR1) in SCH150 for 4 h at 26°C, as well as SCH150 for 4 h followed by 1h SCH incubation at 26°C, showing their reversibility.

Scale bars: 10µm. Errors bars: SEM.

---

Sec body formation. To answer whether SIK activation also plays a role in stress granule formation, we first monitored their formation in cells incubated in SIK inhibitor HG-9-91-01, both upon KRB and SCH50. However, this inhibitor has no effect on stress granule formation (**Figure 2A**), suggesting that SIK is not involved in stress granule formation, neither in KRB and SCH150.

KRB and SCH150 incubation leads to an increase of the protein level of the ER chaperone Bip that we take as a measure of the UPR stimulation by ER stress (Zhang et al., 2021). UPR activation is downstream of the 3 kinases that are ER stress sensors IRE1, PERK and ATF6. Those can be activated upon Bip release from their luminal domain during stress (Hetz, 2012). In the case of IRE1, both its kinase and RNase domains are activated. In order to investigate the role of IRE1 activation in stress granule formation in KRB and SCH150, we incubated the cells with AMG-18 (IRE1 kinase inhibitor) and 4µ8C (IRE1 RNase inhibitor) under conditions of stress (KRB and SCH150). However, neither inhibitor reduce stress granule formation (**Figure 2B**), whereas Sec body formation was strongly inhibited showing that both drugs are efficient in *Drosophila* cells (Zhang et al., 2021). This suggests that IRE1 activation does not play a role in stress granule formation in this system. We then tested the role of PERK and ATF6 using depletion by RNAi. Again, KRB or SCH150 induced stress granule formation was not reduced (**Figure 2C, E**). Furthermore, the PERK inhibitor GSK2606414 did not have any effect on stress granule formation upon KRB and SCH150 (**Figure 2D**). This suggested that PERK and ATF6 activation are not necessary for stress granule formation.

Taken all these together, we conclude that the activation of neither SIK, nor any of the three ER stress sensors (IRE1, PERK and ATF6) are involved in stress granule formation that appears to be mediated by the activation of different kinases than Sec bodies.

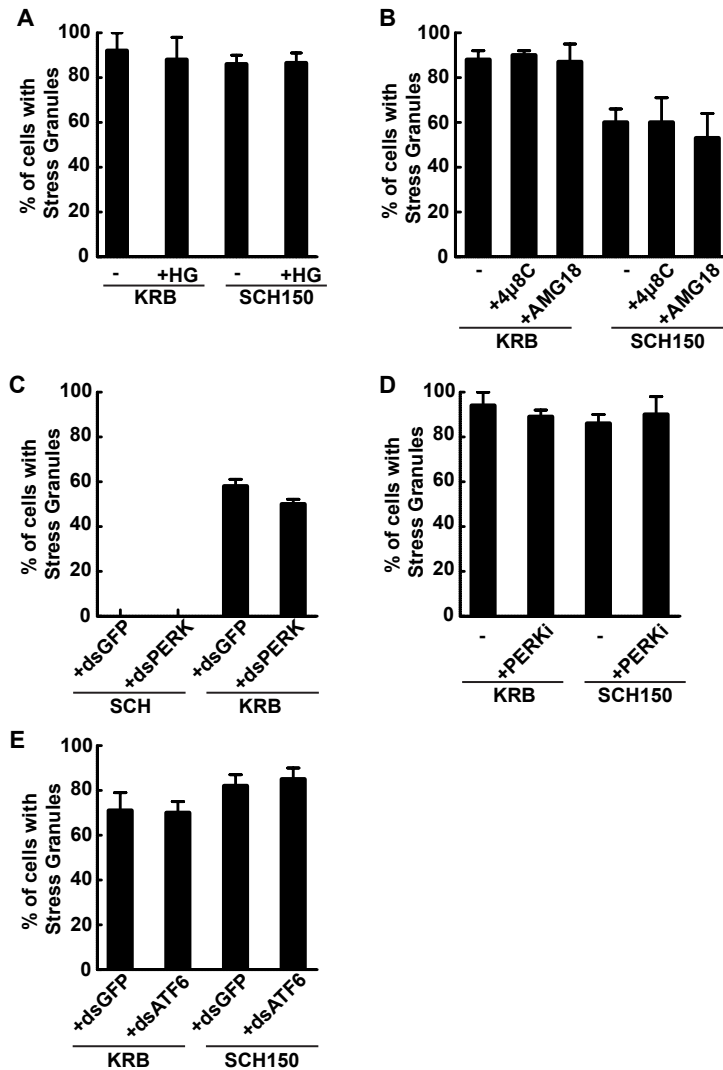


**Figure 2: SIK and ER stress kinases are not involved in KRB and SCH150 induced stress granule formation.**

**(A)** Quantification of stress granule formation (marked by FMR1) in cells incubated in KRB and SCH150 with or without the SIK inhibitor HG-9-91-01 (5μM).

**(B)** Quantification of stress granule formation (marked by FMR1) in cells incubated in KRB and SCH150 with or without the IRE1 RNase inhibitor 4μ8C (30μM) and IRE1 kinase inhibitor AMG-18 (10μM).

**(C)** Quantification of stress granule formation (marked by FMR1) in cells upon mock depletion (dsGFP) or PERK depletion (dsPERK) incubated in KRB.

(D) Quantification of stress granule formation (marked by FMR1) in cells incubated in KRB and SCH150 with or without the PERK inhibitor (5 $\mu$ M).

(E) Quantification of stress granule formation (marked by FMR1) in cells upon mock depletion (dsGFP) or ATF6 depletion (dsATF6) incubated in KRB and SCH150.

Errors bars: SEM

---

*The amino-acid starvation sensor GCN2 is not involved in the KRB and SCH150 induced stress granule formation*

We had shown previously that RNA translation is inhibited in cells incubated in KRB (Aguilera-Gomez et al., 2017). This is characterized by the phosphorylation of elf2alpha (Hetz, 2012). In this regard, we show that elf2alpha is phosphorylated in S2 cells incubated in both KRB and SCH150 (**Figure 3A**). In *Drosophila*, elf2alpha phosphorylation is typically mediated by PERK and GCN2 (General Control Nonderepressible 2). Interestingly, GCN2 is also known as an amino acid starvation sensor (Dever and Hinnebusch, 2005; Towle, 2007) and this might be relevant to the KRB incubation as it does not contain amino-acids. To test whether GCN2 plays a role in KRB and SCH150 induced stress granule formation, we inhibited GCN2 with a specific inhibitor (GCN2iB). However, stress granule still forms as in control conditions (absence of inhibitors) (**Figure 3B**) suggesting that the activation of GCN2 is not involved in stress granule formation either in KRB or SCH150.

*Nutrient sensors pathways mTORC1 and AMPK activation are not involved in stress granule formation upon KRB and SCH150.*

mTORC1 (mechanistic target of rapamycin complex I) activation is also a sensor of the presence of circulating amino acids in the medium (Kim and Guan, 2019; Manifava et al., 2016). It is inhibited when amino-acid level is low in the circulating medium (Condon and Sabatini, 2019). Ribosomal S6 kinase is a direct target of mTORC1, mTORC1 phosphorylates S6 upon its activation (Jacinto et al., 2004; Li et al., 2010). We showed that S6 no longer phosphorylated after KRB incubation (Zhang et al., 2021). Interestingly, the absence of S6 phosphorylation also seal RNA translation, which could lead to stress granule formation. In this regard, we tested whether the sole inhibition of mTORC1 (using Rapamycin) would lead to stress granule formation (Zhang et al., 2021). However, the sole inhibition of mTORC1 by rapamycin did not trigger stress granule formation (**Figure 3C**). This suggested that amino-acid starvation inhibits mTORC1, but only inhibiting mTORC1 is not enough to trigger stress granule formation. Taken together, these results indicate that the KRB and SCH150 induced stress granule formation in S2 cells is not linked to translation inhibition, as neither GCN2 nor PERK activation (**Figure 2**) nor does mTORC1 inhibition modulate their



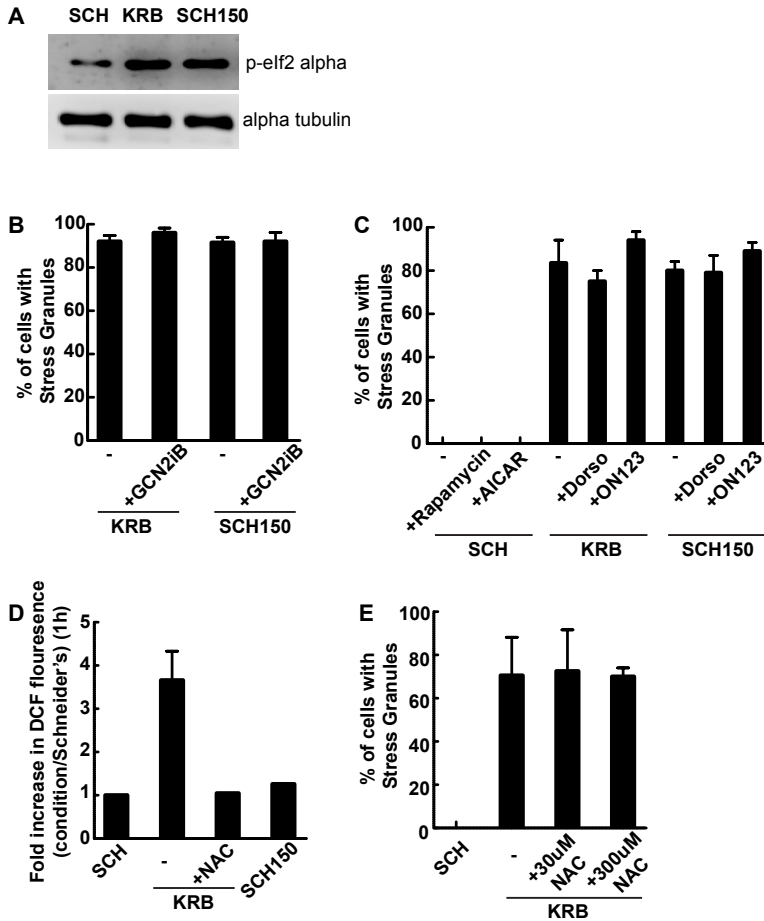


**Figure 3: GCN2, mTORC1, AMPK and ROS production are not involved KRB and SCH150 induced stress granule formation.**

**(A)** Western blot visualization of eIF2alpha phosphorylation in cells in SCH, KRB and SCH150.

**(B)** Quantification of stress granule formation (marked by FMR1) in cells incubated in KRB and SCH150 with or without GCN2 inhibitor GCN2iB (10μM).

**(C)** Quantification of stress granule formation (marked by FMR1) in cells incubated in SCH with or without AICAR (1mM) and Rapamycin (10μM), and cells incubated in KRB and SCH150 with or without Dorsomorphin (Dorso, 1μM) and ON123300 (ON123, 10μM).

**(D)** Quantification of the increase in DCF fluorescence measuring the production of ROS upon KRB, KRB with addition of ROS inhibitor N-acetyl-L-cysteine (NAC) and SCH150 when compared to SCH.

**(E)** Quantification of stress granule formation (marked by FMR1) in cells incubated in SCH, KRB, KRB with addition of N-acetyl-L-cysteine (NAC, 30μM or 300μM).

Errors bars: SEM.

---

formation.

AMPK (AMP-activated protein kinase) is a cellular energy sensor and activated by a decrease in intracellular ATP (Miyamoto et al., 2008; Perera and Turner, 2015). As we observed that a sharp decrease in the intracellular concentration of ATP correlates with Sec body formation in KRB (Zhang et al., 2021), we examined whether AMPK activation is involved in stress granule formation in KRB. To test this, we first incubated S2 cells with AMPK activator AICAR (Ducommun et al., 2014) in growing conditions but this did not lead to stress granule formation (**Figure 3C**). Furthermore, we tested whether an inhibitor of AMPK had an inhibitory effect on KRB and SCH150 induced stress granule formation. However, neither Dorsomorphin (Weiss et al., 2010), nor ON123300 (Zhang et al., 2021) showed an effect of stress granule formation (**Figure 3C**). These results suggest that AMPK activation is not necessary for stress granule formation.

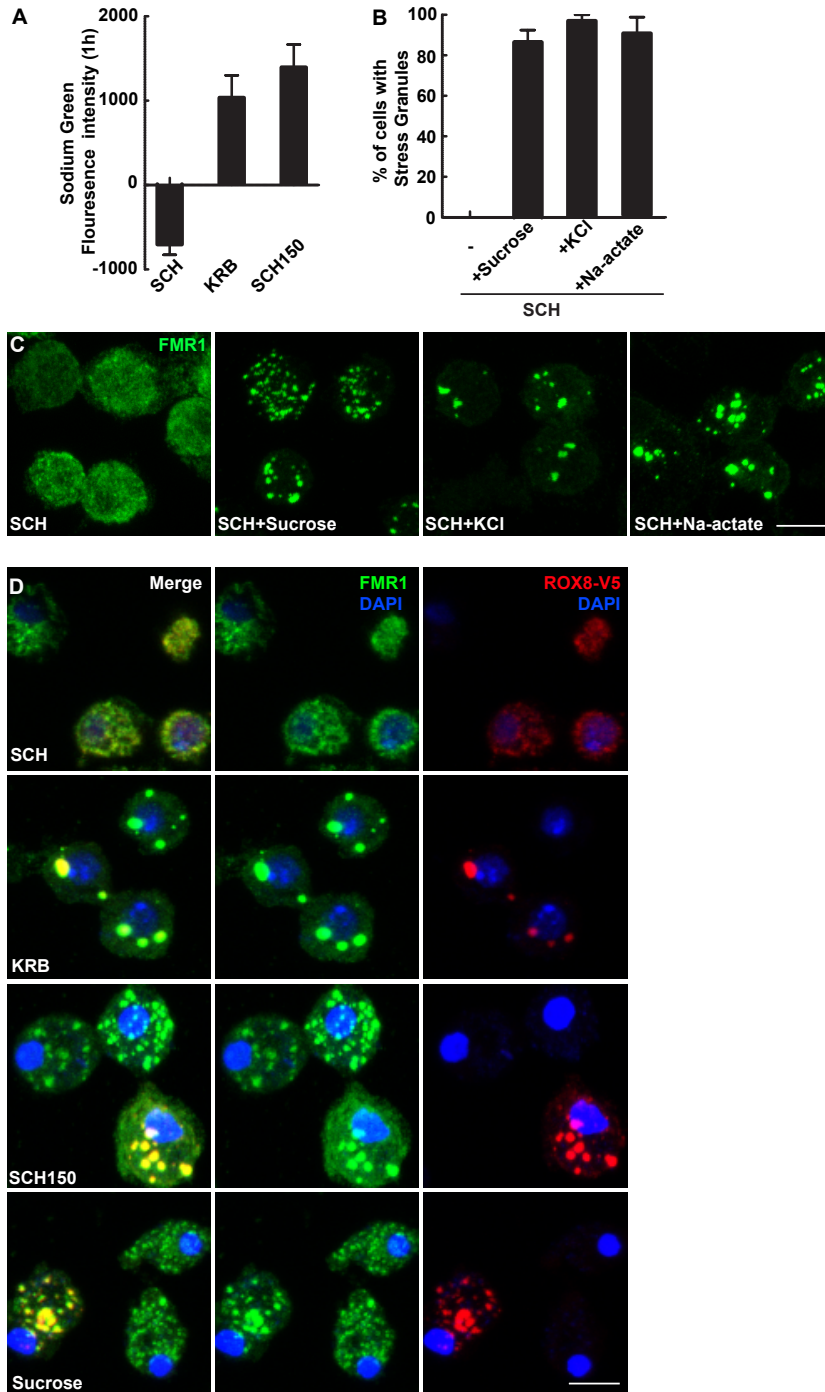
Taken together, the above results indicate that mTOR1 and AMPK are not involved in stress granule formation.

#### *ROS production is not necessary for stress granule formation*

4

To assess which other pathways are stimulated upon KRB incubation that could lead to stress granule formation, we had previously performed an RNA sequencing experiment, the analysis of which suggested that KRB elicits oxidative stress (Zhang et al., 2021). To complete this approach, we performed an analysis by mass spectrometry to identify proteins that are specifically enriched or depleted in cells incubated in this buffer. Overall, KRB incubation for 4h leads to a 30% reduction in protein level, but 59 proteins appear enriched in KRB and 94 appear depleted (**Suppl Table S1**). In particular, the level of the oxidative stress markers peroxiredoxins (Poynton and Hampton, 2014) were reduced after 2h of KRB incubation (not shown), a result in agreement with the RNA sequencing (Zhang et al., 2021). Taken together, the KRB protein and gene signature is suggestive of oxidative stress, indicating that KRB incubation elicits ROS production.

We have previously used DCF fluorescence measurement to visualize ROS production upon KRB and showed that it is efficiently inhibited by N-acetyl-L-cysteine (NAC) (Zhang et al., 2021). In this regard, we tested whether ROS inhibition prevents stress granule formation. However, ROS production inhibition did not modify KRB and SCH150 induced stress granule formation (**Figure 3D**). This is in line with the fact that SCH150 did not elicit ROS (**Figure 3E**). Taken together, ROS production is not necessary for stress granule formation.



---

**Figure 4: Osmotic stress leads to stress granule formation.**

**(A)** Quantification of the increase in Sodium Green fluorescence intensity (measuring the intracellular  $\text{Na}^+$  level) upon SCH, KRB and SCH150.

**(B, C)** Quantification **(B)** and IF visualization **(C)** of stress granule formation (marked by FMR1) in SCH supplemented with sucrose (400mM), KCl (150mM) or Na-acetate (150mM) for 4h at 26°C.

**(D)** IF visualization of overexpressed Rox8-V5 (V5, red) and FMR1 (green) in cells incubated in SCH, KRB, SCH150 and SCH+sucrose (400mM). Note that FMR1 positive stress granules also contain Rox8-V5.

Scale bars: 10 $\mu\text{m}$ . Errors bars: SEM.

---

*Osmotic stress leads to stress granule formation*

We then focused on the non-conventional pathways leading to stress granule formation (see introduction) (Aulas et al., 2017; van Leeuwen and Rabouille, 2019), including osmotic stress. As SCH150 corresponds to a 4-fold increase of  $\text{Na}^+$  in the cell incubation medium (2.6-fold for KRB), we tested whether these media led to an increase of cytoplasmic  $\text{Na}^+$  concentration that can be visualized using Sodium Green Indicator a visible light excitable probe. As expected, we found an  $\text{Na}^+$  concentration increase in KRB and SCH150 (**Figure 4A**).

Accordingly, we asked whether an osmotic shock is enough to induce stress granule formation. Indeed, Addition of 0.4M sucrose leads to a robust stress granule formation (**Figure 4B, C**) and we confirmed that the osmotic stress induced foci are have the same features as stress granule forming upon KRB and SCH150 as they contain also Rox8-v5 (**Figure 4D**) and polyA mRNAs (**Figure 5A**).

To further confirm the role of osmotic stress, we also showed that stress granule strongly formed upon addition of 150mM KCl and Na-acetate (**Figure 4B, C**). This showed that in stark contrast to Sec bodies, stress granule formation is not specific for an increase in NaCl. It also suggests that osmotic stress through an increase in extracellular salt concentration appears to be a factor leading to stress granule formation. It also suggests that KRB and SCH150 leads to this osmotic stress.

*$\text{Ca}^{2+}$  increase is sufficient to drive stress granule formation*

Since the addition of any salt in the medium leads to the formation of stress granule, we also tested  $\text{CaCl}_2$ . This was further motivated by the results of the mass spectrometry (**Figure 6C**), showing that one of the protein whose level most increases upon KRB stress is calmodulin (**Figure 6C; Suppl Table S1**). Calmodulin binds cytoplasmic calcium and acts as

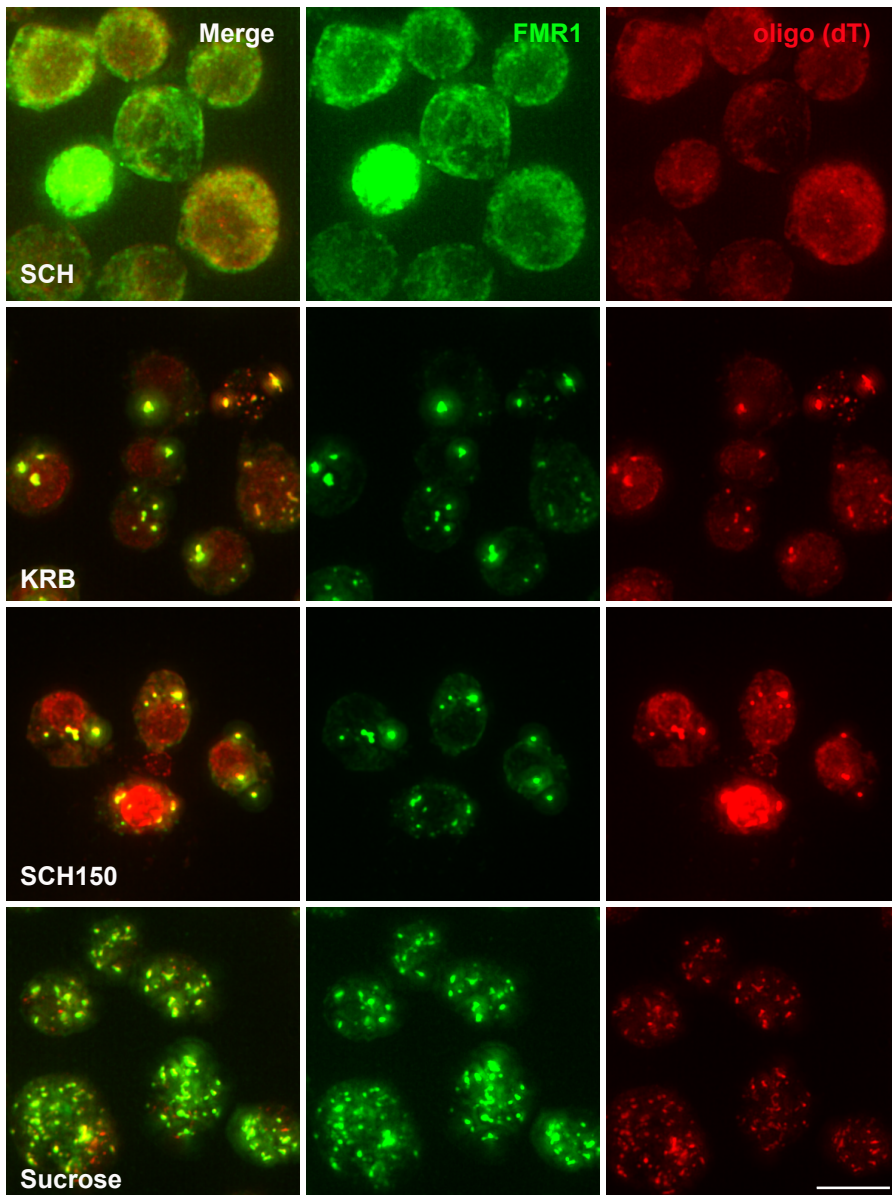


**Figure 5: Stress granule form upon KRB and SCH150 contain polyA mRNA**

Visualization of the oligo (dT) probe (red) by RNA FISH and FMR1 (by IF, green marking stress granules) in cells incubated in KRB and SCH150 and SCH+sucrose. Note that stress granules are positive for polyA mRNAs.

Scale bars: 10µm.

---

signaling hub (Rajan et al., 2017).

Addition of 150mM CaCl<sub>2</sub> in Schneider's strongly induced stress granule formation (**Figure 6A**), as much as NaCl (**Figure 6B**). We then asked whether a decrease in cytoplasmic calcium concentration inhibits stress granule formation. We used BAPTA-AM, a cell permeant calcium chelator, during KRB and SCH150. However, BAPTA-AM did not lead to a decrease in stress granule formation in these conditions (**Figure 6B**). Taken together, the results show that an increase of calcium in the growing medium is sufficient for stress granule formation, but that chelating it in the cytoplasm is not enough to inhibit it.

To further investigate the role of cytoplasmic calcium in stress granule formation calmodulin was depleted from S2 cells by RNAi. Depletion of calmodulin leads to 28% decrease of stress granule formation in KRB and 45% decrease in SCH150 (**Figure 6D**). Although the inhibition is only partial, these results are in line with the notion that the calmodulin, potentially via calcium is instrumental to form stress granules, and with the presence of calcium binding proteins in stress granules (Markmiller et al., 2019; Marmor-Kollet et al., 2020).

Taken together, these results show that stress granules formation in KRB and SCH150 incubated S2 cells is due to osmotic stress partially modulated by calmodulin, suggesting that calcium signaling might be involved.

### *Discussion*

In this study, we found stress granule formation and Sec body formation follow different pathways in *Drosophila* S2 cells, even though these two stress assemblies form under the same stress conditions. Our results show that stress granule formation upon those salt conditions is likely due to osmotic stress modulated by calmodulin activation.

#### *Osmotic stress induces stress granules along non-canonical pathways*

Stress granules are phase separated non-membrane-bound reversible coalescences comprising many RNA binding proteins and RNAs (Buchan and Parker, 2009; Protter and Parker, 2016). The RNA binding protein FMR1 is one of the known stress granule markers in S2 cells. The substantial stress granule formation in salt conditions led us to ask whether those stress granules are bonafide stress granules, not FMR1 aggregation. First, stress granules that form in S2 cells in KRB and SCH150 contain multiple RNA binding proteins such as Rox8 (this study), Caprin and Rasputin (Aguilera-Gomez et al., 2017), although their full protein content has not been investigated as it has in mammalian cells, (Markmiller

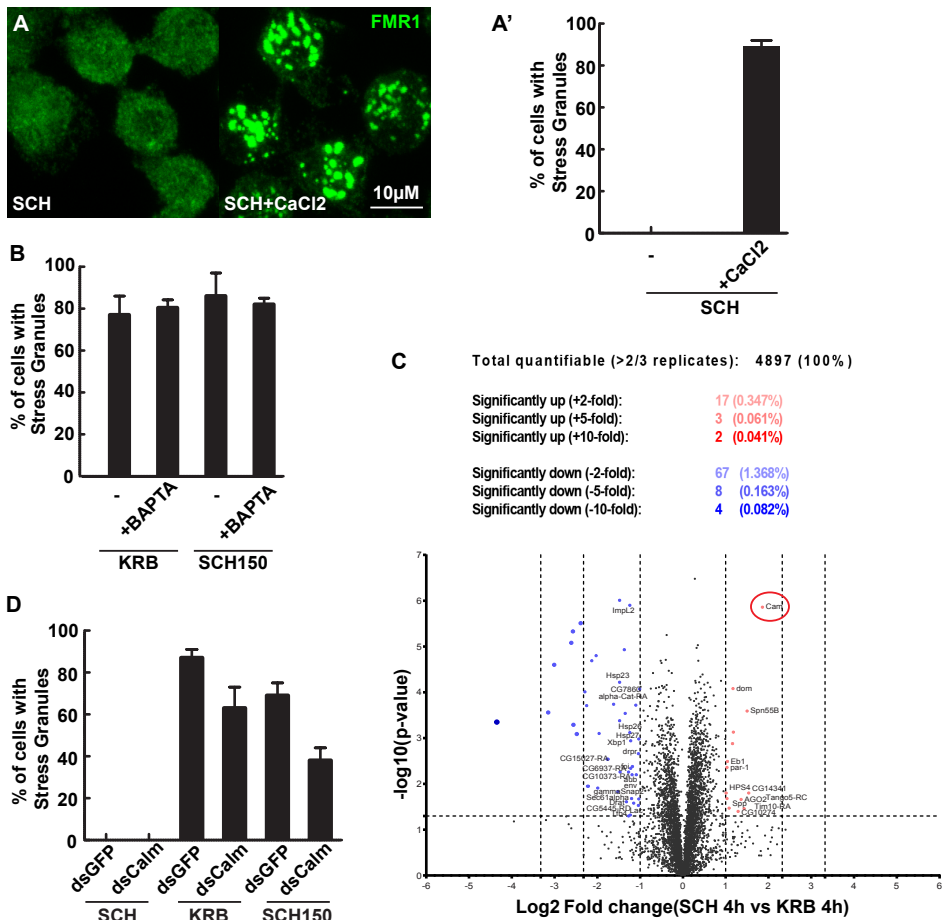


**Figure 6: Calmodulin is involved in KRB and SCH150 driven stress granule formation.**

**(A, A')** IF visualization of stress granule formation (marked by FMR1) in SCH and SCH with addition of CaCl<sub>2</sub> (150mM) after 4 h incubation in 26°C. Quantification of stress granule formation in **(A')**.

**(B)** Quantification of stress granule formation (marked by FMR1) in KRB and SCH150 with or without BAPTA-AM (BAPTA, 100µM).

**(C)** Volcano plot of significantly regulated proteins after KRB 4 h (K) when compared to control cells kept in growing medium Schneider's (S). 59 proteins significantly up-regulated by more than 2-fold (with paired t-test  $p < 0.05$ ) are indicated in red. 94 proteins significantly down-regulated by more than 2-fold (with paired t-test  $p < 0.05$ ) are indicated in blue. The red circle indicates Cam (calmodulin).

**(D)** Quantification of stress granule formation in cells upon mock depletion (dsGFP) and calmodulin depletion (dsCalm) in SCH, KRB or SCH150 after 4 h incubation at 26°C.

Scale bars: 10µm. Errors bars: SEM.

et al., 2019; Marmor-Kollet et al., 2020). Furthermore, they are fully reversible consistent with their formation through phase separation.

Osmotic stress leads to stress granule formation through non-canonical pathways that are independent of eIF2alpha phosphorylation (Anderson and Kedersha, 2002; Aulas et al., 2017), and we find here that it is also the case. Furthermore, mammalian stress granules formed upon osmotic stress appear to contain only a subset of polyA mRNAs (Van Leeuwen and Rabouille, 2019). Here, we show that osmotic stress induces stress granule formation are positive for polyA mRNAs, albeit at a lower level than in other conditions, suggesting that they are potentially non-canonical. Whether eIF4A inhibition by RocA and PatA (Anderson and Kedersha, 2002; Aulas et al., 2017) is involved remains to be elucidated.

#### *Stress granule and Sec body formation in KRB and SCH150 follow different signaling pathways*

Stress granules and Sec bodies form side by side and in similar time frame upon KRB and SCH150 incubation (**Figure 1**). However, their formation follows different pathways. Sec body formation requires the stimulation of two signaling pathways (Zhang et al., 2021). The first is ER stress via IRE1 and PERK activation. However, they do not appear to be sufficient for stress granule formation. The second pathway is high NaCl stress (addition of 150mM NaCl) via SIKs activation, which is sufficient and necessary for Sec body formation (of note, when the NaCl stress is moderate, it does not lead to Sec body formation, IRE1 and PERK activation are needed). However, SIKs activation is not necessary or sufficient for stress granule formation.

Furthermore, Sec body formation requires specific NaCl concentration and only increasing NaCl leads to a substantial formation of Sec bodies. Neither the addition of KCl, Na-acetate nor osmotic shock (sucrose) induces their formation. However, stress granule appears to be formed by the non-differential addition of salts. Addition of sucrose also leads to their formation. As we show that KRB and SCH150 do not lead to a decrease in cell diameter (no apparent shrinkage), it suggests that osmotic salt stress activates other pathways (see below). Taken together, these results suggest that the same cellular stresses induce the formation of two stress assemblies upon the activation of many pathways, a subset of them specifically leading the formation of one assembly while a different subset leads to the formation of the other. It suggests that these incubations are complex. This can also explain that, also they form in close proximity to one another near the ERES (Zacharogianni et al., 2014) and share some components Rasputin (Aguilera-Gomez et al., 2017), these two assemblies remain distinct from one another.



*ER stress can lead to stress granule formation, but it is not required upon KRB and SCH150 induced stress granule formation*

It has been widely reported that stress granules are RNA-containing stress assembly which forms in response to ER stress (Goodier et al., 2007; Kimball, 2003). It is also the case for S2 cells where addition of DTT and ammonium persulfate (APS) and heat stress leads to the formation of stress granules (**Figure 7**).

This strongly suggested that ER stress of S2 cells could be instrumental to stress granule formation, at least upon KRB treatment, as we have shown that it stimulates ER stress (Zhang et al., 2021). However, neither of the ER stress inhibitors (AMG-18, 4u8C, PERKi), nor PERK and ATF6 depletion decrease stress granule formation upon KRB and SCH150. This suggests that although ER stress is sufficient to induce stress granules, ER stress kinases are not involved in KRB and SCH150 induced stress granule formation. of note, this is also the case for mTORC1 signaling. It is inhibited in KRB (Zhang et al., 2021), but its sole inhibition does not lead to stress granule formation.

---

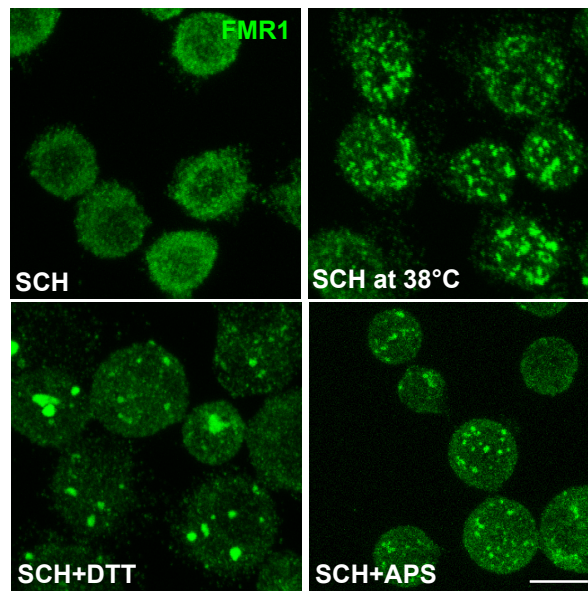


**Figure 7: ER stress leads to stress granule formation in S2 cells.**

**(A)** IF visualization of stress granule formation (marked by FMR1) in SCH and SCH supplemented by DTT (5mM), APS (500uM) for 4 h at 26°C, and SCH for 1 h at 38°C (heat shock).

Scale bars: 10µm.

---

*Ion level change upon osmotic stress leads to stress granule formation via calmodulin*

The assessment of the intracellular  $\text{Na}^+$  concentration suggests that it increases upon KRB and SCH150 incubation. In yeast (Batiza et al., 1996; Matsumoto et al., 2002) and in plant (Tracy et al., 2008), increasing NaCl in the medium is known to lead to an increase of the cytoplasmic calcium concentration through the release of calcium from membrane-bound organelles, such as the ER, the mitochondria, the compartment of the secretory pathway and the endo-lysosomes (Medina et al., 2011). Increasing extracellular  $\text{Ca}^{2+}$  levels have been shown leads to P-body formation in yeast, in a functional calmodulin dependent manner (Kilchert et al., 2010). Here, we show that calmodulin is also involved in stress granule formation in our system, suggesting an involvement of calcium signaling. Interestingly,  $\text{Ca}^{2+}$  binding protein, including calmodulin 1 and 2 have been shown to be incorporated into mammalian stress granules (Markmiller et al., 2019; Marmor-Kollet et al., 2020). Their recruitment is in line with the finding that modulating the intracellular calcium level has an impact on stress granule formation.

Taken together, our study shows that the same cells under the same stresses form two different stress assemblies with similar kinetics by activation of multiple pathways that are differentially used. This could partially explain why the two stress assemblies remain distinct instead of completely phase separating in a single dual structure, even if they form in a close proximity (Zacharogianni et al., 2014) and share component (Aguilera-Gomez et al., 2017).

### *Materials and methods*

#### *Cell culture, KRB incubation, drug treatments and depletions by RNAi*

*Drosophila* S2 cells (R69007, Thermo Fisher Scientific) were cultured in Schneider's medium (Sch, S0146; Sigma) supplemented with 10% insect-tested fetal bovine serum (F4135; Sigma) at 26°C. S2 cells (between passages 5 and 18) were pelleted at 200 g in a microfuge for 3 min, washed once in fresh Schneider's medium, and diluted to 106/ml. 1 ml of cell suspension were plated per well in a 12-well plate containing coverslips. Cells were allowed to attach for 1.5 h before starting the treatment.

Amino acid starvation was performed in Krebs Ringers bicarbonate buffer (KRB) comprising 0.7 mM  $\text{Na}_2\text{HPO}_4$ , 1.5 mM  $\text{NaH}_2\text{PO}_4$ , 15 mM  $\text{NaHCO}_3$  (sodium bicarbonate), 120.7 mM NaCl, 4.53 mM KCl, 0.5 mM MgCl and 10 mM glucose at pH 7.4 as reported (Zhang et al., 2021). SCH84, SCH100 and SCH150 correspond to SCH supplemented with 84, 100 and 150 mM NaCl.

Wild-type *Drosophila* S2 cells were depleted by dsRNAs, as for 5 days previously described (Kondylis and Rabouille, 2003), typically leading to depletion in more than 90% of the cells.

Primers for depletion used were:

dsPERK forward, 5'-TAATACGACTCACTATAGGGAGCTGGAGCTGGCTGTTTT-3';

dsPERK reverse, 5'- TAATACGACTCACTATAGGGTACTGGCGGATATCGGCTTC-3',

dsATF6 forward, 5'- TAATACGACTCACTATAGGGAGCGGCATGTCATAGCTGTA-3',

dsATF6 reverse, 5'- TAATACGACTCACTATAGGGTTGACGAGAAATGCAATCCA-3',

dsCalmodulin forward, 5'- TAATACGACTCACTATAGGGCACCTACAAAAATGGCCGA-3',

dsCalmodulin reverse, 5'- TAATACGACTCACTATAGGGTCTTCGTAATTGACCTGACCG-3'.

### *Molecular cloning and transfection*

To generate pMT-Rox8-V5, Rox8 was amplified from a cDNA library made from S2 cells and cloned into pMT-V5 using the restriction enzymes KpnI and EcoRV. Primer used were:

Rox8 forward: 5'-GGGATCTAGATCGGGGTACCATGGACGAGTCGCAACCG-3',

Rox8 reverse: 5'-GCCACTGTGCTGGATATCTTGGGTCTGGTATTGTGGCATCG-3'.

### *Cell treatment*

Drug treatment was performed on the plated cells at 26°C for 4 h incubated either in Schneider's medium or in KRB or in SCH150 (as in (Zhang et al., 2021)).

### *Antibodies*

For immunofluorescence, we used the rabbit polyclonal anti-Sec16 (1:800) (Ivan et al., 2008) to detect Sec16, the mouse monoclonal anti-FMR1 (1:20, deposited by Siomi, H. DSHB). Donkey anti-rabbit-IgG conjugated to Alexa Fluor 568 (1:200, A10042, Invitrogen) and a goat anti-mouse-IgG conjugated to Alexa Fluor 488 (1:200 A11001, Invitrogen) were used as secondary antibodies.

For western blotting, we used a rabbit a rabbit monoclonal antibody anti-Phospho-eIF2 $\alpha$  (Ser51) (1:1000, 9721S, Cell Signaling) and a mouse monoclonal anti- $\alpha$ -tubulin (1:2500, T5168, Sigma-Aldrich) followed by anti-rabbit-IgG and mouse-IgG antibodies coupled to HRP (1:2000, NA934, NA931, GE Healthcare).

### *Immunofluorescence*

For immunofluorescence, cells were fixed with 4% paraformaldehyde in PBS (pH 7.4) for 20 min. Cells were then washed three times with PBS and subsequently quenched by incubation in 50 mM NH<sub>4</sub>Cl in PBS for 5 min followed by permeabilization with 0.11% Triton X-100 for 5 min. Thereafter, cells were washed three times in PBS and blocked in PBS

---

supplemented with 0.5% fish skin gelatin (G7765, Sigma-Aldrich) for 20 min. Cells were then incubated with the primary antibody (in blocking buffer) for 25 min, washed three times with blocking buffer and incubated with the secondary antibody (in blocking buffer) coupled to a fluorescent dye for 20 min. Cells on the coverslip were washed twice in milliQ water and dried for 3 min on a tissue with cells facing up. Finally, each coverslip with cells was mounted with Prolong antifade medium (+DAPI, P36935, Invitrogen) on a microscope slide. Samples were viewed with a Leica SPE confocal microscope using a 63× oil lens and 2× zoom.

### *Quantification*

The quantification of stress granule formation was performed by counting the cells in which 3-5 FMR1 positive foci form (visualized by Immunofluorescence). Experiments were performed two times or more unless otherwise stated. At least four to five fields (~25–30 cells per field) were recorded and analyzed per experiment as in (Zhang et al., 2021)

### *Sodium Green Indicator assay*

The stock solution of Sodium Green (5 mM in DMSO) was diluted to 5  $\mu$ M in Schneider's medium directly before usage. 106 cells/ml were incubated with 5  $\mu$ M Sodium Green in Schneider's in the dark for 1h at 26°C in a 48-well plate. After incubation, the cells were washed three times with Schneider's medium to remove excess Sodium Green. The cells were then incubated in the treatment medium and the fluorescence intensity of the dye was immediately recorded over a period of 1h at 26°C using a Spark multimode microplate reader (Tecan) with an excitation of 480 nm and an emission of 530 nm. The fluorescence intensity of five fields of cells per condition was measured every 5 min for a period of 1 h. Each experiment was performed at least three times or more. The differences in Sodium Green intensity for each condition was calculated by using the last value (1 h) minus the first value (0 h).

### *RNA FISH*

KRB, SCH150, 0.4M sucrose wild-type S2 cells were fixed and labeled for endogenous FMR1. After incubation with the secondary antibody, cells were washed three times with PBS and cells were post-fixed in 4% paraformaldehyde in PBS (pH 7.4) for 10 min. Following a washing three times in PBS, cells were further incubated for 5 min in 10% formamide (17899, Thermo Fisher Scientific) in DEPC-treated water. They were then incubated overnight on a droplet containing one fluorescent RNA FISH (polydT) probe [125 nM in 1% dextran sulfate (D8906, Sigma-Aldrich), 10% formamide in DEPC-treated water at 37°C] in a moistened chamber to avoid drying. Cells were washed twice for 30 min with 10%

formamide in DEPC-treated water and mounted with Prolong antifade medium (plus DAPI) on a microscope slide. The TMR-oligo(dT) 30× was purchased from IDT. A widefield Leica MM-AF microscope with a 100× lens was used for imaging.

#### *Mass Spectrometry Proteome analysis*

8 million cells per condition were grown in Schneider's and starved in KRB for 2h and 4h in 6 cm dishes at 26°C. After incubation, cells were harvested cells on ice, and cell pellets were and washed twice with ice-cold PBS. Cell material was lysed by gentle vertexing in 8M Urea in 50mM ammonium bicarbonate supplemented with 50µg/ml DNase I (Sigma-Aldrich), 50µg/ml RNase A (Sigma-Aldrich) and 1x complete EDTA-free protease inhibitor cocktail (Roche Diagnostics). Subsequently, the lysate was cleared by centrifugation for 1h at 18,000 x g at 15°C. Protein concentration was determined with the Bradford assay (Bio-Rad). For each sample, 20µg of total protein was reduced, alkylated and digested sequentially with Lys-C (1:100) and trypsin (1:75), and perfectionated pre-fractionated offline on C18 STAGE-tips. Peptides were eluted in 5 high-pH reversed phase fractions, with 11-80% acetonitrile. All samples were dried by vacuum centrifugation and reconstituted in 102% formic acid prior to LC-MS/MS analyses.

MS data was acquired with an UHPLC 1290 system (Agilent) coupled to a Q-Exactive HF mass spectrometer (Thermo Fischer Scientific). Peptides were trapped (Dr Maisch Reprosil C18, 3µM, 2cm x 100µM) for 5min in solvent A (0.1% formic acid in water) before being separated on an analytical column (Agilent Poroshell, EC-C18, 2.7µM, 50cm x 75µM). Solvent B consisted of 0.1% formic acid in 80% acetonitrile. The mass spectrometer operated in data-dependent mode. Full scan MS spectra from m/z 375 – 1600 were acquired at a resolution of 60,000 to a target value of 3x10<sup>6</sup> or a maximum injection time of 20ms. The top 15 most intense precursors with a charge state of 2+ to 5+ were chosen for fragmentation. HCD fragmentation was performed at 27% normalized collision energy on selected precursors with 16s dynamic exclusion at a 1.4m/z isolation window after accumulation to 1x10<sup>5</sup> ions or a maximum injection time of 50ms. Tandem mass spectrometry (MS/MS) spectra were acquired at a resolution of 15,000.

#### *Acknowledgments*

We thank Sem Brussee for the calmodulin depletion experiment, and the Hubrecht Imaging Center for support with microscopy. We acknowledge Genentech for providing us with the IRE1 inhibitor AMG18.

#### *Funding*

C.Z. is supported by a scholarship of the China Scholarship Council (201706670014).

## Supplemental data

**Suppl. Table S1:** Protein list for 4h KRB VS SCH. This table is available as Excel file upon request.

## References

- Aguilera-Gomez, A., Zacharogianni, M., van Oorschot, M.M., Genau, H., Grond, R., Veenendaal, T., Sinsimer, K.S., Gavis, E.R., Behrends, C., and Rabouille, C. (2017). Phospho-Rasputin Stabilization by Sec16 is Required for Stress Granule Formation upon Amino Acid Starvation. *Cell Report* 20, 935-948.
- Anderson, P., and Kedersha, N. (2002). Stressful initiations. *Journal of Cell Science* 115, 3227-3234.
- Aulas, A., Fay, M.M., Lyons, S.M., Achorn, C.A., Kedersha, N., Anderson, P., and Ivanov, P. (2017). Stress-specific differences in assembly and composition of stress granules and related foci. *Journal of Cell Science* 130, 927-937.
- Banani, S.F., Rice, A.M., Peeples, W.B., Lin, Y., Jain, S., Parker, R., and Rosen, M.K. (2016). Compositional Control of Phase-Separated Cellular Bodies. *Cell* 166, 651-663.
- Batiza, A.F., Schulz, T., and Masson, P.H. (1996). Yeast Respond to Hypotonic Shock with a Calcium Pulse. *Journal of Biological Chemistry* 271, 23357-23362.
- Buchan, J.R., and Parker, R. (2009). Eukaryotic stress granules: the ins and outs of translation. *Molecular Cell* 36, 932-941.
- Condon, K.J., and Sabatini, D.M. (2019). Nutrient regulation of mTORC1 at a glance. *Journal of Cell Science* 132, jcs222570.
- Dever, T.E., and Hinnebusch, A.G. (2005). GCN2 whets the appetite for amino acids. *Molecular Cell* 18, 141-142.
- Ducommun, S., Ford, R.J., Bultot, L., Deak, M., Bertrand, L., Kemp, B.E., Steinberg, G.R., and Sakamoto, K. (2014). Enhanced activation of cellular AMPK by dual-small molecule treatment: AICAR and A769662. *American Journal of Physiology, Endocrinology and Metabolism* 306, E688-696.
- Gomes, E., and Shorter, J. (2018). The molecular language of membraneless organelles. *Journal of Biological Chemistry* 294, 7115-7127.
- Goodier, J.L., Zhang, L., Vetter, M.R., and Kazazian, H.H., Jr. (2007). LINE-1 ORF1 protein localizes in stress granules with other RNA-binding proteins, including components of RNA interference RNA-induced silencing complex. *Molecular Cell Biology* 27, 6469-6483.
- Hetz, C. (2012). The unfolded protein response: controlling cell fate decisions under ER stress and beyond. *Nature reviews Molecular Cell Biology* 13, 89-102.
- Ivan, V., de Voer, G., Xanthakis, D., Spoorendonk, K.M., Kondylis, V., and Rabouille, C. (2008). *Drosophila* Sec16 mediates the biogenesis of tER sites upstream of Sar1 through an arginine-rich motif. *Molecular Biology of the Cell* 19, 4352-4365.
- Jacinto, E., Loewith, R., Schmidt, A., Lin, S., Ruegg, M.A., Hall, A., and Hall, M.N. (2004). Mammalian TOR complex 2 controls the actin cytoskeleton and is rapamycin insensitive. *Nature Cell Biology* 6, 1122-1128.
- Kedersha, N., Panas, M.D., Achorn, C.A., Lyons, S., Tisdale, S., Hickman, T., Thomas, M., Lieberman, J., McInerney, G.M., Ivanov, P., et al. (2016). G3BP-Caprin1-USP10 complexes mediate stress granule condensation and associate with 40S subunits. *Journal of Cell Biology* 212, 845-860.
- Kedersha, N.L., Gupta, M., Li, W., Miller, I., and Anderson, P. (1999). RNA-binding proteins TIA-1 and TIAR link the phosphorylation of eIF-2 alpha to the assembly of mammalian stress granules. *Journal*

of Cell Biology 147, 1431-1442.

Kilchert, C., Weidner, J., Prescianotto-Baschong, C., and Spang, A. (2010). Defects in the secretory pathway and high Ca<sup>2+</sup> induce multiple P-bodies. *Molecular Biology of the Cell* 21, 2624-2638.

Kim, J., and Guan, K.-L. (2019). mTOR as a central hub of nutrient signalling and cell growth. *Nature Cell Biology* 21, 63-71.

Kimball, S.R., Rick L. Horetsky, David Ron, Leonard S. Jefferson, and Heather P. Harding (2003). Mammalian stress granules represent sites of accumulation of stalled translation initiation complexes. *American Journal of Physiology-Cell Physiology* 284, C273-C284.

Li, S., Brown, M.S., and Goldstein, J.L. (2010). Bifurcation of insulin signaling pathway in rat liver: mTORC1 required for stimulation of lipogenesis, but not inhibition of gluconeogenesis. *Proceedings of the National Academy of Sciences USA* 107, 3441-3446.

Ma, X., Wang, H., Ji, J., Xu, W., Sun, Y., Li, W., Zhang, X., Chen, J., and Xue, L. (2017). Hippo signaling promotes JNK-dependent cell migration. *Proceedings of the National Academy of Sciences USA* 114, 1934-1939.

Manifava, M., Smith, M., Rotondo, S., Walker, S., Niewczas, I., Zoncu, R., Clark, J., and Ktistakis, N.T. (2016). Dynamics of mTORC1 activation in response to amino acids. *eLife* 5.

Markmiller, S., Soltanieh, S., Server, K.L., Mak, R., Jin, W., Fang, M.Y., Luo, E.C., Krach, F., Yang, D., Sen, A., et al. (2019). Context-Dependent and Disease-Specific Diversity in Protein Interactions within Stress Granules. *Cell* 172, 590-604.

Marmor-Kollet, H., Siany, A., Kedersha, N., Knafo, N., Rivkin, N., Danino, Y.M., Moens, T.G., Olender, T., Sheban, D., Cohen, N., et al. (2020). Spatiotemporal Proteomic Analysis of Stress Granule Disassembly Using APEX Reveals Regulation by SUMOylation and Links to ALS Pathogenesis. *Molecular Cell* 80, 876-891.

Matsumoto, T.K., Ellsmore, A.J., Cessna, S.G., Low, P.S., Pardo, J.M., Bressan, R.A., and Hasegawa, P.M. (2002). An Osmotically Induced Cytosolic Ca<sup>2+</sup> Transient Activates Calcineurin Signaling to Mediate Ion Homeostasis and Salt Tolerance of *Saccharomyces cerevisiae*. *Journal of Biological Chemistry* 277, 33075-33080.

Medina, D.L., Fraldi, A., Bouche, V., Annunziata, F., Mansueto, G., Spampanato, C., Puri, C., Pignata, A., Martina, J.A., Sardiello, M., et al. (2011). Transcriptional activation of lysosomal exocytosis promotes cellular clearance. *Developmental Cell* 21, 421-430.

Miyamoto, T., Oshiro, N., Yoshino, K., Nakashima, A., Eguchi, S., Takahashi, M., Ono, Y., Kikkawa, U., and Yonezawa, K. (2008). AMP-activated protein kinase phosphorylates Golgi-specific brefeldin A resistance factor 1 at Thr1337 to induce disassembly of Golgi apparatus. *J Biol Chem* 283, 4430-4438.

Patel, A., Lee, H.O., Jawerth, L., Maharana, S., Jahnel, M., Hein, M.Y., Stoykov, S., Mahamid, J., Saha, S., Franzmann, T.M., et al. (2015). A Liquid-to-Solid Phase Transition of the ALS Protein FUS Accelerated by Disease Mutation. *Cell* 162, 1066-1077.

Perera, N.D., and Turner, B.J. (2015). AMPK Signalling and Defective Energy Metabolism in Amyotrophic Lateral Sclerosis. *Neurochemical Research* 41, 544-553.

Poynton, R.A., and Hampton, M.B. (2014). Peroxiredoxins as biomarkers of oxidative stress. *Biochimica et biophysica acta* 1840, 906-912.

Protter, D.S., and Parker, R. (2016). Principles and Properties of Stress Granules. *Trends in Cell Biology* 26, 668-679.

Rajan, A., Housden, B.E., Wirtz-Peitz, F., Holderbaum, L., and Perrimon, N. (2017). A Mechanism

---

Coupling Systemic Energy Sensing to Adipokine Secretion. *Developmental Cell* 43, 83-98.

Towle, H.C. (2007). The metabolic sensor GCN2 branches out. *Cell metabolism* 5, 85-87.

Tracy, F.E., Gilliam, M., Dodd, A.N., Webb, A.A., and Tester, M. (2008). NaCl-induced changes in cytosolic free Ca<sup>2+</sup> in *Arabidopsis thaliana* are heterogeneous and modified by external ionic composition. *Plant Cell Environ* 31, 1063-1073.

van Leeuwen, W., and Rabouille, C. (2019). Cellular stress leads to the formation of membraneless stress assemblies in eukaryotic cells. *Traffic* 20(9):623-638

Walter, P., and Ron, D. (2011). The Unfolded Protein Response: From Stress Pathway to Homeostatic Regulation. *Science* 334, 1081-1086.

Weiss, A., Charbonnier, E., Ellertsdottir, E., Tsigos, A., Wolf, C., Schuh, R., Pyrowolakis, G., and Affolter, M. (2010). A conserved activation element in BMP signaling during *Drosophila* development. *Nature structural & molecular biology* 17, 69-76.

Zacharogianni, M., Aguilera-Gomez, A., Veenendaal, T., Smout, J., and Rabouille, C. (2014). A stress assembly that confers cell viability by preserving ERES components during amino-acid starvation. *eLife* 3.

Zhang, C., van Leeuwen, W., Blotenburg, M., Aguilera-Gomez, A., Brussee, S., Grond, R., Kampinga, H.H., and Rabouille, C. (2021). Activation of IRE1, PERK and salt-inducible kinases leads to Sec body formation in *Drosophila* S2 cells. *Journal of Cell Science* 134, jcs258685.







## *Chapter5*

*Novel components of the stress assembly  
Sec body identified by proximity labeling*

Chujun Zhang, J. Mirjam A. Damen, Rianne Ground,  
Catherine Rabouille and Wei Wu (2022)  
Submitted to Journal of Cell Biology

---

## *Novel components of the stress assembly Sec body identified by proximity labeling*

### *Abstract*

Sec bodies are membraneless stress-induced assemblies that form by the coalescence of Endoplasmic Reticulum Exit Sites (ERES). By APEX2 tagging of Sec24AB, we biotinylated and identified the full complement of Sec body proteins. In the presence of biotin-phenol and H<sub>2</sub>O<sub>2</sub> (APEX on), APEX2 facilitates the transfer of a biotin moiety to nearby interactors of chimeric Sec24AB. Using this un-biased approach comparing APEX on and off (-H<sub>2</sub>O<sub>2</sub>) conditions, we identified 52 proteins specifically enriched in Sec bodies. These include a large proportion of ER and Golgi proteins, packaged without defined stoichiometry, which we could selectively verify by imaging. Interestingly, Sec body components are neither transcriptionally nor translationally regulated under the conditions that induce Sec body formation, suggesting that incorporation of these proteins into granules may be driven instead by aggregation of nucleating proteins with high content of intrinsically disordered regions. This reinforces the notion that Sec bodies may act as storage for ERES, ER and Golgi components during stress.

### *Introduction*

The intracellular content is compartmentalized through the formation of either membrane-bound compartments sealed by a lipid bilayer (Mellman and Warren, 2000), or membraneless organelles (Hyman et al., 2014). The latter are formed by phase separation, a process by which diffuse macromolecules coalesce into a mesoscale structure (van Leeuwen and Rabouille, 2019; Zhang and Rabouille, 2019). Although a number of membraneless organelles are stable in growing cells and are critical to their physiology (such as the nucleolus) (Berchtold et al., 2018), others appear to form in response to cellular stress. For instance, ER and oxidative stress can lead to the formation of reversible stress granules (Aulas et al., 2017; Aulas et al., 2018; Jevtov et al., 2015; van Leeuwen and Rabouille, 2019) that contain specific RNA binding proteins (Khong et al., 2017) and a large collection of RNAs (Protter and Parker, 2016) that appear to be stored in these structures during the period of stress.

Interestingly, stress granules can also form in stressed *Drosophila* S2 cells (Aguilera-Gomez et al., 2017; Zacharogianni et al., 2014; Zhang. et al., 2022), along with other stress assemblies that are not RNA-based. In this regard, we have shown that amino-acid starvation combined with salt stress (in the Krebs Ringer Bicarbonate buffer, KRB) can

trigger Sec body formation (Zacharogianni et al., 2014; Zhang et al., 2021).

Sec bodies form around components functioning at ER exit sites (ERES), where proteins destined to the plasma membrane, the extracellular medium and nearly all membrane compartments of the cell exit the ER and transit to the Golgi apparatus and correct downstream compartments. ERES are characterized by COPII coated vesicles of 70 nm in diameter (Barlowe et al., 1994; Barlowe and Schekman, 1993) that are concentrated near an ER cup-shaped membrane (Ivan et al., 2008; Kondylis et al., 2005). COPII coat formation is regulated and requires a defined set of proteins. Sec12 is a key transmembrane protein in this process and acts as a GTP-exchange factor for the small GTPase Sar1. Once in its GTP-bound form, Sar1 is inserted in the ER membrane and recruits the two subunits COPII subunits Sec23/Sec24 that together form the inner COPII coat (Stagg et al., 2006). The outercoat Sec13/31 is then recruited. This coat assembly is concomitant with the budding of vesicles at the ER cup-shaped membrane, leading to the formation of COPII coated vesicles (Gomez-Navarro and Miller, 2016). Importantly, optimal COPII coat assembly also requires a large protein Sec16 that has been shown to interact with all COPII subunits (Sprangers and Rabouille, 2015). This is exemplified by the effect of Sec16 mutation or loss of function in many species that leads to a severe impairment in trafficking through the secretory pathway (Connerly et al., 2005; Farhan et al., 2010; Hughes et al., 2009; Ivan et al., 2008; Joo et al., 2016; Kaiser and Schekman, 1990; Supek et al., 2002; Wilhelmi et al., 2016).

Sec bodies are non-membrane bound compartments that are quickly reversible upon stress relief and display features of liquid-like droplets (Zacharogianni et al., 2014), consistent with their formation by phase separation. This process has been shown to be driven by specific proteins that when depleted prevent condensation of a given structure. These drivers have been shown to contain a large number of low-complexity sequences that are often intrinsically disordered (Banani et al., 2016). In this regard, depletion of the Sec24AB isoform (Zacharogianni et al., 2014) and Sec16 (Aguilera-Gomez et al., 2016) from *Drosophila* S2 cells prevents Sec body formation. Interestingly, these two proteins contain a large proportion of disordered regions that are concentrated in the N-terminal sequence in Sec24AB and throughout the protein in Sec16 (Zacharogianni et al., 2014). Importantly, membraneless organelles also contain many client proteins that passively coalesce. Interestingly, these clients also often contain disordered regions that are thought to help their recruitment (Banani et al., 2016).

To date, immunofluorescence of endogenous and tagged proteins has revealed

that Sec bodies contain Sec16 as a key marker, and most of the COPII subunits Sec24AB, Sec24CD, Sec23 and Sec31 but not Sar1 (Zacharogianni et al., 2014). In addition, few Golgi proteins appear to overlap with these structures. However, the rest of the Sec body composition is still largely unclear. Here, we aim to identify additional Sec body components using APEX2 proximity labeling (Hung et al., 2016). In the presence of biotin-phenol and  $\text{H}_2\text{O}_2$ , APEX facilitates the transfer of a biotin moiety to nearby proteins. When the APEX is fused to a protein of a given compartment, it allows the quantitative identification of other immediate proteins in the same compartment by mass spectrometry. Interestingly, the APEX2 strategy was successfully applied to map the components of stress granules in mammalian cells (Markmiller et al., 2018; Marmor-Kollet et al., 2020).

To identify Sec body components, we tagged the COPII subunit Sec24AB with APEX2 and GFP. This chimera was successfully incorporated to Sec bodies in KRB stressed S2 cells. This allowed the identification of 52 proteins present in Sec bodies, including a large pool of ERES proteins like Sec16 and other COPII subunits, as well as components functioning at the ER and the Golgi apparatus. In line with phase separation, most of the 52 identified components contain intrinsically disordered regions that are proposed to contribute to the coalescence (Babu et al., 2012; Guillen-Boixet et al., 2020). Importantly, these components are neither regulated transcriptionally nor translationally, suggesting a re-location to Sec bodies that likely could act as storage during the period of stress.

## Results and discussion

### *Sec24-APEX2 mediates biotinylation of Sec body proteins*

To investigate the protein species packaged in Sec bodies, we performed proximity labeling using an inducible ascorbate peroxidase (APEX2) system in the S2 cell line (**Figure 1A**). To spatially localize the APEX activity to Sec bodies, we fused GFP-APEX2 C-terminally to Sec24, which is a well-characterized Sec body protein (Zacharogianni et al., 2014). Such a construct allows the fusion protein expression to be monitored by GFP fluorescence, proximity biotin ligation to be assessed by streptavidin-A568 staining, and spatial co-localization of Sec24 and biotinylated sec body proteins to be verified by overlay of fluorescence signals in confocal microscopy images. In our model system, not only is the expression of Sec24-GFP-APEX2 inducible, the APEX activity can be further controlled by the addition or removal of Biotin-Phenol (BP) and  $\text{H}_2\text{O}_2$ , which are critical cofactors essential for biotinylation to take place. The +BP- $\text{H}_2\text{O}_2$  (APEX off) condition serves as the

most stringent control to eliminate background biotinylation events independent of APEX2 (**Figure 1B**). In the absence of APEX reaction triggered by  $H_2O_2$ , Sec bodies can form upon KRB incubation, but proteins surrounding Sec24 will not be biotinylated. In the presence of APEX triggered by  $H_2O_2$ , soluble Sec24 interactors will be labeled by biotin in SCH media, whereas proteins surrounding Sec24 in starvation-induced Sec bodies will be labeled in KRB media, a condition that readily induces Sec body formation (Zhang et al., 2021).

As shown in **Figure 1C**, in APEX off condition, the streptavidin staining is diffuse in the cytoplasm. In SCH APEX on, the streptavidin staining colocalizes with Sec24 at ER exit sites, consistent with the expected localization of Sec24 in growing conditions (Ivan et al., 2008). In KRB APEX on condition, Sec24 co-localizes perfectly with local biotinylation in Sec bodies induced by KRB. Biochemically, proximally biotinylated proteins can be prominently retrieved by streptavidin pulldown (**Figure 1D**), against the background of endogenously biotinylated protein like acetyl-coA carboxylases. With two independent experiments, each activating Sec24-APEX2 under the growing (SCH) or stress (KRB) conditions, we aim to elucidate the protein composition of Sec bodies in a hypothesis-free and unbiased manner (**Figure 1E-F**) by mass spectrometry.

#### *The Sec24 spatial interactome*

Since Sec24 is robustly localized to Sec bodies during amino acid starvation in KRB, the interactome proximal to Sec24 under KRB condition approximates the sub-cellular Sec body proteome, although a physical isolation of such a membrane-less organelle is not yet possible. By virtue of biotin ligation on other proximal proteins in the vicinity of Sec24, it is possible to compare the spatial interactome of Sec24 during growing and starvation conditions respectively, using our Sec24-GFP-APEX2 inducible system, to identify bona fide Sec body proteins. The premise of investigation is that cytosolic Sec24 will localize to Sec bodies upon starvation in KRB, and hence be surrounded by different proteins that together make up the Sec body (**Figure 1E**). Sec24-interacting proteins can be, (1) specific to growing conditions (**Figure 1E**, yellow), (2) specific to KRB stress (**Figure 1E**, blue), or (3) shared in both conditions (**Figure 1E**, pink). To distinguish these different types of Sec24 interactors, we employed two experimental schemes, each compared internally to the APEX off condition, to rule out APEX-independent biotinylation (**Figure 1F**).

After cell lysis and streptavidin pulldown, biotinylated proteins were analyzed by quantitative mass spectrometry in triplicates. In **Figure 2A**, data points of the same colour indicate the close technical reproducibility of mass spectrometry measurements, for samples of the same condition. The overall change in biotinylation from -BP- $H_2O_2$  to

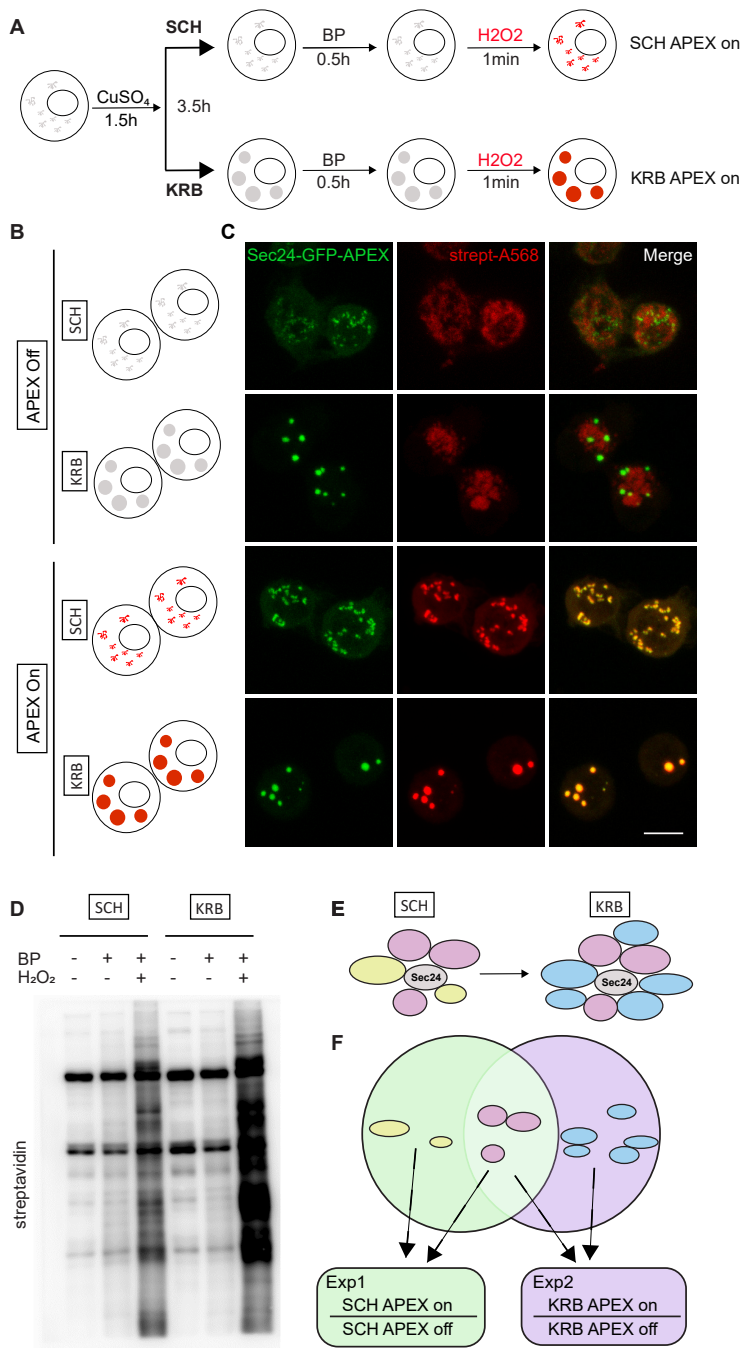




**Figure 1: Modeling the Sec24 interactome during growing and starvation conditions.** (A) Schematic workflow of APEX proximity labeling. For each condition, cells were treated for a total of 4h after 1.5h induction with  $\text{CuSO}_4$ . Biotin-Phenol (BP) was added in the last 0.5h, and  $\text{H}_2\text{O}_2$  in the last 1 min for pulsed biotin labeling within the vicinity of Sec24. The biotinylated Sec14AB interactome is marked in red. (B) Expected outcome of APEX labeling and Sec body formation. In the absence of APEX triggered by  $\text{H}_2\text{O}_2$ , Sec bodies can form upon amino acid starvation buffer KRB incubation, but proteins surrounding Sec24 will not be biotinylated. In the presence of APEX triggered by  $\text{H}_2\text{O}_2$ , soluble Sec24 interactors will be labeled by biotin in SCH media, and proteins surrounding Sec24 in starvation-induced Sec bodies will be labeled in KRB media. (C) Immunofluorescence image of streptavidin staining in Sec24-APEX2 cells. Complete co-localization of Sec24-GFP-APEX2 and biotin (strept-A568) in Sec bodies in KRB media confirms the specificity of local biotinylation in the Sec24-APEX2 model system. Scale bar: 10  $\mu\text{m}$ . (D) Streptavidin-HRP western blot analysis of induced protein biotinylation in lysates from Sec24-GFP-APEX2 cells. Strong biotinylation signals were detected in the +BP+ $\text{H}_2\text{O}_2$  conditions, where full APEX activation is expected. (E) Experimental design to distinguish Sec24 interactors in growing condition and Sec body components during starvation. Soluble Sec24 interactors are annotated in yellow (Exp 1); Sec body proteins during starvation are annotated in blue (Exp 2). Universal interactors that may exist in both conditions are annotated in pink (overlap).

+BP- $\text{H}_2\text{O}_2$  (APEX off) to +BP+ $\text{H}_2\text{O}_2$  (APEX on) conditions can be followed in the PCA plot by black arrows (for growing condition) and red arrows (for KRB condition) respectively. The biggest deviation in path between APEX on and APEX off conditions was observed with KRB, suggesting that the Sec24 interactome shows the biggest change upon KRB stress, and that our experimental setup was highly selective and well-capable of identifying bona fide proteins targeted to Sec bodies. From this, only 19 and 52 proteins (Figure 2B) were specifically enriched in SCH (Exp 1) and KRB (Exp 2) conditions respectively, using a threshold of at least two-fold quantitative enrichment in APEX on: APEX off ( $p < 0.05$ ). These constitute Sec24 interactors and putative Sec body components respectively.

The focused heatmap visualization of only putative Sec body proteins (Figure 2C) clearly shows that these 52 proteins are highly APEX-dependent. In addition, a small sub-cluster (annotated with black sidebar) seems to be significantly more enriched in KRB APEX on condition. Specific Sec24 interactors are quantitatively visualized in Figure 2D and Figure 2E. Interestingly, the overlap between Exp 1 and Exp 2 is small and consists only of Sec31 and Sec24CD (Figure 2B; circle in Figure 2D-E) that were biotinylated in both growing and KRB conditions. This suggests that these proteins are common interactors in both conditions, regardless of whether Sec24AB is at ERES or in Sec bodies. This finding is consistent with the function of these proteins as COPII subunits in COPII coat formation and their known recruitment to KRB induced Sec bodies (Zacharogianni et al., 2014).

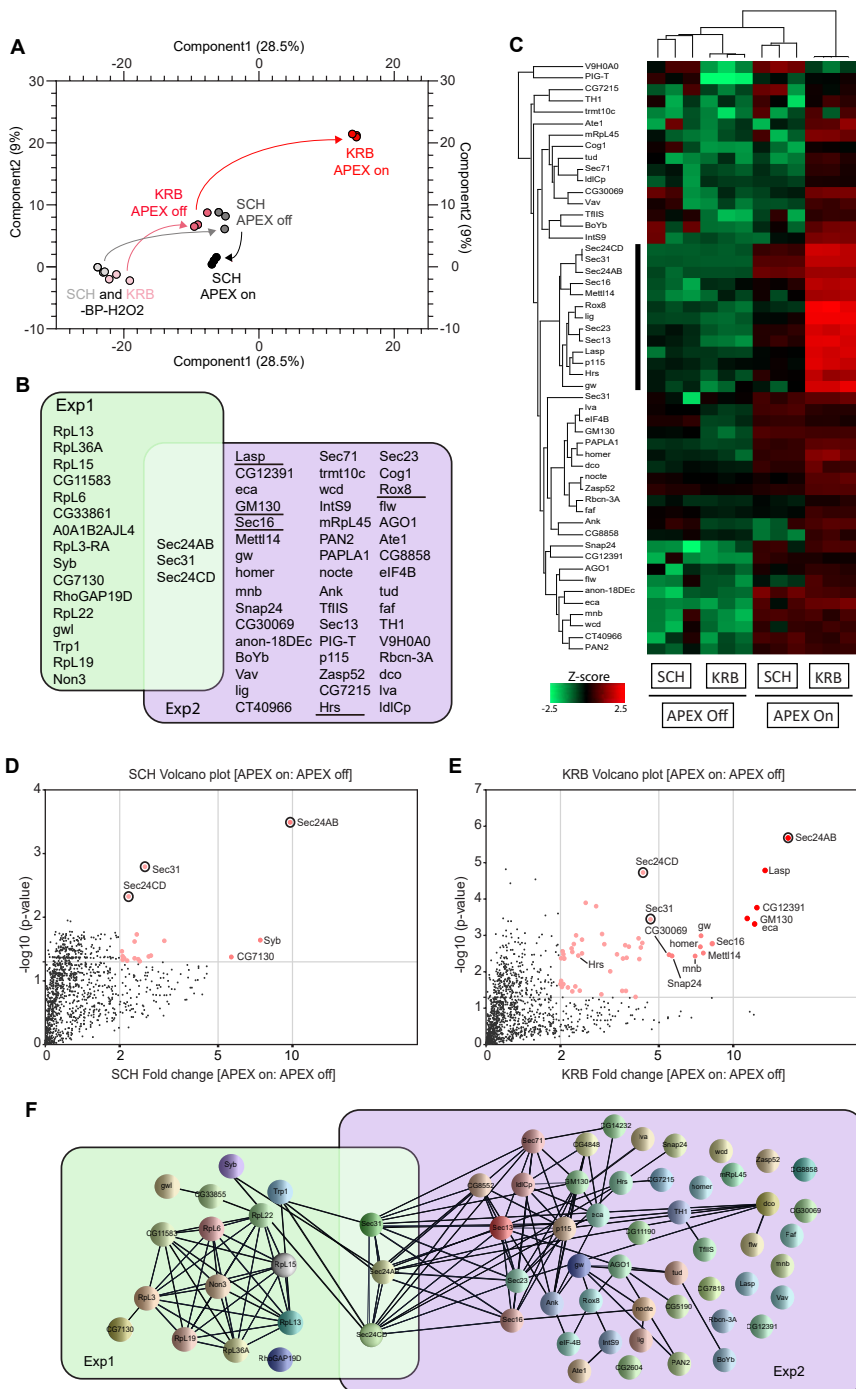


**Figure 2: Sec24-APEX2 mediates biotinylation of Sec body proteins.** (A) Principal component analysis (PCA) depicting impact of BP addition and H<sub>2</sub>O<sub>2</sub> APEX activation. In -BP-H<sub>2</sub>O<sub>2</sub> conditions, APEX labeling in SCH and KRB have similarly low background (light grey and light pink respectively). In +BP-H<sub>2</sub>O<sub>2</sub> conditions, APEX labeling in SCH and KRB remain similar (dark grey and dark pink respectively). Differential proximity biotinylation in Sec bodies (red) depends largely on H<sub>2</sub>O<sub>2</sub>. (B) Overlap of proteins biotinylated in the vicinity of Sec24. Sec24 has a largely distinct protein interactome during growing (green) and starvation (purple) conditions. Proteins underlined have been experimentally verified to co-localise with Sec bodies in this manuscript. (C) Heatmap of differential protein biotinylation in SCH and KRB incubation. Biotinylation is enriched only in APEX on conditions, and preferentially during KRB incubation, where more proteins in Sec bodies are within close proximity to Sec24. Black side bar indicates the most biotinylated 13 proteins in KRB APEX on. (D-E) Analyses of fold change and significance. Volcano plots feature differentially biotinylated proteins in SCH (D) and KRB (E) conditions respectively. Size of points increase with observed fold change. Proteins in red are enriched by at least 2-fold (APEX on: off). Proteins marked in black circles are universal interactors of Sec24 in both conditions. (F) Interaction network analysis of biotinylated proteins. Each line represents a documented interaction between biotinylated proteins, extracted from the STRING functional protein association network database.

To further understand the relationship between the other proteins spatially associated with Sec24, we also retrieved all known protein-protein interactions documented amongst Sec24 interactors in growing and KRB conditions, respectively. Extensive reported interactions provide evidence that formation of Sec body may in part rely on the coalescence of putative complexes forming around COPII subunits (Figure 2F). Collectively, these data systematically reveal the protein components in Sec bodies for the first time.

#### *Validation of Sec body components identified by APEX*

To validate that the predicted Sec body components are true components, we used immunofluorescence to assess their co-localization with Sec16, a known Sec body marker (Zacharogianni et al., 2014; Zhang et al., 2021). Importantly, Sec16 was also on our APEX hit list, and clearly co-localized with Sec24 and biotin (Figure 3A). Co-staining of putative Sec body proteins together with Sec16 instead of Sec24, should further increase confidence, in a manner analogous to reverse IP with a different antibody. Using this strategy, we verified the presence of newly identified components of KRB-induced Sec bodies (Figure 3B). Endogenous GM130 (a Golgi peripheral protein) (Nakamura, 2010), Hrs (an endosome associated protein) (Pullan et al., 2006), Homer (scaffold protein at postsynaptic density) (Luo et al., 2012), and Lasp (an actin associated protein) (Lepa et al., 2020) significantly localized to KRB induced Sec bodies marked with Sec16 (Figure 3B, B'). Interestingly,

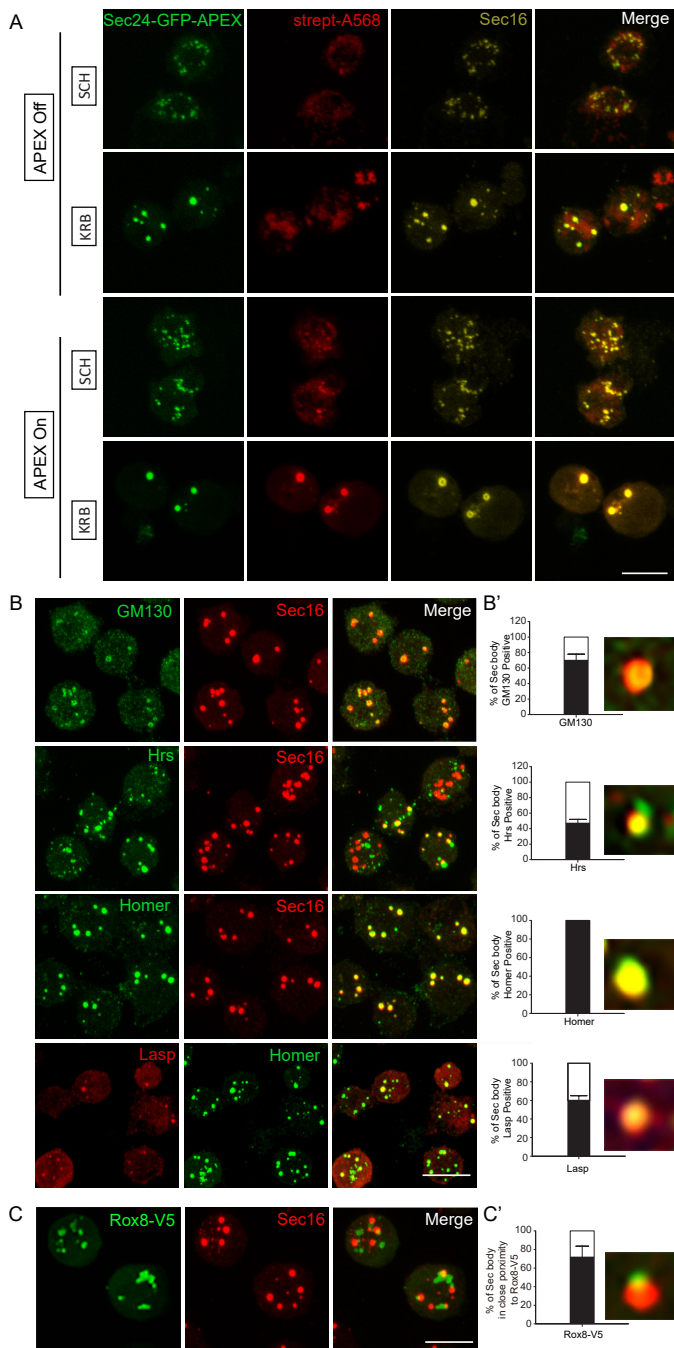


**Figure 3: Validation of Sec body proteins by fluorescence confocal microscopy. (A)** Immunofluorescence visualization of Sec24AB-GFP-APEX2 (green), Sec16 (gold) and biotin (Strept-A568, red). Sec16 completely co-localizes with Sec24-GFP-APEX2 and biotin. **(B, B')** Immunofluorescence visualization of endogenous GM130, Hrs, Homer (green) and in Sec bodies (marked by Sec16, red), as well as LAMP1 (red) and homer (green) **(B)**. Percentage of Sec bodies positive for these candidates **(B')**. **(C, C')** Immunofluorescence visualization of overexpressed Rox8-V5 (anti V5, green) in close proximity of Sec bodies (marked by Sec16). Percentage of Sec bodies positive for Rox8-V5 **(C')**. Scale bar: 10µm.

---

not all the validated Sec proteins were present in every observed Sec body, as shown in Figure 3B'. This reveals that the packaging of proteins into Sec bodies may be somewhat heterogeneous, and not always coordinated in component stoichiometry. This is also a key characteristic of assemblies formed by phase separation.

In addition, V5-tagged Rox8, the *Drosophila* homologue of TIA1, an established stress granule marker in mammalian cells (Waris et al., 2014) was found in close proximity to Sec bodies (**Figure 3C, C'**). This is in agreement with the earlier observation that stress granules form close to Sec bodies (Zacharogianni et al., 2014) and share components (Aguilera-Gomez et al., 2017). The validations of these 5 candidates further strengthen the reliability of our mass spectrometry approach, and that for the first time, we can systematically identify the protein components of KRB-induced Sec bodies.

#### *Sec bodies form from re-localization of existing intracellular proteins*

Since the observation of Sec bodies, the mechanism surrounding their formation of such stress-induced assemblies has remained largely speculative. Of note, specific questions regarding the origin of proteins packaged into these compartments are still unanswered. To investigate this, we supplemented the APEX data with both RNA sequencing (GSE143810; (Zhang et al., 2021)) and total proteome data acquired here, in the same conditions (**Figure 4A**). Since the total cellular proteome considers all proteins, inclusive of proteins packaged into Sec bodies, it is possible to determine if the total quantity of each putative Sec body protein inside the cell has increased during the KRB stress. As shown in **Figure 4B** and **Figure 4C**, none of the putative Sec body proteins was up-regulated at the RNA or proteome level. This provides strong evidence that proteins packaged in Sec bodies are neither newly transcribed nor newly translated. Instead, Sec bodies are likely to be re-organized from existing intra-cellular protein pools.

Detailed Gene Ontology cellular component analysis on the putative Sec body

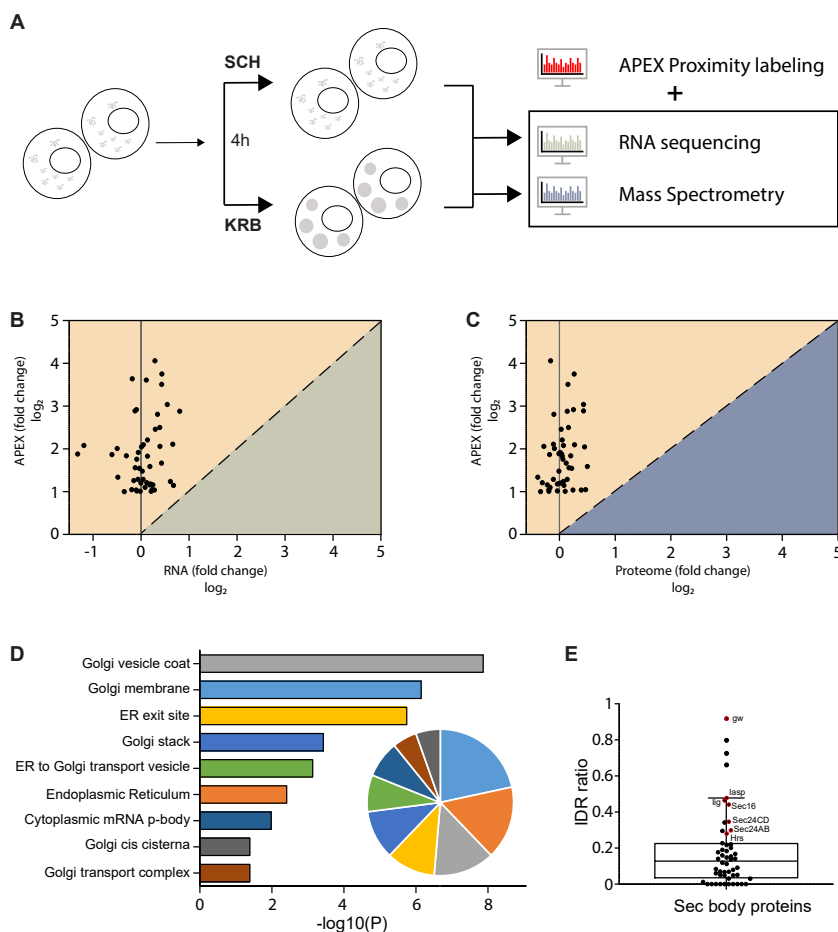


**Figure 4: Sec body formation depends on re-localization of existing cytosolic proteins.** (A) Schematic of combined RNA, protein and APEX analyses of KRB treated cells. Differential changes at 4h starvation, if any, were analyzed for correlative trends. (B-C) Correlation between significantly enriched Sec body proteins and the respective transcript levels (B), or total proteome levels (C). Almost all proteins that accumulate in Sec bodies were not differential at the RNA or total proteome level. (D) Bar graph depicting significantly enriched Gene Ontology Cellular Compartment (GO/CC) terms for proteins in Sec bodies, as calculated by DAVID. Pie graph inset shows the relative proportion of Sec body proteins annotated to these cellular compartments. A large majority of Sec body proteins are of ER and Golgi origin. (E) Box scatter plot showing 52 Sec body proteins ranked by the proportion of intrinsically disordered region (IDR). Proteins annotated in red were significantly enriched in sec bodies, as indicated by black side bar in the heatmap in Figure 2C.

proteins identified in our dataset further revealed that these proteins are largely localized to the ER and Golgi under normal growth conditions (**Figure 4D**), thereby providing further support that Sec bodies may form from re-organization of peripheral proteins functioning at the early secretory pathway.

While other types of stress-induced assemblies such as stress granules have been studied more extensively and also by a similar APEX approach we have used here (Markmiller et al., 2018; Marmor-Kollet et al., 2020), the same Gene Ontology cellular compartment analysis of stress granule components revealed drastically different sub-cellular enrichments, for instance predominantly in the nuclear and cytoplasmic compartments, and were not membrane-associated (**Supplementary Table 1**). Furthermore, stress granules contain reportedly hundreds of different proteins from diverse subcellular compartments, whereas Sec bodies are composed of relatively fewer proteins that are mostly from the ER and Golgi. These differences critically distinguish their formation.

Sec bodies have the properties of phase-separated liquid droplets (Zacharogianni et al., 2014), similar to stress granules. The components of phase-separated liquid droplets have been reported to often contain intrinsically disordered regions (IDRs) (Oldfield and Dunker, 2014) that may facilitate droplet formation. Many IDRs contain low-complexity domains (LCDs), which are regions with low amino-acid diversity (Jain et al., 2016; Kato et al., 2012). We have previously established that Sec24AB/CD and Sec16 display high LCD content (Zacharogianni et al., 2014). Uniprot sequence annotation of the 52 putative Sec body proteins identified in this current dataset revealed a wide range of IDR ratio, as defined by the fraction of the total sequence length predicted to be intrinsically disordered. It was intriguing to find that the cluster of proteins most enriched in Sec bodies (**Figure 2C**, black side bars), are also amongst the proteins with the highest IDR ratio in our dataset (**Figure 4E**, data points in red). In addition, 42 out of the 52 putative Sec body proteins contain IDRs (**Figure 4E**). This further implies that Sec bodies may form from the coalescence of ERES, ER and Golgi components as driven by lattice arrangement between intrinsically disordered regions of driver proteins, such as Sec16 and Sec24AB at ERES. These can in turn nucleate the other proteins that function normally at the early secretory pathway.

---

## *Materials and methods*

### *Cell culture and amino acid starvation*

Drosophila S2 cells (R69007, Thermo Fisher Scientific) were cultured in Schneider's medium (SCH, S0146; Sigma) supplemented with 10% insect-tested fetal bovine serum (F4135; Sigma) at 26°C. S2 cells (between passages 5 and 18) were pelleted at 200g in a microfuge for 3 min, washed once in fresh Schneider's medium, and diluted to 106/ml. 1ml of cell suspension were plated per well in a 12-well plate containing coverslips. Cells were allowed to attach for 1.5h before starting the treatment. Amino acid starvation was performed in Krebs Ringers bicarbonate buffer (KRB) comprising 0.7mM NaH<sub>2</sub>PO<sub>4</sub>, 15mM NaHCO<sub>3</sub> (sodium bicarbonate, BIC), 120.7mM NaCl, 4.53mM KCl, 0.5mM MgCl and 10mM glucose at pH 7.4 as described previously (Zacharogianni et al., 2014; Zhang et al., 2021).

### *Molecular cloning and transfection*

To generate pMT-Sec24AB-GFP-APEX2, GFP-APEX2 was amplified from the plasmid encoding Connexin43-GFP-APEX2 (44440, addgene) and cloned into pMT using the restriction enzymes BstBI and PmeI. Sec24AB was amplified from a cDNA library made from S2 cells and cloned into pMT-GFP-APEX2 using the restriction enzymes EcoRI and ApaI. To generate pMT-Rox8-V5, Rox8 was amplified from a cDNA library made from S2 cells and cloned into pMT-V5 using the restriction enzymes KpnI and EcoRV. Transfection of pMT constructs were performed using Effectene transfection reagent (301425, Qiagen) (Zacharogianni and Rabouille, 2013) for 48h. Chimeric protein expression was induced with 1mM CuSO<sub>4</sub> for 1.5h before incubation in KRB.

Primers used were:

GFP-APEX2 forward: 5'-CATGTTCTGAACTATGGTGAGCAAGGGCG-3',

GFP-APEX2 reverse: 5'-CATGGTTTAACTTAGGCATCAGCAAACCC-3'

Sec24AB forward: 5'-CATGGAATCCACCATGTCGACTTACAATCCGAACCTC-3'

Sec24AB reverse: 5'-CATGGGGCCCTTTAACCTGAGCCCGAATGT-3'

Rox8 forward: 5'-GGGATCTAGATCGGGGTACCATGGACGAGTCGCAACCG-3',

Rox8 reverse: 5'-GCCACTGTGCTGGATATCTGGGTCTGGTATTGTGGCATCG-3'.

### *Stable cell line*

To generate pMT-Sec24AB-GFP-APEX2 stable cell line, pMT-Sec24AB-GFP-APEX2 was co-transfected with a plasmid encoding for pCoHygro in S2 cells using Effectene transfection reagent (Qiagen) with a 1:10 ratio of DNA to Effectene Reagent. After culturing the transfected cells in antibiotic-free medium for 2 days, the selection of the transfected cells was performed with 150µg/ml Hygromycin B (ThermoFisher). Stable S2 cells were cultured



in Schneider's medium with additional 300µg/ml Hygromycin B.

### *Antibodies*

Immunofluorescence was performed with rabbit polyclonal anti-Sec16 (1:800) (Ivan et al., 2008); mouse monoclonal anti-GM130 (4A3 at 1:500; gift from Martin Lowe) (Seeman. et al., 2002); mouse monoclonal anti-Hrs (1:10, deposited by Munro, S. DSHB) (Riedel et al., 2016); guinea pig antibody dHNG2 against Homer (1:100; gift from Ulrich Thomas) (Diagana. et al., 2002); and rabbit polyclonal antibody against N-terminal Lasp (1:200, gift from Anne Ephrussi) (Suyama et al., 2009). For western blotting, biotinylated proteins were detected with streptavidin-HRP conjugates (1:1000, SA10001, life technologies). As loading control, mouse monoclonal anti- $\alpha$ -tubulin (1:2500, T5168, Sigma-Aldrich) was used. As secondary antibodies, we used donkey anti-rabbit-IgG conjugated to Alexa Fluor 568 (1:200, A10042, Invitrogen), goat anti-guinea pig-IgG conjugated to Alexa Fluor 488 (1:200, A-11073, Invitrogen), donkey anti-rabbit-IgG conjugated to Alexa Fluor 647 (1:200, A31573, Life technologies) and streptavidin conjugated to Alexa Fluor 568 (1:200, S11226, Invitrogen), as well as mouse-IgG antibodies coupled to HRP (1:2000, NA934, NA931, GE Healthcare).

### *Immunofluorescence*

Cells were fixed with 4% paraformaldehyde in PBS (pH 7.4) for 20 min. Cells were then washed three times with PBS and subsequently quenched by incubation in 50 mM NH<sub>4</sub>Cl in PBS for 5 min. Followed by permeabilization with 0.11% Triton X-100 for 5 min. Thereafter, cells were washed three times in PBS and blocked in PBS supplemented with 0.5% fish skin gelatin (G7765, Sigma-Aldrich) for 20 min. Cells were then incubated with the primary antibody (in blocking buffer) for 25 min, washed three times with blocking buffer and incubated with the secondary antibody (in blocking buffer) coupled to a fluorescent dye for 20 min. Cells on the coverslip were washed twice in milliQ water and dried for 3 min on a tissue with cells facing up. Finally, each coverslip with cells was mounted with Prolong antifade medium (+DAPI, P36935, Invitrogen) on a microscope slide. Samples were viewed with a Leica SPE confocal microscope using a 63× oil lens and 2× zoom.

### *Western blotting*

A total of 4x10<sup>6</sup> cells per condition were harvested on ice and lysed in 50 mM Tris-HCl pH 7.5, 150 mM NaCl, 1% Triton X- 100, 50 mM NaF, 1 mM Na<sub>3</sub>VO<sub>4</sub>, 25 mM Na<sub>2</sub>- $\beta$ -glycerophosphate, supplemented with a protease inhibitor tablet (Roche). The lysates were cleared by centrifugation at 20,000 x g for 20 min at 4°C. Supernatants were collected and the protein concentration was determined with a BCA protein assay kit (ThermoFisher).

---

50µg of protein was mixed with 5x SDS loading dye, boiled for 5 min and separated on an 8% SDS-PAGE gel. Then, separated proteins were transferred to a polyvinylidene difluoride (PVDF) membrane. Hereafter, the PVDF membrane was blocked in TBS+0.05% Tween-20 and 5% BSA (Sigma-Aldrich) (Blocking buffer). Primary antibodies were added to blocking buffer. After an overnight incubation at 4°C, the membrane was washed 3 times in TBS+0.05% Tween-20 over 45 min and incubated with secondary antibodies for 1 hour at room temperature. The membrane was washed 3 times washing in TBS+0.05%Tween-20 and developed by enhanced chemiluminescence (Bio-Rad) with Image Quant™ LAS 4000.

#### *APEX proximity labeling and analysis of biotinylated proteins*

After induction cells were incubated in Schneider's or KRB for 4h. To induce APEX activity, 500µM biotin-phenol was added to the medium in the last 30min, and 1mM H<sub>2</sub>O<sub>2</sub> was added for 1min just before harvesting. Biotinylation reaction was quenched with 5mM Trolox and 10mM solidum L-ascorbate in PBS. After cold-PBS wash, cells were harvested by scrapping and lysed in ice-cold lysis buffer (8M urea, 150mM NaCl, 20mM Tris-HCl pH 8.0, Protease Inhibitor Cocktail, 5mM Trolox and 10mM sodium L-ascorbate) for 30min on ice. Lysates were cleared at 18,000 x g for 30min at 4°C and the protein concentration was determined with a BCA protein assay kit (Thermo Fisher Scientific). 50ul streptavidin-coated magnetic beads (Thermo Fisher Scientific) were incubated for pulldown experiments with 380ug protein for each condition with end-to-end rotation for 2h at room temperature.

Biotinylated proteins captured by Steptavidin-coated magnetic beads were washed 5 times with PBS, and 3 times with 50mM ammonium bicarbonate. Reduction was performed at 20°C for 1h with 10mM dithiothreitol (DTT). Alkylation was then performed at 20°C for 0.5h with 20mM iodoacetamide (IAA) in the dark. Digestion was performed at 37°C, first with 1 µg of Lys C for 4 h, then with 1 µg of Trypsin overnight. Digested peptide were cleaned up with home-made c18 STAGE tips. Peptides were analysed by LC-MS/MS on an UHPLC 1290 system (Agilent, USA) coupled to an Orbitrap HF-X mass spectrometer (Thermo Scientific, USA). Peptides were trapped (Dr. Maisch Reprosil-Pur C18-AQ, 3 µm, 2.5 cm × 100 µm) for 5 min in solvent A (0.1% Formic acid in water) and then separated on an analytical column (Agilent Poroshell, 120 EC-C18, 2.7 µm, 50 cm × 75 µm) using a linear gradient of solvent B (0.1% Formic acid in 80% acetonitrile). An LC gradient of 10–40 % B in 115 min was used.

The mass spectrometer was operated in data-dependent mode, at a resolution of 60,000 for MS1 and 30,000 for MS2. Peptide data were acquired at 375–1600 m/z

and precursor ions were accumulated for 20 ms or until a AGC target value of 3e6 was reached. The 15 most abundant doubly and triply charged precursors were selected for fragmentation, after accumulation to the AGC target value of 1e5 within 50 ms. HCD fragmentation was performed at 27% NCE. Dynamic exclusion time was set to 16 s.

### *Mass Spectrometry Proteome analysis*

8 million cells per condition were grown in Schneider's and starved in KRB for 2h and 4h in 6 cm dishes at 26°C. After incubation, cells were harvested cells on ice, and cell pellets were and washed twice with ice-cold PBS. Cell material was lysed by gentle vortexing in 8M Urea in 50mM ammonium bicarbonate supplemented with 50µg/ml DNase I (Sigma-Aldrich), 50µg/ml RNase A (Sigma-Aldrich) and 1x cOmplete EDTA-free protease inhibitor cocktail (Roche Diagnostics). Subsequently, the lysate was cleared by centrifugation for 1h at 18,000 x g at 15°C. Protein concentration was determined with the Bradford assay (Bio-Rad). For each sample, 20µg of total protein was reduced, alkylated and digested sequentially with Lys-C (1:100) and trypsin (1:75), and perfectionated pre-fractionated offline on C18 STAGE-tips. Peptides were eluted in 5 high-pH reversed phase fractions, with 11-80% acetonitrile. All samples were dried by vacuum centrifugation and reconstituted in 102% formic acid prior to LC-MS/MS analyses.

MS data was acquired with an UHPLC 1290 system (Agilent) coupled to a Q-Exactive HF mass spectrometer (Thermo Fischer Scientific). Peptides were trapped (Dr Maisch Reprosil C18, 3µM, 2cm x 100µM) for 5min in solvent A (0.1% formic acid in water) before being separated on an analytical column (Agilent Poroshell, EC-C18, 2.7µM, 50cm x 75µM). Solvent B consisted of 0.1% formic acid in 80% acetonitrile. The mass spectrometer operated in data-dependent mode. Full scan MS spectra from m/z 375 – 1600 were acquired at a resolution of 60,000 to a target value of 3x10<sup>6</sup> or a maximum injection time of 20ms. The top 15 most intense precursors with a charge state of 2+ to 5+ were chosen for fragmentation. HCD fragmentation was performed at 27% normalized collision energy on selected precursors with 16s dynamic exclusion at a 1.4m/z isolation window after accumulation to 1x10<sup>5</sup> ions or a maximum injection time of 50ms. Tandem mass spectrometry (MS/MS) spectra were acquired at a resolution of 15,000. The APEX proteomics dataset has been deposited to ProteomeXchange Consortium via the PRIDE repository and can be accessed through the identifier PXD031601.

### *Mass spectrometry database search*

Raw files were searched using MaxQuant version 1.5.3.30 and the Andromeda search engine against the drosophila uniprot database (42477 entries, downloaded in September 2018). Enzyme specificity was set to trypsin and up to 2 missed cleavages were allowed.

---

Cysteine carbamidomethylation was set as fixed modification. Methionine oxidation and N-terminal acetylation were set as variable modifications. The false discovery rate (FDR) was restricted to 1% in both protein and peptide identification. For quantitative comparisons, label-free quantification (LFQ) was performed with “match between runs” enabled. Data normalization, imputation and statistics were performed with Perseus version 1.6.2.2. The data was visualized with Graphpad PRISM 8.

### *Acknowledgments*

We thank Marinke van Oorschot for making the Sec24AB-APEX2-GFO construct and generating the stable cell line. We thank the Hubrecht imaging facility for support with confocal microscopy.

### *Funding*

C.Z. is supported by a scholarship of the China Scholarship Council (201706670014).

### *References*

- Aguilera-Gomez, A., van Oorschot, M.M., Veenendaal, T., and Rabouille, C. (2016). In vivo visualization of mono-ADP-ribosylation by dPARP16 upon amino-acid starvation. *eLife* 5.
- Aguilera-Gomez, A., Zacharogianni, M., van Oorschot, M.M., Genau, H., Grond, R., Veenendaal, T., Sinsimer, K.S., Gavis, E.R., Behrends, C., and Rabouille, C. (2017). Phospho-Rasputin Stabilization by Sec16 Is Required for Stress Granule Formation upon Amino Acid Starvation. *Cell Rep* 20, 935-948.
- Aulas, A., Fay, M.M., Lyons, S.M., Achorn, C.A., Kedersha, N., Anderson, P., and Ivanov, P. (2017). Stress-specific differences in assembly and composition of stress granules and related foci. *J Cell Sci* 130, 927-937.
- Aulas, A., Lyons, S.M., Fay, M.M., Anderson, P., and Ivanov, P. (2018). Nitric oxide triggers the assembly of “type II” stress granules linked to decreased cell viability. *Cell Death & Disease* 9, 1129.
- Babu, M.M., Kriwacki, R.W., and Pappu, R.V. (2012). Structural biology. Versatility from protein disorder. *Science* 337, 1460-1461.
- Banani, S.F., Rice, A.M., Peeples, W.B., Lin, Y., Jain, S., Parker, R., and Rosen, M.K. (2016). Compositional Control of Phase-Separated Cellular Bodies. *Cell* 166, 651-663.
- Barlowe, C., Orci, L., Yeung, T., Hosobuchi, M., Hamamoto, S., Salama, N., Rexach, M.F., Ravazzola, M., Amherdt, M., and Schekman, R. (1994). COPII: a membrane coat formed by Sec proteins that drive vesicle budding from the endoplasmic reticulum. *Cell* 77, 895-907.
- Barlowe, C., and Schekman, R. (1993). SEC12 encodes a guanine-nucleotide-exchange factor essential for transport vesicle budding from the ER. *Nature* 365, 347-349.
- Berchtold, D., Battich, N., and Pelkmans, L. (2018). A Systems-Level Study Reveals Regulators of Membrane-less Organelles in Human Cells. *Molecular cell* 72, 1035-1049.e1035.
- Connerly, P.L., Esaki, M., Montegna, E.A., Strongin, D.E., Levi, S., Soderholm, J., and Glick, B.S. (2005). Sec16 is a determinant of transitional ER organization. *Current biology : CB* 15, 1439-1447.
- Diagana, T.T., Thomas, U., Prokopenko, S.N., Xiao, B., Worley, P.F., and Thomas, J.B. (2002).

Mutation of *Drosophila* homer Disrupts Control of Locomotor Activity and Behavioral Plasticity. *The Journal of Neuroscience*.

Farhan, H., Wendeler, M.W., Mitrovic, S., Fava, E., Silberberg, Y., Sharan, R., Zerial, M., and Hauri, H.P. (2010). MAPK signaling to the early secretory pathway revealed by kinase/phosphatase functional screening. *J Cell Biol* 189, 997-1011.

Gomez-Navarro, N., and Miller, E. (2016). Protein sorting at the ER-Golgi interface. *J Cell Biol* 215, 769-778.

Guillen-Boixet, J., Kopach, A., Holehouse, A.S., Wittmann, S., Jahnel, M., Schlussler, R., Kim, K., Trussina, I., Wang, J., Mateju, D., et al. (2020). RNA-Induced Conformational Switching and Clustering of G3BP Drive Stress Granule Assembly by Condensation. *Cell* 181, 346-361 e317.

Hughes, H., Budnik, A., Schmidt, K., Palmer, K.J., Mantell, J., Noakes, C., Johnson, A., Carter, D.A., Verkade, P., Watson, P., et al. (2009). Organisation of human ER-exit sites: requirements for the localisation of Sec16 to transitional ER. *J Cell Sci* 122, 2924-2934.

Hung, V., Udeshi, N.D., Lam, S.S., Loh, K.H., Cox, K.J., Pedram, K., Carr, S.A., and Ting, A.Y. (2016). Spatially resolved proteomic mapping in living cells with the engineered peroxidase APEX2. *Nature protocols* 11, 456-475.

Hyman, A.A., Weber, C.A., and Julicher, F. (2014). Liquid-liquid phase separation in biology. *Annual review of cell and developmental biology* 30, 39-58.

Ivan, V., de Voer, G., Xanthakis, D., Spoorendonk, K.M., Kondylis, V., and Rabouille, C. (2008). *Drosophila* Sec16 mediates the biogenesis of tER sites upstream of Sar1 through an arginine-rich motif. *Mol Biol Cell* 19, 4352-4365.

Jain, S., Wheeler, J.R., Walters, R.W., Agrawal, A., Barsic, A., and Parker, R. (2016). ATPase-Modulated Stress Granules Contain a Diverse Proteome and Substructure. *Cell* 164, 487-498.

Jevtov, I., Zacharogianni, M., van Oorschot, M.M., van Zadelhoff, G., Aguilera-Gomez, A., Vuillez, I., Braakman, I., Hafen, E., Stocker, H., and Rabouille, C. (2015). TORC2 mediates the heat stress response in *Drosophila* by promoting the formation of stress granules. *J Cell Sci* 128, 2497-2508.

Joo, J.H., Wang, B., Frankel, E., Ge, L., Xu, L., Iyengar, R., Li-Harms, X., Wright, C., Shaw, T.I., Lindsten, T., et al. (2016). The Noncanonical Role of ULK/ATG1 in ER-to-Golgi Trafficking Is Essential for Cellular Homeostasis. *Mol Cell* 62, 491-506.

Kaiser, C.A., and Schekman, R. (1990). Distinct sets of SEC genes govern transport vesicle formation and fusion early in the secretory pathway. *Cell* 61, 723-733.

Kato, M., Han, T.W., Xie, S., Shi, K., Du, X., Wu, L.C., Mirzaei, H., Goldsmith, E.J., Longgood, J., Pei, J., et al. (2012). Cell-free formation of RNA granules: low complexity sequence domains form dynamic fibers within hydrogels. *Cell* 149, 753-767.

Khong, A., Matheny, T., Jain, S., Mitchell, S.F., Wheeler, J.R., and Parker, R. (2017). The Stress Granule Transcriptome Reveals Principles of mRNA Accumulation in Stress Granules. *Mol Cell* 68, 808-820.

Kondylis, V., Spoorendonk, K.M., and Rabouille, C. (2005). dGRASP localization and function in the early exocytic pathway in *Drosophila* S2 cells. *Mol Biol Cell* 16, 19870-19875.

Lepa, C., Moller-Kerutt, A., Stolting, M., Picciotto, C., Eddy, M.L., Butt, E., Kerjaschki, D., Korb-Pap, A., Vollenbroeker, B., Weide, T., et al. (2020). LIM and SH3 protein 1 (LASP-1): A novel link between the slit membrane and actin cytoskeleton dynamics in podocytes. *FASEB journal : official publication of the Federation of American Societies for Experimental Biology* 34, 5453-5464.

Luo, P., Li, X., Fei, Z., and Poon, W. (2012). Scaffold protein Homer 1: implications for neurological

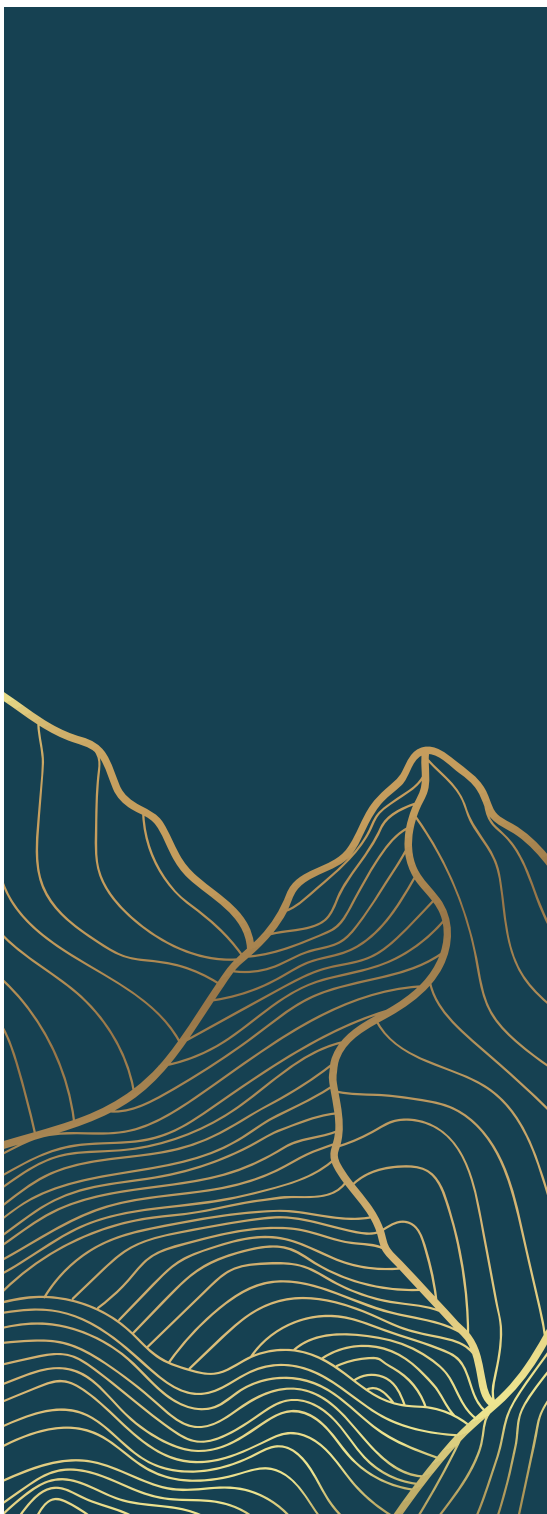
- diseases. *Neurochemistry international* 61, 731-738.
- Markmiller, S., Soltanieh, S., Server, K.L., Mak, R., Jin, W., Fang, M.Y., Luo, E.-C., Krach, F., Yang, D.S., Sen, A., et al. (2018). Context-Dependent and Disease-Specific Diversity in Protein Interactions within Stress Granules. *Cell* 172, 590-604.e513.
- Marmor-Kollet, H., Siany, A., Kedersha, N., Knafo, N., Rivkin, N., Danino, Y.M., Moens, T.G., Olender, T., Sheban, D., Cohen, N., et al. (2020). Spatiotemporal Proteomic Analysis of Stress Granule Disassembly Using APEX Reveals Regulation by SUMOylation and Links to ALS Pathogenesis. *Mol Cell* 80, 876-891.e876.
- Mellman, I., and Warren, G. (2000). The road taken: past and future foundations of membrane traffic. *Cell* 100, 99-112.
- Nakamura, N. (2010). Emerging new roles of GM130, a cis-Golgi matrix protein, in higher order cell functions. *J Pharmacol Sci* 112, 255-264.
- Oldfield, C.J., and Dunker, A.K. (2014). Intrinsically disordered proteins and intrinsically disordered protein regions. *Annual review of biochemistry* 83, 553-584.
- Protter, D.S., and Parker, R. (2016). Principles and Properties of Stress Granules. *Trends in cell biology* 26, 668-679.
- Pullan, L., Mullapudi, S., Huang, Z., Baldwin, P.R., Chin, C., Sun, W., Tsujimoto, S., Kolodziej, S.J., Stoops, J.K., Lee, J.C., et al. (2006). The endosome-associated protein Hrs is hexameric and controls cargo sorting as a "master molecule". *Structure (London, England : 1993)* 14, 661-671.
- Riedel, F., Gillingham, A.K., Rosa-Ferreira, C., Galindo, A., and Munro, S. (2016). An antibody toolkit for the study of membrane traffic in *Drosophila melanogaster*. *Biology open* 5, 987-992.
- Seeman, J., Pypaert, M., Taguchi, T., Malsam, J., and WarrEN, G. (2002). Partitioning of the Matrix Fraction of the Golgi Apparatus During Mitosis in Animal Cells. *Science*.
- Sprangers, J., and Rabouille, C. (2015). SEC16 in COPII coat dynamics at ER exit sites. *Biochemical Society transactions* 43, 97-103.
- Stagg, S.M., Gurkan, C., Fowler, D.M., LaPointe, P., Foss, T.R., Potter, C.S., Carragher, B., and Balch, W.E. (2006). Structure of the Sec13/31 COPII coat cage. *Nature* 439, 234-238.
- Supek, F., Madden, D.T., Hamamoto, S., Orci, L., and Schekman, R. (2002). Sec16p potentiates the action of COPII proteins to bud transport vesicles. *J Cell Biol* 158, 1029-1038.
- Suyama, R., Jenny, A., Curado, S., Pellis-van Berkel, W., and Ephrussi, A. (2009). The actin-binding protein Lasp promotes Oskar accumulation at the posterior pole of the *Drosophila* embryo. *Development* 136, 95-105.
- van Leeuwen, W., and Rabouille, C. (2019). Cellular stress leads to the formation of membraneless stress assemblies in eukaryotic cells. *Traffic* 0.
- Waris, S., Wilce, M.C., and Wilce, J.A. (2014). RNA recognition and stress granule formation by TIA proteins. *International journal of molecular sciences* 15, 23377-23388.
- Wilhelmi, I., Kanski, R., Neumann, A., Herdt, O., Hoff, F., Jacob, R., Preußner, M., and Heyd, F. (2016). Sec16 alternative splicing dynamically controls COPII transport efficiency. *Nature Communications* 7, 12347.
- Zacharogianni, M., Aguilera-Gomez, A., Veenendaal, T., Smout, J., and Rabouille, C. (2014). A stress assembly that confers cell viability by preserving ERES components during amino-acid starvation. *eLife* 3.
- Zacharogianni, M., and Rabouille, C. (2013). Trafficking along the secretory pathway in *Drosophila* cell

line and tissues: a light and electron microscopy approach. *Methods in cell biology* 118, 35-49.

Zhang, C., and Rabouille, C. (2019). Membrane-Bound Meet Membraneless in Health and Disease. *Cells* 8.

Zhang, C., van Leeuwen, W., Blotenburg, M., Aguilera-Gomez, A., Brussee, S., Grond, R., Kampinga, H.H., and Rabouille, C. (2021). Activation of IRE1, PERK and salt-inducible kinases leads to Sec body formation in *Drosophila* S2 cells. *J Cell Sci* 134.

Zhang, C., Grond, R., Damen, M.J., Wu, W., and Rabouille, C. (2022). Salt stress via calmodulin lead to the formation of stress granule in *Drosophila* S2 cells (in preparation).



## *Chapter 6*



## *Summary and general discussion*

---

## *Summary and general discussion*

In this thesis, we have addressed the formation of two stress assemblies, Sec bodies and stress granules, in response to stressing *Drosophila* S2 cells, either by amino-acid starvation in KRB (Krebs Ringer bicarbonate buffer) or in high NaCl stress (SCH150). Both Sec bodies and stress granules are phase separated membraneless organelles. It is interesting that they can form at the same time with the same kinetics upon the incubation of KRB and SCH150, yet remain distinct without significant intermixing. Furthermore, we have identified Sec body components using proximity labeling and mass spectrometry.

**Chapter 1** introduces the key concepts addressed in this thesis, including the formation of membraneless organelles under stress. Sec bodies form by coalescence of ER exit sites (ERES) components, and stress granules form by coalescence of specific RNA-binding proteins and RNAs. Membraneless organelles compartmentalize the cell cytoplasm alongside membrane bound compartments.

In **Chapter 2**, prompted by the finding of Sec bodies form from components of a membrane compartment ERES), we have explored further the relationship between cellular phase separation and membrane. Although the term “membraneless organelle” is language-wise correct and defines a compartment that is non-sealed by a lipidic membrane, it also alludes to the notion that phase separation in a cellular context “has nothing to do” with membrane. This is in fact not the case. Many membraneless organelles form in a close proximity or even template on membrane. Consequently, the term membraneless organelles should be replaced by “non-membrane bound condensates/assemblies/ compartments.

Furthermore, the contact between these assemblies and membrane needs to be defined in a more systematic manner as they influence each other’s biology. P-bodies appear to form near the ER, Sec bodies also. What about other condensates given that the ER pervades the entire cell?

Last, a large amount of data leading to a deep understanding of the biophysical and material properties of these condensates are performed in vitro using purifying proteins. However, given that the cell is an environment crowded with membrane-bound organelles that interact with condensates, now is a good time to add membrane to in vitro phase separation experiments.

In **Chapter 3**, we have identified the signaling pathways that cause Sec body formation and find that two pathways are critical. The first is the activation of salt-inducible kinases

(SIKs; SIK2 and SIK3 in *Drosophila*) by Na<sup>+</sup> stress, which is sufficient when it is high (i.e., a Na<sup>+</sup> concentration 4-fold higher than in the growing medium). The second is activation of two kinases IRE1 and PERK (also known as PEK in flies) downstream of ER stress induced by the absence of amino acids. This activation on its own is not enough to lead to Sec body formation. It needs to be combined with moderate salt stress to induce Sec body formation.

Interestingly, amino acid starvation in KRB and high salt both lead to the formation of another stress assembly, the stress granules, which stores mRNAs and RNA binding proteins (**Chapter 4**). However, we found that the formation of this second stress assembly is not downstream of the same kinases as Sec bodies. Indeed, inhibition of SIK, IRE1 and PERK does not affect the KRB and SCH150 induced stress granule formation. Instead, we found that osmotic stress through the addition of several salt or sucrose leads to the formation of stress granules and this is partly modulated by calmodulin activation, in stark contrast to Sec body formation. This might partly explain why the two assemblies remain distinct from one another.

In **Chapter 5**, we have identified the Sec body proteome by proximity labeling using the ascorbate peroxidase APEX2. We fused APEX2 to Sec24AB, the COPII subunit that localizes to ERES in cells in basal conditions (Schneiders') and to Sec bodies in KRB. In the presence of biotin-phenol and H<sub>2</sub>O<sub>2</sub> (APEX on), APEX2 facilitates the transfer of a biotin moiety to nearby interactors of chimeric Sec24AB. Using an un-biased approach comparing APEX on and off (-H<sub>2</sub>O<sub>2</sub>) in SCH and KRB, we identified 52 specifically enriched Sec body components. This included a large proportion of ER and Golgi proteins. After validation by immunofluorescence microscopy of endogenous proteins, we show that the expression of these components is not transcriptionally and translationally regulated. Instead, they appear to coalesce in Sec bodies under stress due to their high content of intrinsically disordered regions.

### *Phase separation*

Biomolecular phase separation has promoted a radically different explanation for how membraneless compartments assemble. Membraneless compartments are formed under the activation of phase separation driver proteins. These membraneless compartments are not formed or are not stable without out driver proteins (Musacchio, 2022).

Phase separation can be a transition which can concentrate specific molecules seemingly diffuse, leading to a liquid-liquid phase separation (LLPS, (liquid into a liquid) or

---

a liquid-solid transition (Li et al., 2012).

Proteins associated with membraneless organelles often exhibit multivalent interactions. Folded proteins are proteins with well-defined interaction surfaces which can form stable secondary structures. On the other hand, proteins with IDRs (intrinsically disordered regions) cannot form stable secondary structures and many IDRs contain a small biased amino acid composition which is referred to as low complexity domains (LCDs) (Das et al., 2014; Jones et al., 2006). IDRs have been shown to be prone to aggregation upon stress conditions (Uversky, 2017).

Similar to stress granule, Sec bodies may also have the properties of phase-separated liquid droplets (Zacharogianni et al., 2014). We have previously established that Sec24AB/ and Sec16 display a high content of LCDs, and the IDRs of Sec24 is sufficient and necessary to induce Sec body formation (Zacharogianni et al., 2014).

In **Chapter 5**, we identified 42 out of 52 putative Sec body proteins contain IDRs. This further suggested that Sec body formation is driven by lattice arrangement between IDRs of driver proteins (Sec16 and Sec24AB).

#### *KRB is more than just amino acid starvation*

KRB buffer does not contain amino-acids but simply removing amino-acids from buffers does not lead to Sec body formation (or stress granules). KRB is therefore more than just amino acid starvation.

mTORC1 inhibition: amino acid starvation triggered by KRB leads to the inhibition of mTORC1 (mechanistic target of rapamycin complex 1). It has been widely reported that when amino acid level is low or absent in the circulating medium the amino acid sensor mTORC1 is inhibited, which results in the dephosphorylation of mTORC1 direct target ribosomal S6 kinase (Jacinto et al., 2004; Kim and Guan, 2019; Li et al., 2010; Manifava et al., 2016). In **Chapter 3**, we observed S6 kinase no longer phosphorylated after KRB incubation, suggesting that mTORC1 is inhibited. However, the sole inhibition of mTORC1 by rapamycin or Torin in growing condition (Schneider's) does trigger neither Sec body nor stress granule formation (**Chapter 3** and **Chapter 4**). Furthermore, inhibition of mTORC1 during KRB does not increase the formation of these stress assemblies. This suggests mTORC1 inhibition takes place during the KRB incubation but does not play a role during the formation of stress assemblies.

Activation of IRE1 and PERK: Amino acid starvation during the KRB incubation leads to the activation of the UPR (unfolded protein response). In **Chapter 3**, we show that KRB elicits ER stress and activation of two downstream kinases, IRE1 and PERK leading to the stimulation of UPR. probably occur through the clustering of two ER membrane kinases IRE1 and PERK. Interestingly, UPR stimulation has been shown that linked to the MARYlation Drosophila PARP16 (Jwa and Chang, 2012), which is also a transmembrane protein of the ER and the activation of PARP16 in KRB is essential for Sec body formation (Aguilera-Gomez et al., 2016). Whether the UPR stimulation during KRB incubation induces Sec body formation via this mechanism or independently remains to be further investigation. It could also be events that are downstream of the UPR, the Bip upregulation itself, and/or cytoplasmic changes. One interesting aspect is whether the activation of UPR might affect biophysical properties, membrane association dynamics, and conformation and post-translational modifications of Sec16 and COPII subunits, which would lead to their enhanced phase separation properties under stress. Importantly the sole stimulation of the UPR alone (through DTT) is not sufficient to form Sec bodies.

KRB appears to be a combination of UPR stimulation through amino acid starvation and SIK stimulation by a moderate salt stress. To form Sec bodies, the stimulation of both IRE1 and PERK needs to be combined to a moderate NaCl stress, through the activation of SIKs.

Interestingly, a high NaCl stress, even in the presence of amino-acids also induces the formation of Sec bodies in a sufficient manner. It therefore suggests that the absence of amino acid potentiates the moderate NaCl stress. At present, this is not understood, as IRE1 and PERK inhibitors do not influence SCH150-induced Sec body formation, so the exact link between IRE1, PERK, SIKs and the UPR remains to be further investigated.

Alternatively, the salt stress could potentiate the UPR kinases but it does not appear to be via SIKs, as HG-9-91-01 (the pan-SIK inhibitor) does not modulate the UPR, yet strongly reduces Sec body formation.

*The formation of Sec body and stress granules is governed by different intracellular pathways*

As mentioned above, both KRB and SCH150 (high NaCl stress) leads to the formation of Sec bodies as well as Stress granules. Both stress assemblies form by phase separation in the same time frame and in close proximity to one another, but without intermixing.

Stimulation of the UPR. Sec body formation is triggered by UPR activation combined to SIK activation, mimicked in the dish by addition of DTT and 100 mM NaCl. Inhibition of IRE1,

---

PERK and SIK affects the KRB and SCH150 induced Sec body formation, but interestingly not at all the stress granule formation.

This is remarkable as it has been widely reported that stress granules form in response to ER stress (Kimball, 2003; Lin et al., 2007). It is also the case for S2 cells where DTT, Heat stress, APS leads to the formation of stress granules (**Chapter 4**). This strongly suggested that ER stress of S2 cells could be instrumental to stress granule formation, at least upon KRB treatment, as we have shown that it does stimulate ER stress (**Chapter 3**) (Zhang et al., 2021). However, none of the ER stress inhibitors (AMG-18, 4u8C, PERKi) or depletions (PERK and ATF6 depletion) lead to a decrease in stress granule formation upon KRB and SCH150. This suggests that even though ER stress can lead to stress granule formation, the downstream kinases are not involved in stress granule formation in KRB and SCH150.

Taken together, these results suggest that the same cellular stresses induce the formation of two stress assemblies upon the activation of many pathways, a subset of them specifically leading the formation of one assembly while a different subset leads to the formation of the other (**Figure1**). It suggests that these incubations are complex.

NaCl stress for Sec bodies and Osmotic stress for Stress granules: Second, Addition of NaCl to the growing medium triggers the formation of both stress assemblies. But Sec body formation requires the specific presence of NaCl. Only increasing NaCl led to a substantial formation of Sec bodies. Indeed, neither addition of KCl, Na-acetate nor osmotic shock (sucrose) induces their formation, suggesting that it is not downstream of osmotic stress. We have also shown that NaCl addition activates the SIKs.

Conversely, stress granule formation appears to be formed by the non-differential addition of salt (+150mM of NaCl, KCl, Na-acetate, LiCl, CaCl<sub>2</sub>), and addition of sucrose also leads to their formation, supporting that their formation is downstream of osmotic (and/or hypertonic) stress. However, we have shown that KRB and SCH150 do not lead to a decrease in cell diameter (no apparent shrinkage). It suggests that osmotic salt stress activates specific pathways that still need to be fully elucidated. Osmotic stress induced stress granule formation falls in the category of non-canonical pathway as it appears to be independent of elf2alpha phosphorylation (Aulas et al., 2017; Kedersha et al., 2002). The KRB and SCH150 induced stress granule formation in S2 cells are also independent of the phosphorylation of this factor as its inhibition does not modulate the response. This suggests that this is also non canonical. In other systems, RocA and PatA have been involved and it could be interesting to test these enzymes in our system (Aulas et al., 2017; Kedersha et al., 2002).

Furthermore, the formation of stress granules upon KRB and SCH150 appears to

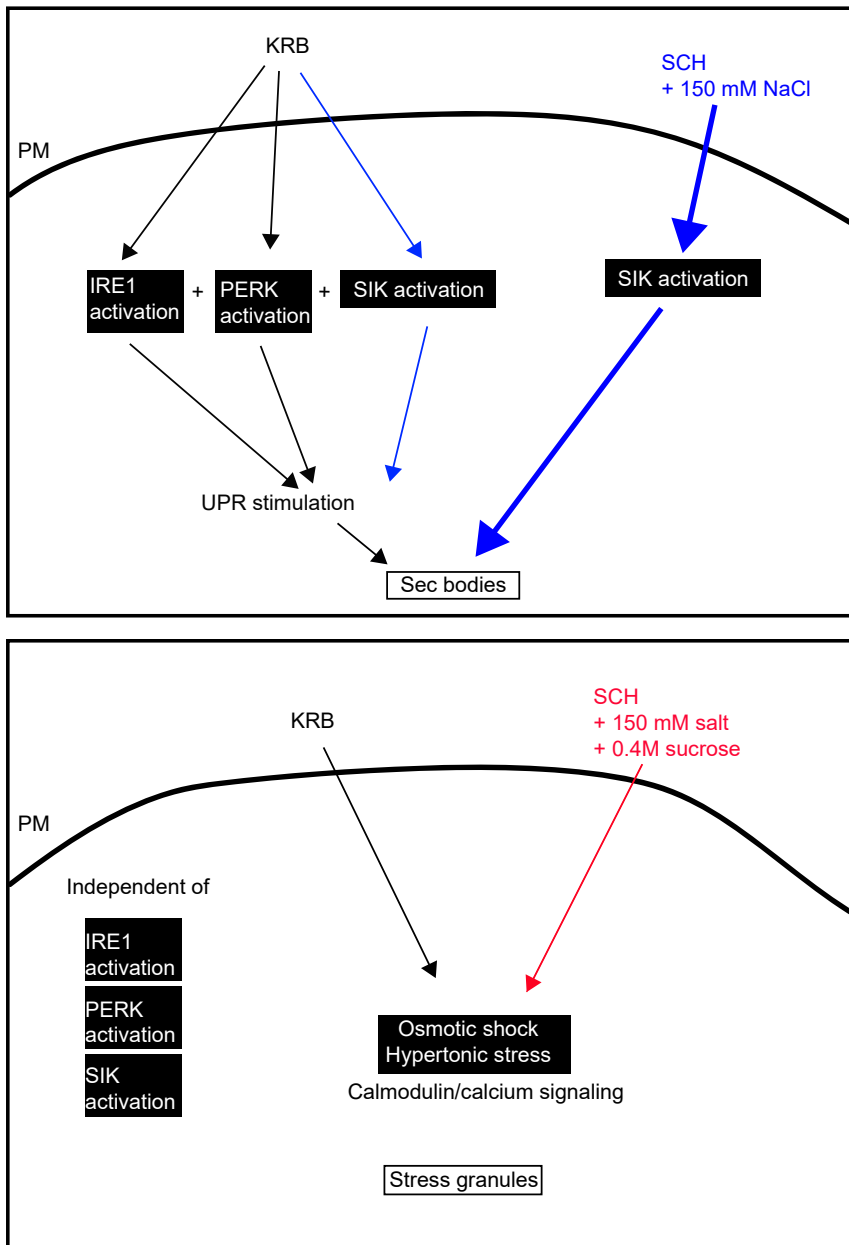


**Figure 1: The formation of Sec body and stress granules is governed by different intracellular pathways.** Sec body formation is triggered by UPR activation combined to SIK activation, mimicked in the dish by addition of DTT and 100 mM NaCl. Stress granule formation is downstream of osmotic/hypertonic stress.

---

involve calmodulin, a protein that is the most elevated in KRB S2 cell stressed (Chapter 4). This is relevant as calcium binding proteins are now clearly components of stress granules in mammalian cells (Markmiller et al., 2019; Marmor-Kollet et al., 2020). Their recruitment is in line with the finding that modulating the intracellular calcium level has an impact on stress granule formation.

Taken together, the same cells stressed by the same extracellular conditions form two assemblies through different and non-overlapping intracellular pathways. This illustrates the complexities of the stress response in general and may explain why the two assemblies remain distinct instead of collapsing into a single structure.

### *Identification of the Sec body proteome*

The fact that they remain distinct has allowed the identification of the Sec body proteome by the APEX strategy by tagging Sec24AB (a known component of the Sec bodies). We identified 52 proteins including large number of them being components of the ER, such as Sec16 (the key Sec body marker and driver), other COPII subunits, as well as components functioning at the Golgi apparatus.

Interestingly, in line with phase separation, most of the 52 identified components contain intrinsically disordered regions (IDRs) that are proposed to contribute to coalescence (Babu et al., 2012; Guillen-Boixet et al., 2020). Importantly, these components are neither regulated transcriptionally nor translationally, suggesting a re-location to Sec bodies that likely act as storage during the period of stress.

Previous research in our group has shown that Sec bodies formation is related to the inhibition of protein secretion in the early secretory pathway and proteins recruit into Sec bodies protect them from degradation (Zacharogianni et al., 2014). Recent study in our group on the formation of Sec body in mammalian INS-1 cells suggests that Sec body formation is the cause of the inhibition of ER exit (van Leeuwen et al., 2022), not the consequence. Whether this is also the case in S2 cells remains to be explored in more detail. The incorporation of key components functioning in this pathway may store components and modulates the secretion and endocytosis capacity of the cells during stress.

More specifically, we found P115 and GM130 (that we validated) but also Hrs, Homer, Lasp, and Rox8.

-GM130 localized at ERES and cis-Golgi in Drosophila cells (Kondylis and Rabouille, 2009). In mammalian cells, GM130 forms a complex with p115 on the Golgi cisternae to help with building and maintaining Golgi stack, a similar complex (Kondylis and Rabouille, 2003;



Nakamura et al., 1997). GM130 contain IDRs and this could contribute to its Sec body recruitment.

-Hrs is homologous to yeast Vps27p (vacuolar protein sorting), which regulates protein trafficking from a perivacuolar compartment to the vacuole in yeast (R C Piper et al., 1995). Drosophila and mammalian Hrs regulate inward budding of endosome membrane and (Multivesicular body) formation (Thomas, 2002). In both drosophila and mammalian cells, endosome enlarged phenotype were observed upon Hrs depletion or mutation (Thomas, 2002). Why Hrs is recruited into Sec bodies and whether Sec body formation correlates with inhibition (or modulation) of inward budding in late endosomes during stress still need further investigation.

-Homer colocalizes with an ER marker Bip suggested its location to the cytoplasmic face of the ER compartment (Thierry et al., 2002). Homer proteins are key components modulating calcium- and glutamate-induced calcium release from ER stores in neurons (Thomas, 2002; Xiao et al., 2000). Interestingly, as mentioned above, calcium signaling through calmodulin may be involved in stress granule formation in KRB and SCH150 stress, suggesting that Homer recruitment to Sec bodies may participate to their formation through  $\text{Ca}^{2+}$  release from the ER. Depletion of this factor will help understanding its role in the formation of both assemblies.

-Drosophila Lasp is an actin-binding protein (Suyama et al., 2009) which highly similar to vertebrate and Caenorhabditis elegans Lasp (Chenard et al., 1998; Chew et al., 1998). Lasp consists of an N-terminal LIM domain, followed by two nebulin-like repeats, a spacer regain and a C-terminal SH3 domain (Grunewald and Butt, 2008). SH3 domains (60 amino acids) are one of the most prevalent families of modular binding domains which present on signaling proteins. These 60 amino acid domains are evolutionarily conserved protein-protein interaction domains (Musacchio et al., 1992). SH3 domains mediate interactions have been showed that are able to drive phase separation. For example, the linker between the first two SH3 domains in Nck enhances phase separation of Nck with N-WASP (Banjade et al., 2015). Whether SH3 domain of Lasp contributes Sec body formation under KRB incubation still need further investigation.

-Last, Rox8 (TIA1 in mammals) is an RNA binding protein and established stress granule marker in mammalian cells (Waris et al., 2014). It is now identified as a binding partner of Sec24AB specifically in KRB. Upon KRB, Rox8 localises in stress granules that are found in a close proximity to Sec bodies (marked by Sec16) near the ERES. This is in line with results

---

previously described in (Zacharogianni et al., 2014) (Aguilera-Gomez et al., 2017) showing that these two assemblies form side by side but remain distinct one another.

Taken together, the identification of the Sec body proteome increases our knowledge of Sec bodies but also of other assemblies forming in their vicinity, such as stress granules (Rox8) but also Hrs containing coalescences that overlap with Sec16 without complete colocalization.

This technique opens the possibility for identifying the Sec body component in high salt condition. It will be interesting to figure out whether any of these newly identified Sec body proteins are playing a role in controlling Sec body formation and other stress assemblies and how they modulate membrane trafficking steps.

### *References*

- Aguilera-Gomez, A., van Oorschot, M.M., Veenendaal, T., and Rabouille, C. (2016). In vivo visualization of mono-ADP-ribosylation by dPARP16 upon amino-acid starvation. *Elife* 5.
- Aguilera-Gomez, A., Zacharogianni, M., van Oorschot, M.M., Genau, H., Grond, R., Veenendaal, T., Sinsimer, K.S., Gavis, E.R., Behrends, C., and Rabouille, C. (2017). Phospho-Rasputin Stabilization by Sec16 Is Required for Stress Granule Formation upon Amino Acid Starvation. *Cell Report* 20, 935-948.
- Aulas, A., Fay, M.M., Lyons, S.M., Achorn, C.A., Kedersha, N., Anderson, P., and Ivanov, P. (2017). Stress-specific differences in assembly and composition of stress granules and related foci. *Journal of cell science* 130, 927-937.
- Babu, M.M., Kriwacki, R.W., and Pappu, R.V. (2012). Structural biology. Versatility from protein disorder. *Science* 337, 1460-1461.
- Banjade, S., Wu, Q., Mittal, A., Peeples, W.B., Pappu, R.V., and Rosen, M.K. (2015). Conserved interdomain linker promotes phase separation of the multivalent adaptor protein Nck. *Proceedings of the national academy of sciences* 112, E6426-6435.
- Chenard, V.S.C.M.-L.C.H.R.M.-P., Boeuf, H., and Rio, J.-L.V.C.T.M.-C. (1998). Lasp-1, a Novel Type of Actin-Binding Protein Accumulating in Cell Membrane Extensions. *Molecular Medicine* 4, 675-687.
- Chew, C.S., Jr., J.A.P., Zhou, C.-J., Baranco, E., and Chen, X. (1998). Lasp-1 is a regulated phosphoprotein within the cAMP signaling pathway in the gastric parietal cell. *American journal of Physiology Cell Physiology* 275, C56-C67.
- Das, S., Pal, U., Das, S., Bagga, K., Roy, A., Mrigwani, A., and Maiti, N.C. (2014). Sequence complexity of amyloidogenic regions in intrinsically disordered human proteins. *PloS one* 9, e89781.
- Grunewald, T.G., and Butt, E. (2008). The LIM and SH3 domain protein family: structural proteins or signal transducers or both? *Molecular cancer* 7, 31.
- Guillen-Boixet, J., Kopach, A., Holehouse, A.S., Wittmann, S., Jahnel, M., Schlusser, R., Kim, K., Trussina, I., Wang, J., Mateju, D., et al. (2020). RNA-Induced Conformational Switching and Clustering of G3BP Drive Stress Granule Assembly by Condensation. *Cell* 181, 346-361 e317.
- Jacinto, E., Loewith, R., Schmidt, A., Lin, S., Ruegg, M.A., Hall, A., and Hall, M.N. (2004). Mammalian TOR complex 2 controls the actin cytoskeleton and is rapamycin insensitive. *Nature Cell Biology* 6, 1122-1128.

- Jones, N.L., Blasutig, I.M., Eremina, V., Ruston, J.M., Bladt, F., Li, H., Huang, H.L., Larose, L., Li, S.S.C., Takano, T., et al. (2006). Nck adaptor proteins link nephrin to the actin cytoskeleton of kidney podocytes. *Nature* 440, 818-823.
- Jwa, M., and Chang, P. (2012). PARP16 is a tail-anchored endoplasmic reticulum protein required for the PERK- and IRE1 $\alpha$ -mediated unfolded protein response. *Nature Cell Biology* 14, 1223-1230.
- Kedersha, N., Chen, S., Gilks, N., Li, W., Miller, I.J., Stahl, J., and Anderson, P. (2002). Evidence that ternary complex (eIF2-GTP-tRNA(i)(Met))-deficient preinitiation complexes are core constituents of mammalian stress granules. *Molecular Biology of the Cell* 13, 195-210.
- Kim, J., and Guan, K.-L. (2019). mTOR as a central hub of nutrient signalling and cell growth. *Nature Cell Biology* 21, 63-71.
- Kimball, S.R., Rick L. Horetsky, David Ron, Leonard S. Jefferson, and Heather P. Harding (2003). Mammalian stress granules represent sites of accumulation of stalled translation initiation complexes. *American Journal of Physiology-Cell Physiology* 284, 273-284.
- Kondylis, V., and Rabouille, C. (2003). A novel role for dp115 in the organization of tER sites in *Drosophila*. *Journal of cell biology* 162, 185-198.
- Kondylis, V., and Rabouille, C. (2009). The Golgi apparatus: lessons from *Drosophila*. *FEBS letters* 583, 3827-3838.
- Li, P., Banjade, S., Cheng, H.C., Kim, S., Chen, B., Guo, L., Llaguno, M., Hollingsworth, J.V., King, D.S., Banani, S.F., et al. (2012). Phase transitions in the assembly of multivalent signalling proteins. *Nature* 483, 336-340.
- Li, S., Brown, M.S., and Goldstein, J.L. (2010). Bifurcation of insulin signaling pathway in rat liver: mTORC1 required for stimulation of lipogenesis, but not inhibition of gluconeogenesis. *Proceedings of the national academy of sciences* 107, 3441-3446.
- Lin, J.H., Li, H., Yasumura, D., Cohen, H.R., Zhang, C., Panning, B., Shokat, K.M., Lavail, M.M., and Walter, P. (2007). IRE1 signaling affects cell fate during the unfolded protein response. *Science* 318, 944-949.
- Manifava, M., Smith, M., Rotondo, S., Walker, S., Niewczas, I., Zoncu, R., Clark, J., and Ktistakis, N.T. (2016). Dynamics of mTORC1 activation in response to amino acids. *Elife* 5.
- Markmiller, S., Soltanieh, S., Server, K.L., Mak, R., Jin, W., Fang, M.Y., Luo, E.C., Krach, F., Yang, D., Sen, A., et al. (2019). Context-Dependent and Disease-Specific Diversity in Protein Interactions within Stress Granules. *Cell* 172, 590-604.
- Marmor-Kollet, H., Siany, A., Kedersha, N., Knafo, N., Rivkin, N., Danino, Y.M., Moens, T.G., Olender, T., Sheban, D., Cohen, N., et al. (2020). Spatiotemporal Proteomic Analysis of Stress Granule Disassembly Using APEX Reveals Regulation by SUMOylation and Links to ALS Pathogenesis. *Molecular Cell* 80, 876-891 e876.
- Musacchio, A. (2022). On the role of phase separation in the biogenesis of membraneless compartments. *The EMBO journal* 41, e109952.
- Musacchio, A., Noble, M., Pauptit, R., Wierenga, R., and Saraste, M. (1992). Crystal structure of a Src-homology 3 (SH3) domain. *Nature* 359, 851-855.
- Nakamura, N., Lowe, M., Levine, T.P., Rabouille, C., and Warren, G. (1997). The vesicle docking protein p115 binds GM130, a cis-Golgi matrix protein, in a mitotically regulated manner. *Cell* 89, 445-455.
- R C Piper, A A Cooper, H Yang, and Stevens, T.H. (1995). VPS27 controls vacuolar and endocytic traffic

---

through a prevacuolar compartment in *Saccharomyces cerevisiae*. *Journal of cell biology* 131, 603-617.

Suyama, R., Jenny, A., Curado, S., Pellis-van Berkel, W., and Ephrussi, A. (2009). The actin-binding protein Lasp promotes Oskar accumulation at the posterior pole of the *Drosophila* embryo. *Development* 136, 95-105.

Thierry T. D, Ulrich T, Sergei N. P, Bo Xiao, Paul F. Worley, and Thomas, J.B. (2002). Mutation of *Drosophila* homer Disrupts Control of Locomotor Activity and Behavioral Plasticity. *The Journal of Neuroscience* 22, 428-436.

Thomas, G. (2002). Furin at the cutting edge: from protein traffic to embryogenesis and disease. *Nature reviews Molecular cell biology* 3, 753-766.

Uversky, V.N. (2017). How to Predict Disorder in a Protein of Interest. *Methods in molecular biology* (Clifton, NJ) 1484, 137-158.

van Leeuwen, W., Nguyen, D.T.M., Grond, R., Veenendaal, T., Fariás, G.G., and Rabouille, C. (2022). Stress-induced phase separation of ERES components into Sec bodies precedes ER exit inhibition in mammalian cells. *bioRxiv*.

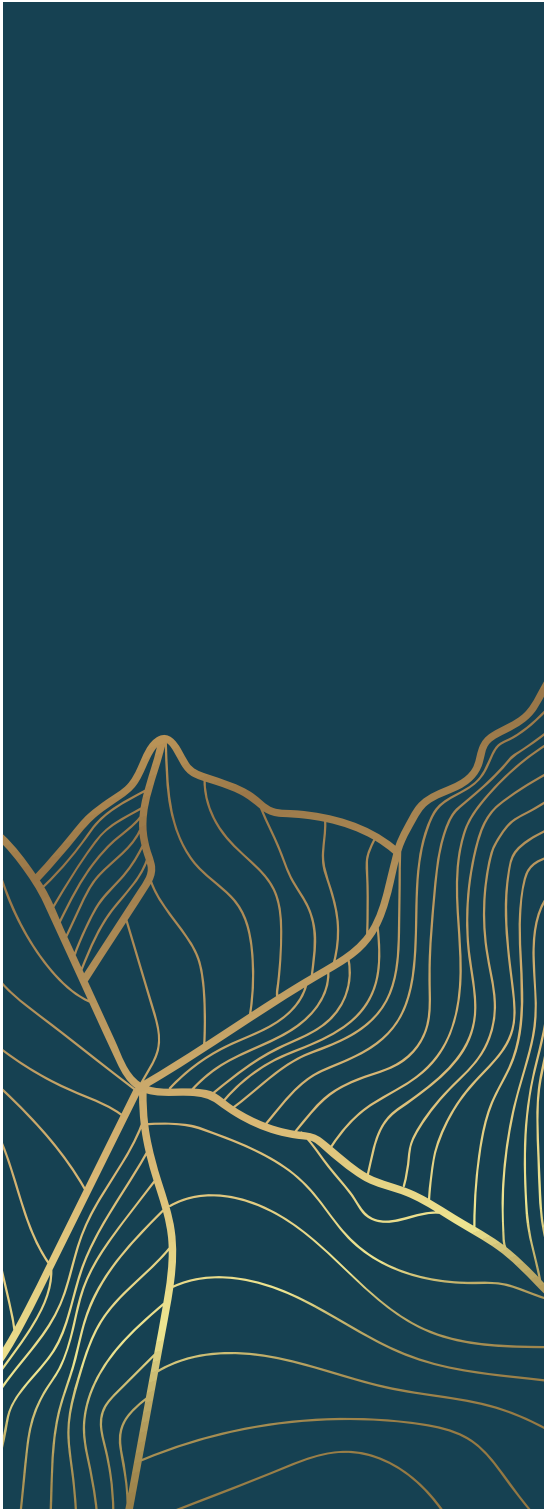
Waris, S., Wilce, M.C., and Wilce, J.A. (2014). RNA recognition and stress granule formation by TIA proteins. *International journal of molecular sciences* 15, 23377-23388.

Xiao, B., Tu, J., and Worley, P.F. (2000). Homer: a link between neural activity and glutamate receptor function. *Current opinion in neurobiology* 10, 370-374.

Zacharogianni, M., Aguilera-Gomez, A., Veenendaal, T., Smout, J., and Rabouille, C. (2014). A stress assembly that confers cell viability by preserving ERES components during amino-acid starvation. *Elife* 3.

Zhang, C., van Leeuwen, W., Blotenburg, M., Aguilera-Gomez, A., Brussee, S., Grond, R., Kampinga, H.H., and Rabouille, C. (2021). Activation of IRE1, PERK and salt-inducible kinases leads to Sec body formation in *Drosophila* S2 cells. *Journal of cell science* 134.





## *Chapter 7*

## *Addendum*

---

## *Nederlandse samenvatting*

In dit proefschrift hebben we de vorming van twee stress-assemblages, Sec-lichaampjes en stresskorrels, behandeld als reactie op stressvolle *Drosophila* S2-cellen, hetzij door aminozuuruithongering in KRB (Krebs Ringer-bicarbonaatbuffer) of in hoge NaCl-stress (SCH150). Zowel Sec-lichamen als stresskorrels zijn fasegescheiden membraanloze organellen (MLO's). Het is interessant dat ze zich tegelijkertijd met dezelfde kinetiek kunnen vormen bij de incubatie van KRB en SCH150, maar toch verschillend kunnen blijven zonder significante vermenging. Verder hebben we Sec-lichaamscomponenten geïdentificeerd met behulp van proximity-labeling en massaspectrometrie.

**Hoofdstuk 1** introduceert de belangrijkste concepten die in dit proefschrift worden behandeld, inclusief de vorming van membraanloze organellen onder stress. Sec-lichamen vormen door samensmelting van ER-uitgangsplaatsten (ERES) componenten, en stresskorrels vormen door samensmelting van specifieke RNA-bindende eiwitten en RNA's. Membraanloze organellen compartimenteren het celcytoplasma naast membraangebonden compartimenten.

In **Hoofdstuk 2** hebben we, naar aanleiding van de vondst van Sec-lichaampjes uit componenten van een membraancompartiment ERES, de relatie tussen celfasescheiding en membraan verder onderzocht. Hoewel de term "membraanloos organel" taalkundig correct is en een compartiment definieert dat niet wordt afgesloten door een lipidisch membraan, verwijst het ook naar het idee dat fasescheiding in een cellulaire context "niets te maken heeft" met membraan. Dit is in feite niet het geval. Veel MLO's vormen zich dicht bij elkaar of zelfs sjabloon op membraan. Daarom moet de term membraanloze organellen worden vervangen door "niet-membraangebonden condensaten/assemblages/compartimenten".

Bovendien moet het contact tussen deze samenstellingen en het membraan op een meer systematische manier worden gedefinieerd, omdat ze elkaars biologie beïnvloeden. P-lichamen lijken zich te vormen in de buurt van de ER, ook Sec-lichamen. Hoe zit het met andere condensaten, aangezien het ER de hele cel doordringt?

Ten slotte wordt een grote hoeveelheid gegevens die leiden tot een diep begrip van de biofysische en materiële eigenschappen van deze condensaten in vitro uitgevoerd met behulp van zuiverende eiwitten. Aangezien de cel echter een omgeving is vol met membraangebonden organellen die interageren met condensaten, is dit een goed moment om membraan toe te voegen aan in vitro fasescheidings experimenten.



---

In **Hoofdstuk 3** hebben we de signaalroutes geïdentificeerd die Sec-lichaamsvorming veroorzaken en we hebben vastgesteld dat twee routes cruciaal zijn. De eerste is de activering van door zout induceerbare kinasen (SIK's; SIK2 en SIK3 in *Drosophila*) door  $\text{Na}^+$ -stress, wat voldoende is wanneer deze hoog is (d.w.z. een  $\text{Na}^+$ -concentratie die 4 keer hoger is dan in het groeimedium). De tweede is activering van twee kinasen IRE1 en PERK (ook bekend als PEK in vliegen) stroomafwaarts van ER-stress veroorzaakt door de afwezigheid van aminozuren. Deze activering alleen is niet voldoende om tot Sec-lichaamsvorming te leiden. Het moet worden gecombineerd met matige zoutstress om Sec-lichaamsvorming te veroorzaken.

Interessant is dat uithongering van aminozuren in KRB en een hoog zoutgehalte beide leiden tot de vorming van een andere stressgroep, de stresskorrels, waarin mRNA's en RNA-bindende eiwitten worden opgeslagen (**Hoofdstuk 4**). We ontdekten echter dat de vorming van deze tweede spanningsassemblage niet stroomafwaarts is van dezelfde kinasen als Sec-lichamen. Remming van SIK, IRE1 en PERK heeft inderdaad geen invloed op de door KRB en SCH150 geïnduceerde vorming van stresskorrels. In plaats daarvan ontdekten we dat osmotische stress door de toevoeging van verschillende zouten of sucrose leidt tot de vorming van stresskorrels en dit wordt gedeeltelijk gemoduleerd door calmoduline-activering, in schril contrast met Sec-lichaamsvorming. Dit zou gedeeltelijk kunnen verklaren waarom de twee assemblages van elkaar gescheiden blijven.

In **Hoofdstuk 5** hebben we het Sec-lichaamsproteoom geïdentificeerd door middel van proximity-labeling met behulp van het ascorbaatperoxidase APEX2. We hebben APEX2 gefuseerd met Sec24AB, de COPII-subeenheid die lokaliseert naar ERES in cellen in basale omstandigheden (Schneiders') en met Sec-lichamen in KRB. In aanwezigheid van biotine-fenol en  $\text{H}_2\text{O}_2$  (APEX aan), vergemakkelijkt APEX2 de overdracht van een biotine-eenheid naar nabijgelegen interactoren van chimere Sec24AB. Met behulp van een onbevooroordeelde benadering waarbij APEX aan en uit ( $-\text{H}_2\text{O}_2$ ) in SCH en KRB werd vergeleken, identificeerden we 52 specifiek verrijkte Sec-lichaamscomponenten. Dit omvatte een groot deel van de ER- en Golgi-eiwitten. Na validatie door immunofluorescentiemicroscopie van endogene eiwitten, laten we zien dat de expressie van deze componenten niet transcriptioneel en translationeel gereguleerd is. In plaats daarvan lijken ze samen te smelten in Sec-lichamen onder stress vanwege hun hoge gehalte aan intrinsiek ongeordende regio's.

In **Hoofdstuk 6** bediscussieren we onze bevindingen en suggereren directies voor toekomstig onderzoek.

---

*List of publications*

**Zhang C**, Rabouille C. Membrane-bound meet membraneless in health and disease[J]. **Cells**, 2019, 8(9): 1000.

**Zhang C**, van Leeuwen W, Blotenburg M, et al. Activation of IRE1, PERK and salt-inducible kinases leads to Sec body formation in Drosophila S2 cells[J]. **Journal of cell science**, 2021, 134(17): jcs258685.

**Zhang C**, Grond R, Damen J M A, et al. Osmotic stress via calmodulin lead to the formation of stress granule in Drosophila S2 cells[J]. **bioRxiv**, 2022.

**Zhang C**, Damen JMA, Ground R, et al. Novel components of the stress assembly Sec body identified by proximity labelling [J]. **Submitted to Journal of cell biology**, 2022.

---

## Acknowledgements

### 致谢

终于提笔写下致谢二字，此刻又是一年芳草绿，心中思绪繁杂。

过去的四年半很长，长到花开花谢，春去秋来，叶生叶落，反反复复；却又很短，短到一年一岁，逝如朝霞。过往的每一幕都化成斑斓，闪烁在记忆的屏障中。

博士期间所有的经历都是学习，所有的相遇都值得感恩。

Thanks to my promotor **Prof. A. van Oudenaarden** and my thesis committee members **Prof. H. Kampinga, Prof. R. Korswagen, Prof. J. Klumperman, Prof. M. Maurice, Prof. M. Boxem** and **Dr. W. Wu** for all the usefull suggestions during the PhD evaluation meetings and taking the time to read and comment my thesis.

In ancient times those who wanted to learn would seek out a teacher, one who could propagate the doctrine, impart professional knowledge, and resolve doubts. Here I would like to thank my supervisor **Professor Catherine Rabouille**, who taught me volumes of knowledges and offered professional guidance in the past four and half years. This thesis could not be finished without your patient help. Thank you for all your support!

**Rianne**, thank you for the "Stress cells, not yourself". **Wessel**, thank you for all the "European History Lessones". Thank you both for all the discussion and help at work!

Thanks everyone at the **Hubrecht Institute**!

感谢爽和丹丹，帮我驱散 Bunnik 时的孤独。

感谢鹏，之涵，璐璐和庆午的鼓励和帮助。

感谢蔡苗和许锐的慰藉。

感谢楚慧 33 以及她的两只猫猫 Feifei 和 Miya 的陪伴。

感谢家人对我的无条件支持、理解和包容。

感谢卢叶茂毫无保留的爱，你的存在是爱人也是朋友和伙伴。有你在再多的困难也不会感到害怕。未来的每一天我们都要更坚定的走下去。

Chujun

楚琚，

Wrote on the train to Interlaken

写于驶往因特拉肯的火车上

---

### *Curriculum vitae*

Chujun Zhang was born on September 18th 1991 in Hubei, China. In 2010 she started her Bachelor in Pharmaceutical Engineering at Wuhan University of Bioengineering and graduated at 2014. After that she joined Prof. D. Gao's lab and started her Master in Basic Veterinary Medicine at Guizhou University.

In September 2017 she started her PhD at the Hubrecht Institute in the group of Prof Catherine Rabouille, investigating the pathways leading to stress assemblies formation in *Drosophila* S2 cells. The results developed on this subject are described in this thesis.

---

---



